

This file is part of the following work:

Bodhinayake, Geeth Gayantha (2020) *Correlation of internal and external pressure fluctuations in industrial buildings*. PhD Thesis, James Cook University.

Access to this file is available from:

<https://doi.org/10.25903/806q%2Dsk10>

Copyright © 2020 Geeth Gayantha Bodhinayake.

The author has certified to JCU that they have made a reasonable effort to gain permission and acknowledge the owners of any third party copyright material included in this document. If you believe that this is not the case, please email

researchonline@jcu.edu.au

JAMES COOK UNIVERSITY



COLLEGE OF SCIENCE AND ENGINEERING

**Correlation of Internal and External Pressure
Fluctuations in Industrial Buildings**

Geeth Gayantha Bodhinayake

DOCTORAL THESIS

This Thesis is submitted to the college of science and engineering for the degree of
Doctor of Philosophy

29 September 2020

Correlation Of Internal And External Pressure Fluctuations

In Industrial Buildings – Geeth Bodhinayake – 29 September 2020

To
Sharika,
Bithum,
and
Dehan

ඔබ හෙට මිය යාම් යැයි සිතා ජීවත්වන්න, ඔබ සදාකල් ජීවත් වේ යැයි සිතා ඉගෙන ගන්න....

Live as if you were to die tomorrow, Learn as if you were to live forever....

By Mahatma Gandhi

DECLARATION

I declare that this thesis is my work and has not been submitted for another degree or diploma at any university or other institution of tertiary education. Information derived from published or unpublished work of others has been acknowledged in the text and a list of references given.

Signed: _____

Date: _____

Geeth Bodhinayake

STATEMENT OF ACCESS

I, the author of this thesis, understand that James Cook University will make it available for use within the University Library and via the Australian Digital Theses network for use elsewhere.

I understand that as an unpublished work, a thesis has significant protection under the Copyright act, and I do not wish to place restrictions on access to this work.

Signed: _____

Date: _____

Geeth Bodhinayake

STATEMENT ON THE CONTRIBUTION OF OTHERS

Supervision: Prof. J. D. Ginger and Dr. D. J. Henderson were the principal supervisors of this work.

Editorial Assistance: Principal editorial assistance was provided by Prof. J. D. Ginger and Dr. D. J. Henderson. Additional editorial assistance was provided by Adjunct Prof. G. R. Walker.

Experimental Assistance: Assistance during the experimental setup of the wind tunnel testing was provided by Dr. Mitchell Humphreys. Assistance during the model construction and preparing was provided by Mr. Don Braddick and Mr. Denis Smith.

Funding: Financial support from the Australian Research Council linkage grant (project ID: LP150101206), and the project partners, the Australian Steel Institute Ltd, JDH Consulting, and Scott Woolcock Consulting Pty Ltd is gratefully acknowledged.

ACKNOWLEDGEMENTS

I first and foremost thank my advisors, Prof. John Ginger and Dr. David Henderson, for directing me throughout my PhD journey with their encouragements and guidance. Thank you for patience, advice and criticism at the many meetings to keep things on track and also for support during the thesis writing.

I would like to especially thank Mr. Neil Creek, national manager, Australian Steel Institute for initiating this research project and reviewing the project progress. I also would like to thank Prof. John Holmes for been a partner of this project, his stimulating inputs in project progress, and guidance for successful completion.

I would especially thank Prof. George Walker for all his time and effort reviewing my thesis and providing valuable comments and feedback to complete a good thesis. I also would like to thank Dr. Mitchell Humphreys and Dr. Korah Parackal for there support, and suggestions after the proofread of my thesis.

I am very grateful to acknowledge the Cyclone Testing Station (CTS) for their support of this research through the use of wind tunnel and resources. I also like to thank CTS staff Mr. John Doolan, Mr. Simon Ingham, Mr. Denis Smith, Mr. Don Braddick and Mrs. Lucy Crowley, and staff of the college of science and engineering for their grateful support. Appreciation is also expressed to my colleagues and friends over the years of providing stimulating discussions.

I am grateful and most fortunate to have a family who has been able to support me through good and bad times over the last four years. Special thanks to the special woman in my life, Sharika for accepting the pressures associated with the PhD, and taking care of our two lovely sons.

Finally, thank you all for the time and support to the many others who have contributed and whom I may not have mentioned.

ABSTRACT

Internal pressure fluctuations in a building depend on the external pressures generated by approaching wind flow, the opening area and location of openings in the envelope, building porosity and building volume. The approach wind flow generates spatially and temporally varying external pressure fluctuations on the walls and roof of the building. The internal pressure fluctuations in the building are influenced by the external pressures around the envelope so that a large opening in the envelope generates highly fluctuating internal pressures in strong wind conditions. Combinations of large internal pressures with large external pressures generate large resultant net pressures on the walls and roof of the building. Application of accurate internal pressures and their correlation with external pressure fluctuations enables the optimal design of typical industrial buildings.

The design internal pressure data in wind loading standards are based on the quasi-steady approximation to provide net wind pressures on the building envelope. The combination of internal and external pressures on different parts of a building and the parameters specified to account for the lack of correlation between internal and external pressure fluctuations have not been studied in detail.

The parameters have not been satisfactorily characterised previously from model-scale wind tunnel tests, full-scale tests or analytical techniques. This study characterises the external and internal pressure fluctuation and their correlation to generate large net pressure on the building envelope. The correlation between internal and external pressures and net pressure fluctuations were examined with two wind tunnel models representation of open-plan, rectangular, low roof pitch industrial buildings, 80 m long \times 40 m wide \times 20 m high, and 160 m long \times 40 m wide \times 20 m high. A series of wind tunnel tests were conducted on nominally sealed buildings and building with large openings. Further, simultaneously measured internal, external and net pressure fluctuations are analysed to study the effect of opening size and location in the building envelope, building porosity and building volume.

Internal pressure fluctuations are damped in the nominally sealed buildings due to the restricted wind flow in and out through the porous holes in the building envelope. Internal pressure fluctuations are small for all wind directions compared to the external pressure fluctuations. Large internal pressure fluctuations are experienced in a building with a large wall opening. The amplification and attenuation of peak and fluctuating internal pressures are presented as a function of the non-dimensional opening area to building

volume parameter, $S^* = (A^{3/2}/V)(a_s/\bar{U}_h)^2$. The ratios, $C_{\sigma_{pi}}/C_{\sigma_{pe}}$ and $C_{\hat{p}_i}/C_{\hat{p}_e}$ are discussed for different building configurations as a function of S^* .

The correlation between internal and external pressure fluctuations ($r_{pepi}(0)$) are analysed for different cladding locations on walls and roof. For the roof, internal and external pressure fluctuations are poorly, positively correlated ($r_{pepi}(0) < 0.3$) near windward roof edge and moderately correlated at the middle of the roof of the nominally sealed building. This is because the internal pressure fluctuations generated by leakage through all walls do not correlate with highly fluctuating suction external pressures generated by the conical vortices and separation bubbles at the leading edge. Similarly, internal and external pressure fluctuations on the walls are poorly correlated in the nominally sealed building.

When the building has a large windward wall opening, the $r_{pepi}(0)$ is moderately correlated around -0.6 and -0.7 at roof corners and near the windward roof edge above the opening where the flow separates. Furthermore, internal and external pressure fluctuations are poorly correlated ($-0.2 < r_{pepi}(0) < 0.3$) in the middle of the roof in the flow reattachment region. The correlation coefficients do not vary significantly for different building configurations for $1 < S^* < 120$. Internal and external pressure fluctuations are moderately correlated near the opening edge on the wall and poorly correlated further away from the opening.

The peak net pressures are large at the leading windward edge of the roof and side wall of the building following the combination of large external suction pressures and positive internal pressures when the building has a large windward wall opening. The probability of peak internal, external, and net pressure events occurring at the same time acting on the roof and wall cladding is less than 1% (i.e., peak events of internal, external and net pressures acting on roof and wall cladding do not coincide).

The correlation between external and internal pressures is a critical parameter used in the covariance integration method to determine the net peak pressure using the statistical properties of the overall external and internal pressure signals (i.e., peaks, means, standard deviations and correlation coefficients). The covariance integration method satisfactorily estimates the peak net pressures on cladding elements of nominally sealed building and building with a large opening and confirms that the external, internal and net peak events are random events.

The reduction factors for net pressure coefficients is derived considering the peak internal, external, and net pressures to optimise the design of the typical industrial building. The net pressure factor, F_C is defined for different roof zones and wall cladding of the nominally sealed buildings and buildings with large opening with the different opening area to building volume ratios. The net pressure factor provides a 5% to 10% reductions to the maximum magnitude net pressures on roof and wall cladding of the typical industrial buildings.

The results and conclusions in this thesis provide information to optimise the net pressures applied to the envelope of industrial buildings with wall openings, and further this information can be used to revise internal pressure provisions and combination factors in wind loading standards.

CONTENTS

1 Introduction	1
1.1 Objectives.....	5
1.2 Thesis Structure.....	6
2 Literature Review and Theory	8
2.1 External pressure fluctuations on buildings	8
2.1.1 Area-averaged external pressures	10
2.2 Internal pressure fluctuations	10
2.2.1 Characteristics of wind flow-through openings.....	11
2.2.2 Internal pressure in a nominally sealed building	12
2.2.3 Internal pressure in a building with a large opening	14
2.2.4 Internal pressure in a building with multiple openings	17
2.2.5 Internal pressure in a building with openings and background leakage.....	19
2.2.6 Internal pressure provisions in wind loading standards	20
2.3 Dimensional analysis	21
2.4 Correlation between external and internal pressure	25
2.5 Net pressures and net pressure factors	28
2.6 Covariance integration method	30
2.7 Chapter summary	31
3 Experimental Setup and Methodology	33
3.1 Wind tunnel boundary layer simulation.....	33
3.2 Building models	35
3.2.1 Opening geometries	37
3.2.2 Wall porosity on Model #1.....	39
3.2.3 Building volume of Model #1	40
3.2.4 External pressure tap layout.....	42
3.2.5 Internal pressure taps	45
3.2.6 Roof zones	45
3.3 Wind tunnel test configurations	46
3.4 Pressure time-history analysis.....	50
3.4.1 Pressure measurement system	50
3.4.2 External and internal pressures.....	51

3.4.3	<i>Net pressure fluctuations</i>	52
3.4.4	<i>Correlation coefficient between external and internal pressures</i>	53
4	External and Internal Pressure Fluctuations	56
4.1	External pressure fluctuations- Nominally sealed building	56
4.1.1	<i>External pressure on Wall #1</i>	56
4.1.2	<i>External pressure on the roof</i>	60
4.1.3	<i>Area-averaged external pressures on openings</i>	64
4.1.4	<i>External pressure spectra</i>	67
4.2	Internal pressure fluctuations	68
4.2.1	<i>Nominally sealed building</i>	69
4.2.2	<i>Building with a large opening in a wall</i>	71
4.2.3	<i>A large opening in a building with background porosity</i>	79
4.2.4	<i>Effect of the building volume</i>	80
4.2.5	<i>Building with multiple openings on the same wall</i>	82
4.3	Non-dimensional representation	85
4.4	Chapter summary	89
5	Correlation of External and Internal Pressure Fluctuations	91
5.1	Cross-correlation coefficient	91
5.2	Building with a large opening- effect of opening size and locations	94
5.2.1	<i>Correlation coefficients on the roof cladding- openings on the Wall #4</i>	95
5.2.2	<i>Correlation coefficients on the roof cladding- opening on Wall #1</i>	110
5.2.3	<i>Correlation coefficients on the wall cladding</i>	112
(i)	<i>Opening on Wall #4</i>	112
(ii)	<i>Opening on Wall #1</i>	115
5.3	Effect of the building volume on the correlation coefficient	117
5.4	Net pressure and net pressure factors for roof and wall cladding	120
5.4.1	<i>Roof cladding - net pressures</i>	121
5.4.2	<i>Roof cladding- net pressure factors based on point pressures</i>	138
5.4.3	<i>Wall Cladding</i>	144
5.5	Chapter summary	151
6	Conclusions and Recommendations	154
6.1	Conclusions	155
6.2	Recommendations	159

References	160
Appendices	164
Appendix A : Wind tunnel model details	165
Appendix B : Area averaged external pressure coefficient and area reduction factor (Ka)	173
Appendix C: Area-averaged net pressure and net pressure factors for roof Zones	181

LIST OF TABLES

Table 2.1: Area reduction factors (K_a) in AS/NZS 1170.2, 2011	10
Table 2.2: Measured Helmholtz frequency, mean and peak internal pressures for opening configurations for $\theta = 0^\circ$ (Guha et al. (2012)).....	19
Table 2.3: Cross-correlation coefficients for roof and wall areas- Beste et al. (1997) ...	27
Table 2.4: Combination factors for internal and external pressures, Xu and Lou (2017)	29
Table 3.1: Opening configurations of Model #1	38
Table 3.2: Wall porosity Model #1	39
Table 3.3: Notations for external pressure taps.....	43
Table 3.4: Wind tunnel test configurations – Model #1.....	47
Table 3.5: Wind tunnel test configurations – Model #2.....	49
Table 4.1: Area to volume ratio for different single opening configurations	86
Table 5.1: Interpretation for cross-correlation coefficient	92
Table 5.2: Selected single opening cases for detail analysis.....	94
Table 5.3: Estimated minimum net pressures using covariance integration method and measured minimum net pressures on selected roof locations for (a) Case #02 and (b) Case #09 for $\theta = 90^\circ$	129
Table 5.4: Peak to standard deviation ratios for external, internal and net pressures of an average of five runs for $\theta = 90^\circ$, RP1-1	132
Table 5.5: Number of peak events exceeding 3 standard deviations from the mean for five runs – Case #09, RP1-1, $\theta = 90^\circ$	133
Table 5.6: Number of net, external, and internal peak events for wind directions 90° to 135° for RP1-1	137
Table 5.7: Point net pressure factors, F_{C1} and F_{C2} for roof Zones #2B, #3B and #4B for different S^* values	144
Table B.1: Patch combinations and notations	174
Table B.2: Individual area reduction factors for each tap location on the side wall patch by adding one patch at a time to patch “a”	176
Table B.3: Individual area reduction factors for each tap location on the windward wall patch by adding one patch at a time to patch “a”	178
Table B.4: Individual area reduction factors for each tap location on the Leeward wall patch by adding one patch at a time to patch “a”	179
Table B.5: Proposed area reduction factor for wall cladding design for $h < 20\text{m}$	180
Table C.1: Net pressure factors for different roof Zones #1B, 2B, 3B, and 4B based on point pressures and area-averaged pressures for each S^* values	188

LIST OF FIGURES

Figure 1.1: Typical large span industrial type building	1
Figure 1.2: External and internal pressure distribution on the building envelope	2
Figure 1.3: Structural damage to industrial buildings (a) Loss of entire roof - CTS Report TR57 (b) Windward roller door failure –Stehle and Henderson (2001).....	3
Figure 1.4: Structural damage observed after Cyclone Debbie, 2017	4
Figure 2.1: Wind flow around the low-rise building (page-180; Holmes, 2007)	8
Figure 2.2: External pressure distribution on low rise building-(Holmes and Syme,1994)	9
Figure 2.3: Inflows and outflows of the multiple openings	12
Figure 2.4: Spectra of the internal and external pressures for the building with background leakage– Oh et al. [2007]	13
Figure 2.5: Wind Engineering Research Field Laboratory (WERFL) full scale low rise test building (dimensions in ft; 1ft -0.305m)- Ginger et al.(1997)	14
Figure 2.6: Experimental wind tunnel model used by Holmes (1979)	15
Figure 2.7: Windward wall, roof windward edge and internal pressure spectra for building with 2% windward wall opening (Ginger et al.,1997).....	17
Figure 2.8: Wind tunnel model with openings - 1: 100 scale (Guha et al.-2012).....	18
Figure 2.9: a) measured standard deviation pressure ratio versus S^* * b) measured peak pressure ratio versus S^* (Ginger et al.,2010)	22
Figure 2.10: Measured standard deviation pressure ratio versus S^* (Holmes and Ginger, 2012)	23
Figure 2.11: Standard deviation pressure ratio versus C_L ; a) Different opening sizes b) Different internal volume (Xu et al.,2017)	24
Figure 2.12: Wind tunnel model with openings and wind directions –Beste et al. (1997)	26
Figure 2.13: Wind tunnel model - 1:50 scale (Sharma and Richards (2005))	27
Figure 3.1: Boundary layer wind profile simulated in the wind tunnel at a length scale of 1/200	34
Figure 3.2: 1/200 scale wind velocity spectra at $z=100$ mm (20 m in full scale)	34
Figure 3.3: Schematic of wind tunnel Model #1 - 1/200 scale (all dimensions are in mm)	35
Figure 3.4: Model #1 fixed in the wind tunnel	36
Figure 3.5: Model #2 fixed in the wind tunnel	36
Figure 3.6: Layout of the porous holes in walls of Model #1	39
Figure 3.7: Three volume cases for Model #1	40

Figure 3.8: External pressure taps layout Model #1 –Walls and Roof	43
Figure 3.9: External pressure taps layout for Roof Purlins RP1-RP6; taps 1 to 17- Model #1.....	44
Figure 3.10: External pressure taps layout for Wall Girts WG1- WG3; taps 1 to 17-Model #1.....	44
Figure 3.11: Four internal pressure tap layout - Model #1	45
Figure 3.12: Roof zones , $\theta = 0^\circ \pm 45^\circ$	46
Figure 3.13: Roof zones , $\theta = 90^\circ$	46
Figure 3.14: 1.2m Long flexible tube connected to module	50
Figure 3.15: Peak events in the internal pressures time-history signal	55
Figure 3.16: Venn diagram for internal, external and net pressure peak events.....	55
Figure 4.1: Selected external pressure taps in the Wall #1	57
Figure 4.2: Mean, maximum, minimum and standard deviation pressure coefficients for FA 25, FA31, FC25 and FC31 on Wall #1	59
Figure 4.3: Selected external pressure taps on the roof	60
Figure 4.4: Mean, maximum, minimum, and standard deviation coefficients- roof cladding, RP6-1, RP4-1, RP6-9, RP4-9, RP6-17 and RP4-17 in Case #02.....	64
Figure 4.5: Area-averaged mean, maximum, minimum and Standard deviation pressure coefficients on the opening area LO1 and LO2 – Nominally sealed building.....	65
Figure 4.6: Area-averaged mean, maximum, minimum and Standard deviation pressure coefficients on the opening area LO5 and LO6 – Nominally sealed building.....	67
Figure 4.7: External pressures spectra for windward wall (Wall #1), side wall (Wall #2) and leeward wall (Wall #3) at $\theta = 0^\circ$	68
Figure 4.8: Internal pressure fluctuations at four locations in the building and cross-correlation between the taps (a)-(b) nominally sealed building at $\theta = 0^\circ$, (c)-(d) Building with a large opening when opening perpendicular to approach wind direction	69
Figure 4.9: Mean, standard deviation, minimum, and maximum internal pressure coefficient for $\theta = 0^\circ - 360^\circ$ for the nominally sealed buildings.....	71
Figure 4.10: Mean, standard deviation, minimum, and maximum internal pressure coefficient for single large opening on Wall #4 – Cases #09, #11, and #12.....	73
Figure 4.11: Area-averaged external pressure spectrum on Wall #4 and internal pressure spectra for Cases #09, #11, and #12, (a) $\theta = 90^\circ$, (b) $\theta = 180^\circ$	75
Figure 4.12: Mean, standard deviation, minimum, and maximum internal pressure coefficient for single large opening on Wall #1- Cases #04 and #08	77
Figure 4.13: Area-average external pressure spectrum and internal pressure spectra for Cases #04, #07, and #08 - (a) $\theta = 0^\circ$, (b) $\theta = 90^\circ$	78

Figure 4.14: Mean, standard deviation, minimum, and maximum internal pressure coefficient for single large opening in Case #04, and LO1 with three different porosities, 0.62, 0.30 and 0.08 for Cases #30, #31 and #32.....	80
Figure 4.15: Mean, standard deviation, minimum, and maximum internal pressure coefficient for a single large opening, LO1 for two volumes, Case #04 in Model #1 and Case #52 in Model #2	81
Figure 4.16: Area-average external pressure spectrum and internal pressure spectra for Case #4 (Model #1) and #52 (Model #2) at $\theta = 0^\circ$	82
Figure 4.17: Mean, standard deviation, maximum and minimum internal pressure coefficients for Cases #13, #14 and #15	84
Figure 4.18: Area-average external pressure spectrum for LO2 and internal pressure spectra for $\theta = 0^\circ$	85
Figure 4.19: Internal and external pressure standard deviation ratio versus S^* for different opening configurations- when wind perpendicular to the opening.....	87
Figure 4.20: Peak internal and peak external pressure ratio versus S^* for different single opening configurations- when wind perpendicular to the opening.....	88
Figure 5.1: Typical cross-correlation between internal and external pressures vs lag time (τ).....	92
Figure 5.2: (a) Negative internal and negative external pressures in the building (b) Positive correlation between negative external and negative internal pressure.....	93
Figure 5.3: (a) Negative external and positive internal pressures in the building, (b) negative correlation between negative external and positive internal pressures	94
Figure 5.4: Correlation between external and internal pressure on roof cladding for $\theta = 90^\circ$ (a) Case #02, (b) Case #09, (c) Case #11, and (d) Case #12.....	96
Figure 5.5: External and internal pressure fluctuations on the roof of the nominally sealed building, for $\theta = 90^\circ$ – Case #02.....	97
Figure 5.6: Fluctuating component of external and internal pressures on the roof for Case #09 at $\theta = 90^\circ$	98
Figure 5.7: Correlation between internal and external pressure fluctuations at RP3-1 and RP3-17 for Case #09 at $\theta = 90^\circ$	99
Figure 5.8: $r_{pepi}(0)$ for RP1-1, RP3-3, and RP3-8 for wind directions 90° to 270° ; (a) Case #02, (b) Case #09, (c) Case #11, (d) Case #12.....	102
Figure 5.9: $r_{pepi}(0)$ on $Fc2$ roof cladding for $\theta = 135^\circ$ (a) Case #02-nominally sealed, (b) Case #09-LO6 open, (c) Case #11-LO5 open, and (d) Case #12-LO4 open	104
Figure 5.10: Fluctuating component of external and internal pressure at RP1-3 and RP5-13 for Case #02 at $\theta = 135^\circ$	105
Figure 5.11: Correlation between internal and external pressures at RP1-7 and RP2-1 for Case #09 at $\theta = 135^\circ$	105
Figure 5.12: Fluctuating component of internal and external pressures at RP2-1, RP4-2, RP1-3 and RP2-8 for Case #09 at $\theta = 135^\circ$	106

Figure 5.13: Fluctuating component of internal and external pressures at RP5-13, and RP6-7 for Case #09 at $\theta = 135^\circ$	107
Figure 5.14: Correlation between internal, external and net pressure time-histories of Case #09 for wind directions 90° to 135° (a) RP3-1, (b) RP3-8, and (c) RP3-16	108
Figure 5.15: Correlation between internal, external and net pressure time-histories of Case #09 for wind directions 90° to 135° (a) RP4-1, (b) RP4-8, and (c) RP4-16	109
Figure 5.16: $r_{pepi}(0)$ for selected locations on the roof purlins, RP5 and RP6 for LO1 opening (Case #04) – $\theta = 0^\circ$ to 180°	111
Figure 5.17: $r_{pepi}(0)$ for selected locations on the roof purlins, RP5 and RP6 for LO3 opening (Case #08) – $\theta = 0^\circ$ to 180°	111
Figure 5.18: Selected external pressure taps on Wall #1	112
Figure 5.19: $r_{pepi}(0)$ on WG2-1, WG2-3, WG2-8 and WG2-17 on Wall #1 for wind directions 90° to 270° (a) Case #02, (b) Case #09, and (c) Case #11	115
Figure 5.20: $r_{pepi}(0)$ on WG3-2, WG3-5, WG3-9 and WG3-12 on Wall #1 with the opening on Wall #1 for wind directions 0° to 180° for Case #04	116
Figure 5.21: $r_{pepi}(0)$ on WG1-2, WG1-5, WG1-9 and WG1-12 on Wall #3 with the opening on Wall #1 for wind directions 0° to 180° for Case #04	117
Figure 5.22: $r_{pepi}(0)$ for Cases #9 and #23 at RP1-1 and RP2-2 for $\theta = 90^\circ$ to 270° ..	118
Figure 5.23: Area-averaged $r_{pepi}(0)$ for Zone #1B for Cases #9 and #23 for $\theta = 90^\circ - 270^\circ$	118
Figure 5.24: Largest $r_{pepi}(0)$ for roof zone #1B for single opening cases LO6, LO5 and LO4 for different building volumes- $\theta = 90^\circ$ to 135°	119
Figure 5.25: Largest $r_{pepi}(0)$ for roof zone #2B for single opening cases LO6, LO5 and LO4 for different building volumes- $\theta = 90^\circ$ to 135°	120
Figure 5.26: Mean, standard deviation, maximum and minimum net pressure coefficients for Case #02 at $\theta = 90^\circ$	123
Figure 5.27: Mean, standard deviation, maximum and minimum net pressure coefficients for Case #09 at $\theta = 90^\circ$	124
Figure 5.28: Minimum net pressure coefficient at wind directions $\theta = 0^\circ - 270^\circ$ (a) Case #02, (b) Case #09, and (c) Case #11	127
Figure 5.29: Estimated and measured minimum net pressure coefficients at RP1-1 for Cases #09 and #11 for wind directions 90° to 270°	130
Figure 5.30: External, internal, and net pressures vs time with respective peaks at the RP1-1 at $\theta = 90^\circ$ for Case #09	131
Figure 5.31: Peak events with time on the RP1-1 for Case #09 at $\theta = 90^\circ$; (a) internal pressure fluctuation, (b) external pressure fluctuation, (c) net pressure fluctuation	133
Figure 5.32: Theoretical and wind tunnel data PDFs, and Histogram of peak events for Case #09, RP1-1, $\theta = 90^\circ$	134

Figure 5.33: Venn diagram for external, internal, and net peak events	134
Figure 5.34: Venn diagrams for peak events for Cases #02, #09, and #11 for RP1-1 and RP3-17 at $\theta = 90^\circ$	136
Figure 5.35: Point net pressure factors (F_{C2}) for roof cladding for Case #02 – $\theta = 90^\circ$ to 135°	139
Figure 5.36: Point net pressure factors, F_{C2} for roof cladding for Case #09 – $\theta = 90^\circ$ to 135°	140
Figure 5.37: Point net pressure factors, F_{C1} for roof cladding for Case #07 (LO2 opening) – $\theta = 225^\circ$ to 315°	141
Figure 5.38: Roof zones for the net pressure factors when wind flows $\theta 90^\circ \pm 45^\circ$ perpendicular to the opening.....	142
Figure 5.39: Point net pressure factors for Zone #1B vs S^* (a) F_{C2} for windward opening cases; (b) F_{C1} for leeward or side wall opening cases.....	143
Figure 5.40: Minimum net pressures coefficient on Wall #1 cladding when the LO6 open for $\theta = 90^\circ - 135^\circ$	145
Figure 5.41: Point net pressure factor, F_{C2} for Wall #1 for $\theta = 90^\circ - 135^\circ$	145
Figure 5.42: Maximum net pressure coefficients on Wall #2 with the opening on Wall #1 in Case #07 – $\theta = 270^\circ \pm 45^\circ$	146
Figure 5.43: External, internal and net pressure time-histories for Wall #2 (a) W2-5 for $\theta = 260^\circ$, (b) W2-1 for $\theta = 290^\circ$	147
Figure 5.44: Point net pressure factor, F_{C1} for Wall #2 when the opening on adjacent side wall for $\theta = 270^\circ \pm 45^\circ$	148
Figure 5.45: Maximum net pressure coefficient for Wall #3 with the opening on Wall #1, Case #04 for $\theta = 135^\circ - 180^\circ$	149
Figure 5.46: Minimum net pressure coefficient for Wall #3 with the opening on Wall #1, Case #04 for $\theta = 0^\circ - 45^\circ$	149
Figure 5.47: Point net pressure factor, F_{C1} for Wall #3 (windward wall) with the opening on Wall #1, Case #4, $\theta = 135^\circ - 180^\circ$	150
Figure 5.48: Point net pressure factors, F_{C2} for Wall #03(leeward wall) with the opening on Wall #1 -Case #04, $\theta = 0^\circ - 45^\circ$	150
Figure 5.49: Schematic view of the walls and roof zones on the building envelope....	151
Figure A.1: External pressure taps layout - Model #1	165
Figure A.2: Model #1-external pressure taps layout on the roof (All dimensions in millimetres).....	166
Figure A.3: Model #1-external pressure taps layout on Wall #1 and #3 (All dimensions in millimetres).....	167

Figure A.4: Model #1-external pressure taps layout on Wall #2 (All dimensions in millimetres).....	168
Figure A.5: Model #1-external pressure taps layout on Wall #4 (All dimensions in millimetres).....	168
Figure A.6: Model #2 dimensions and opening locations (All dimensions in millimetres).....	169
Figure A.7: External and internal pressure tubes are connected to Model #2	169
Figure A.8: Model #2-external pressure taps layout on the roof (All dimensions in millimetres).....	170
Figure A.9: Model #2- external pressure taps layout on Wall #1 and #3 (All dimensions in millimetres).....	171
Figure A.10: Model #2- external pressure taps layout on Wall #4 (All dimensions in millimetres).....	172
Figure A.11: Model #2- external pressure taps layout on Wall #2 (All dimensions in millimetres).....	172
Figure B.1: Eight patches on the nominally sealed building	173
Figure B.2: External pressure tap layout.....	174
Figure B.3: Area-averaged minimum external pressure coefficients for each tributary area on side wall	176
Figure B.4: Area-averaged minimum external pressure coefficients for each tributary area on the windward wall.....	177
Figure B.5: Area-averaged minimum external pressure coefficients for each tributary area on the leeward wall	179
Figure C.1: Roof zones for the net pressure factors when wind flows $90^\circ \pm 45^\circ$	181
Figure C.2: Point pressures and area-averaged pressures for Zone #1B of nominally sealed building (Case #02) (a) Minimum external pressures (b) minimum net pressures for $\theta= 90^\circ$ to 135°	182
Figure C.3: Area-averaged minimum net pressures for roof Zones 1B,2B,3B and 4B of the nominally sealed building (Case #02) for $\theta = 90^\circ$ - 135°	183
Figure C.4: Area-averaged net pressure factors (F_{C2}) for roof zones based area-averaged external and net pressures for nominally sealed building (Case #02), $\theta= 90^\circ$ to 135°	184
Figure C.5: Point pressures and area-averaged pressures for Zone #1B of a building with a large opening (Case #09) (a) Minimum external pressures (b) minimum net pressures for $\theta= 90^\circ$ to 135°	185
Figure C.6: Area-averaged minimum net pressures for roof Zones 1B,2B,3B, and 4B of a building with a large opening (Case #09) for $\theta= 90^\circ$ - 135°	186
Figure C.7: Area-averaged net pressure factors (F_{C2}) for roof zones based on area-averaged external and net pressures for building with a large opening (Case #09), $\theta= 90^\circ$ to 135°	187

LIST OF ABBREVIATIONS AND ACRONYMS

A	Area of single opening (m^2)
A_L	Combined leeward opening area (m^2)
A_o	Combined porous opening area (m^2)
A_T	Total surface area (m^2)
A_W	Combined windward opening area (m^2)
a_s	Speed of sound through air (340m/s)
C_I	Inertial coefficient
C_L	Loss coefficient of a single opening
C_{pe}	External pressure coefficient
C_{pi}	Internal pressure coefficient
$C_{p,net}$	Net pressures coefficient
$C_{\sigma p}$	Standard deviation pressure coefficient
f_C	Characteristic frequency (Hz)
f_H	Helmholtz frequency (Hz)
g	Acceleration due to gravity ($9.81 m/s^2$)
h	Mid-roof-height of the building (m)
k	Discharge coefficient of a single opening
l_e	Effective length of air-slug (m)
p	Pressure (Pa)
Q	Volumetric flow rate (m^3/s)
r_{pepi}	Correlation coefficient between external and internal pressures
Re	Reynolds number
S^*	Opening area to building volume parameter
t	Time (s)
t^*	Non-dimensional time
U	Wind velocity (m/s)
U_z	Wind velocity at reference height z (m/s)
\bar{U}_h	Mean wind velocity at the mid-roof-height (m/s)
V	Building volume (m^3)

GREEK LETTERS

Φ_1	Opening area to volume ratio
Φ_2	Inverse of Mach number
Φ_3	Reynolds number
Φ_4	Turbulence intensity
Φ_5	Mean gust length relative to opening size parameter
Φ_6	Background leakage area to large opening area ratio
ε	Porosity, porous opening area relative to total surface area
λ_u	Integral length-scale of turbulence (m)
ρ_a	Density of air (1.2 kg/m ³)
γ	Ratio of specific heats of air (1.4)
τ	Lag-time
θ	Wind direction (deg)

JOURNAL PUBLICATIONS

Bodhinayake, G.G., Ginger, J. D., & Henderson, D. J. (2020). “Correlation of internal and external pressures and net pressure factors for cladding design”, *Journal of Wind and Structures*, <https://doi.org/10.12989/was.2020.30.2.000>.

CONFERENCE PUBLICATIONS

Bodhinayake, G.G., Ginger, J. D., & Henderson, D. J. (2019). “Internal and External Pressure Fluctuations, Combination and Area Reduction Factors”, *The 15th International Conference on Wind Engineering*, China.

Bodhinayake, G.G., Ginger, J. D., & Henderson, D. J. (2018). “ Correlation of Internal and External Pressures on Building Cladding Elements”, *19th Australasian Wind Engineering Society Workshop*, Torquay, Victoria.

Bodhinayake, G.G., Ginger, J. D., & Henderson, D. J. (2018). “Net Cladding Pressures on Industrial Building Roofs”, *25th Australasian Conference on Mechanics of Structures and Materials*, Brisbane, Australia.

Bodhinayake, G.G., Ginger, J. D., & Henderson, D. J. (2017). “External and Internal Pressure Fluctuations on Industrial-Type Buildings”, *9th Asia-Pacific Conference on Wind Engineering*, Auckland, New Zealand.

1 INTRODUCTION

Engineered steel shed buildings are used for domestic, commercial, industrial and agricultural purposes. These industrial buildings such as that shown in Figure 1.1 are often open plan, and large span industrial sheds, that have steel cladding fixed to purlins and girts supported by portal frames. Industrial buildings with a large internal volume are designed and constructed using standard engineering concepts, having one or more roller doors, access doors and windows that can be vulnerable to damage in a windstorm. Damage may occur due to the high wind loads generated by a combination of external and internal pressures across the building envelope. The wind load is thus critical design action for these buildings, and such failures can be mitigated by optimising the building design using reliable internal and external pressure design data.



Figure 1.1: Typical large span industrial type building

The approach wind flow generates spatially and temporally varying external pressures around the building envelope. These external pressures are positive on the windward wall and negative on sidewalls, leeward wall, and roof. The pressure around the envelope influences the internal pressure, which depends on the airflow in and out of the openings in the building envelope. In typical nominally sealed industrial buildings, air flows through small openings or construction gaps in the envelope and generates small internal pressure fluctuations.

In strong wind conditions, a large opening can be created by an open or debris impacted door or window on the windward wall, sidewall or leeward wall. Internal pressure fluctuations depend on a spatially averaged external pressure distribution on the opening area and location of the opening (i.e., windward wall), as illustrated in Figure 1.2. When an opening is on the windward wall, these large positive internal pressures in combination with negative external pressures generate large outward net pressures on the roof, sidewall and leeward wall, as shown in Figure 1.2a. When the opening is on the sidewall or leeward wall, suction internal pressures generate large positive net pressures on the windward wall and some parts of the roof, as shown in Figure 1.2b.

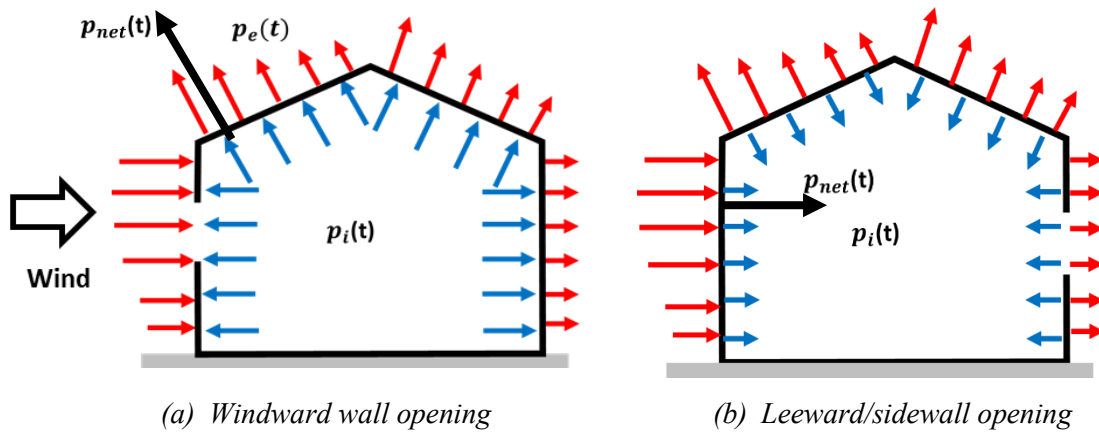


Figure 1.2: External and internal pressure distribution on the building envelope

Large net pressures generated by the combination of internal and external pressures may lead to failures in the cladding and structural system of a building. Generally, damage is caused by internal pressurisation of a building when the opening is on the windward wall. In windstorms, these large positive internal pressures can also cause catastrophic failures of the structural system of industrial buildings.

Windstorms are recognised as a common natural hazard that causes the most damage to buildings worldwide. Hurricanes Andrew (1992), Katrina (2005), Irma (2017), and Michael (2018) in the USA, and Cyclones Tracy (1975), Larry (2006), George (2007), Yasi (2011), and Debbie (2017) in Australia have caused damaged to large industrial buildings. Numerous post-windstorm damage investigations by the Cyclone Testing Station (CTS) in Australia and the Natural Hazard Engineering Research Infrastructure

(NHERI) in the USA have shown that internal pressurisation is one of the main causes leading to structural damage in these types of buildings.

Cyclone Yasi caused significant damage to industrial buildings where Figure 1.3a shows the failure of the windward wall resulted in internal pressurisation and loss of the entire roof. The combined uplift loading on the roof resulted in buckled purlins and damaged the structural system. Figure 1.3b also shows the failure of windward roller door resulting in damage to roof and wall cladding, purlins and first portal frame knee. Here, large positive internal pressure in the building contributed significantly to generate large net wind load on the windward roof edge of the building.



Figure 1.3: Structural damage to industrial buildings (a) Loss of entire roof - CTS Report TR57 (b) Windward roller door failure –Stehle and Henderson (2001)

Figure 1.4 shows damage to two steel buildings where the whole gable end wall was open during cyclone Debbie in 2017. Figure 1.4a shows deformation of the structural system (i.e. ridgeline and lintel over the opening) due to the internal pressurisation when the wind flowed towards the large windward opening of the building. Figure 1.4(b) shows damage to the windward gable end wall cladding when the leeward wall was completely open. This failure may have occurred as a result of the combination of large positive external and negative internal pressure on the windward wall. Damage shown in Figures 1.4a and 1.4b is caused by conditions described in Figures 1.2a and 1.2b, respectively.

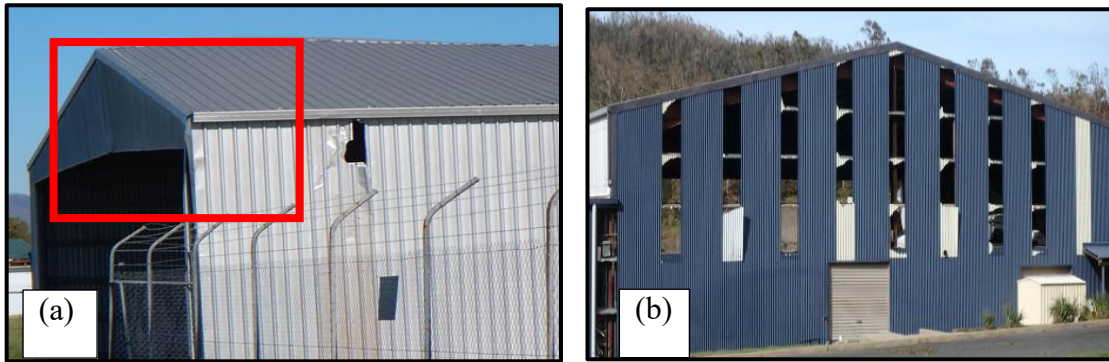


Figure 1.4: Structural damage observed after Cyclone Debbie, 2017

The design internal pressure data provided in wind loading standards (i.e. AS/NZS 1170.2) are based on quasi-static analysis and mean pressure data from wind tunnel model-scale studies. Designers have to choose the appropriate internal pressure data from wind-loading standards based on assumed possible opening sizes on the envelope. When designing, they may use conservative or uncertain internal pressure data because of a lack of understanding or a limited range of internal pressure data in these standards. Selection of unconservative internal pressure data may lead to cladding and structural component failures. A better assessment of the internal pressure fluctuations can therefore improve the structural design of these buildings.

Large internal pressure fluctuations can contribute to a significant portion of the net wind loads on a building. Internal pressure studies have been conducted in model-scale wind tunnel experiments, full-scale tests and analytical model since the early 1970s. Detailed model-scale studies conducted by Liu (1975), Holmes (1979), Stathopoulos et al. (1979), and Vickery (1986) derived the fundamental theories on internal pressure fluctuations in nominally sealed buildings and buildings with large openings. Further wind tunnel studies conducted by Harris (1990), Oh et al. (2007), Sharma et al. (2003), Guha et al. (2011a and b), Kim et al. (2013), and Xu et al. (2014 and 2017) assessed the effect of sizes and locations of openings and porosity in the envelope, and flexibility, the volume of the building, and external pressure fluctuations at the openings have on internal pressure fluctuations.

Furthermore, net pressures depend on the correlation between internal and external pressure fluctuations. Limited studies have been conducted on the correlation between internal and external pressures on the building envelope. Beste et al. (1997) and Sharma

and Richards (2005) studied the combination of external and internal pressures in model-scale studies. Both studies obtained the highest correlation coefficient of about -0.6 between internal and external pressures at the leading roof edge when the building has an opening on the windward wall. Sharma and Richards (2005) also found that the peak net pressures are smaller than the magnitude of the difference between peak external and peak internal pressures since the peak external and peak internal pressures do not occur at the same time. In wind loading standards, a combination factor (i.e., K_C) is defined to account for the lack of correlation between internal and external pressures to reduce the net pressures on the building envelope. Thus, improvement of the assessment of the correlation between internal and external pressures will enable combination factors to be specified based on different building configurations for different roof and wall areas for the optimal building design.

This thesis focuses on the correlation between internal and external pressure fluctuations and the relationship between correlation coefficients on different areas on the roof and walls of a range of building with a range of large openings and background leakages, and building volumes. The analysis of internal and external pressure characteristics from this wind tunnel study will further provide data for assessing the net pressures fluctuations on different parts of the building envelope. In addition, the effect of the correlation coefficient on net pressure fluctuations on different parts of the roof and wall cladding will be studied. This thesis further analyses the occurrence of peak net pressures relative to the peak external and internal pressures, and defines a range of net pressure factors to quantify the reduction in the peak net pressures.

1.1 Objectives

This study characterises the wind-induced internal pressure fluctuations and analyses the net pressures that generate peak wind loads on a range of industrial-type building configurations, a range of large openings and porosities in the envelope and building volumes.

This thesis assesses the hypothesis of the coincidence of peak internal pressure with the peak external suction pressure causing large net design pressures on the roof and walls of buildings.

The main objective is to quantify the correlation between internal and external pressure fluctuations to analyse the peak net pressures in terms of peak external and peak internal

pressures on the different parts of the building envelope. This is achieved by undertaking a wind tunnel model-scale study to:

- i. Measure external and internal pressure fluctuations in a building with a range of opening configurations (single or multiple), building volumes, and building porosity. Analyse the internal and net pressure fluctuations with respect to the opening area to building volume ratio.
- ii. Determine the relationship between the correlation coefficients, peak net pressure coefficients by analysing the occurrence of peak external and peak internal pressures and their contributions to producing peak net pressure.
- iii. Define the net pressure factors for different parts of the roof and walls cladding, and structural elements of the building.

The internal and net pressures obtained from this study will enable the optimal design of these type of buildings by providing the relationship between correlation coefficients and peak net pressure coefficients. In addition, the outcomes will produce relevant data for wind loading design guidelines.

1.2 Thesis Structure

Chapter 2 presents a review of the previous research on internal and net pressure. The Chapter includes a detailed study of the relevant parameters influencing internal pressure fluctuations and discusses their importance for the current study.

Chapter 3 describes the building model configurations and the experimental setup in the boundary layer wind tunnel. Further, analytical methods and numerical equations are presented along with the details of the wind tunnel tests.

Chapter 4 presents the external pressure variations around the building, and the internal pressure fluctuations in each building configuration based on the opening sizes and locations, building porosity, and building volume.

Chapter 5 presents the correlation between external and internal pressures on different parts of the building envelope and discusses the effect of the size of the opening on the correlations. The analysis also describes the external and internal pressure peak events, which generates peak net pressure on the envelope. In addition, Chapter 5 provides net pressure factors for different roof and wall areas as a function of opening area to building volume ratio.

Chapter 6 provides the conclusion of this research and recommendation for further research.

2 LITERATURE REVIEW AND THEORY

Chapter 2 introduces the theory and past/previous research conducted on internal pressure fluctuations in a building. This includes the internal and external pressure fluctuations that are imposed on the building envelope, and their characteristics for buildings with different sizes and locations of openings and background leakage in the envelope, and volumes.

2.1 External pressure fluctuations on buildings

The approach wind flow produces spatially and temporally varying external pressures around buildings. The external pressure fluctuations are an important parameter that influences internal pressure fluctuations in a building. Many studies on bluff-body aerodynamics have discussed the spatial and temporal variation of external pressures around buildings. Holmes (1979) described the wind flow around a low-rise building, as shown in Figure 2.1, which shows flow separation at the windward roof edge and reattachment at a further downwind region on the roof. High suction and high turbulence occur in the separation bubble, while lower turbulence develops in the reattachment zone, and the windward wall experiences positive pressures.

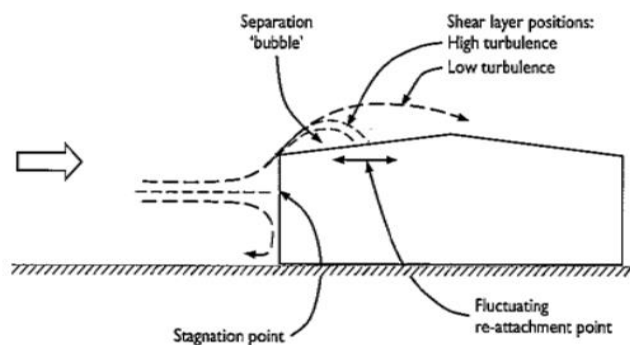


Figure 2.1: Wind flow around the low-rise building (page-180; Holmes, 2007)

External pressure fluctuations are different for the building's roof and wall areas. Figure 2.2 illustrates the time-varying spatially varying distribution of wind pressures by showing the instantaneous distribution of pressures at 3 different times in the same wind flow and approximate design pressures in wind codes (Holmes and Syme, 1994). Here, positive pressures are applied towards the surface of the windward wall, and negative pressures occur on the roof, sidewalls, and leeward wall, which act away from the surface. At the windward roof edge experiences high negative pressures because of flow separation (i.e., separation bubble) and the roll-up of vortices, and the lower negative pressures occur in the attached flow region. A similar external pressure variation is observed on the sidewall in different magnitudes. Smaller suction pressures are experienced on the leeward wall in the wake regions behind the building.

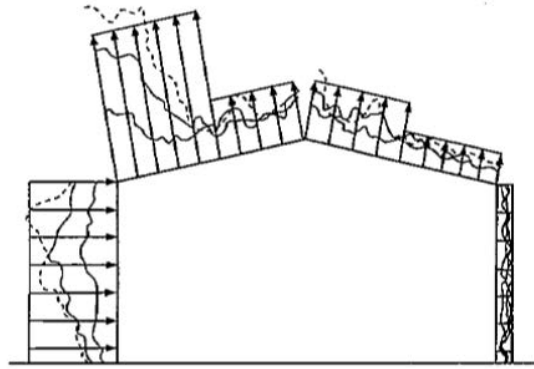


Figure 2.2: External pressure distribution on low rise building-(Holmes and Syme, 1994)

The time-varying pressure, $p(t)$ on the building surface depends on the time-varying wind speed $U(t)$ of the approaching wind flow which is a combination of the steady (i.e., mean) component and the fluctuating (i.e., turbulent) component, $U(t) = \bar{U} + U'(t)$, respectively. The time-varying pressures are converted to pressure coefficients, $C_p(t) = p(t)/(0.5\rho_a\bar{U}_h^2)$, where ρ_a is the density of air and \bar{U}_h is the mean wind speed at the reference roof height, respectively. Accordingly, mean, standard deviation, maximum and minimum pressure coefficients over an observation period are described as;

$$C_{\bar{p}} = \frac{\bar{p}(t)}{(1/2)\rho_a\bar{U}_h^2}; C_{\sigma_p} = \frac{\sigma_p(t)}{(1/2)\rho_a\bar{U}_h^2}; C_{\hat{p}} = \frac{\hat{p}(t)}{(1/2)\rho_a\bar{U}_h^2}; C_{\check{p}}(t) = \frac{\check{p}(t)}{(1/2)\rho_a\bar{U}_h^2}$$

2.1.1 Area-averaged external pressures

External pressure is temporally and spatially varying on the walls and roof surfaces and produces lower peak area-averaged external pressure as the area increases. Davenport et al. (1977), Holmes and Best (1981), Roy and Holmes (1981), Kim and Metha (1997), Kopp and Morrison (2011) studied the linearly averaged pressures over the tributary area to define the area-averaged external pressures. Area reduction factors (i.e., K_a) are given in wind loading standards for a reduction in peak wind loads on large areas on roof and walls. AS/NZS 1170.2,2011 specifies three reduction factor values, as shown in Table 2.1. ASCE 7-16 gives continuous function of load with an area for Components and Cladding (C&C) loading, which varies from 0.6 to 1.0. For flat roof buildings, loading curve D ($K_a \sim 0.7- 1.0$) is applicable for roof cladding, while loading curve C ($K_a \sim 0.8 - 1.0$) and E ($K_a \sim 0.6 -1.0$) are applicable for wall cladding (Table 30.6.2, ASCE 7-16). The area reduction factor reduces with the increasing tributary area. However, area reduction factors are not specified for windward and leeward walls. This thesis will review the area reduction factors given in wind loading standards for roof and sidewalls, and provide area reduction factors for the windward wall and leeward wall of a building.

Table 2.1: Area reduction factors (K_a) in AS/NZS 1170.2, 2011

Tributary area,(m²)	K_a
≤ 10	1.0
25	0.9
≥ 100	0.8

2.2 Internal pressure fluctuations

Internal pressure studies have been conducted since the 1960s, but have received less attention than external pressure fluctuations. Model-scale and full-scale studies have characterised the internal pressure fluctuations, which are dependent on the external pressure fluctuations, size and location of the openings and porosity in the envelope, and building volume. The unsteady discharge equation, flow continuity, and Bernoulli equation are used to describe the airflow through openings and internal pressure fluctuations in a nominally sealed building and building with a large opening.

2.2.1 Characteristics of wind flow-through openings

The approaching wind enters and exits the building through openings in the envelope and influences the internal pressure fluctuations, which can be large or small depending on the pressure difference between external and internal pressures and size of openings. The unsteady flow through an opening, $Q(t)$ is dependent on the pressure difference, $\Delta p(t)$, across the opening in terms of flow, and opening area A as described in the unsteady discharged equation given in Equation 2.1. The first and second components of the right-hand side of the equation represent the damping and inertial terms respectively, where the C_L is the loss coefficient, and C_I is the inertial coefficient. $U_o(t) = Q(t)/A$, is the area-averaged flow velocity through the opening of area A , and $\partial U_o(t)/\partial t$ is the acceleration through the opening. Vickery and Bloxham(1992) noted that the inertial and loss coefficients could be theoretically determined from potential flow theory, where the flow passes through an opening between two large volumes.

$$\Delta p(t) = \frac{1}{2} C_L \rho_a (U_o(t))^2 + C_I \rho_a \frac{\partial U_o(t)}{\partial t} \sqrt{A} \quad (2.1)$$

When a building contains multiple openings as shown in Figure 2.3, the continuity equation shows that mean inflow (Q_{in}) equals to the mean outflow (Q_{out}) through the multiple openings ($\sum Q_{in} = \sum Q_{out}$). Internal pressure fluctuations in these buildings depend on the inflow and outflow through openings. The mean internal pressure ($C_{\bar{p}i}$) can be derived from combining the unsteady discharge equation and flow continuity, as explained by Liu (1978), in Equation 2.2. Here, A_W , is the total windward open area, A_L is the total leeward open area, $C_{\bar{p}eW}$ and $C_{\bar{p}eL}$ are the area-averaged mean external pressures on the windward openings and leeward openings, respectively.

Equation 2.2 is applied in many codes and standards to find a corresponding $C_{\bar{p}i}$ value for a given A_W/A_L ratio. When the building contains only a windward opening (i.e. total leeward wall area, $A_L=0$) Equation 2.2 simplifies to $C_{\bar{p}i} = C_{\bar{p}eW}$. When there are only leeward openings ($A_W = 0$), $C_{\bar{p}i} = C_{\bar{p}eL}$. Accordingly, $C_{\bar{p}i}$ varies between $C_{\bar{p}eW}$ and $C_{\bar{p}eL}$ for all other A_L/A_W ratios.

$$C_{\bar{p}i} = \frac{C_{\bar{p}eW}}{1 + (A_L/A_W)^2} + \frac{C_{\bar{p}eL}}{1 + (A_W/A_L)^2} \quad (2.2)$$

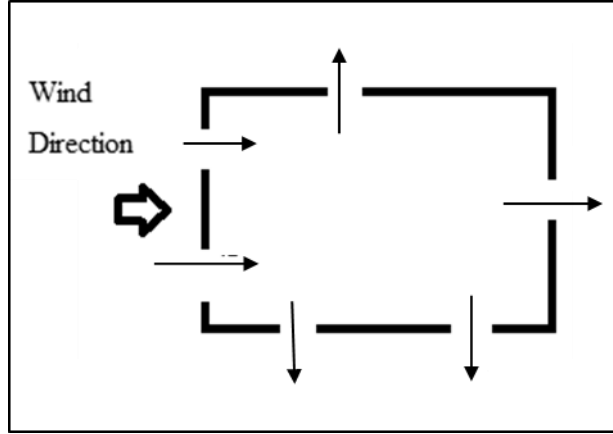


Figure 2.3: Inflows and outflows of the multiple openings

2.2.2 Internal pressure in a nominally sealed building

A building with only small openings or construction gaps in the envelope (typically known as background leakage or porosity) is referred to as a nominally sealed building. Model-scale and full-scale studies have revealed small internal pressure fluctuations resulting from a small amount of airflow through these openings. Vickery (1986, 1994) and Harris (1990) studied internal pressure fluctuations in these buildings using the relationship of wind flow through windward and leeward walls by combining the unsteady discharge equation with mass conservation. Equation 2.3 was developed by simplifying the flow through porous openings into two groups, the flow into the building as windward openings, A_W and the flow out from the building as leeward openings, A_L . Here C_{LW} is the loss coefficient of the windward openings, C_{LL} is the loss coefficient of the leeward openings, a_s is the speed of sound, and V is the volume of the building.

$$\frac{A_W}{\sqrt{C_{LW}}} \sqrt{2\rho_a(p_w - p_i)} - \frac{A_L}{\sqrt{C_{LL}}} \sqrt{2\rho_a(p_i - p_L)} = \frac{V}{a_s^2} \frac{dp_i}{dt} \quad (2.3)$$

Vickery (1986) also reported that the flow through small openings is laminar and unsteady, and the inertial effect is small, which produces a significant reduction in internal pressure fluctuations. Vickery (1986) defined the characteristic frequency, f_c , of the building as given in Equation 2.4 and discovered that the external pressure fluctuations above f_c are increasingly attenuated. Considering the unsteady flow through multiple leakage paths simultaneously, Oh et al. (2004, 2007) used multiple discharge equations (MDE) proposed by Vickery (1986) and demonstrated that internal pressure fluctuations in a nominally sealed building are of smaller magnitude than the external pressure fluctuations. Figure 2.4 displays the power spectral densities of measured and simulated internal pressure $C_{pi}(exp)$ and $C_{pi}(MDE)$ that are much smaller than the external pressures on windward, leeward and sidewalls. In another study, Yu et al. (2008) proved the internal pressure fluctuations contain much less energy and found a sharp drop-off compared with external pressure fluctuations across the range of frequencies.

$$f_c = \frac{1}{2\pi} \left(\frac{a_s(A_W^2 + A_L^2)^{3/2}}{V_o \bar{U}_h A_W A_L C_L \sqrt{C_{pW} - C_{pL}}} \right) \quad (2.4)$$

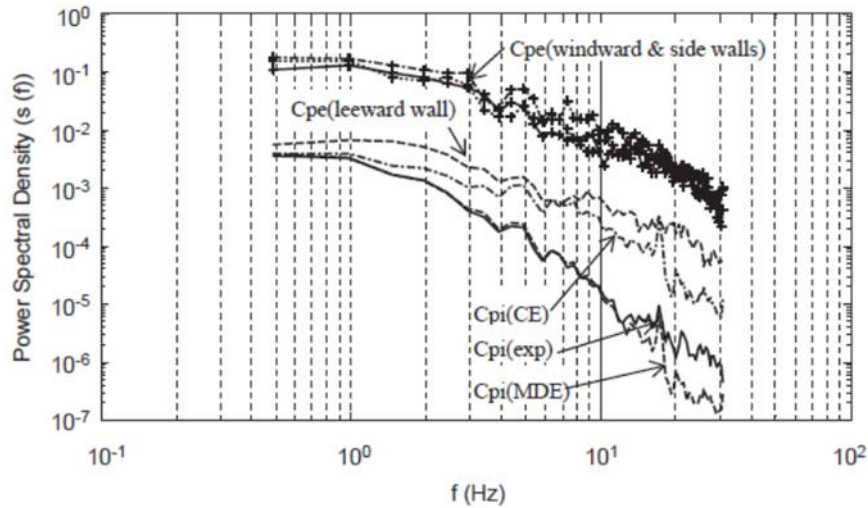


Figure 2.4: Spectra of the internal and external pressures for the building with background leakage– Oh et al. [2007]

Ginger et al. (1997) conducted a full-scale study of the nominally sealed WERFL test building shown in Figure 2.5 and validated model scale studies by demonstrating that the internal pressure fluctuations are significantly smaller than external pressure fluctuations.

The measured mean and peak internal pressure coefficients in the nominally sealed WERFL test building were -0.14 and -0.38, respectively. In contrast, the peak positive pressure coefficient on the windward wall was +2.76, and the peak negative external pressures coefficients on the sidewall, roof and leeward wall were -1.95, -1.72, and -0.85 respectively. Further, assuming uniform porosity around the nominally sealed WERFL building, Ginger et al. (1997) obtained the characteristic frequency, $f_c \cong 0.54$ Hz.

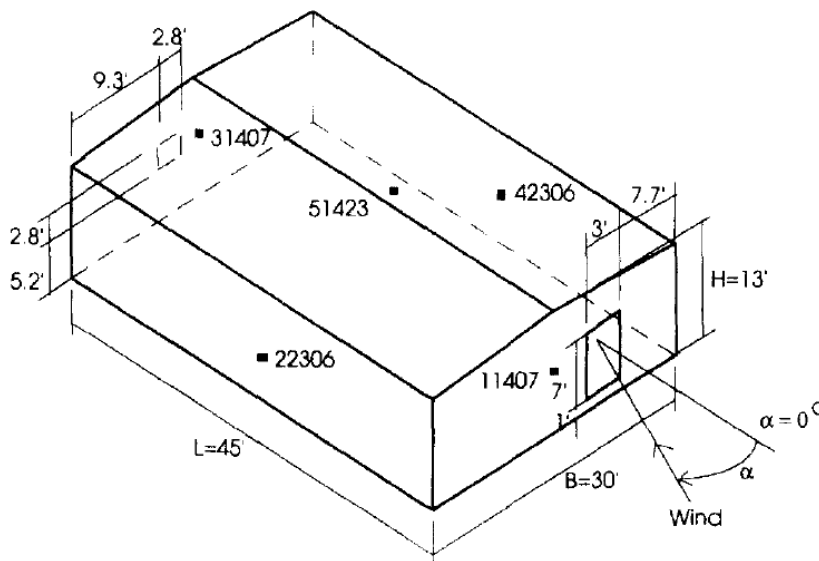


Figure 2.5: Wind Engineering Research Field Laboratory (WERFL) full scale low rise test building (dimensions in ft; 1ft =0.305m)- Ginger et al.(1997)

2.2.3 Internal pressure in a building with a large opening

Strong winds or windborne debris can damage the envelope of a building and create a large opening, produce large internal pressure fluctuations. An opening on the windward wall generates positive internal pressures while an opening on the leeward or sidewall produces negative internal pressures inside the building. Model-scale and full-scale tests have investigated the wind-induced internal pressure in buildings with various opening configurations. Liu (1975 and 1981), Holmes (1979), and Vickery (1986) derived the fundamental equations on internal pressure fluctuations in model scale and theoretical studies.

Figure 2.6 shows the wind tunnel model used by Holmes (1979) to describe the air oscillation in and out through an opening similar to a Helmholtz resonator. He described the amplification of internal pressure fluctuations compared to the external pressure fluctuations when a building has a large windward opening. Holmes (1979) considered the internal pressure dynamic response as a simple mass-spring-damper system and used a fundamental second-order differential equation to derive Equation 2.5. Here, A is the opening area, V is the volume of the building, a_s is the speed of sound, C_L loss coefficient, C_I inertial coefficient and $\dot{C}_{pi}(t)$ and $\ddot{C}_{pi}(t)$ are the first and second derivatives of $C_{pi}(t)$ with respect to time, t . Liu and Saathoff (1981) derived an equation similar to Equation 2.5 with an additional term of the orifice contraction coefficient. Vickery (1986) derived an identical equation to Holmes (1979) by applying unsteady flow theory.

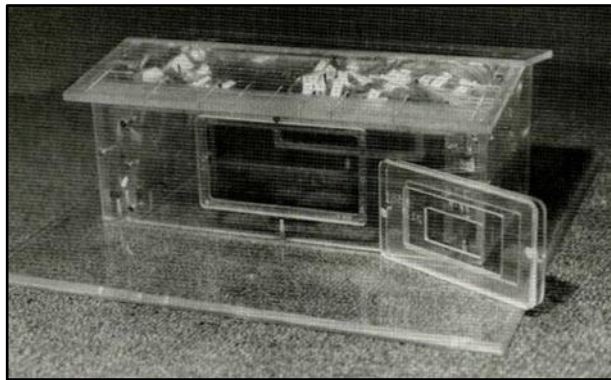


Figure 2.6: Experimental wind tunnel model used by Holmes (1979)

$$\frac{C_I V}{a_s^2 \sqrt{A}} \ddot{C}_{pi}(t) + C_L \left(\frac{V \bar{U}_h}{2 a_s^2 A} \right)^2 \dot{C}_{pi}(t) |\dot{C}_{pi}(t)| + C_{pi}(t) = C_{pe}(t) \quad (2.5)$$

Holmes (1979) showed that internal pressure resonance occurs at the undamped Helmholtz frequency (f_H) given in Equation 2.6, for a range of dominant windward and leeward openings. He further suggested that internal pressure resonance depends on the

opening area to building volume ratio, and it occurs at higher frequencies as the opening area increases, relative to the building volume.

$$f_H = \frac{1}{2\pi} \sqrt{\frac{a_s^2 \sqrt{A}}{C_I V}} \quad (2.6)$$

The inertial coefficient, C_I , can be calculated from the measured Helmholtz frequency using Equation 2.6 from model-scale and full-scale experiments. Holmes (1980), Liu and Rhee (1986) and Vickery (1991) have applied an inertial coefficient of 0.89. However, literature shows that the inertial coefficient is not constant and depends on the shape and size of the opening. Vickery and Bloxham (1992), Sharma (1996), Sharma and Richards (1997), Ginger et al. (2010), and Humphreys (2019) have derived a range of inertial coefficients from 0.89 to 3, based on Helmholtz frequency measurements in model-scale and full-scale studies.

In the full-scale study on the WERFL test building (Figure 2.5), Ginger et al. (1997) discussed the internal pressure fluctuations when the building has a 2% windward wall opening. They found an increase in internal pressure energy close to the Helmholtz frequency of 1.58 Hz, as shown in Figure 2.7. Ginger et al. (1997) also found a similar increase in the building's internal pressure energy with 1% windward opening at 1.34 Hz and the 5% windward opening at 2.0 Hz. In other full-scale studies, Humphreys et al. (2019) showed similar variations in internal pressure energy in a building with a single dominant opening and identified that damping of the internal pressure increases as the size of the opening decreases. Humphreys et al. (2019) showed that porosity in the building envelope also decreases internal pressure energy and attenuates the Helmholtz resonance.

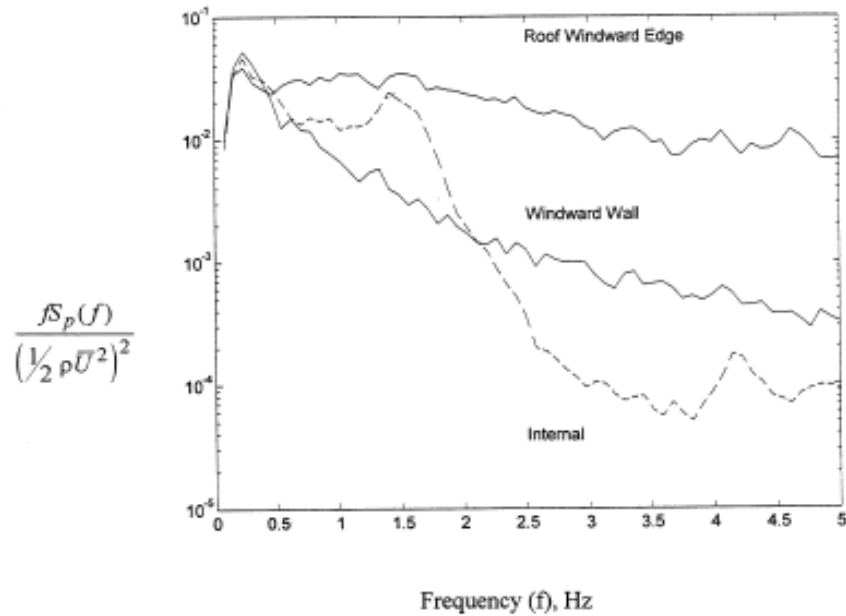


Figure 2.7: Windward wall, roof windward edge and internal pressure spectra for building with 2% windward wall opening (Ginger et al., 1997)

Woods and Blackmore (1995) conducted a series of wind tunnel tests for five opening areas to wall area ratios, 25%, 16%, 9%, 4% and 1% on a 1:200 length scale model. They demonstrated that the mean internal pressure tends to follow the area-averaged external pressure at the opening and observed differences between mean internal and external pressures when the opening is in a transition region between the separated and attached flow.

2.2.4 Internal pressure in a building with multiple openings

In industrial buildings, it is quite common to have two or more roller doors on the same wall. The influence of multiple openings on internal pressure fluctuations has been studied by Guha et al. (2012) in a 1:100 scale wind tunnel model shown in Figure 2.8. They considered single windward openings and multiple openings equal in size to the single opening area on the same wall.

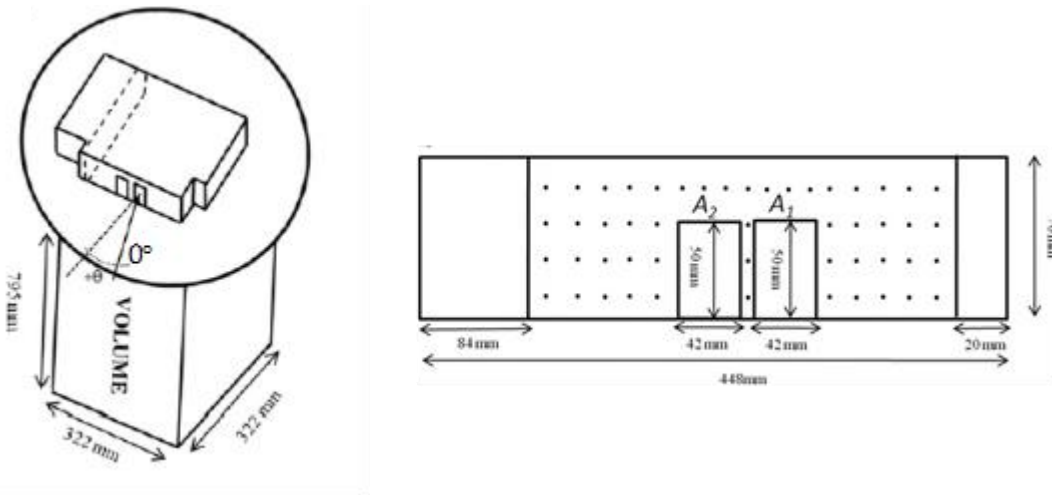


Figure 2.8: Wind tunnel model with openings - 1: 100 scale (Guha et al.-2012)

Guha et al. (2012) summarised the results of Helmholtz frequency, mean, and maximum internal pressure coefficients for different opening configurations, as shown in Table 2.2. The mean and peak internal pressure coefficients are obtained from the measurements of internal pressure data sampled at 600 Hz for 2 min for each angle of attack yielding 72,000 samples. Comparison between single opening configurations, A1, A2, and two opening configurations, C1 and C2, of the same opening area indicate that the single opening configurations produce higher peak internal pressures. This is due to the reduced correlation between airflows at the two openings compared to a single opening. For normal or near-normal wind flows (i.e., $0 \pm 20^\circ$), the peak internal pressure coefficient for multiple openings A1 and A2 (i.e., D) is found to be slightly lower compared to the single opening configuration A1, and almost equal to that of A2. For wind angles within $\pm 30^\circ$, the peak internal pressure coefficients for D are much higher than the single opening configurations A1 and A2. Helmholtz resonance was observed for opening these cases; it occurred at higher frequencies with increasing opening area. This thesis considers the variation of f_H with a single opening vs multiple openings in different locations on the same wall.

Table 2.2: Measured Helmholtz frequency, mean and peak internal pressures for opening configurations for $\theta = 0^\circ$ (Guha et al. (2012))

Configuration ID	Opening Size (mm × mm)	Measured		
		f_H (Hz)	\bar{C}_{pi}	\hat{C}_{pi}
A1	50 × 42	33.8	0.61	1.67
A2	50 × 42	34.3	0.59	1.64
B1 = (A2 & 0.5A1)	50 × 42 , 25 × 42	41.6	0.57	1.48
B2 = (0.5A2 & A1)	50 × 42 , 25 × 42	42.7	0.61	1.59
C1= (0.5A2 & 0.5A1) bottom halves	25 × 42 , 25 × 42	37.4	0.54	1.37
C2 = (0.5A2 & 0.5A1) top halves	25 × 42 , 25 × 42	39.1	0.57	1.49
D = (A2 & A1)	50 × 42 , 50 × 42	46.3	0.61	1.63

2.2.5 Internal pressure in a building with openings and background leakage

Stathopoulos et al. (1979), Vickery and Bloxham (1992), Oh et al. (2007), Yu et al. (2008), Guha et al. (2011, 2013a and b), Kim and Ginger (2013), and other researchers have shown that the background leakage reduces the internal pressures in a building with a dominant opening. The total background leakage area is considered as the total opening area on the wall while the porosity of the wall is calculated as the ratio between total background leakage area to the total wall area.

Stathopoulos et al. (1979) performed model-scale wind tunnel studies on a building with uniform porosities (0%, 0.5% and 3.0%) on the walls. He stated that the internal pressure coefficients in building with a large opening are not affected by the background leakage when the opening size is more than 20% of the total wall area. Vickery and Bloxham (1992) found that the effect of background leakage on internal pressure fluctuations are

minor if the porous area is less than 10% of the windward dominant opening area ($A_L/A_W < 10\%$).

Ignoring the background leakage, Oh et al. (2007) predicted much higher values of the fluctuating internal pressures, indicating that the background leakage plays an important role in determining the internal pressures. Oh et al. (2007) theoretically predicted and experimentally observed the Helmholtz resonance in a building with a dominant opening and background leakage. Further, their experiment and predictions illustrated that the background leakage attenuates the total fluctuating energy of the internal pressures when a porosity ratio reaches 70% of the dominant opening area. Yu et al. (2008) and Guha et al. (2011a, 2012) introduced an additional damping term to Equation 2.5 to determine the internal pressure in a building with background leakage. Using this theoretical method, Guha et al. (2011a) satisfactorily estimated the damping effect in a model-scale building with porosity.

2.2.6 Internal pressure provisions in wind loading standards

Internal pressures coefficients in wind loading codes and standards are defined using a quasi-steady approximation. This thesis is concerned with the internal pressure coefficients in two primary wind loading standards, AS/NZS 1170.2, 2011, and ASCE07-16 (2018).

In AS/NZS 1170.2, 2011, the internal pressure coefficients (C_{pi}) are classified based on envelope permeability (a ratio of total open area to total surface area) and wind directions. When permeability is less than 0.5%, buildings are defined as nominally sealed buildings, and internal pressures coefficients vary within a range of -0.3 and 0 (Table 5.1 (A), AS/NZS 1170.2). When the permeability is more than 0.5%, buildings are deemed to have large openings, and internal pressure coefficients are defined as a fraction of the wall's external pressure coefficient at the location of the opening (Table 5.1 (B), AS/NZS 1170.2). For example, when the windward opening area is higher than 6 times the total of other opening areas, the mean internal pressure coefficient is +0.7. When the opening is on side wall near the leading edge, mean internal pressure is -0.65, which is the mean external pressure.

In ASCE 7-16 (2018), the internal pressure coefficient (GC_{pi}) is based on the enclosure classification of enclosed, partially enclosed, or open. The highest internal pressure coefficient of ± 0.55 (i.e. equivalent to $\pm 0.55/0.85 = \pm 0.65$ in AS/NZS 1170.2) is given

for partially enclosed buildings, while the lowest GC_{pi} of 0 is for open buildings if each wall is at least 80% open. For enclosed buildings and partially enclosed buildings, the lowest internal pressure coefficient of ± 0.18 (i.e. equivalent to $\pm 0.18/0.85 = \pm 0.21$ in AS/NZS 1170.2) is applicable for building design. Selecting the internal pressure coefficient is more simplified for designers since a single pressure coefficient applies to any approach wind direction ($0^\circ - 360^\circ$).

Designers are responsible for selecting the appropriate internal pressure coefficients provided in wind loading standards. Sometimes designers need to estimate the internal pressure coefficients if the code or standard does not cover the desired building enclosure or configuration. Accordingly, there is a limitation of internal pressure data for industrial type buildings when considering some unique building characteristics such as large volume, porosity, and the size of possible openings. In this thesis, internal pressure fluctuations in open-plan industrial buildings are analysed for different single and multiple openings, building volume, and porosity, and the results non-dimensionally compared for different building configurations.

2.3 Dimensional analysis

Internal pressure fluctuations in a building with a dominant opening were represented as a function of five non-dimensional parameters by Holmes (1979); $\Phi_1 = A^{3/2}/V$, $\Phi_2 = a_s/\bar{U}_h$, $\Phi_3 = \rho_a \bar{U}_h \sqrt{A}/\mu$, $\Phi_4 = \sigma_u/\bar{U}_h$, and $\Phi_5 = \lambda_u/\sqrt{A}$, where λ_u is the integral length scale of turbulence, μ is viscosity of air, and Φ_4 is turbulence intensity of the flow. These parameters were applied to Equation 2.5 with a non-dimensional time $t^* = t\bar{U}_h/\lambda_u$ to produce Equation 2.7.

$$C_l \frac{1}{\Phi_1 \Phi_2^2 \Phi_5^2} \frac{d^2 C_{pi}}{dt^{*2}} + \left(\frac{C_L}{4}\right) \left(\frac{1}{\Phi_1 \Phi_2^2 \Phi_5}\right)^2 \frac{dC_{pi}}{dt^*} \left| \frac{dC_{pi}}{dt^*} \right| + C_{pi} = C_{pe} \quad (2.7)$$

Ginger et al. (2008) defined the non-dimensional parameter, $S^* = (A^{3/2}/V) \times (a_s/\bar{U}_h)^2$, which is the product of $\Phi_1 \Phi_2^2$, and modified Equation 2.7 by substituting S^* . Vickery and Bloxham (1992), Irwin and Dunn (1994), Yu et al. (2006), Kim and Ginger (2013), and Sharma (2013) discussed the ratio between peak internal and peak external

pressure at the opening area, (\hat{p}_i / \hat{p}_e) , and the ratio of the standard deviation of internal to external pressures at the opening, $(\sigma_{pi}/\sigma_{pe})$ as a function of a non-dimensional parameter similar to that introduced by Ginger et al. (2008).

Figure 2.9 (a) and (b) show the \hat{p}_i/\hat{p}_e and σ_{pi}/σ_{pe} for different opening areas ($\Phi_5 = 4.7, 6, 8.5$ and 15) as a function of S^* by Ginger et al. (2010). Figure 2.9 (b) shows the effect of the opening area to volume ratio where internal pressure fluctuations \hat{p}_i/\hat{p}_e increases with increasing S^* . Further, internal pressure fluctuations for a larger opening (i.e. $\Phi_5 = 15$) are less than the external pressure fluctuations for a small S^* (< 0.4), as shown in Figure 2.9 (a). The internal pressure fluctuations tend to exceed the external pressure fluctuations when the S^* exceeds 1.0.

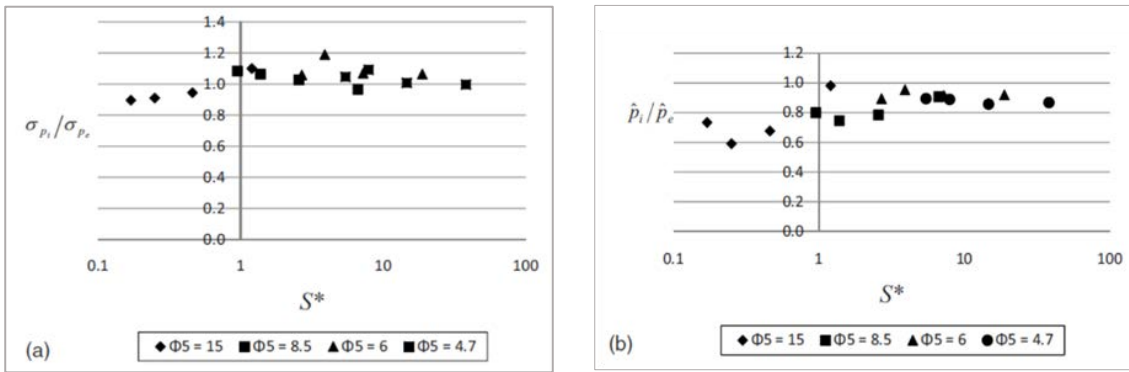


Figure 2.9: a) measured standard deviation pressure ratio versus S^* b) measured peak pressure ratio versus S^* (Ginger et al.,2010)

Holmes and Ginger (2012) reviewed the internal pressure fluctuations in a building with a dominant windward opening and discussed Vickery and Bloxham (1992) formula and Irwin and Dunn (1994) formula for σ_{pi}/σ_{pe} . They compared the experimental results obtained by Holmes (1979), Liu and Rhee (1986), Vickery and Bloxham (1992), Sharma and Richards (2003), Ginger et al. (2008) and Ginger et al. (2010) as presented in Figure 2.10 and introduced two empirical formulas (Equation 2.8 and 2.9).

$$\frac{\sigma_{pi}}{\sigma_{pe}} = 1.1 \quad \text{for } S^* \geq 1.0 \quad (2.8)$$

$$\frac{\sigma_{pi}}{\sigma_{pe}} = 1.1 + 0.2 \log_{10} S^* \quad \text{for } 0.1 < S^* < 1.0 \quad (2.9)$$

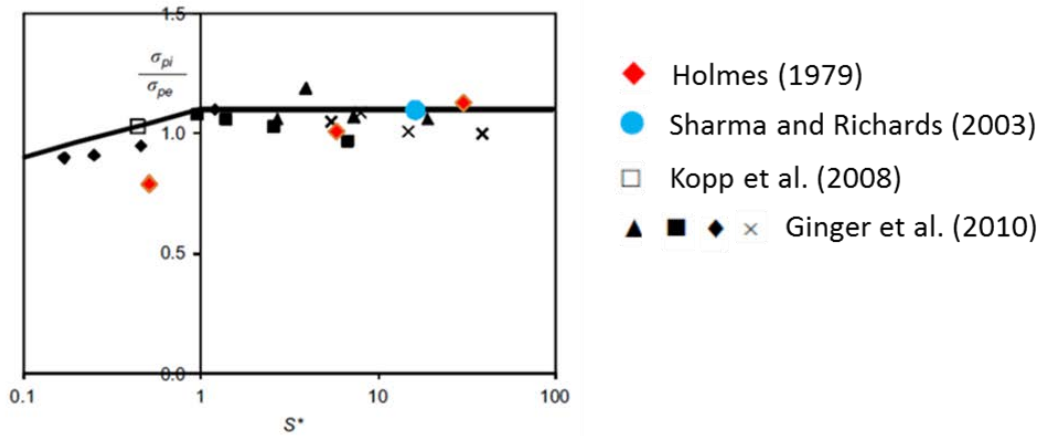


Figure 2.10: Measured standard deviation pressure ratio versus S^* (Holmes and Ginger, 2012)

Furthermore, Xu et al. (2017) compared the ratio of the standard deviation of internal and external pressure variation with C_L for different opening sizes (i.e., S^*) in Figure 2.11a and different internal volumes (i.e., S^*) in Figure 2.11b. Large internal pressure fluctuations were identified for small loss coefficients, and internal pressure fluctuation decreased with an increasing loss coefficient from 1 to 100. In addition, $\sigma_{cpi}/\sigma_{cpe}$ significantly decreased when S^* decreases (i.e., decreasing opening areas with a constant volume, and increasing internal volume with a fixed opening area). They also introduced two empirical formulas to describe the variation of loss coefficient with S^* as shown in Equation 2.10 and 2.11.

$$C_L = \frac{1}{\left(0.15 \log\left(\frac{30}{S^*}\right) + 0.07\right)^2} \quad \text{for } S^* \leq 30 \quad (2.10)$$

$$C_L = \frac{1}{0.07^2} \quad \text{for } S^* > 30 \quad (2.11)$$

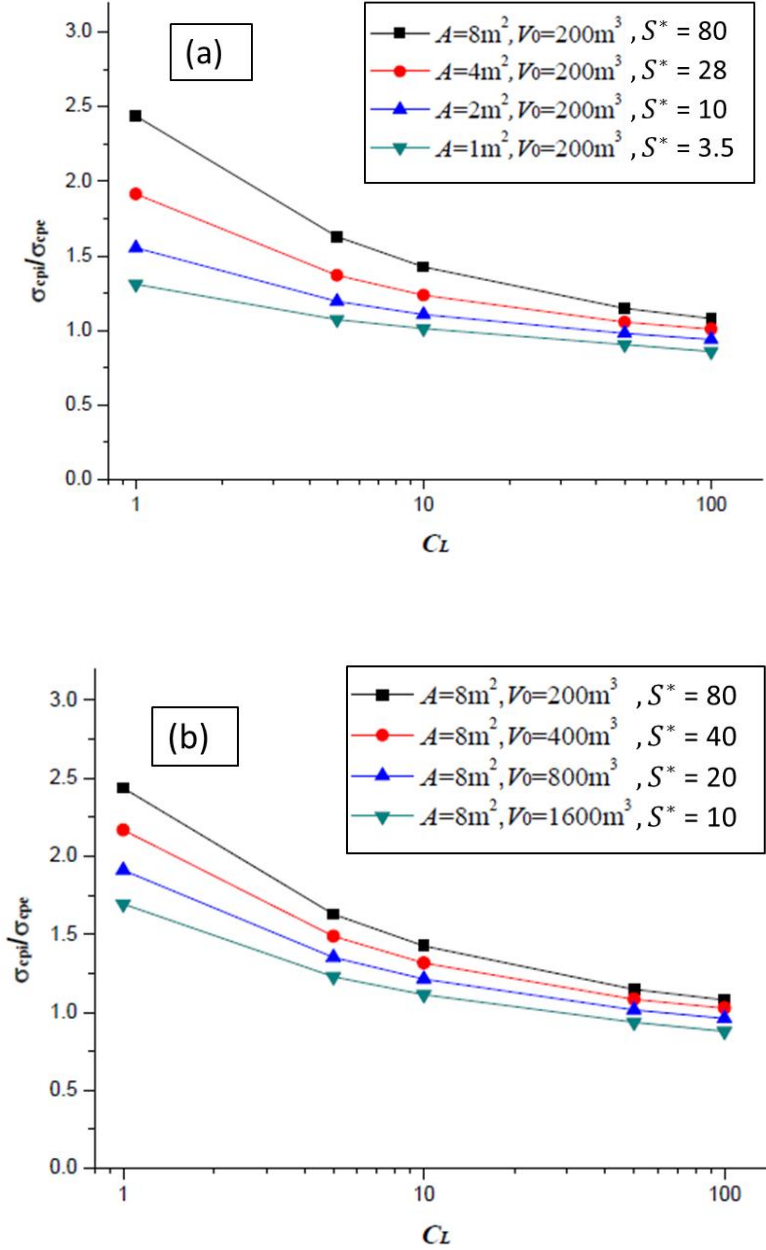


Figure 2.11: Standard deviation pressure ratio versus C_L ; a) Different opening sizes b) Different internal volume (Xu et al.,2017)

The loss coefficient, C_L depends on the geometry of the opening, and the Re of the leakage paths. Vickery (1986) defined the pressure difference through the opening as $\Delta p_{loss} = C_L \rho U^2 / 2$ and calculated the effective wall porosity area for experimental data by

assigning a value of $C_L = 2.5$. Liu and Saathoff (1981), Stathopoulos and Luchian (1989), and Vickery and Bloxham (1992) used 2.78 as the empirical value for C_L . Sharma (1996), and Sharma and Richards (1997) compared experimental data with Computational Fluid Dynamic analysis for a range of C_L between 1.5 to 2.8. Ginger et al. (2010) found that the loss coefficient spreads within a broader range from 6.25 to 100 for different opening sizes and internal volumes (i.e., S^* varies from 0.17 to 38). Similar results were obtained by Xu et al. (2016,2017) with large C_L varies from 1 to 100 when S^* decreases from 80 to 3.5 as shown in Figures 2.11a and b.

The effect of non-dimensional parameters (i.e., S^*) on internal and external pressure characteristics is also studied in this thesis. Besides, this objective of this thesis, the combination of internal and external pressures that generate high net pressures on different parts of the building also examined.

2.4 Correlation between external and internal pressure

Beste et al. (1997) defined the cross-correlation between external and internal pressures by taking the product of the fluctuating components of the external pressure at the time, t , and internal pressure at the time, $(t + \tau)$, where τ is the lag time between external and internal pressures. Beste et al. (1997) conducted a wind tunnel model-scale study on a 1:100 scale model of TTU experimental building with a windward wall opening shown in Figure 2.12. They defined eight cladding zones as per the specifications in the ASCE7-95, and each zone is concentrated by external pressure taps connected to a manifold to measure area-averaged external pressure fluctuations in each zone.

Beste et al. (1997) obtained a positive correlation for zero lag time when the external and internal pressures are of the same sign, and negative correlation when the external and internal pressures are of opposite signs. For example, when the wind flows towards a windward wall opening, positive internal pressures and area-averaged negative external pressures on the roof are negatively correlated. They defined that the internal and external pressures are highly correlated if the correlation coefficient was higher than ± 0.6 and poorly correlated if the correlation coefficient was below ± 0.2 .

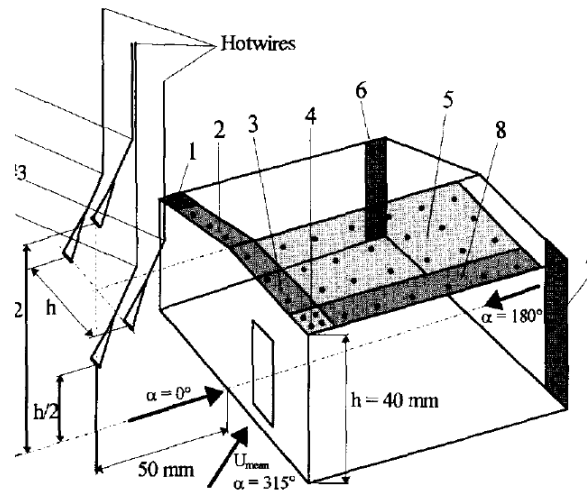


Figure 2.12: Wind tunnel model with openings and wind directions –Beste et al. (1997)

Beste et al. (1997) found that internal and area-averaged external pressures are highly correlated at the windward roof edges and wall corners that border a wall having a dominant opening. Table 2.3 presents the internal-external pressure cross-correlation coefficients for roof and wall areas. The internal pressure measured for $\alpha = 315^\circ$ are generally lower than for $\alpha = 0^\circ$, however, the highest cross-correlation coefficient between internal and area-averaged external pressure at the roof leading edge (Area #3) is about -0.6 at wind direction $\alpha = 315^\circ$. The cross-correlation between area-averaged external pressure and internal pressures on Area #8 is about -0.15. Both building Areas #3 and #8 are located in the corner vortex regions typically for separated flow over the windward edge for $\alpha = 315^\circ$ but magnitude of the correlation coefficient is higher on Area #3 than Area #8 because Area #3 is above the dominant opening.

In addition, Beste et al. (1997) concluded that internal and area-averaged external pressures for a roof corner (Area #4, $\alpha = 315^\circ$) covered by vortices during cornering flow are poorly correlated. For Area #5, the central roof area, this coefficient becomes positive (+0.15) for $\alpha = 315^\circ$ which implies that the two pressure fluctuations more often subtract than add and is negative (-0.25) for $\alpha = 0^\circ$. When the opening faced the wind direction, $\alpha = 180^\circ$, the positive internal pressures are poorly correlated with positive external pressures due to flow separation at the windward wall edge (Area #7). Beste et al. (1997) recommended investigating the correlation coefficient for a range of building parameters such as building geometry and opening sizes and locations.

Table 2.3: Cross-correlation coefficients for roof and wall areas- Beste et al. (1997)

Area	$\alpha = 0^\circ$	$\alpha = 180^\circ$ ^a	$\alpha = 315^\circ$	Area	$\alpha = 0^\circ$	$\alpha = 180^\circ$ ^a	$\alpha = 315^\circ$
1	-0.45	—	-0.25	5	-0.25	—	+0.15
2	-0.45	—	-0.40	6	—	-0.40	—
3	-0.45	—	-0.60	7	-0.10	+0.20	—
4	-0.50	—	-0.02	8	-0.10	—	-0.15

^a Door opening moved to windward wall.

Sharma and Richards (2005) studied a 1:50 geometric scale model of the TTU building and examined the cross-correlation coefficients between internal pressure and area-averaged external pressures on the roof edges (RF1 and RF2) for two separate wall openings (WO1 and WO2), as shown in Figure 2.13. When WO1 is open for wind directions 0° to 90° , correlation coefficients for RF1 varied between -0.2 and -0.4. On the other hand, the near-zero values of the correlation coefficient between wind angles of 90° and 320° indicate that fluctuating (negative) internal pressures are not correlated with (negative) roof external pressures.

When WO2 is open, the highest correlation coefficient for the corner roof area (RF1) was about -0.6 (at 350°). Correlation coefficients varied between -0.4 to -0.6 in the wind angle range $-40^\circ \leq \theta \leq +65^\circ$, indicating a significant addition between internal and roof external pressure fluctuations. Furthermore, for a sidewall and leeward wall opening at the wind angles of 85° and 310° , correlation coefficients were positive, showing cancellation of fluctuating internal and roof external pressures.

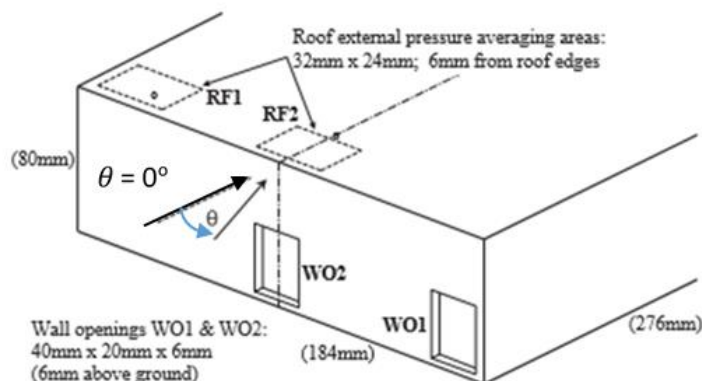


Figure 2.13: Wind tunnel model - 1:50 scale (Sharma and Richards (2005))

For the roof area (RF2), Sharma and Richards (2005) found the highest correlation coefficient about -0.6 (at $\theta = 30^\circ$) for WO1 opening and about -0.64 (at $\theta = 40^\circ$) for WO2 opening. Furthermore, conical vortices were formed along the leading roof edges for oblique wind directions, but the correlation between external and internal pressures was highest at the RF2 when WO2 was open because RF2 was located over the WO2 opening compared to WO1 opening.

These studies have determined the correlation between internal and external pressures. They have considered the area-averaged external pressures on the roof and wall areas with a few opening sizes and locations in the walls. However, the effect of correlation between external and internal pressures that generate peak net pressures and the effects of the porosity and the building volume on the correlation coefficient of internal and external pressures were not studied.

This thesis focuses on the correlation between internal and external pressures at the roof and wall cladding (i.e., individual taps) and structural components (i.e., area-averaged external pressure) to characterise the peak net pressures based on the opening area to volume ratio. Further, the effect of size and location of the openings and porosity in the envelope, and building volume on the correlation between external and internal pressures are examined in detail.

2.5 Net pressures and net pressure factors

Ginger et al. (1997) analysed the net pressure fluctuations on the WERFL test building by combining external and internal pressure time histories, as shown by Equation 2.12. Compared to the nominally sealed building, when the building has an opening on the windward wall, they found that net positive loads on the windward wall were decreased and net suction loads on the roof, side walls, and leeward walls were increased due to large positive internal pressure fluctuations.

$$C_{p,net}(t) = C_{pe}(t) - C_{pi}(t) \quad (2.12)$$

Ginger et al. (1997) showed that the peak net pressure coefficients were 76% to 90% in magnitude compared to the difference between peak external and peak internal pressures. When the building has an opening on the windward wall (i.e., $A_W = 0.8 \text{ m}^2$ and 2.0 m^2)

net peak suction pressures at the roof windward edge region were 93% of the difference between peak external and peak internal pressures. They postulated that high net peak suction pressures occurred at the windward roof edge because the high positive internal pressures and high suction external pressures were highly correlated, negatively.

Combinations of peak external and peak internal pressure have been studied by Xu and Lou (2017), who produced reductions to net peak pressure by defining combination factors with Equation 2.12. Accordingly, it was rearranged as, $C_{\hat{p},net} = \varphi'_{e1}C_{\hat{p}e} - \varphi'_{i1}C_{\hat{p}i}$ and $C_{\check{p},net} = \varphi'_{e2}C_{\check{p}e} - \varphi'_{i2}C_{\check{p}i}$ where combination factors φ'_e (φ'_i) are the ratio between maximum or minimum external pressure magnitude (or internal) and maximum or minimum net pressure magnitude (i.e. $\varphi'_{e1} = C_{\hat{p}e}/C_{\hat{p},net}$). Table 2.4 provides the calculated combination factors for external and internal pressures for different openings. Accordingly, for roof net pressures, they introduced a combination factor of 0.98 for peak internal pressures and a combination factor of 0.43 for external pressure. Further, combination factors for internal and external pressure are almost equal to 1 for wall maximum net pressures, showing the equivalent maximum pressures in net, external and internal pressures.

Table 2.4: Combination factors for internal and external pressures, Xu and Lou (2017)

Opening size (mm × mm)	S^*	$C_{\check{p},net}$ for roof		$C_{\hat{p},net}$ for wall		$C_{\hat{p},net}$ for roof	
		φ'_{i2}	φ'_{e2}	φ'_{i1}	φ'_{e1}	φ'_{i2}	φ'_{e2}
400 × 208	49.8	0.98	0.43	0.97	0.96	0.89	0.81
200 × 208	17.6	0.98	0.45	0.92	0.84	0.93	0.78
120 × 208	8.2	0.98	0.43	0.95	0.95	0.86	0.82

Peak net pressure coefficients are lower in magnitude than the difference between peak external and peak internal pressures because the peak external and peak internal pressures do not happen simultaneously. Wind loading standard AS/NZS 1170.2, 2011 provides combination factors, K_C , which account for the lack of correlation between internal and external pressures. For example, if pressures on two contributing surfaces act together (i.e., large external and internal pressure), AS/NZS 1170.2, 2011 gives a K_C of 0.9, where $C_{\check{p},net} = 0.9(C_{\check{p}e} - C_{\check{p}i})$. The Eurocode EN 1991-1-4-2005 defines the background factor (similar to K_C in AS/NZS 1170), which varies between 0.85 to 1.0 based on the building height to width ratio.

Combination factors in standards are derived from limited wind tunnel studies and are neither well-understood nor well-defined to accommodate net loads on different roof areas considering the size and location of the opening and the opening area to building volume ratio. This thesis focuses on the net reduction factor similar to the combination factor in AS/NZS 1170.2, 2011. Accordingly, this study has derived two net pressure factors based on the maximum net pressure coefficient ($C_{p,net}$) and the minimum net pressure coefficient, $C_{p,net}$ for roof and wall cladding in the building envelope.

2.6 Covariance integration method and L.R.C method

Holmes and Best (1981) developed the covariance integration method, which can determine the peak load effects, given the correlation between pressures acting on panels on a tributary area supporting a structure. Kasperski and Niemann (1992) further refined this as the “Load-Response-Correlation” (L.R.C.) method, which has been used by Holmes (1992) to determine the equivalent static load distributions on a tributary area. The wind loads applied on ‘ N ’ number of panels on the tributary area are used to determine the wind load effect $x(t)$ as given in Equation 2.13, where β_j and p_j are the influence coefficient and the pressure at the panel ‘ j ’ of area A_j .

$$x(t) = \sum_{j=1}^N \beta_j p_j(t) A_j \quad (2.13)$$

The peak value of the load effect, \hat{x} or \check{x} is defined in Equation 2.14 where \bar{x} is the mean, σ_x is the standard deviation, and g_x is the peak factor of x .

$$\hat{x}, \check{x} = \bar{x} \pm g_x \sigma_x \quad (2.14)$$

Holmes and Best (1981), Kasperski and Niemann (1992), and Ginger et al. (2000) defined σ_x and g_x as shown in Equations 2.15 and 2.16, where β_j and β_k are the influence coefficients and $A_j; A_k$ are the area of two panels ‘ j ’ and ‘ k ’ respectively. The peak factors, g_{pj} and g_{pk} are also estimated for pressure fluctuations on panels “ j ” and “ k ”

using $g_{pj}^+ = (\hat{p}_j - \bar{p}_j)/\sigma_{pj}$ when β_j is positive and $g_{pj}^- = (\bar{p}_j - \check{p}_j)/\sigma_{pj}$ when β_j is negative for deriving g_x in Equation 2.16. The $r_{p_j p_k}(0)$ in Equation 2.16a is the correlation between p_j and p_k at zero lag time (See Section 3.4.4 for further details).

$$\sigma_x = \left(\sum_{j=1}^N \sum_{k=1}^N \overline{p'_j(t)p'_k(t)} \beta_j \beta_k A_j A_k \right)^{1/2} \quad (2.15)$$

$$\begin{aligned} g_x &= \left(\sum_{j=1}^N \sum_{k=1}^N \overline{p'_j(t)p'_k(t)} \beta_j \beta_k g_{p_j} g_{p_k} \right)^{1/2} / \sigma_x \\ &= \left(\sum_{j=1}^N \sum_{k=1}^N r_{p_j p_k}(0) \sigma_{p_j} \sigma_{p_k} \beta_j \beta_k g_{p_j} g_{p_k} \right)^{1/2} / \sigma_x \end{aligned} \quad (2.16)$$

The L.R.C. method is used to determine the expected pressure distributions corresponding to peak load effects. Kasperski and Niemann (1989) derived Equation 2.17 for load at j , P_j which generates peak value of the load \hat{x} . Here, $r_{P_j x}$ is the correlation between P and load x .

$$(P_j)_{\hat{x}} = \bar{P}_j \pm g_x r_{P_j x} \sigma_{P_j} \quad (2.17)$$

These equations can be used to calculate the peak net pressures by considering external and internal pressure fluctuations on the building roof and wall (i.e., substitute suffix of x , j , and k by *net*, *external* and *internal* pressure data). The application of covariation method in this study is presented in Chapter 5.

2.7 Chapter summary

Research on internal pressure fluctuations has been conducted in model-scale and full-scale studies on nominally sealed buildings and buildings with a large opening since 1970s. Internal pressure fluctuations inside a nominally sealed building depend on the flow through the porous surfaces of the envelope leading to small internal pressure fluctuations. Internal pressure fluctuations inside a building with a large opening are

positive when the opening is on the windward wall and negative when the opening is on side wall or leeward wall. During a windstorm, internal pressure can contribute significantly to generate large net pressure on the envelope; thus, further study of internal pressure will provide a better understanding of wind loading enabling the optimal structural design of industrial type buildings.

The correlation between internal and external pressures have also been examined by Beste et al. (1997) and Sharma and Richards (2005). They focused on the correlation coefficient between internal pressure and area-averaged external pressures for building with a large opening. Sharma and Richards (2005) also studied the combination of external and internal pressures on the windward roof edge of a building with a large opening. However, the combined effects of internal and external pressure fluctuations on net pressure fluctuations on cladding and structural elements of large industrial buildings with a range of openings and porosity in the envelope and building volumes have not been studied in detail.

Current gaps in the research include:

- Lack of data discussing the effect of building parameters (i.e., S^*) on the correlation between internal and external pressures.
- Limited information on net pressures that determine the contribution of external and internal pressure peaks on peak net pressures when the internal and external pressure fluctuations exceed a threshold value on different areas and components in the building envelope
- Few studies on combination factors that define a reduction to peak net pressures on different parts of the roof and walls.

This thesis analyses the correlation between internal and external pressures on industrial type steel-clad buildings by conducting a series of model-scale wind tunnel tests. The combination of internal and external pressures generating net pressure fluctuations on different parts of the building envelope are analysed considering a range of different size openings and porosity in the envelope, and building volume. The relationship of correlation coefficients and net pressure fluctuations to generate peak net pressure is studied to define reduction to peak net pressures with respect to the non-dimensional parameter S^* . The outcomes of this study will enable optimising the design of an industrial building, by providing the relationship between correlation coefficients, peak net pressure coefficients, and structural effects.

3 EXPERIMENTAL SETUP AND METHODOLOGY

This Chapter presents details of a 1/200 model-scale wind tunnel study conducted on rectangular plan industrial buildings to record time-varying external and internal pressure data. External and internal pressure tap layouts on the roof and walls and the different opening geometries are presented in this Chapter. Further, the data analysis methods and the configurations tested are listed.

3.1 Wind tunnel boundary layer simulation

A wind tunnel study was conducted to determine the internal and external pressures simultaneously at the roof and walls of typical industrial buildings. Tests were performed in the 2.0 m high \times 2.5 m wide \times 22 m long boundary layer wind tunnel at James Cook University, in Townsville, Australia.

The approach wind flow was simulated at a length scale of 1:200 for a terrain category 2 approach as per AS/NZS 1170.2. A Turbulent Flow Instrument, Cobra Probe was used to measure the approach wind velocity and turbulence intensity at a range of heights (z) above the wind tunnel floor. The Cobra Probe measurements were taken at the upwind end of turntable near the model. Figure 3.1(a)-(b) show the measured mean velocity and the turbulence intensity profiles, compared with the values specified for terrain category 2 in the wind loading standard AS/NZS 1170.2, 2011. Figure 3.2 presents the velocity spectrum of the approach wind flow which compares satisfactorily with the von-Karman spectrum at a length scale of 1/200. Measured wind tunnel data closely match the approach velocity profiles in the wind loading standard AS/NZS 1170.2 (terrain category 2) and the von Karman spectrum.

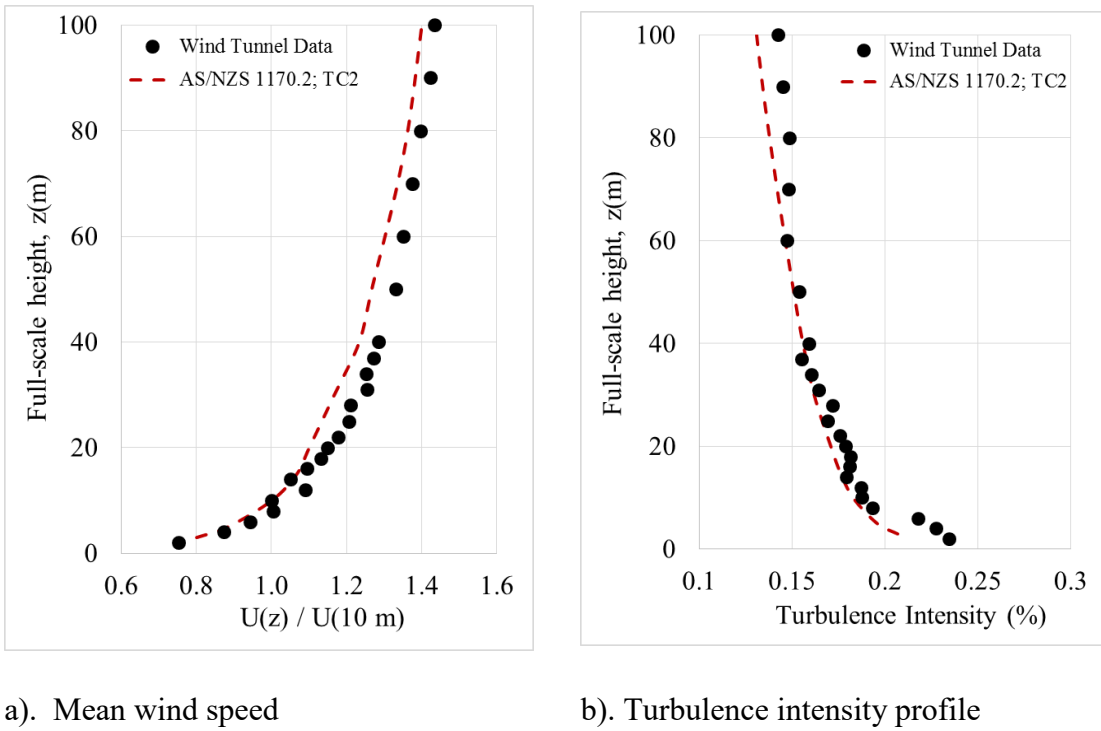


Figure 3.1: Boundary layer wind profile simulated in the wind tunnel at a length scale of 1/200

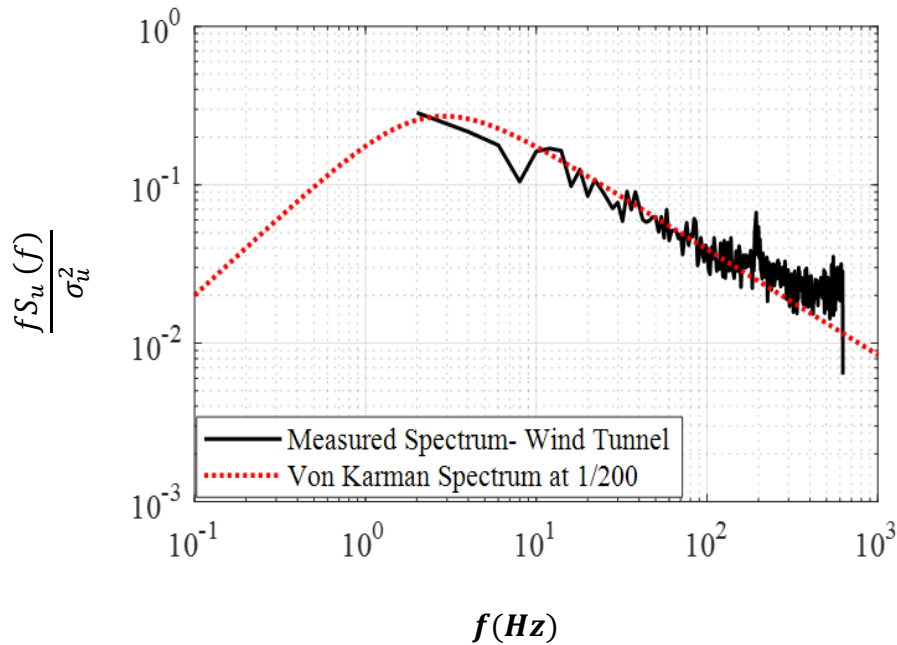


Figure 3.2: 1/200 scale wind velocity spectra at $z = 100 \text{ mm}$ (20 m in full scale)

3.2 Building models

Two open plan, rectangular, low pitch industrial buildings, 80 m long \times 40 m wide \times 20 m high (Model #1), and 160 m long \times 40 m wide \times 20 m high (Model #2), were constructed from 6 mm thick perspex at a length scale, $L_r = L_{model-scale} / L_{full-scale}$, of 1/200. Figure 3.3 shows Model #1, 400 mm long \times 200 mm wide \times 100 mm high with an additional volume of 400 mm \times 200 mm \times 600 mm below the turntable of the wind tunnel. The only difference between Model #1 and Model #2 is the length of Model #2 is two times the length of Model #1.

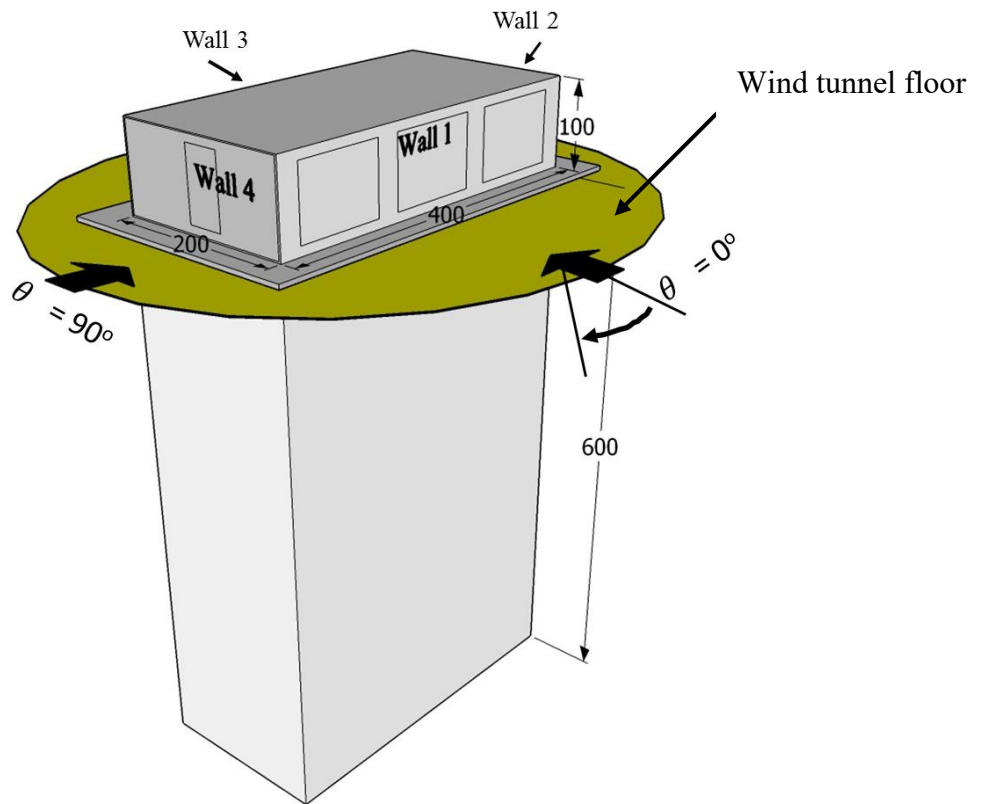
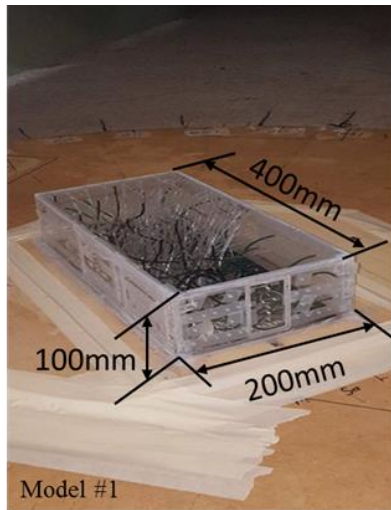


Figure 3.3: Schematic of wind tunnel Model #1 - 1/200 scale (all dimensions are in mm)

Figure 3.4(a) shows the top part of Model #1 attached to the wind tunnel turntable, and Figure 3.4(b) shows the bottom part of the model under the wind tunnel turntable. Figure 3.5 (a-b) show the top and bottom of Model #2 fixed to the wind tunnel turntable, and all other details of Model #2 are described in Appendix A. The model was installed on the wind tunnel turntable where Wall #1 is the windward wall for $\theta = 0^\circ$, and Wall #4 is the

windward wall for $\theta = 90^\circ$, as shown in Figure 3.3. This orientation was followed for every test configuration (Cases), discussed in Chapters 4 and 5.

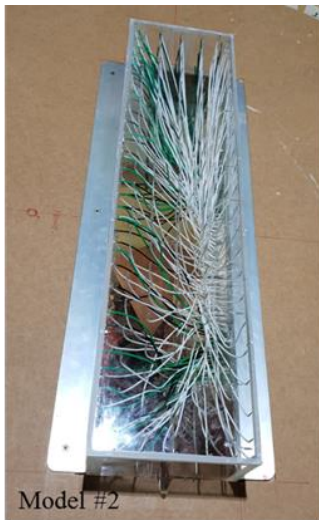


(a) Top of the wind tunnel turntable



(b) Under the turntable

Figure 3.4: Model #1 fixed in the wind tunnel



(a) Top of the wind tunnel turntable



(b) Under the turntable

Figure 3.5: Model #2 fixed in the wind tunnel

3.2.1 Opening geometries

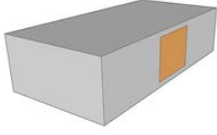

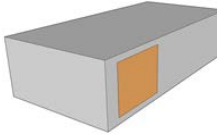
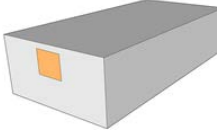
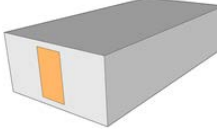
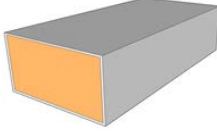

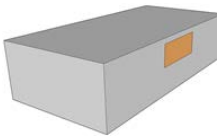
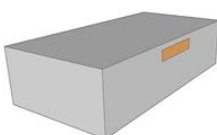
3.2.1.1 Model #1

Tests were performed on a number of building configurations, with a range of wall openings in Walls #1 to #4 for varying approaching wind directions as defined in Table 3.1. LO4, LO5, and LO6 on Wall #4 and LO1, LO8, and LO9 on Wall #1 are two sets of opening sizes for assessing the effect of opening size influencing internal pressure fluctuations. LO1, LO2, and LO3 on Wall #1 are the same opening size at different locations on the building, which addresses the effect of the location of the opening on internal pressure fluctuations. LO7 on Wall #2 is the same opening size of LO5 on Wall #4, which are on two opposite walls. Further, combinations of these openings are used for testing multiple openings on the same wall, two adjacent or opposite walls. The opening sizes (i.e., LO4, LO5, LO8 and LO9) are selected to match practical openings in standard industrial buildings. Other openings (i.e., LO1, LO2, LO3 and LO5) are selected to represent other possible opening sizes (including complete wall opening) used in very large industrial buildings.

3.2.1.2 Model #2

A range of wall openings, LO4, LO5, and LO6 in Wall #4 and LO1, LO2, LO3 and LO8 in Wall #1 are similar to openings in Model #1. Additionally, LO10 (100 mm × 90 mm) in Wall #1 and LO11 (150 mm × 90 mm) in Wall #4 are tested. Additional figures are shown in Appendix A.

Table 3.1: Opening configurations of Model #1

Notation	Size (mm)	Wall #	Figure
LO1	100 × 80	1	
LO2	100 × 80	1	
LO3	100 × 80	1	
LO4	40 × 40	4	
LO5	80 × 40	4	
LO6	190 × 95	4	
LO7	100 × 80	2	
LO8	100 × 40	1	
LO9	100 × 20	1	

3.2.2 Wall porosity on Model #1

The porosity of the walls on Model #1 was simulated by installing uniformly distributed holes on the walls. Figure 3.6 illustrates the distribution of 60 × 3 mm diameter holes and 180 × 1.5 mm diameter holes on Walls #1 to #4. These holes could be taped as needed to simulate a range of porous areas on the walls. Accordingly, four porosity configurations were tested, as described in Table 3.2. The percentage ratio between total wall porous area to total wall area is defined as the wall porosity. For example, total porous area on Wall #1 is 247.5 mm² (i.e., $20 \times \pi \times (3/2)^2 + 60 \times \pi \times (1.5/2)^2$) and total wall area is 40000 mm² (i.e., 400×100) that creates a porosity of 0.62 % (i.e., $(247.5/40000) \times 100$). Equal porosities were maintained on each wall for each building configuration tested. The porous holes are not modelled across the roof because the actual porosity level is very small compared to the wall porosity in these types of buildings (Humphreys, 2020).

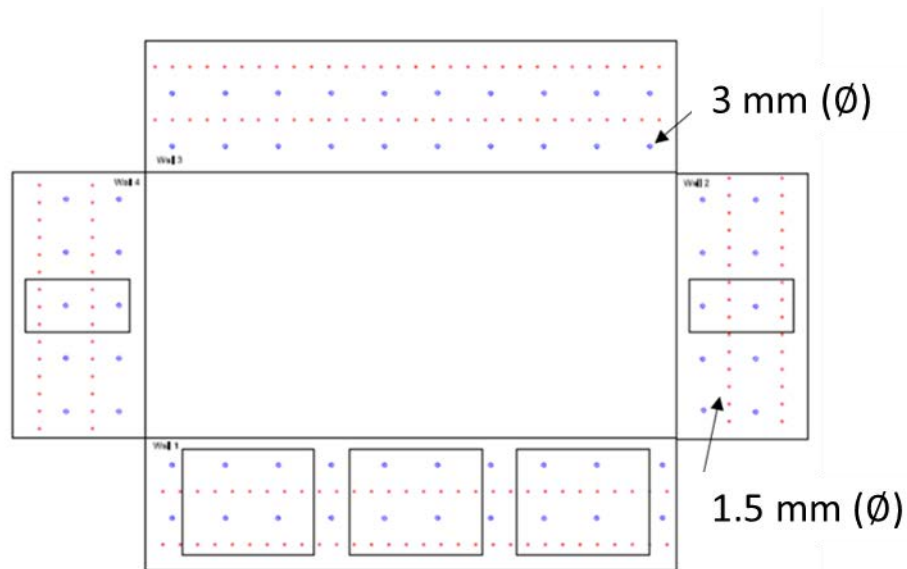


Figure 3.6: Layout of the porous holes in walls of Model #1

Table 3.2: Wall porosity Model #1

Description	No. of holes on each Walls #1 and #3		No. of holes on each Walls #2 and #4		Wall Porosity (%)
	3 mm	1.5 mm	3 mm	1.5 mm	
P1	0	0	0	0	0
P2	0	18	0	9	0.08
P3	10	32	5	16	0.32
P4	20	60	10	30	0.62

3.2.3 Building volume of Model #1

Three building volumes were considered in Model #1 to study the effect of building volume on internal pressure fluctuations for selected opening configurations. Figure 3.7(a) shows the original wind tunnel model with an internal volume of $388 \text{ mm} \times 188 \text{ mm} \times 688 \text{ mm}$ ($V_1 = 0.050 \text{ m}^3$). Foam blocks were inserted to reduce the volume, giving internal volumes of $388 \text{ mm} \times 188 \text{ mm} \times 344 \text{ mm}$ ($V_2 = 0.025 \text{ m}^3$) and $388 \text{ mm} \times 188 \text{ mm} \times 194 \text{ mm}$ ($V_3 = 0.014 \text{ m}^3$), as shown in Figure 3.7(b) and 3.7(c), respectively. The model contains 250 flexible tubes (see in Section 3.4) that the total volume of tubing is less than 0.25% of the total volume of the model and was not subtracted to give the volume of the model.

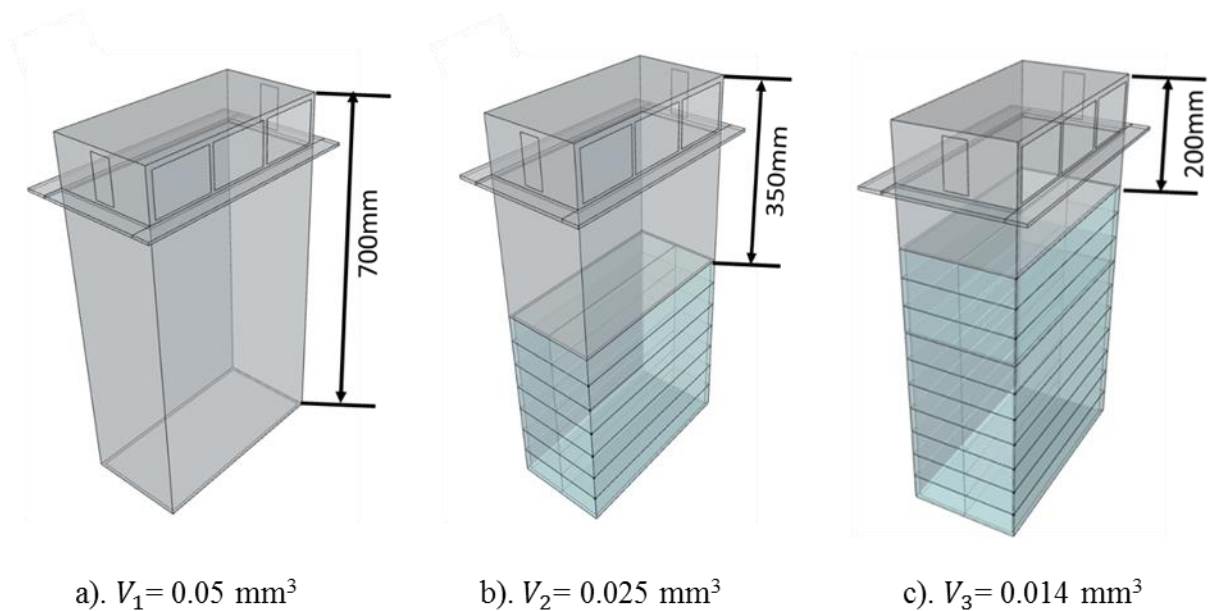


Figure 3.7: Three volume cases for Model #1

3.2.3.1 Internal volume distortion

Holmes (1979) applied dimensional analysis and defined the internal volume distortion in model scale studies to ensure that the internal pressure fluctuations in the building are scaled correctly. Correspondingly, the internal volume of the models was distorted to satisfy scaling requirements and the volume ratio V_r , between model-scale and full-scale is maintained as described as;

For wind tunnel testing at atmospheric pressure, the ratio of model-scale to full-scale (subscript- r) is considered as;

$$\text{Length scale ratio; } [L]_r = L_{ms}/L_{fs}$$

$$\text{Velocity scale ratio; } [U]_r = U_{ms}/U_{fs}$$

$$\text{Time scale ratio; } [T]_r = [L]_r/[U]_r$$

$$\text{Frequency scale ratio; } [f]_r = 1/[T]_r = [U]_r/[L]_r$$

From Helmholtz resonance frequency: $f_H^2 \propto \sqrt{A}p_0/\rho_a V_0$

$$[f]_r = [L]_r[p_0]_r/[\rho_a]_r[V]_r = [L]_r/[V]_r ;$$

for atmospheric pressure; $[p_0]_r = 1$ and $[\rho_a]_r = 1$

To satisfy frequency scaling; $[f]_r^2 = [f_H]_r^2$ and then, $[U]_r^2/[L]_r^2 = [L]_r/[V]_r$

Gives the Equation 3.1;

$$[V]_r = \frac{[L]_r^3}{[U]_r^2} \quad (3.1)$$

Accordingly, the volume ratio V_r between model-scale and full-scale is maintained as $[V]_r = [L]_r^3/[U]_r^2$. If the test (model-scale and full-scale) is done at a $[U]_r \neq 1$ then the model-scale building volume must be distorted.

Wind tunnel tests carried out with volumes $V_1 = 0.05 \text{ m}^3$, $V_2 = 0.025 \text{ m}^3$, and $V_3 = 0.014 \text{ m}^3$ gives $[V]_r = 7, 3.5$, and 2 respectively. Combined with $[L]_r = 1/200$ thus gives $[U]_r = 0.38, 0.54$, and 0.71 respectively. These different building volumes, velocity ratios and opening areas enables the results to be discussed with respect to a non-dimensional parameter, $S^* = (A^{3/2}/V) \times (a_s/\bar{U}_h)^2$. The opening non-dimensional parameter, S^* in model-scale and full-scale should be equal (i.e., $S_{ms}^* = S_{fs}^*$) gives the same relationship for volume ratio, $[V]_r$ as shown in Equation 3.1.

$$\left(\frac{A^{3/2}}{V}\right)_{ms} \times \left(\frac{a_s}{\bar{U}_h}\right)_{ms}^2 = \left(\frac{A^{3/2}}{V}\right)_{fs} \times \left(\frac{a_s}{\bar{U}_h}\right)_{fs}^2$$

$$\left(\frac{A_{ms}}{A_{fs}}\right)^{3/2} \times \left(\frac{\bar{U}_{fs}}{\bar{U}_{ms}}\right)^2 = \left(\frac{V_{ms}}{V_{fs}}\right)$$

$$[V]_r = ([L^2]_r)^{\frac{3}{2}} \times \frac{1}{[U]_r^2} = \frac{[L]_r^3}{[U]_r^2}$$

Accordingly, the volume ratio $[V]_r$ in Equation 3.1 can be satisfied by considering the non-dimensional parameter S^* .

This analysis indicates that the internal pressure fluctuations for given external pressure fluctuations at the opening in a building will depend on the parameter S^* . The relationship between internal and external pressures at an opening can be described by the ratio of $C_{\sigma pi}/C_{\sigma pe}$ and $C_{\hat{p}i}/C_{\hat{p}e}$, across the range of S^* and enable insight into the provisions of design guidelines.

3.2.4 External pressure tap layout

A total of two hundred and forty-three (243) external pressure taps were installed on Model #1 to measure the external pressures for each wind direction simultaneously. External pressure taps were located to obtain pressures on wall and roof cladding of the buildings. Details for both Model #1 and Model #2 are given in Appendix A.

All external pressure taps were numbered with a specific notation based on the wall and roof cladding and structural components, as described in Table 3.3. Figure 3.8 shows the external pressure taps on the walls and roof. External pressures on seven roof purlins were measured at 17 locations on each purlin, as shown in Figure 3.9. Further, Figure 3.10 shows the external pressure taps on three wall girts.

Table 3.3: Notations for external pressure taps

Description	No of external pressure taps	Tap Notation	Figure
Wall #1	6	W1-1 to W1-6	Figure 3.8
Wall #2	7	W2-1 to W2-7	Figure 3.8
Wall #3	10	W3-1 to W3-10	Figure 3.8
Wall #4	6	W4-1 to W4-6	Figure 3.8
Roof	19	R1 to R19	Figure 3.8
Purlin 1 to 6 (RP1 to RP6)	17 nos. for each purlin	RP1-1 to RP1-17 (change the purlin number to get tap location)	Figure 3.9
Wall Girt 1 to 3 (WG1 to WG3)	17 nos. for each wall girt	WG1-1 to WG1-17 (change the purlin number to get tap location)	Figure 3.10

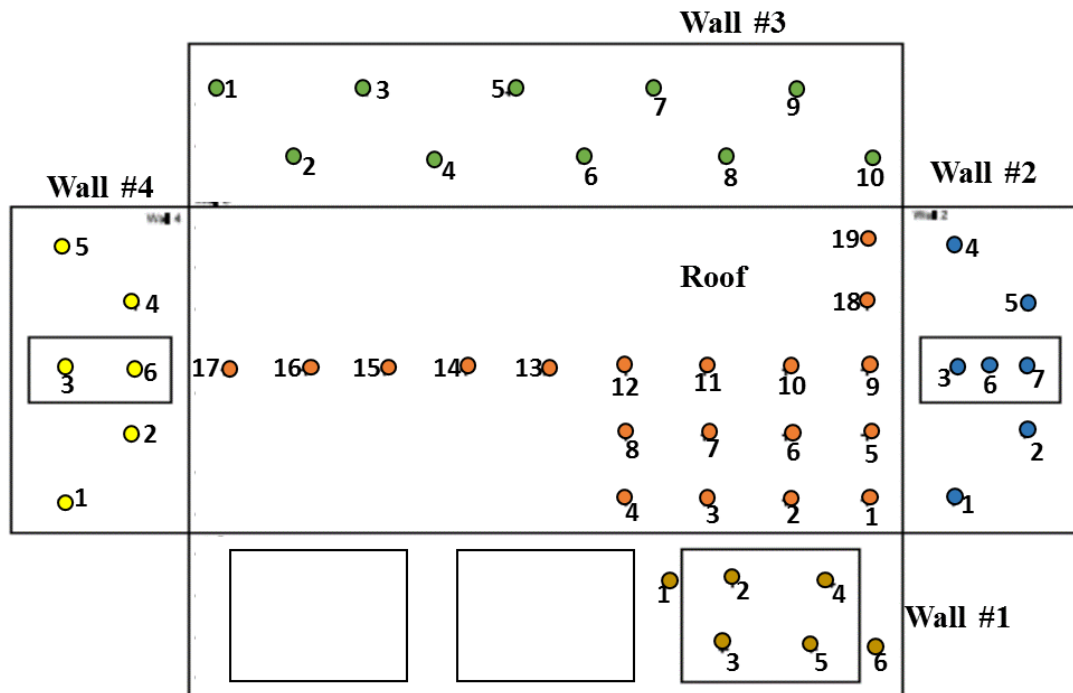


Figure 3.8: External pressure taps layout Model #1 –Walls and Roof

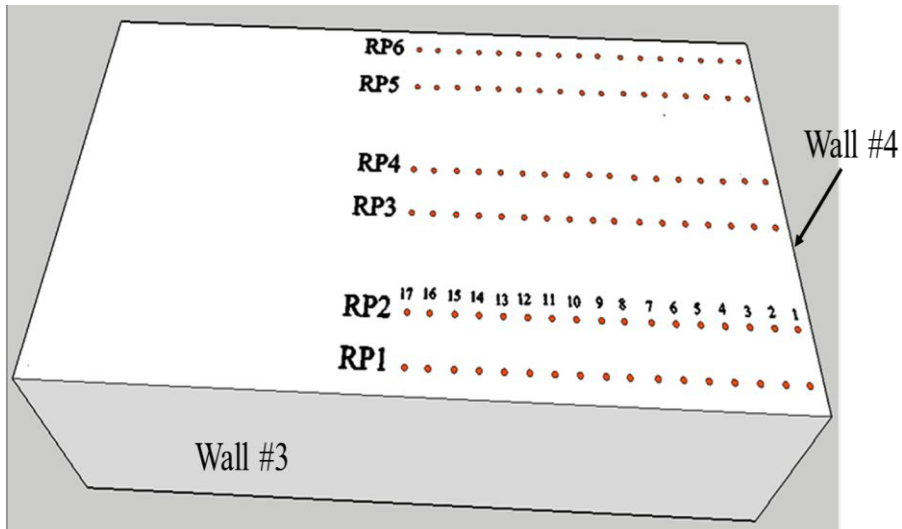


Figure 3.9: External pressure taps layout for Roof Purlins RP1-RP6; taps 1 to 17- Model #1

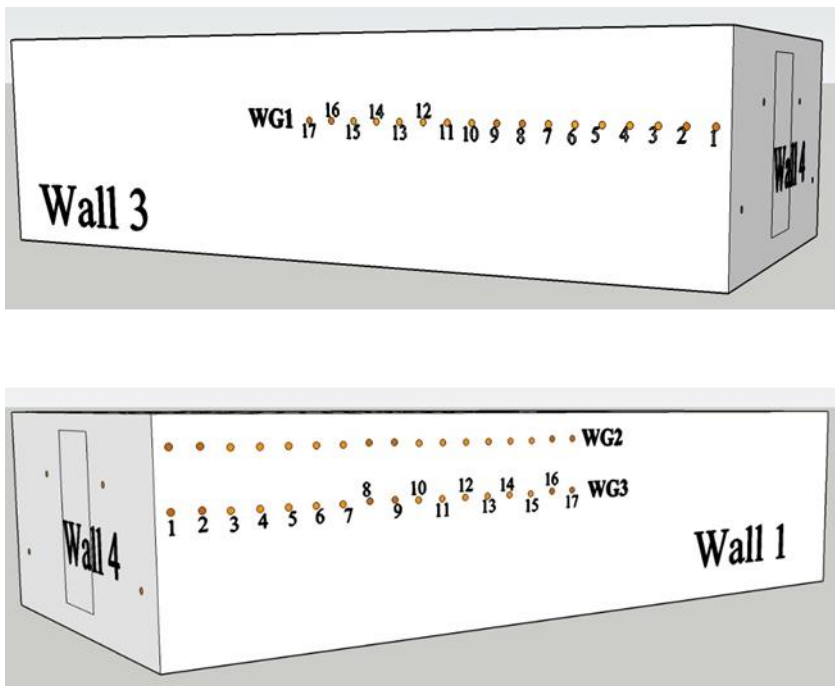


Figure 3.10: External pressure taps layout for Wall Girts WG1- WG3; taps 1 to 17- Model #1

3.2.5 Internal pressure taps

Figure 3.11 shows the four internal pressure taps installed at different positions in Model #1 to obtain the spatial variations of the internal pressure fluctuations. A detailed analysis of the internal pressure fluctuations is presented in Chapter 4 for the range of the size and location of the openings, building volume and building porosity.

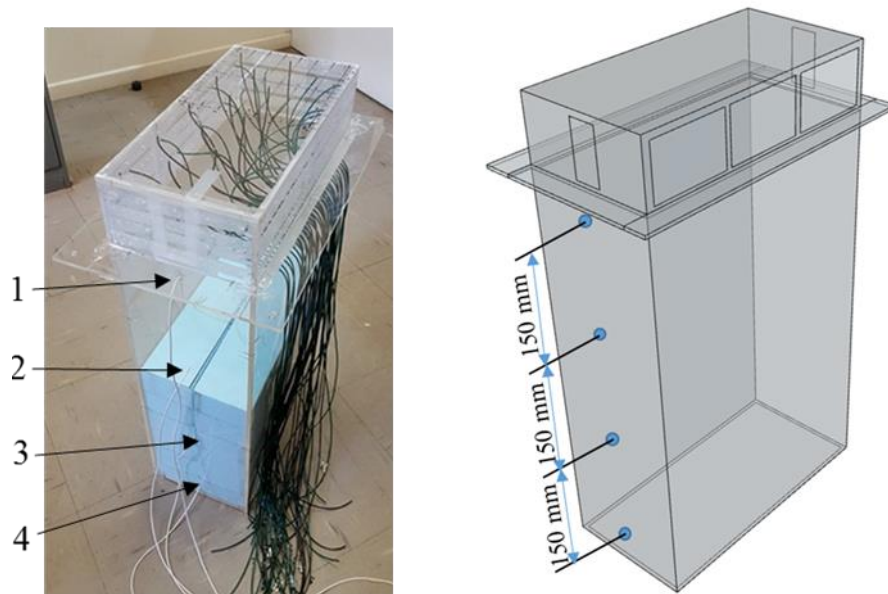


Figure 3.11: Four internal pressure tap layout - Model #1

3.2.6 Roof zones

The roof was divided into five zones to analyse the net pressure fluctuations, net pressure factors and the correlation of external and internal pressures on the roof. Figure 3.12 and Figure 3.13 describe the selected roof zones when wind flows within a range of $\pm 45^\circ$ to orthogonal wind directions $\theta = 0^\circ$ and 90° , respectively to accommodate the wind loading standard AS/NZS 1170.2. The roof zone size is defined based on the distance from the windward roof edge (a), which is the minimum of $0.2b$ or $0.2d$ or height (h) as described in Section 5.4.4 of AS/NZS 1170.2. For Model #1, $b = 40$ m, $d = 80$ m and $h = 20$ m, so, distance from windward edge, $a = 0.2b = 8$ m in full-scale (40 mm in model-scale).

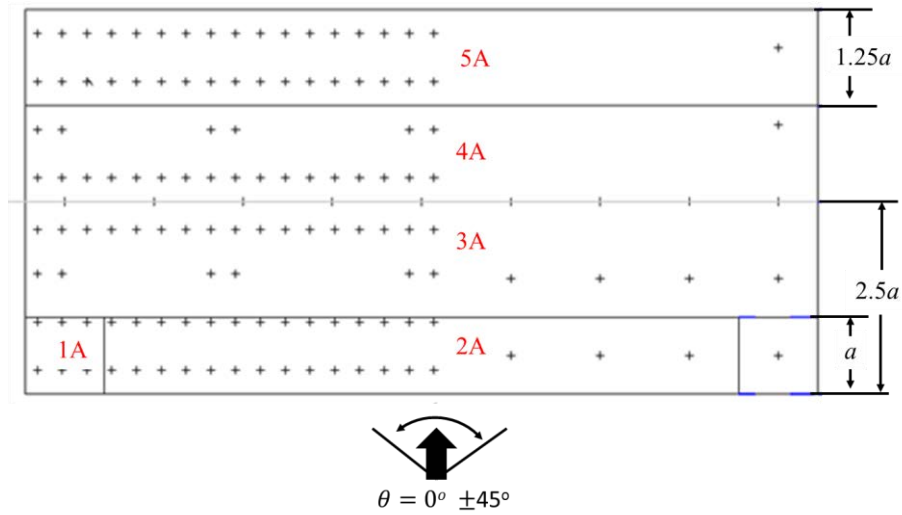


Figure 3.12: Roof zones , $\theta = 0^\circ \pm 45^\circ$

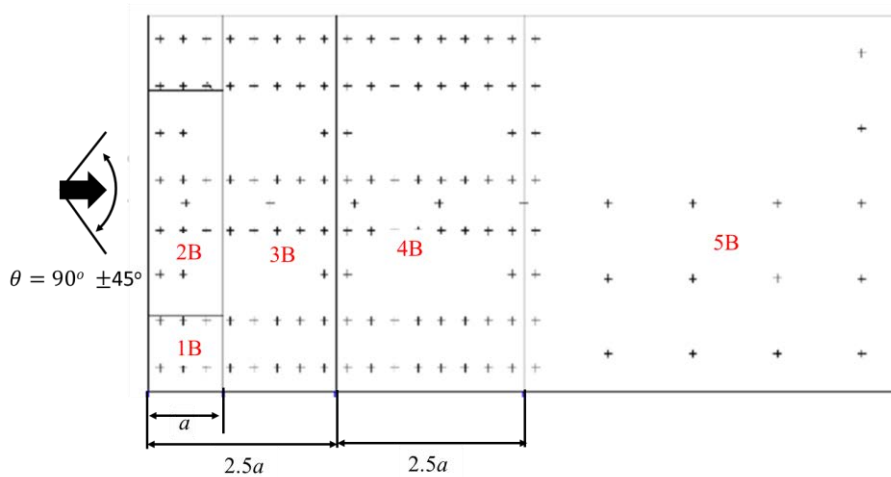


Figure 3.13: Roof zones , $\theta = 90^\circ$

3.3 Wind tunnel test configurations

Table 3.4 and Table 3.5 list the wind tunnel test configurations with the wind directions, model volume, wall porosity of the models, and opening geometry Model #1 and #2 respectively. The sealed building model (Case #1) was tested to obtain the external pressure distribution around the building, while Cases #2 and #3 represents the nominally sealed building. Single wall opening cases are Cases #4 to #12, while Cases #13 to #18 presents the multiple wall openings in the building with full volume (V_1). Selected cases were tested for different volumes (Cases #20 to #29) and different porosity levels (Cases #30 to #45) in Model #1. Cases #46 to #55 show the single and multiple opening configurations in Model #2.

Table 3.4: Wind tunnel test configurations – Model #1

Case #	Description	Wind Direction (θ°)	V (m^3)	$\frac{A_o}{A_T}$ (%)	Porosity * (%)	Opening Location		
						Wall #1	Wall #2	Wall #4
1	Sealed	0°-360°	0.05		-	-	-	-
2	Nominally sealed	0°-360°	0.05		0.62	-	-	-
3	Nominally sealed	0°-360°	0.05		0.32	-	-	-
4	Single opening	0°-180°	0.05	20	-	LO1	-	-
5	Single opening	0°-180°	0.05	10	-	LO8	-	-
6	Single opening	0°-180°	0.05	5	-	LO9	-	-
7	Single opening	0°-360°	0.05	20	-	LO2	-	-
8	Single opening	0°-360°	0.05	20	-	LO3	-	-
9	Single opening	90°-270°	0.05	92	-	-	-	LO6
10	Single opening	90°-270°	0.05	16	-	-	LO7	-
11	Single opening	90°-270°	0.05	16	-	-	-	LO5
12	Single opening	90°-270°	0.05	8	-	-	-	LO4
13	Multiple opening	0°-360°	0.05	40	-	LO1+ LO3	-	-
14	Multiple opening	0°-180°	0.05	40	-	LO2+ LO3	-	-
15	Multiple opening	0°-180°	0.05	60	-	LO1+LO2 +LO3	-	-
16	Multiple opening	90°-270°	0.05		-	-	LO7	LO5
17	Multiple opening	90°-270°	0.05		-	-	LO7	LO6
18	Multiple opening	0°-360°	0.05		-	LO3	-	LO6
19	Nominally sealed	0°-180°	0.025		0.62	-	-	-

Correlation of internal and external pressure fluctuations in industrial buildings

Case #	Description	Wind Direction (θ°)	V (m^3)	$\frac{A_o}{A_T}$ (%)	Porosity * (%)	Opening Location		
						Wall #1	Wall #2	Wall #4
20	Single opening	0°-180°	0.025	20	-	LO1	-	-
21	Single opening	90°-270°	0.025	92	-	-	-	LO6
22	Single opening	90°-270°	0.025	16	-	-	-	LO5
23	Single opening	90°-270°	0.014	92	-	-	-	LO6
24	Single opening	90°-270°	0.014	16	-	-	-	LO5
25	Single opening	90°-270°	0.014	8	-	-	-	LO4
26	Multiple opening	0°-180°	0.025	40	-	LO2+ LO3	-	-
27	Multiple opening	0°-180°	0.025	60	-	LO1+LO2 +LO3	-	-
28	Multiple opening	0°-180°	0.014	40	-	LO2+ LO3	-	-
29	Multiple opening	0°-180°	0.014	60	-	LO1+LO2 +LO3	-	-
30	Single opening	0°-360°	0.05	20	0.62	LO1	-	-
31	Single opening	0°-360°	0.05	20	0.32	LO1		
32	Single opening	0°-360°	0.05	20	0.08	LO1		
33	Single opening	0°-360°	0.05	20	0.62	LO2	-	-
34	Single opening	0°-360°	0.05	20	0.32	LO2	-	-
35	Single opening	0°-360°	0.05	20	0.08	LO2	-	-
36	Single opening	0°-180°	0.05	10	0.5	LO8	-	-
37	Single opening	0°-180°	0.05	10	0.3	LO8	-	-
38	Single opening	0°-180°	0.05	10	0.13	LO8	-	-
39	Single opening	0°-180°	0.05	5	0.26	LO9	-	-

Case #	Description	Wind Direction (θ°)	V (m^3)	$\frac{A_o}{A_T}$ (%)	Porosity* (%)	Opening Location		
						Wall #1	Wall #2	Wall #4
40	Single opening	0°-180°	0.05	5	0.15	LO9	-	-
41	Single opening	0°-180°	0.05	5	0.07	LO9	-	-
42	Single opening	0°-360°	0.05	92	0.62	-	-	LO6
43	Single opening	90°-270°	0.05	16	0.32	-	-	LO7
44	Single opening	90°-270°	0.05	16	0.17	-	-	LO7
45	Single opening	90°-270°	0.05	16	0.04	-	-	LO7

Table 3.5: Wind tunnel test configurations – Model #2

Case #	Description	Wind Direction (θ°)	V (m^3)	$\frac{A_o}{A_T}$ (%)	Opening Location		
					Wall #1	Wall #2	Wall #4
46	Nominally sealed	0°-180°	0.112		-	-	-
47	Single opening	0°-180°	0.112	67	LO10	-	-
48	Single opening	0°-180°	0.112	2.5	LO8	-	-
49	Single opening	0°-360°	0.112	92	-	-	LO6
50	Single opening	0°-360°	0.112	16	-	-	LO5
51	Single opening	0°-360°	0.112	8	-	-	LO4
52	Single opening	0°-180°	0.112	10	LO1	-	
53	Single opening	0°-360°	0.112	54	-	-	LO11
54	Multiple opening	0°-180°	0.112	30	LO1+LO2+LO3	-	-
55	Multiple opening	0°-180°	0.112	20	LO2+ LO3	-	-

3.4 Pressure time-history analysis

3.4.1 Pressure measurement system

The Dynamic Pressure Measuring System (DPMS) from Turbulent Flow Instruments (TFI), was used to collect internal and external pressures. There are four pressure transducer modules, and a total of 256 pressure transducers in four modules (64 nos in each module). As per Figure 3.14, 1.2 m long \times 1.2 mm diameter flexible tubes connect each pressure tap to the pressure transducer in the DPMS.

The DPMS measures fluctuating pressures by accounting for the distortions caused by the flexible tubes that connect pressure taps to pressure transducers. These distortions are mainly dependent on the tube length and diameter of the tubing from the pressure tap to the transducer diaphragm (inside the DPMS), including the transducer's internal volume. The specified percentage error in the calibrated TFI system is about 2%. At the beginning of each test, DPMS is zeroed to minimise offset pressures.

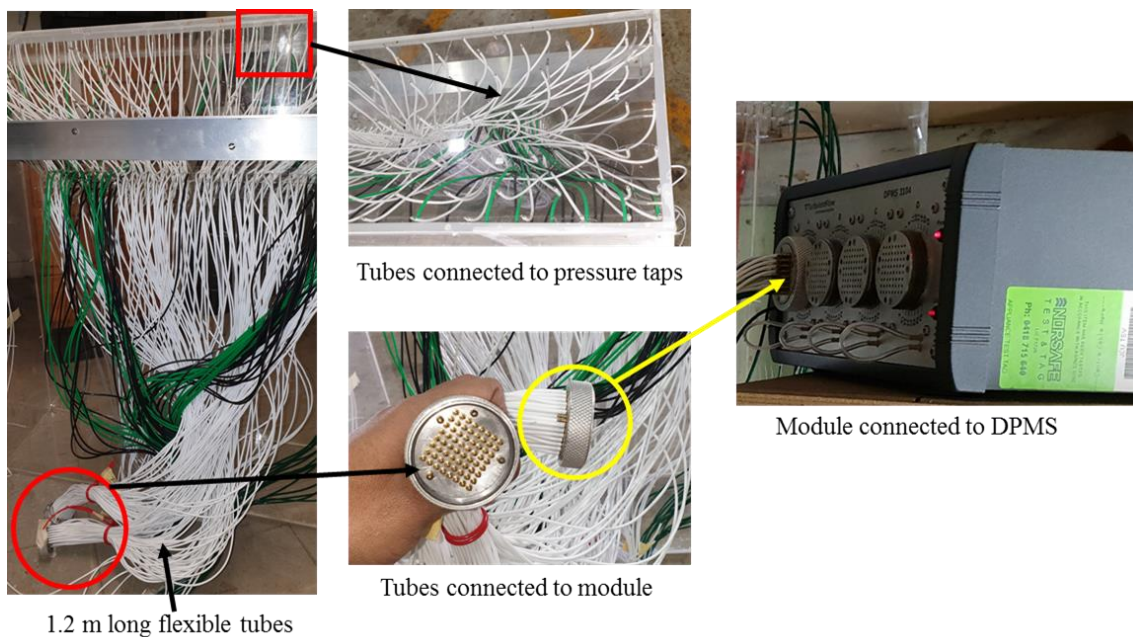


Figure 3.14: 1.2m Long flexible tube connected to module

3.4.2 External and internal pressures

The external and internal pressures were measured simultaneously for each wind direction from $\theta = 0^\circ$ to 360° in 5° intervals by rotating the turntable. However, considering the symmetry of the model, some configurations were tested only for 0° to 180° or 90° to 270° .

The approach flow velocity ratio is defined as $[U]_r = [L]_r/[T]_r$, where $[L]_r=1/200$ and the velocity scale ratio $[U]_r \approx 0.4$ (see Section 3.2.3.1) and $[T]_r$ is time scale ratio of model-scale to full scale, which is denoted as $[T]_r = 1/(200 \times 0.4) = 0.0125$. The equivalent full-scale time, T_{fs} is defined as $T_{fs} = T_{ms}/0.0125$, giving $T_{ms} \approx 16$ s in model scale equivalent to about 20 minutes in full-scale. Thus, $1/625$ s time steps recorded at the model represents 0.128 s in full-scale. Accordingly, external and internal pressures were measured for 16 s at a frequency of 625 Hz (10240 sample points per one time-history), and each test was repeated five times.

The reference pressure (p_{ref}) was measured through a pitot tube installed inside the wind tunnel at the height of 500 mm. The recorded time (t) varying external pressure, $p_e(t)$, and internal pressure, $p_i(t)$, were converted into pressure coefficients (i.e., $C_p(t) = [p(t)/(0.5\rho_a\bar{U}_{500}^2)] \times (\bar{U}_{500}^2/\bar{U}_h^2)$; \bar{U}_{500} is mean wind speed at 500 mm). The mean, standard deviation, maximum and minimum, external pressure coefficients, $C_{pe}(t)$ and internal pressure coefficients, $C_{pi}(t)$ were obtained for each approach wind direction as follows:

$$C_{\bar{p}} = \frac{\bar{p}}{(1/2) \rho_a \bar{U}_h^2}, C_{\sigma_p} = \frac{\sigma_p}{(1/2) \rho_a \bar{U}_h^2}, C_{\hat{p}} = \frac{\hat{p}}{(1/2) \rho_a \bar{U}_h^2}, C_{\check{p}} = \frac{\check{p}}{(1/2) \rho_a \bar{U}_h^2}$$

Where,

- \bar{p} , σ_p , \hat{p} and \check{p} are the mean, standard deviation, maximum and minimum pressures in each 16 s period
- \bar{U}_h is the mean wind speed at the roof-height ($h = 100$ mm)
- ρ_a is the density of air.

The aerodynamic shape factor in AS/NZS 1170.2 (2011) $C_{fig} = C_{peak}/G_u^2$ where C_{peak} is $C_{\hat{p}}$ or $C_{\check{p}}$ obtained in the wind tunnel study, and the velocity gust factor $G_u = \hat{U}_{0.2s}/\bar{U}$

at the roof height. Here $G_u = 1 + 3.4 \sigma_u / \bar{U}$ (Holmes et al., 2014) = $1 + 3.4 \times 0.18 = 1.61$ for this study.

3.4.3 Net pressure fluctuations

External and internal pressure time histories were recorded for five repeat runs for each wind direction, and the time-varying net pressure coefficients, $C_{p,net}(t)$ (as defined in Equation 3.2) were generated for each pressure tap location.

$$C_{p,net}(t) = C_{pe}(t) - C_{pi}(t) \quad (3.2)$$

Net pressure coefficients were obtained for each building configuration listed in Tables 3.4 and 3.5, for a range of openings and porosities, and building volumes. The peak net pressures on different parts of the building are presented with respect to the parameter, S^* . This thesis examined the relationship between peak external and peak internal pressures that generate peak net pressures on different parts of the building envelope. Further, peak net pressures were obtained using the correlation between external and internal pressures and the covariance-integration method defined in Chapter 2.

The mean, standard deviation, and peak (maximum and minimum) external, internal and net pressure coefficients are obtained by taking the average values from five repeat runs each of 16 s duration. These results focus on the mean and peak ratios between the external, internal and net pressures obtained in the same consistent manner. In addition, the spectra and the cross-correlation coefficients (Section 3.4.4) are also derived from the averages of these five repeat runs. The peak net C_p values obtained from the analysis carried out using the covariance-integration method also use this data, enabling these to be directly compared to the measured peak net pressure coefficients.

3.4.3.1 Net pressures factor

The peak external and peak internal pressures at a point do not coincide in time. Therefore peak net pressure coefficients in magnitude are less than the difference between peak external and peak internal pressures (i.e., $|C_{\check{p},net}| < |C_{\check{p}e} - C_{\check{p}i}|$). These differences are related to the correlation between external and internal pressure. Two net pressure factors, F_{C1} and F_{C2} , are defined related to the maximum net pressure coefficient ($C_{\hat{p},net}$) and the

minimum net pressure coefficient, ($C_{\tilde{p},net}$), as defined in Equations 3.3 and 3.4. F_{C1} accounts for the inward pressures while F_{C2} accounts for the outward pressure on the building envelope. Different net pressure factors are obtained for different roof areas shown in Figure 3.12 and Figure 3.13 for each 5° wind direction for intervals. The final net pressure factor for each roof zone is selected based on the critical wind direction which produces the highest peak net pressures, and F_C values are compared with the combination factor K_C given in the wind loading standard AS/NZS 1170.2 (2011).

$$F_{C1}(\theta) = \frac{C_{\tilde{p},net}(\theta)}{C_{\tilde{p}e}(\theta) - C_{\tilde{p}i}(\theta)} \quad (3.3)$$

$$F_{C2}(\theta) = \frac{C_{\tilde{p},net}(\theta)}{C_{\tilde{p}e}(\theta) - C_{\tilde{p}i}(\theta)} \quad (3.4)$$

3.4.4 Correlation coefficient between external and internal pressures

Cross-correlation is a standard method for assessing the relationship between two data series. The measured time-varying internal and external pressure data over the 16 s period represent two sets of data series (i.e., 10240 points for each) that produces the cross-correlation between internal and external pressures with respect to time-lag, τ . The covariance (COV) between internal and external pressures is defined in Equation 3.5 as the product of the fluctuating components of the external pressure at the time, t , and the internal pressure at the time, $(t + \tau)$, over the total time, T . The cross-correlation coefficient, $r_{pepi}(\tau)$, in Equation 3.6, is obtained by dividing the covariance over the time by the standard deviations of external and internal pressures.

$$COV(C_{pe}, C_{pi})(\tau) = \frac{1}{T} \int_0^T [(C_{pe}(t) - \bar{C}_{pe}) \times (C_{pi}(t + \tau) - \bar{C}_{pi})] dt \quad (3.5)$$

$$r_{pepi}(\tau) = \frac{COV(C_{pe}, C_{pi})(\tau)}{C_{\sigma pe} \times C_{\sigma pi}} \quad (3.6)$$

The cross-correlation coefficient, $r_{pepi}(\tau)$, varies between -1 and +1. External and internal pressures are positively correlated (i.e., $0 < r_{pepi}(\tau) < +1$), when both external and internal pressure increase, or decrease together. In contrast, when external pressure increases and internal pressure decrease or vice versa, represents the negative correlation coefficient (i.e., $0 > r_{pepi}(\tau) > -1$) between internal and external pressures. For example, when the wind flows towards a large windward wall opening, positive internal pressure and negative external pressures acting on the roof are negatively correlated while positive internal pressures and positive external pressures on the windward wall are positively correlated.

The net pressures acting on the building envelope are generated by a combination of external and internal pressures as given in Equation 3.2. Therefore the cross-correlation coefficient with $\tau = 0$ relates to combining internal and external pressure at the same instant to give the net pressure. Sharma and Richards (2005) explained that positive internal pressures and external suction pressures are well correlated at zero lag-time and generate large suction net pressures at the windward roof edge of the building with large windward wall opening. This thesis focuses on the cross-correlation coefficients at zero lag-time ($r_{pepi}(0)$) for different parts of the roof and walls on the building envelope. Further, the effect of opening size and location of the openings and building volumes on the correlation coefficient is examined for building configurations listed in Table 3.1. The $r_{pepi}(0)$ is used in covariance integration method method to calculated the theoretical peak net pressure in Chapter 5.

The cross-correlation coefficient, $r_{pepi}(0)$ provides the relationship between the external and internal pressures over the entire time of the time-history signal. This correlation coefficients do not explain the combined effect of peak external and internal pressures on generating peak net pressure. Therefore, local maxima and minima in the external, internal and net pressure time-history signals are defined as peak events when the pressures exceeded the threshold value of $\pm 3C_{\sigma p}$ from the mean (i.e., $C_{\bar{p}} \pm 3C_{\sigma p}$). Figure 3.15 shows the measured internal pressure fluctuation in the building with a large windward opening, the threshold value and the selected peak events for particular time-history.

The internal, external, and net pressure time-histories' peak events are analysed using a conditional probabilistic approach. The occurrence of individual peak events of internal and external time-histories at the same instant shows the contribution of these individual

peak events to generate net peak events. This coincidence of the peak events is further discussed using the standard Venn diagram analyses shown in Figure 3.16 on the building envelope's different locations. Here in the Venn diagram, NEI represents the number of the net (N), external (E) and internal (I) peak events which occur at the same time, while NEI' represents the number of peak events of net and external pressures that occurred at the same time but not for internal (N') pressure peak events.

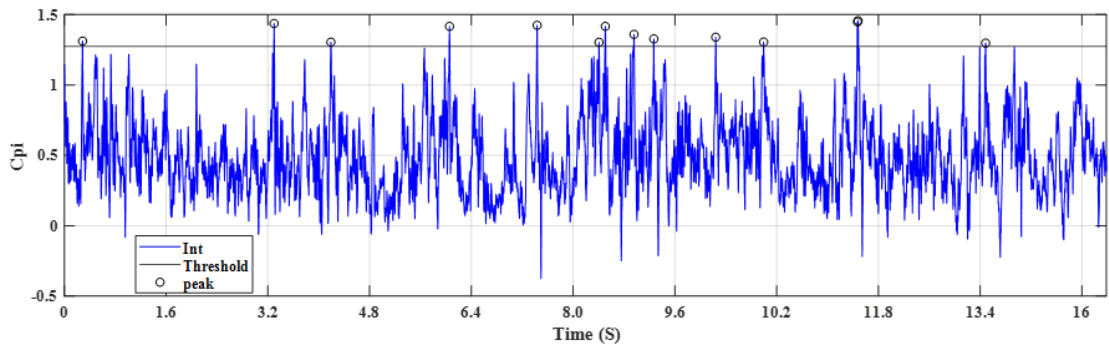


Figure 3.15: Peak events in the internal pressures time-history signal

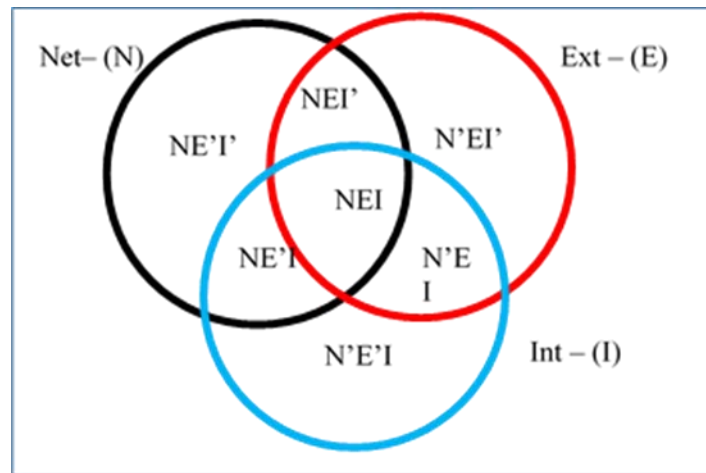


Figure 3.16: Venn diagram for internal, external and net pressure peak events

4 EXTERNAL AND INTERNAL PRESSURE FLUCTUATIONS

This Chapter presents an analysis of the fluctuating external and internal pressures measured on the 1/200 scale wind tunnel models described in Chapter 3. External pressure fluctuations on the walls and roof cladding are presented, along with area-averaged external pressures on the potential wall openings while the wall openings are closed (i.e., nominally sealed building). Further, internal pressure fluctuations are analysed in nominally sealed buildings and building with large wall openings. The effects of the size and location of the wall openings, porosity of the envelope, and building volume on internal pressure fluctuations are also discussed in this Chapter. The detailed study of external and internal pressure dynamics leads to a better understanding of the correlation between internal and external pressure fluctuations and net wind loads on the building envelope that are analysed in the next Chapter.

4.1 External pressure fluctuations- Nominally sealed building

The nominally sealed building (Case #2) consists of 60×3 mm holes and 180×1.5 mm holes uniformly distributed around the walls (detailed in Table 3.2). The measured time-varying external pressures are analysed as pressure coefficients with the statistical properties described in Section 2.1 as $C_{\bar{p}_e}$, $C_{\sigma_{pe}}$, $C_{\hat{p}_e}$ and $C_{\check{p}_e}$.

4.1.1 External pressure on Wall #1

Figure 4.1 shows four pressure taps selected on Wall #1 to analyse the external pressure variations across Wall #1 with approaching wind direction, θ . Figure 4.2 shows mean, standard deviation, maximum, and minimum pressure coefficients on taps FA25, FA31, FC25, and FC31 for wind directions 0° to 360° . On the windward wall ($\theta = 0^\circ \pm 45^\circ$), the highest mean external pressure, of about +0.6 to +0.7, is observed at the middle of the wall (FC25) for $\theta = 0^\circ$ and the edge of the wall (FA25) for $\theta = 40^\circ$ illustrating the variation of the stagnation zone with wind direction along the windward wall. The $C_{\bar{p}_e}$

variation matches other previous model scale studies (i.e., Holmes, 1979, Guha et al. 2011, etc.).

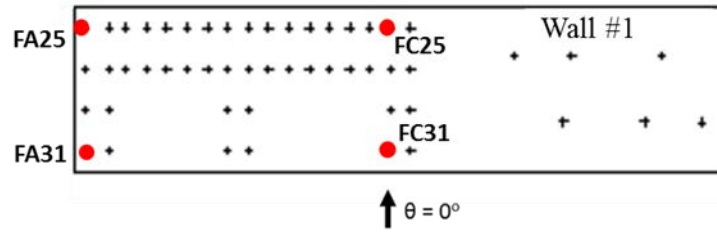
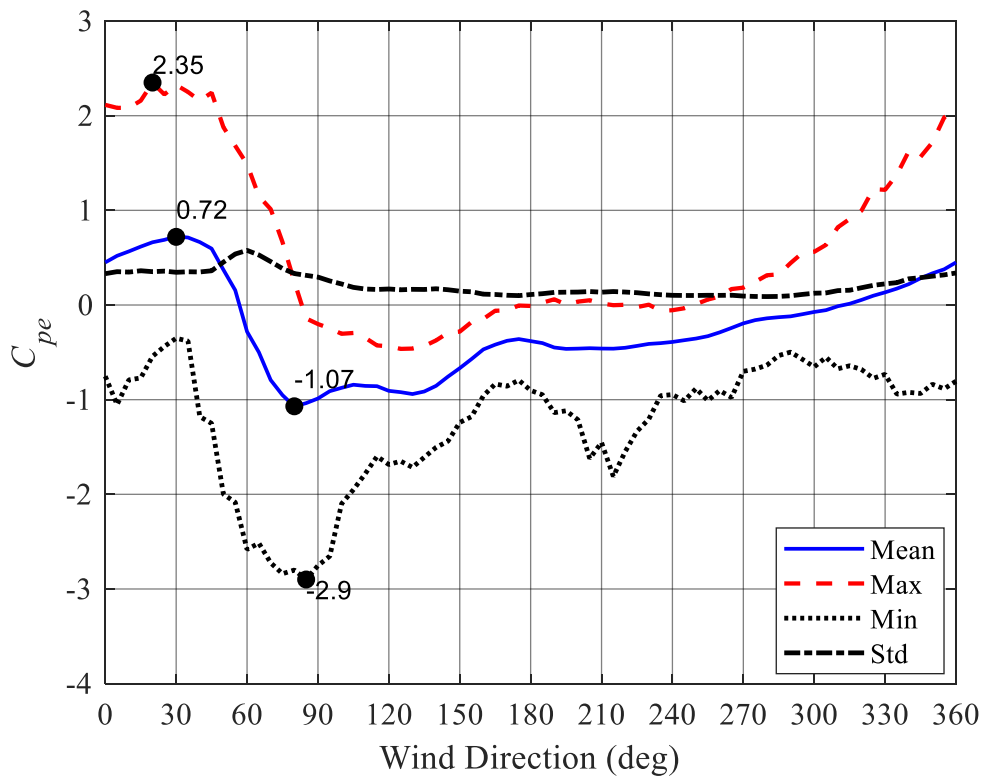
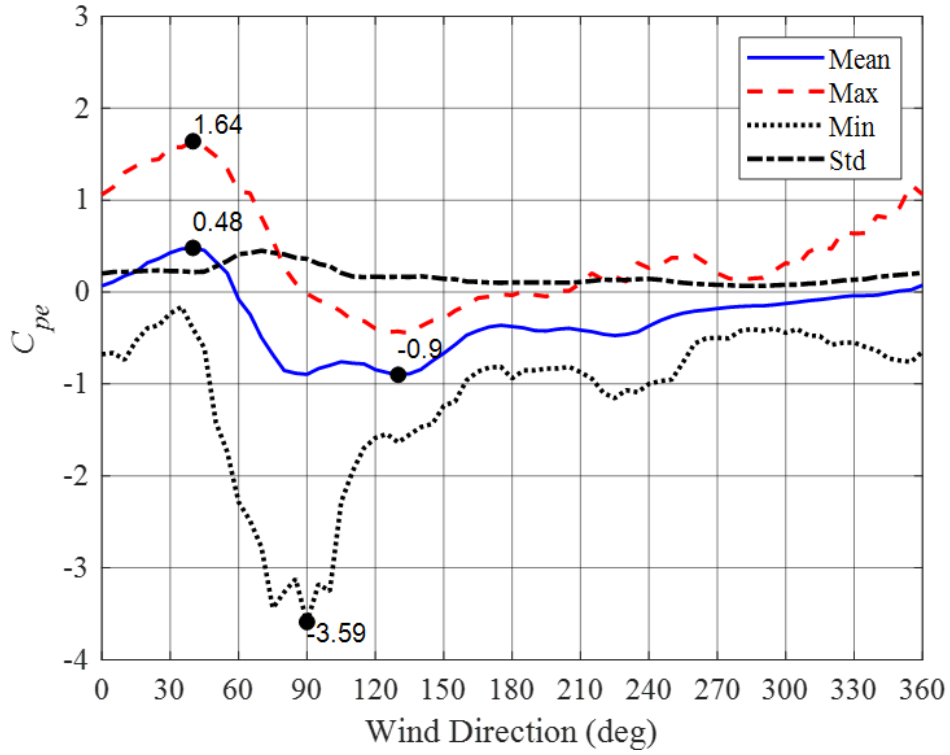


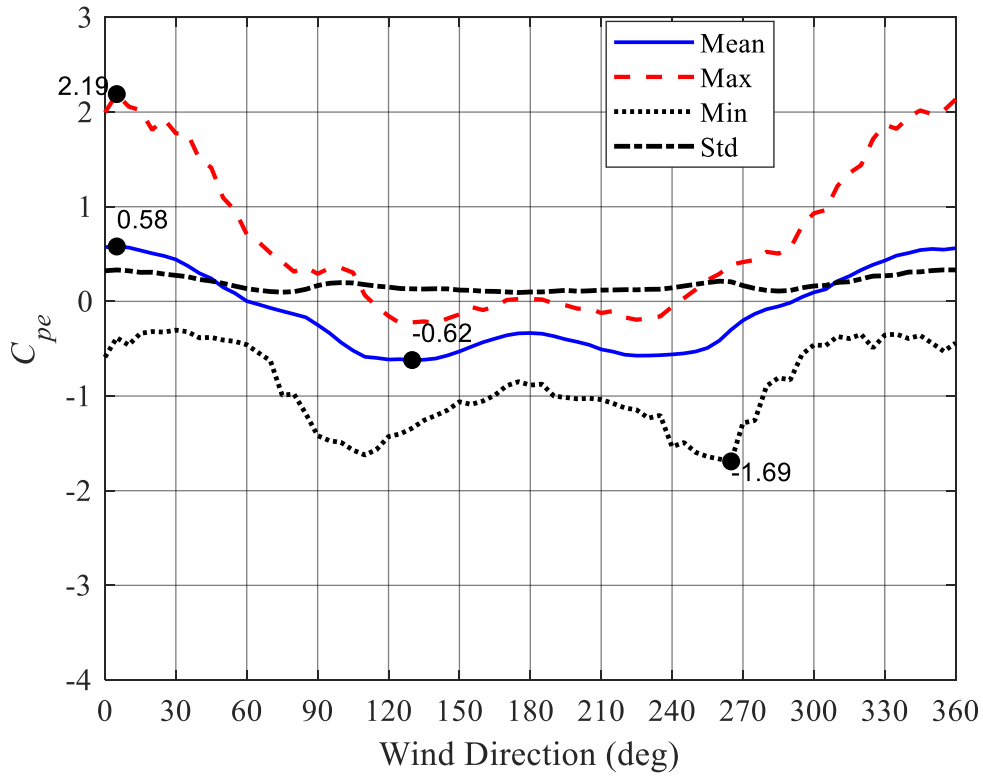
Figure 4.1: Selected external pressure taps in the Wall #1



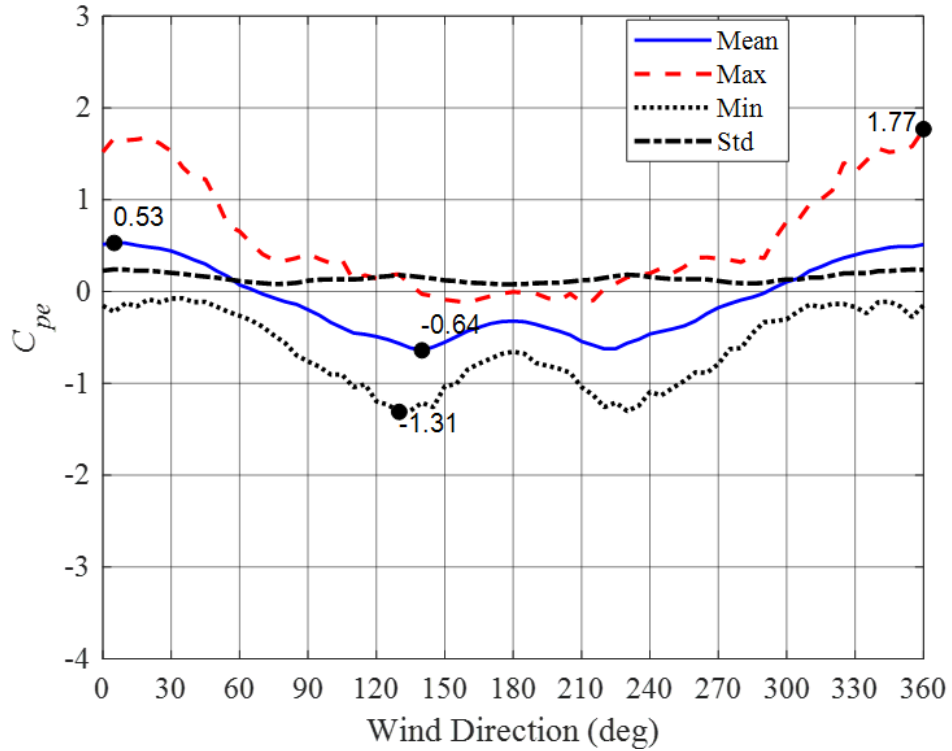
(a) Case #02- FA25



(b) Case #02- FA31



(c) Case #02- FC25



(d) Case #02- FC31

Figure 4.2: Mean, maximum, minimum and standard deviation pressure coefficients for FA 25, FA31, FC25 and FC31 on Wall #1

For wind directions, $\theta = 90^\circ \pm 45^\circ$, Wall #1 is on the side of the building, and experiences large external suction pressures at the pressure taps next to the leading edge (FA25, and FA31), as they are in the flow separation region. The largest peak suction pressure coefficient, C_{pe} of about -3.6 was recorded at FA31 for $\theta = 90^\circ$, due to flow separation at the leading edge of this wall compared to the middle of Wall #1 (FC25) which recorded a C_{pe} of -1.6 for $\theta = 110^\circ$, illustrating the significant difference between pressures in the flow separation and reattachment regions.

For wind directions $\theta = 180^\circ \pm 45^\circ$, Wall #1 is the leeward wall of the building (i.e., wake region) and is subjected to small suction pressures with less variation from the mean (small standard deviation), matching previous studies with a mean external pressure coefficient C_{pe} of about -0.5.

4.1.2 External pressure on the roof

Figure 4.3 shows six external pressure taps selected on the roof to analyse the external pressure variation with wind direction. The variations of the external pressures across the roof are discussed with respect to the distance from the windward roof edge, i.e., leading roof edge, upwind half of the roof (about h from the leading edge) and downwind half of the roof (greater than h from the leading edge), based on the wind flow direction.

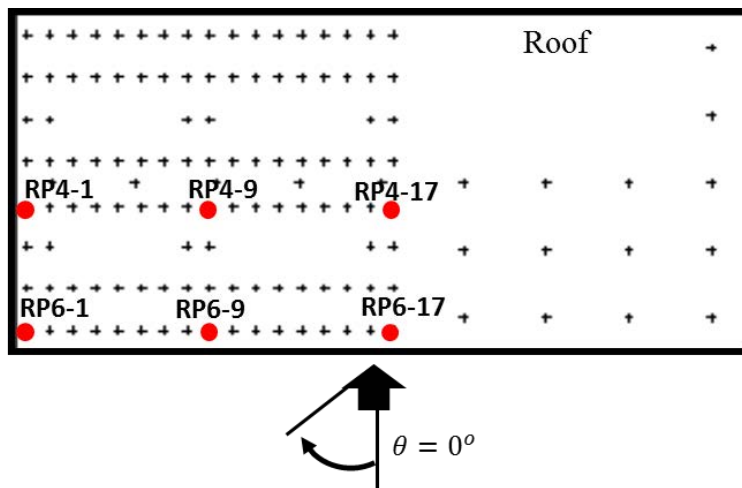


Figure 4.3: Selected external pressure taps on the roof

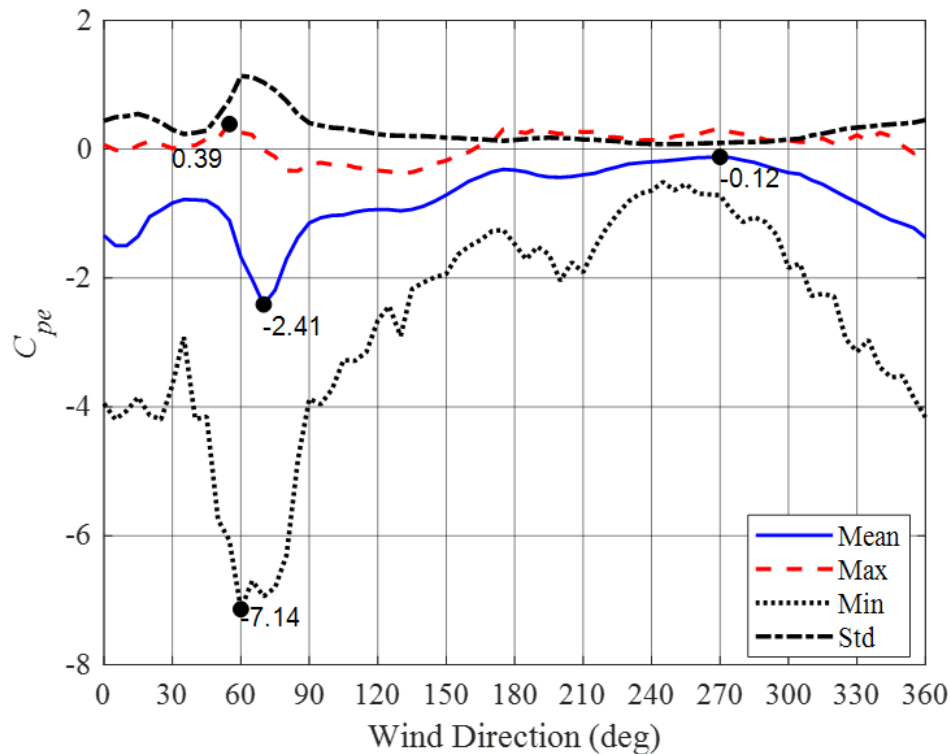
Figure 4.4 shows the $C_{\bar{p}_e}$, $C_{\sigma p_e}$, $C_{\hat{p}_e}$ and $C_{\check{p}_e}$ on the six selected roof taps with wind direction $\theta = 0^\circ - 360^\circ$. Pressure taps RP6-1, RP6-9 and RP6-17 capture the external pressures behind the roof leading edge for wind direction $\theta = 0^\circ$, RP6-1 is located in the corner of the roof, and RP6-9 and RP6-17 are about one building height length ($1h$) and $2h$ from the roof corner respectively. RP4-1, RP4-9 and RP4-17 are parallel to the first row of pressure taps ($1h$ apart) and are situated close to the middle of the roof.

For wind directions $\theta = 0^\circ \pm 45^\circ$, RP6-1, RP6-9 and RP6-17 experience large mean and peak suction pressures at the leading edge of the roof, with a highest $C_{\bar{p}_e} \approx -1.5$ at the windward corner ($\theta = 5^\circ$) at RP6-1 compared to $C_{\bar{p}_e}$ of -1.2 ($\theta = 0^\circ$) at the middle of the roof (RP6-17). Figure 4.4 (d) and (f) (taps RP4-9 and RP4-17) show that the $C_{\bar{p}_e}$, about $1h$ from the leading edge, are 20-30% less than the mean pressure near the leading edge.

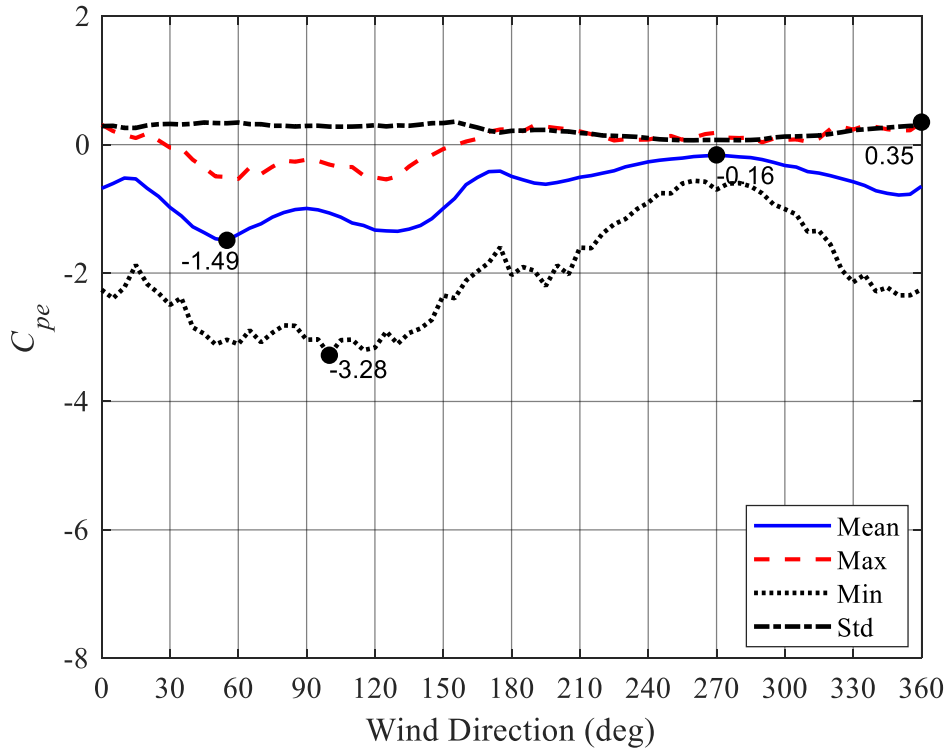
For wind directions $\theta = 90^\circ \pm 45^\circ$, RP6-1 and RP4-1 are located near the leading edge, RP6-9 and RP4-9 are about $1h$ from the leading edge and RP6-17, and RP4-17 are about

$2h$ from the leading edge and are in the middle of the roof. Figure 4.4(a) shows that the formation of the conical vortices generate large magnitude mean and fluctuating suction pressures for roof corner RP6-1. The highest magnitude minimum pressure coefficient of -7.1 at RP6-1 occurred at $\theta = 60^\circ$, and C_{pe} decreases towards the middle of the roof, as shown in Figure 4.4(c) and Figure 4.4(e). Figure 4.4(d) and Figure 4.4(f) show a reduction in the magnitude of minimum external pressures near the reattached flow region (taps RP4-9 and RP3-17).

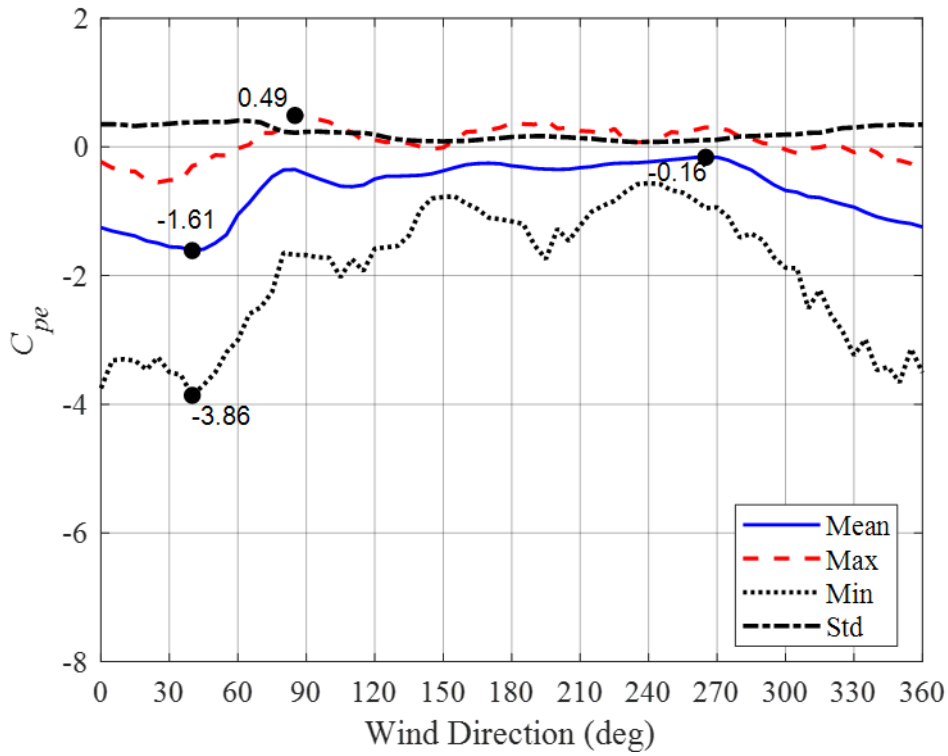
For wind directions $\theta = 180^\circ \pm 45^\circ$, roof pressure taps are located about $1h$ away from the leading edge where smaller mean and minimum external suction pressures are observed. The minimum external suction pressure close to the middle (RP4) is higher compared to the pressure taps further down nearly (\approx) $2h$ from the leading edge (RP6). Similarly, for wind directions $\theta = 270^\circ \pm 45^\circ$, the small magnitude in minimum external pressures are identified from the middle of the roof towards the leeward roof edge (i.e., RP-17 to RP4-1). These external pressure fluctuations are similar in magnitude to the studies conducted by Ginger and Letchford (1999) and Ginger et al. (1997), and many other researchers.



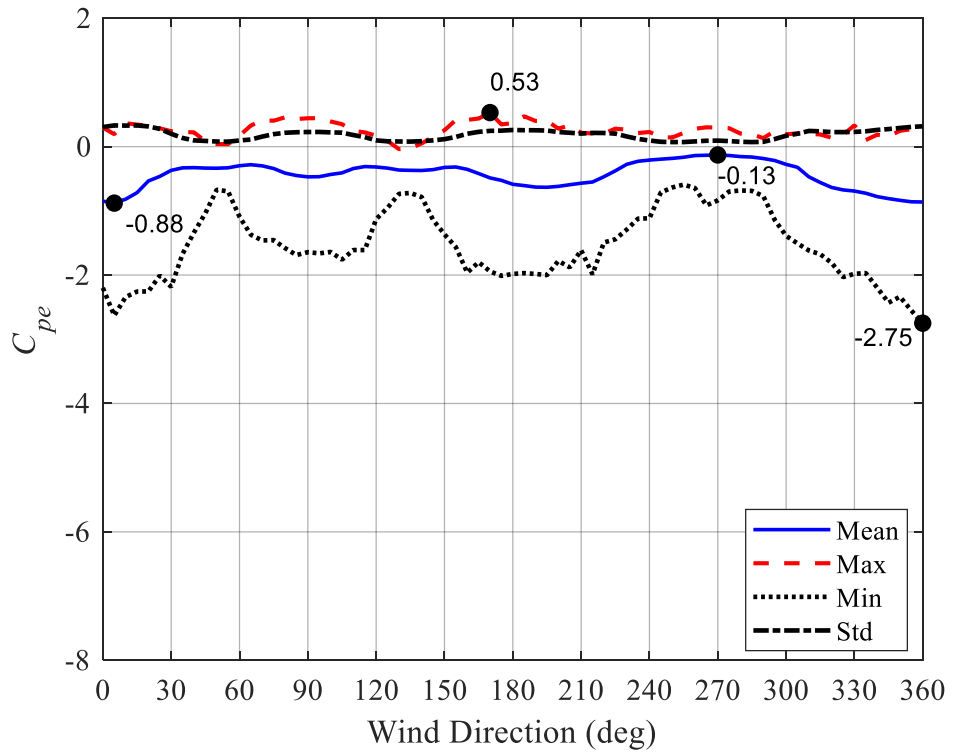
(a) Case #02- RP6-1



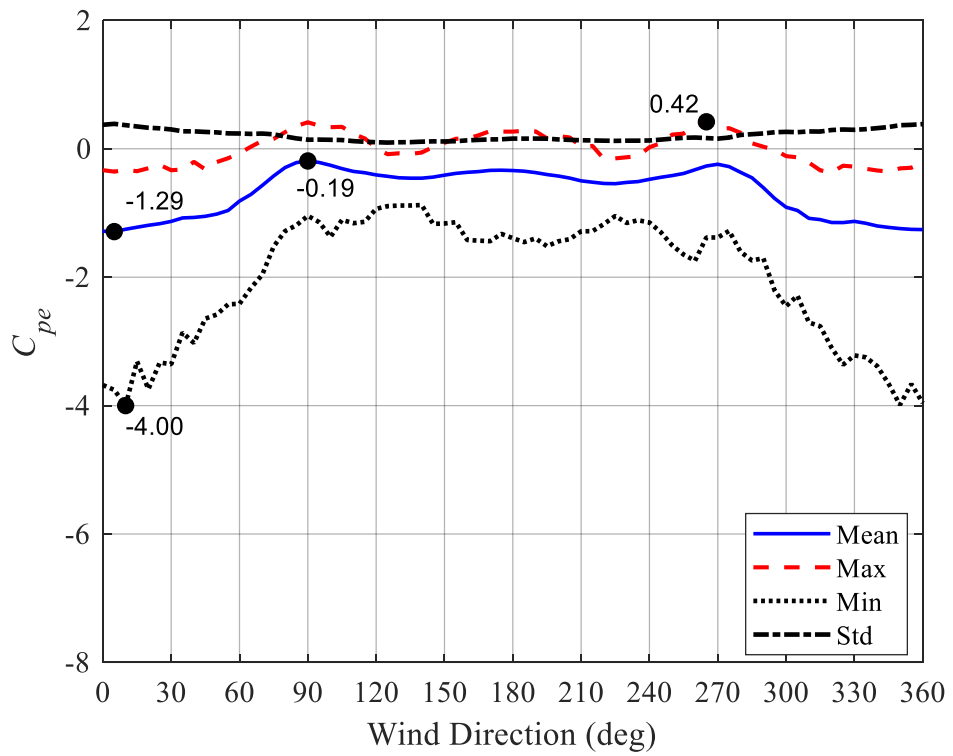
(b) Case #02- RP4-1



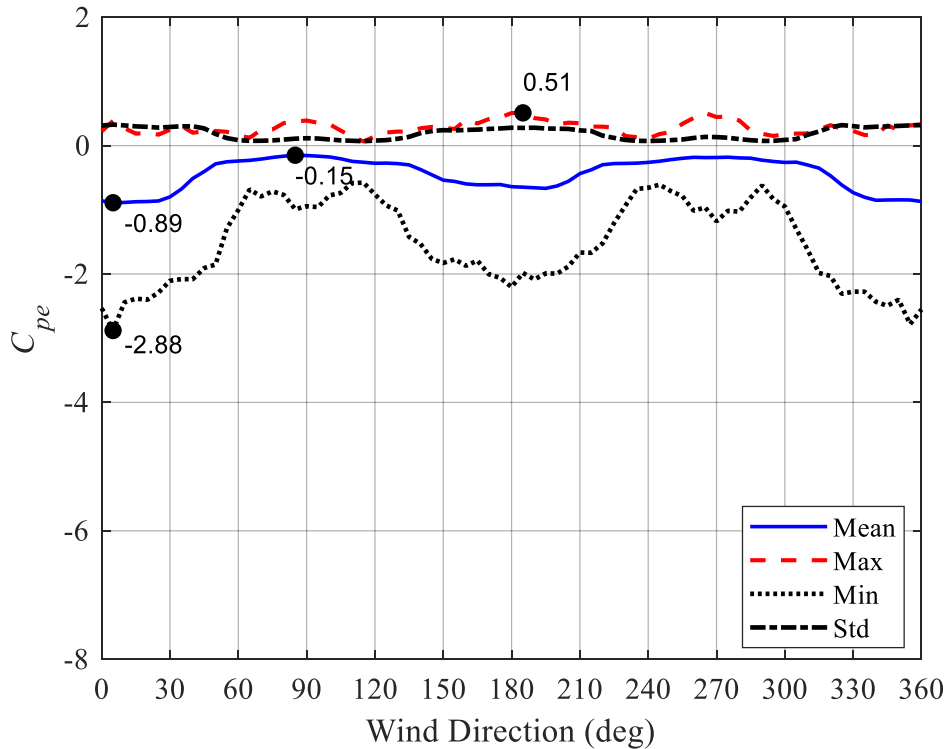
(c) Case #02- RP6-9



(d) Case #02- RP4-9



(e) Case #02- RP6-17



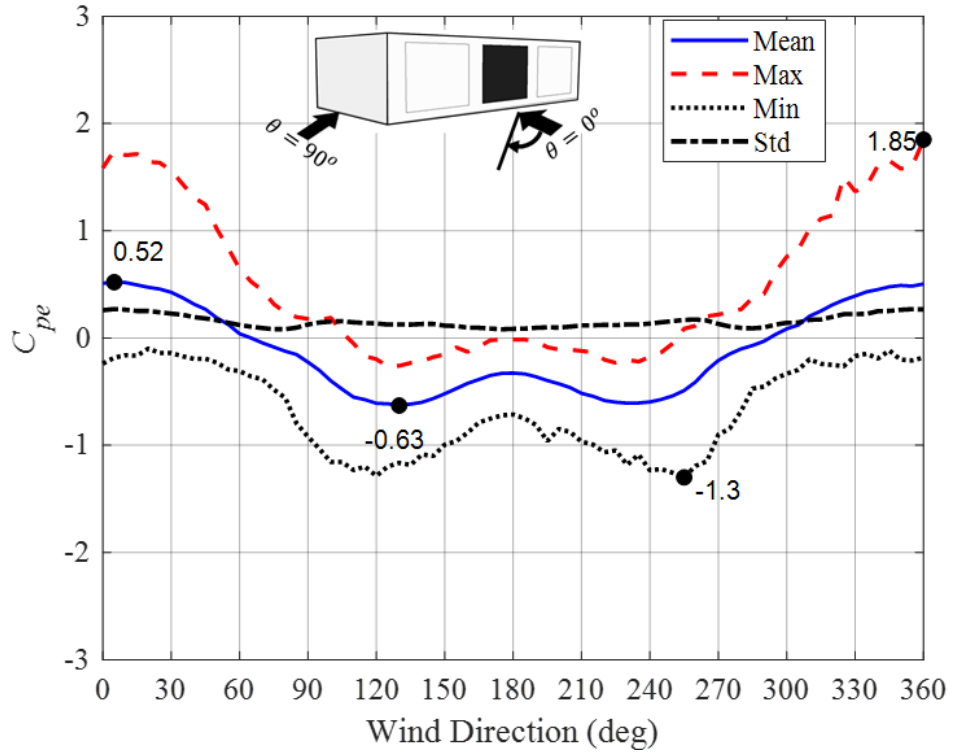
(f) Case #02- RP4-17

Figure 4.4: Mean, maximum, minimum, and standard deviation coefficients- roof cladding, RP6-1, RP4-1, RP6-9, RP4-9, RP6-17 and RP4-17 in Case #02

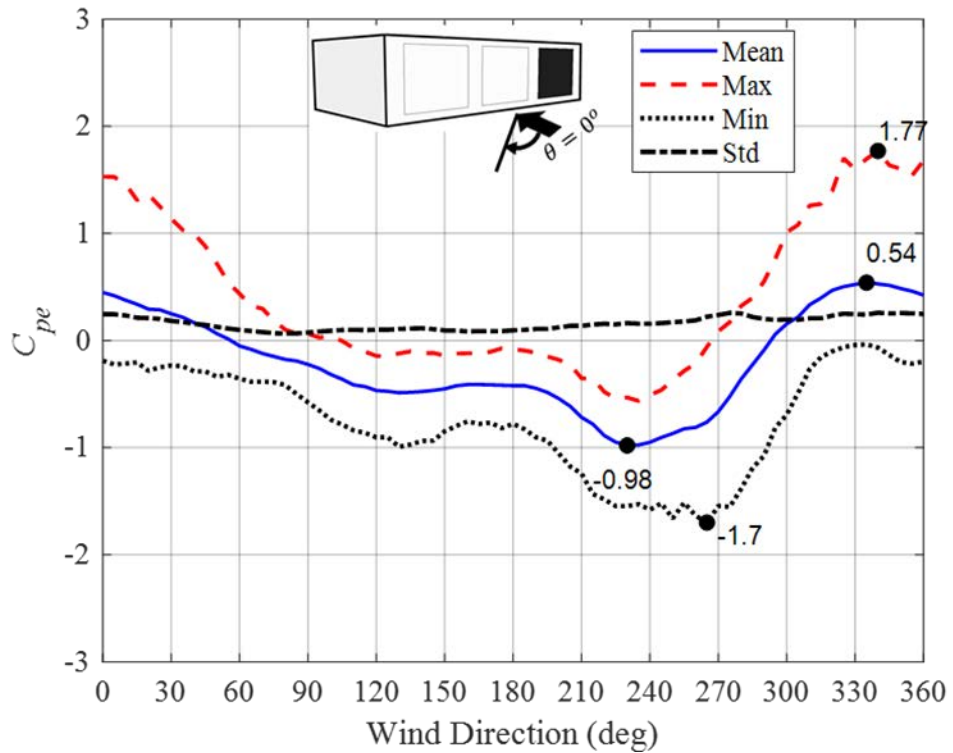
4.1.3 Area-averaged external pressures on openings

External pressures measured on individual taps on Wall #1 and #4 of the nominally sealed building are used to obtain the area-averaged external pressure coefficients on opening areas of LO1, LO2, LO5 and LO6. Area-averaged external pressures on LO1 and LO2 were derived by numerically averaging the simultaneously measured pressures on taps on each opening area. Area-averaged external pressures on LO5 and LO6 are obtained by averaging two taps and six taps, respectively within these areas (see Figure 3.8).

Figure 4.5(a)-(b) show area-averaged external pressures on LO1 and LO2 on Wall #1 for $\theta = 0^\circ$ to 360° . The largest area-averaged positive C_{pe} on LO1 and LO2 is about +0.55 when wind flows from $\theta = 0^\circ \pm 45^\circ$. The largest C_{pe} of about +1.85 and +1.77 are obtained for LO1 and LO2 for wind directions $\theta = 5^\circ$ and 340° respectively, and the largest C_{pe} of -1.2 was for LO1 and -1.7 for LO2, for $\theta = 120^\circ$ and 265° , respectively. For wind direction $\theta = 180^\circ$, Wall #1 becomes the leeward wall and area-averaged C_{pe} is about -0.75 on both LO1 and LO2, but slightly higher on the LO2. The variations of peak area-averaged external pressures are based on the location of the opening due to the spatial variation of external pressures.



(a) Area-averaged external pressures on opening LO1 – Case #02

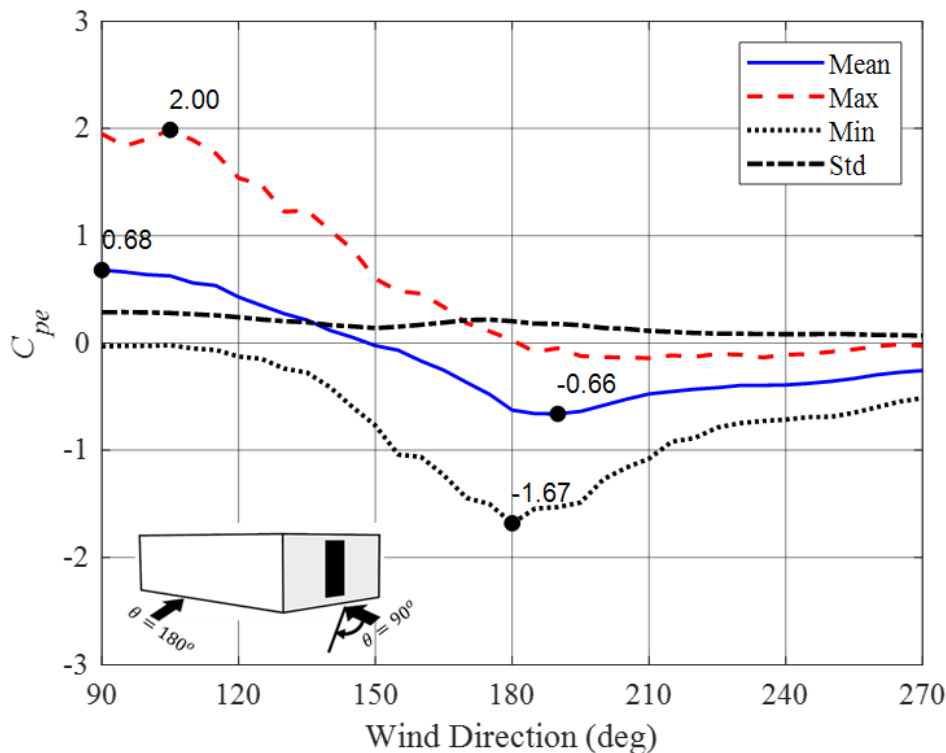


(b) Area-averaged external pressures on opening LO2 – Case #02

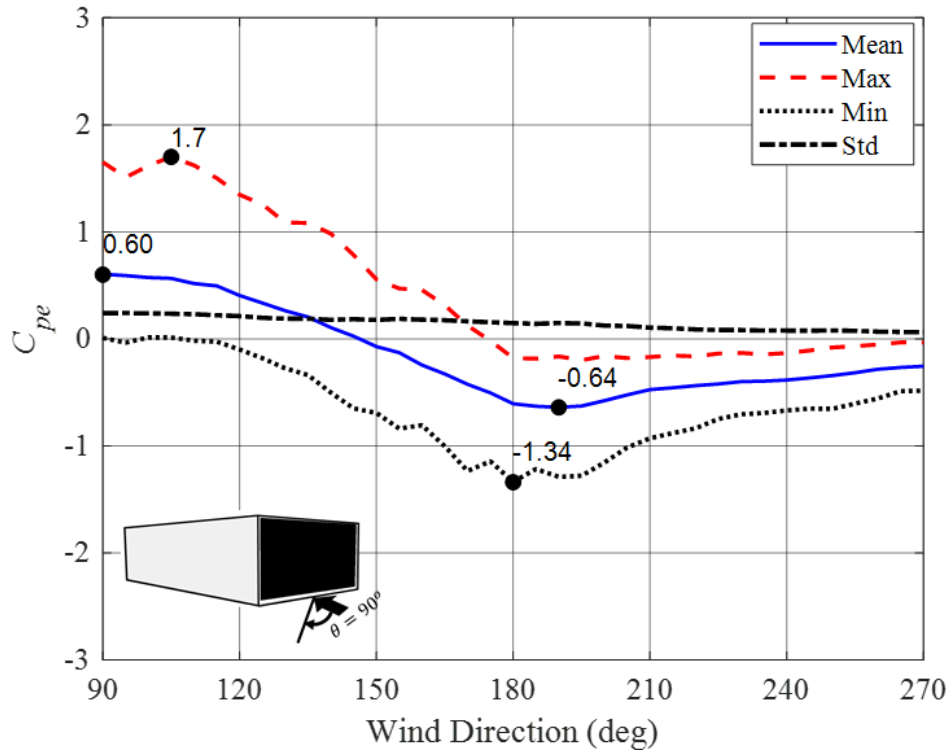
Figure 4.5: Area-averaged mean, maximum, minimum and Standard deviation pressure coefficients on the opening area LO1 and LO2 – Nominally sealed building

Figures 4.6(a) and 4.6(b) present the area-averaged external pressures on LO6 and LO5 for wind directions 90° to 270° . The area-averaged $C_{\bar{p}_e}$ on LO6 and LO5 are $+0.6$ and $+0.68$ when these areas are on the windward wall ($\theta = 90^\circ$). The largest $C_{\hat{p}_e}$ and $C_{\check{p}_e}$ for LO6 (whole wall opening) of $+1.7$ and -1.34 occurred at $\theta = 105^\circ$ and 180° , when the LO6 is on the windward and sidewall, respectively. Additionally, $C_{\hat{p}_e}$ on LO5 is 18% higher than LO6 for wind directions $90^\circ \leq \theta \leq 120^\circ$, and $C_{\check{p}_e}$ is 25% more negative for wind directions 160° to 200° . The opening LO5 is closer to the stagnation zone on the windward wall, which has a larger mean positive pressure than LO6, which is a combination of pressures at the stagnation point and lower mean positive pressures close to windward edge. The increasing lack of spatial correlation with increasing area reduces the positive and negative peak pressures with an increasing area from LO5 to LO6 (i.e., LO6 is $6 \times$ LO5).

The detailed study on area-averaged external pressures on the windward wall, leeward wall, and side wall were conducted and analysed the area reduction factors for these walls as presented in Appendix B.



(a) Area-averaged external pressures on opening LO5- Case #02



(b) Area-averaged external pressures on opening LO6- Case #02

Figure 4.6: Area-averaged mean, maximum, minimum and Standard deviation pressure coefficients on the opening area LO5 and LO6 – Nominally sealed building.

4.1.4 External pressure spectra

The pressure fluctuations are further characterised by the non-dimensional pressure spectrum $fSC_p(f)$, which gives the distribution of energy with frequency, f . Accordingly, external pressure spectra of the area-averaged external pressures on the windward wall, side wall, and leeward wall of the nominally sealed building, for $\theta = 0^\circ$ are presented in Figure 4.7. Figure 4.7 shows the energy distributions of the area-averaged pressure fluctuations on the windward wall are induced by the approaching wind turbulence (see velocity spectrum in Figure 3.2). Figure 4.7 further shows the energy distributions of external pressures on the side wall and leeward wall are induced by the wind and building generated turbulence. The pressure fluctuations on side walls are greatly influenced by building induced fluctuations in the flow separation and reattachment regions. Figure 4.7 shows the area-averaging of these pressures along the wall has less energy than the windward wall, with most of the energy at pressure fluctuations less than 15Hz. Further, Figure 4.7 shows the leeward wall pressure (wake)

fluctuations have significantly less energy than fluctuating on windward and side walls. Ginger et al. (1997) in a full-scale study and Guha et al. (2011) in a model-scale study have shown similar spectra for external pressure fluctuations on the windward wall, side wall, and leeward wall.

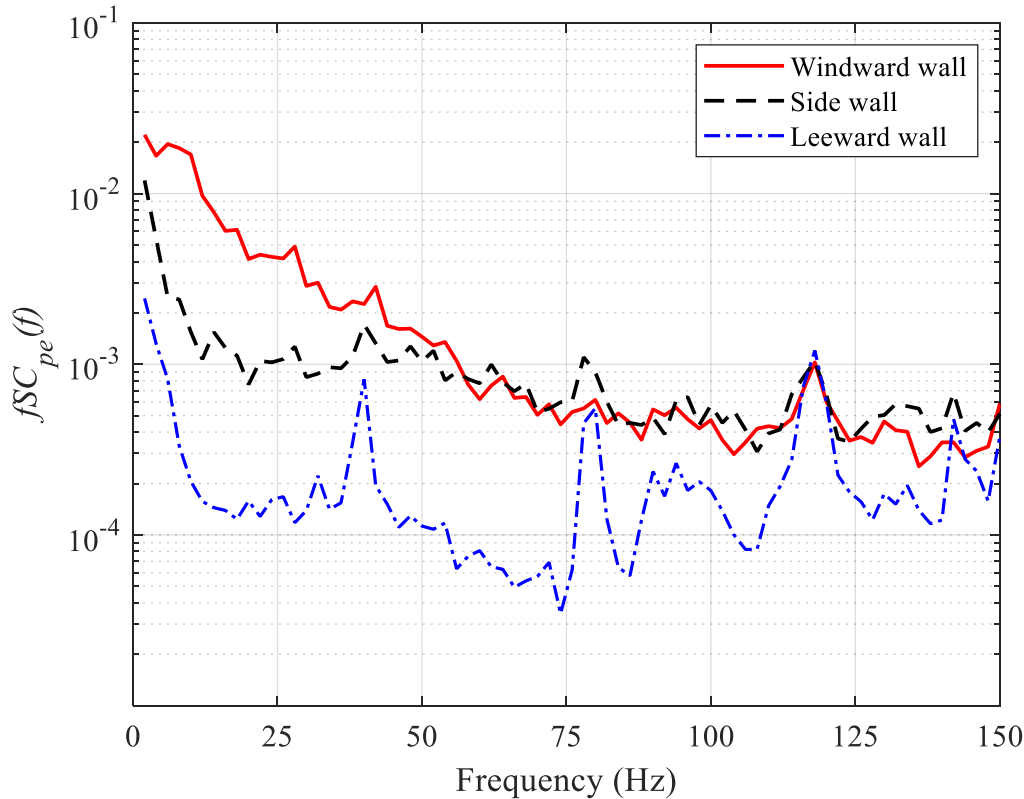


Figure 4.7: External pressures spectra for windward wall (Wall #1), side wall (Wall #2) and leeward wall (Wall #3) at $\theta = 0^\circ$

4.2 Internal pressure fluctuations

Figure 4.8(a) and (c) show a single 16 s (model-scale) record of temporally varying internal pressure fluctuations in the nominally sealed building (Case #02) for $\theta = 0^\circ$ and building with a large opening in Case #09 for $\theta = 90^\circ$ measured at the four internal taps. Figure 4.8(c) and (d) show cross-correlation between internal pressure taps for Cases #02 and #09). The internal pressure at all four locations in the building have spatially similar fluctuations, and are fully correlated giving $r_{pip_i}(0) = +1$ as shown in Figure 4.8(b) and

(d). Therefore taking an average of the pressures from four taps or considering a single tap gives the internal pressure fluctuations in the building.

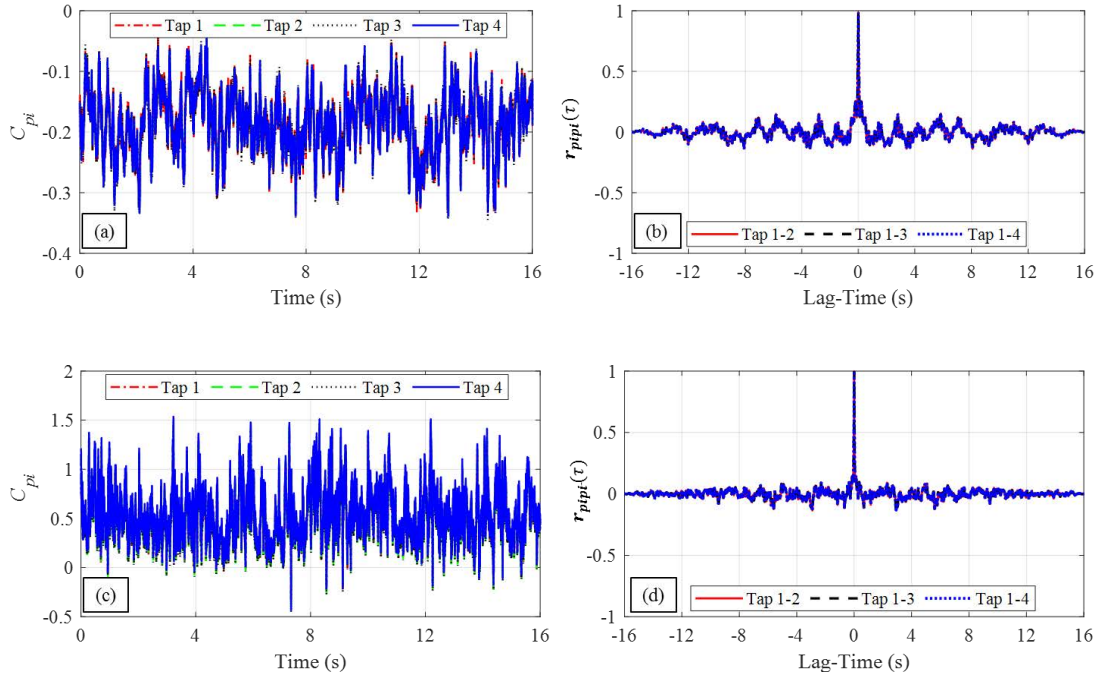


Figure 4.8: Internal pressure fluctuations at four locations in the building and cross-correlation between the taps (a)-(b) nominally sealed building at $\theta = 0^\circ$, (c)-(d) Building with a large opening when opening perpendicular to approach wind direction

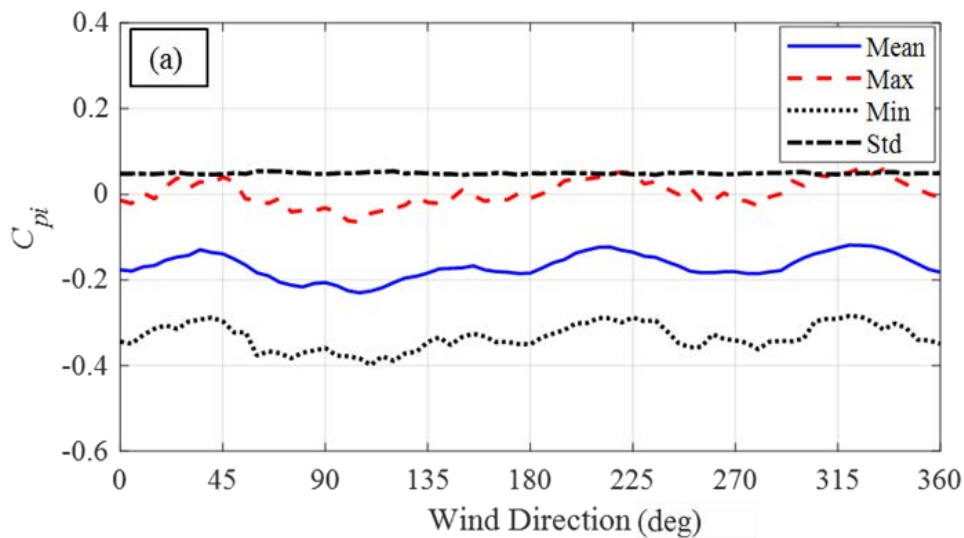
4.2.1 Nominally sealed building

Figure 4.9(a) and (b) show the mean, standard deviation, minimum and maximum internal pressure coefficients for the nominally sealed buildings with two different porosities (Case #02 and #03) for wind directions $\theta = 0^\circ$ to 360° . In Case #02 and #03, the C_{pi} is negative and fluctuates around -0.2, which is in good agreement with the quasi-steady pressure coefficients in AS/NZS 1170.2. Further, C_{pi} and C_{pi} fluctuate around -0.05 and -0.35, respectively for all wind directions.

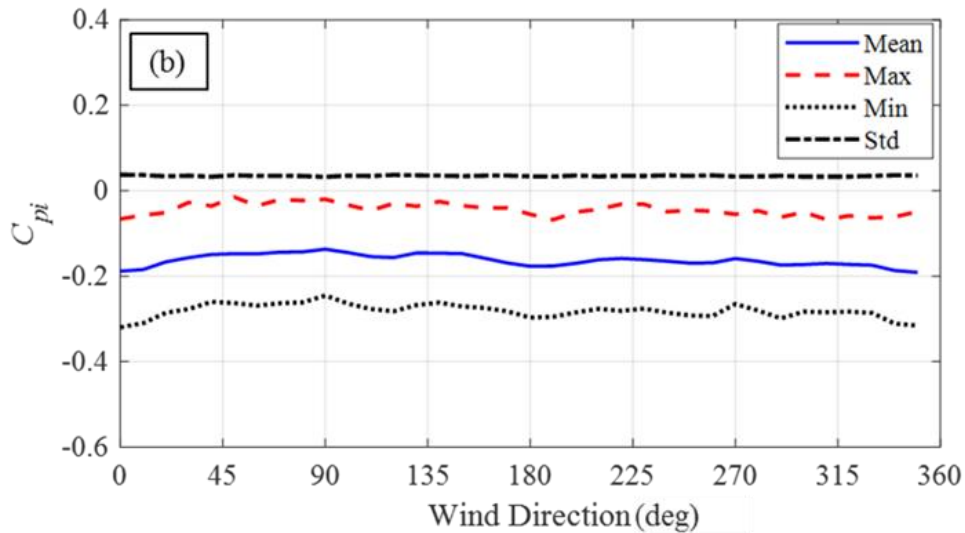
The total porous area in the windward wall, A_{pW} is less than the total porous area in leeward and side walls, A_{pL} (i.e., $A_{pW}/A_{pL} < 1$) for all wind directions. The combination of negative pressures on the side and leeward walls generates mean suction internal pressures according to the continuity equation (Equation 2.2). The restricted flow in and out of the building through the porous holes around the envelope attenuate the internal

pressure fluctuations relative to external pressure fluctuations, reducing fluctuating internal pressures compared to the area-averaged external pressures on walls. Thus, the $C_{\bar{p}i}$, $C_{\hat{p}i}$, and $C_{\tilde{p}i}$ do not vary significantly in the nominally sealed building when the porosity is decreased in Case #03 compared to Case #02. However, in full-scale studies by Humphreys et al. (2020) showed that the internal pressure fluctuations in the nominally sealed building could be significantly influenced by levels of building porosity.

The similarities in Figure 4.9(a) and (b) show that the wind tunnel model scale studies may not satisfactorily simulate the envelope porosity because the Re of the flow through the small holes does not satisfactorily simulate the flow in the full-scale studies. In this model-scale study, Re is small when the porous hole diameter is 3 mm in 6 mm thick wall. However, in full-scale, when the length scale ratio is 200 and wind speeds are higher Re number very much larger, which can be in the turbulent range. Further, the shapes of the porous openings are different and may significantly effect the flow through the openings in full-scale industrial buildings.



(a) Case #02- 0.62% porosity



(b) Case #03- 0.32% porosity

Figure 4.9: Mean, standard deviation, minimum, and maximum internal pressure coefficient for $\theta = 0^\circ - 360^\circ$ for the nominally sealed buildings

4.2.2 Building with a large opening in a wall

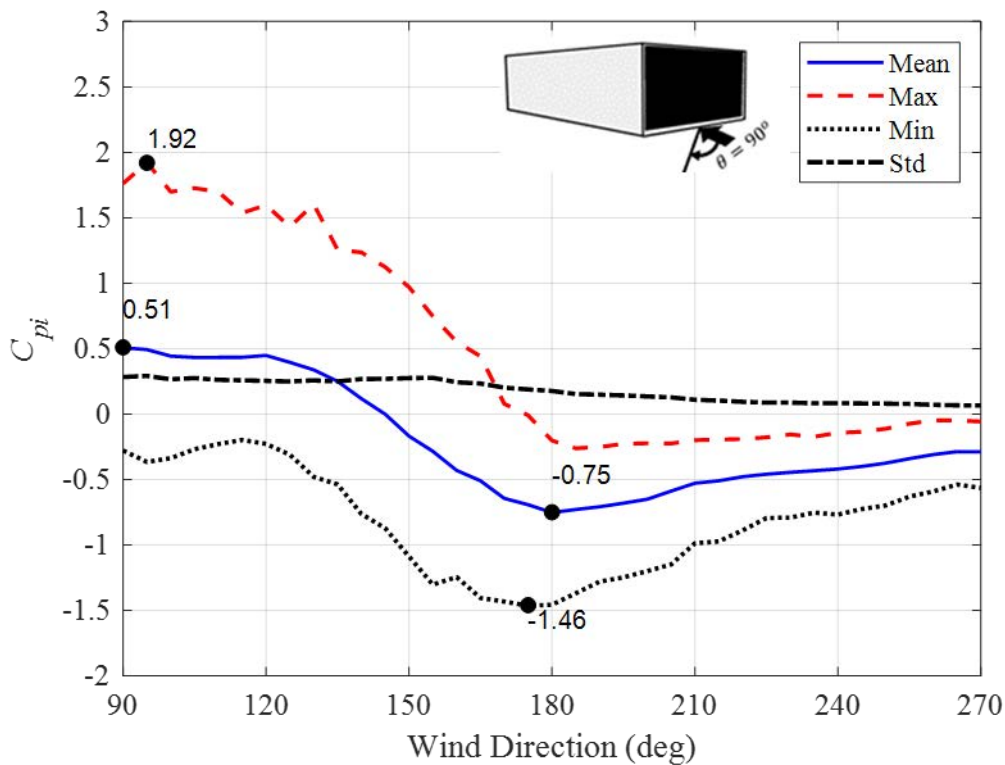
(i) Effect of the opening area

The effect of the size of a single opening on the internal pressure fluctuations is studied for three openings LO6, LO5, and LO4 (Cases #09, #11, and #12 in Table 3.4, respectively). The variation of mean, standard deviation, maximum, and minimum internal pressure coefficients for $\theta = 90^\circ$ to 270° for Cases #09, #11, and #12 are presented in Figure 4.10(a)-(c).

The $C_{\bar{p}_i}$ are positive and large when the approaching wind blows towards the openings (i.e. $\theta = 90^\circ$ to 135°). Figure 4.10 shows that as the windward opening area to wall area ratio decreases, the positive mean internal pressure increases. These values closely follow the area-averaged $C_{\bar{p}_e}$ shown in Figure 4.6 for Case #09 and #11 (LO6 and LO5). The largest positive $C_{\bar{p}_i}$ is +0.51, +0.7, and +0.82 for Cases #09, #11, and #12, respectively when $\theta = 90^\circ$. Furthermore, the largest negative mean internal pressure coefficients are -0.75 for Case #09 at $\theta = 180^\circ$, -0.72 for Case #11 at $\theta = 190^\circ$, and -0.63 for Case #12 at $\theta = 185^\circ$ (i.e., when the opening is on the sidewall). Internal pressure is more negative in

Case #09 compared to the other two cases since the portion of LO6 is closer to the side wall leading edge at $\theta = 180^\circ$.

When the opening area becomes larger, the peak internal pressure decreases due to the lack of spatial correlation of the external pressures on the opening in Cases #09, #11, and #12. However, the peak internal pressure amplifies due to Helmholtz resonance for each building configuration and the measured peak internal pressures in Figure 4.10 are larger compared to the area-averaged peak external pressures. For example, the largest $C_{\hat{p}i}$ of +2.27 at $\theta = 90^\circ$ and $C_{\check{p}i}$ of -1.59 at $\theta = 180^\circ$ in Figure 4.10(c) are about 20% and 13% larger in magnitude compared to area-averaged $C_{\hat{p}e}$ (+2.0) and $C_{\check{p}e}$ (-1.34) for Case #11 in Figure 4.6. The $C_{\hat{p}i}$ and $C_{\check{p}i}$ in Figure 4.10(a)-(b) follow a similar pattern as $C_{\hat{p}e}$ and $C_{\check{p}e}$ in Figure 4.6 for $\theta = 90^\circ$ to 270° .



(a) Case #09 - LO6

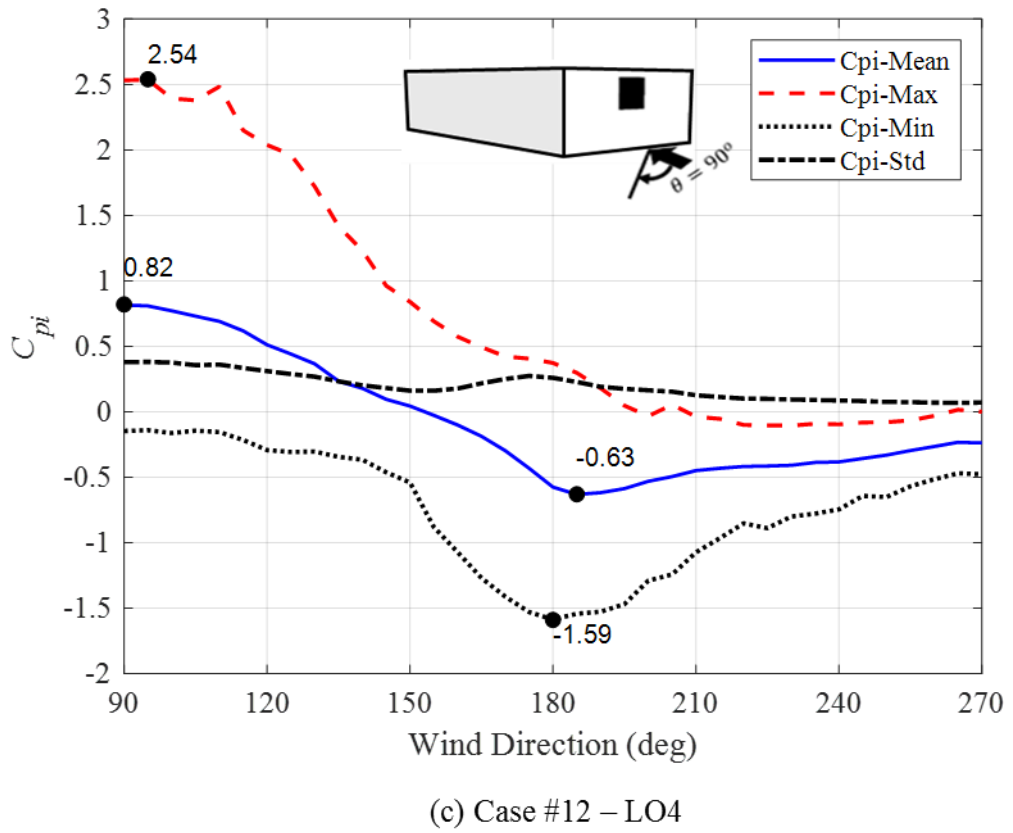
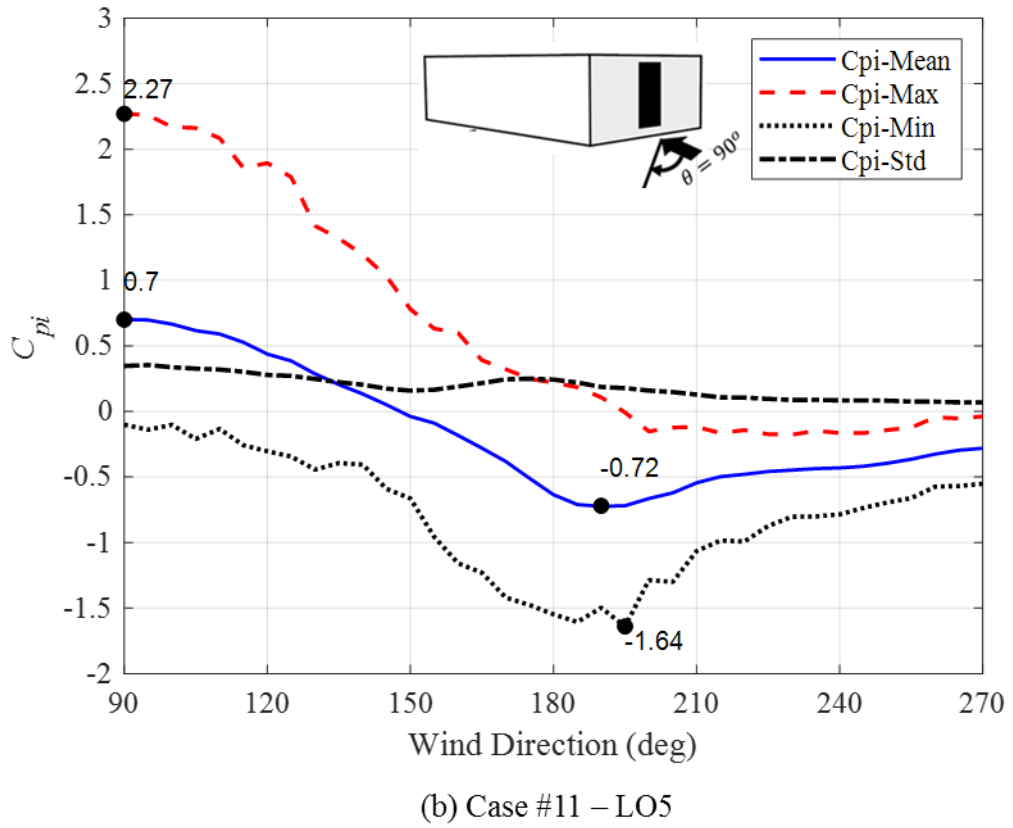


Figure 4.10: Mean, standard deviation, minimum, and maximum internal pressure coefficient for single large opening on Wall #4 – Cases #09, #11, and #12

Figure 4.11(a) and (b) show the area-averaged external pressure spectra on the opening area of LO6 (i.e., Wall #4) and the internal pressure spectra for Cases #09, #11, and #12 for wind directions, $\theta = 90^\circ$ and $\theta = 180^\circ$. Helmholtz resonance is observed at f_H of 38 Hz, 32 Hz, and 28 Hz for Cases #09, #11, and #12. Accordingly, f_H increases with increasing the opening area, which is consistent with $f_H = 1/2\pi \sqrt{((a_s^2 \sqrt{A})/(C_I V))}$. Furthermore, Figure 4.11(a) and (b) illustrates that Helmholtz resonance occurred at the same frequencies for windward wall opening ($\theta = 90^\circ$) and side wall opening ($\theta = 180^\circ$). However, the magnitude of the internal pressure spectra changed in Figure 4.11(b) with relative to the external pressure fluctuation on the opening.

For Cases #09, #11, and #12, the inertial coefficients, C_I are calculated as 4.4, 2.9 and 2.7, respectively using the measured Helmholtz frequencies f_H , where $a_s = 340$ m/s, and known area of the opening and volume of the model. Sathopolulos and Luchian (1989), Vickery and Bloxham (1992), Ginger (1997), Sharma and Richards (1997), Xu et al. (2014), and Humphreys et al. (2019) stated that a range of C_I values vary within the range of 0.8 to 2.0 from wind tunnel and full-scale studies. However, no other studies have examined very large openings, including whole wall opening (i.e. 3-wall building) before and the calculated C_I values are higher than the theoretical value of 0.89 for steady flow through and orifice connecting infinite volumes, as explained by Vickery (1986).

A secondary peak is observed at higher frequencies for all single opening configurations. For example, a secondary peak for Case #12 occurred at about 80 Hz an order of magnitude of 10^{-4} below the Helmholtz resonance magnitude. Sharma and Richards (2003), Kim and Ginger (2013) also observed a similar secondary peak and the order of magnitude is small. Ghanadi et al. (2013, 2014) also observed harmonic in Helmholtz resonance in a self-excited Helmholtz resonator model. The energy at the peak is in order of magnitude lower and therefore does not significantly influence the magnitude of internal pressure fluctuations.

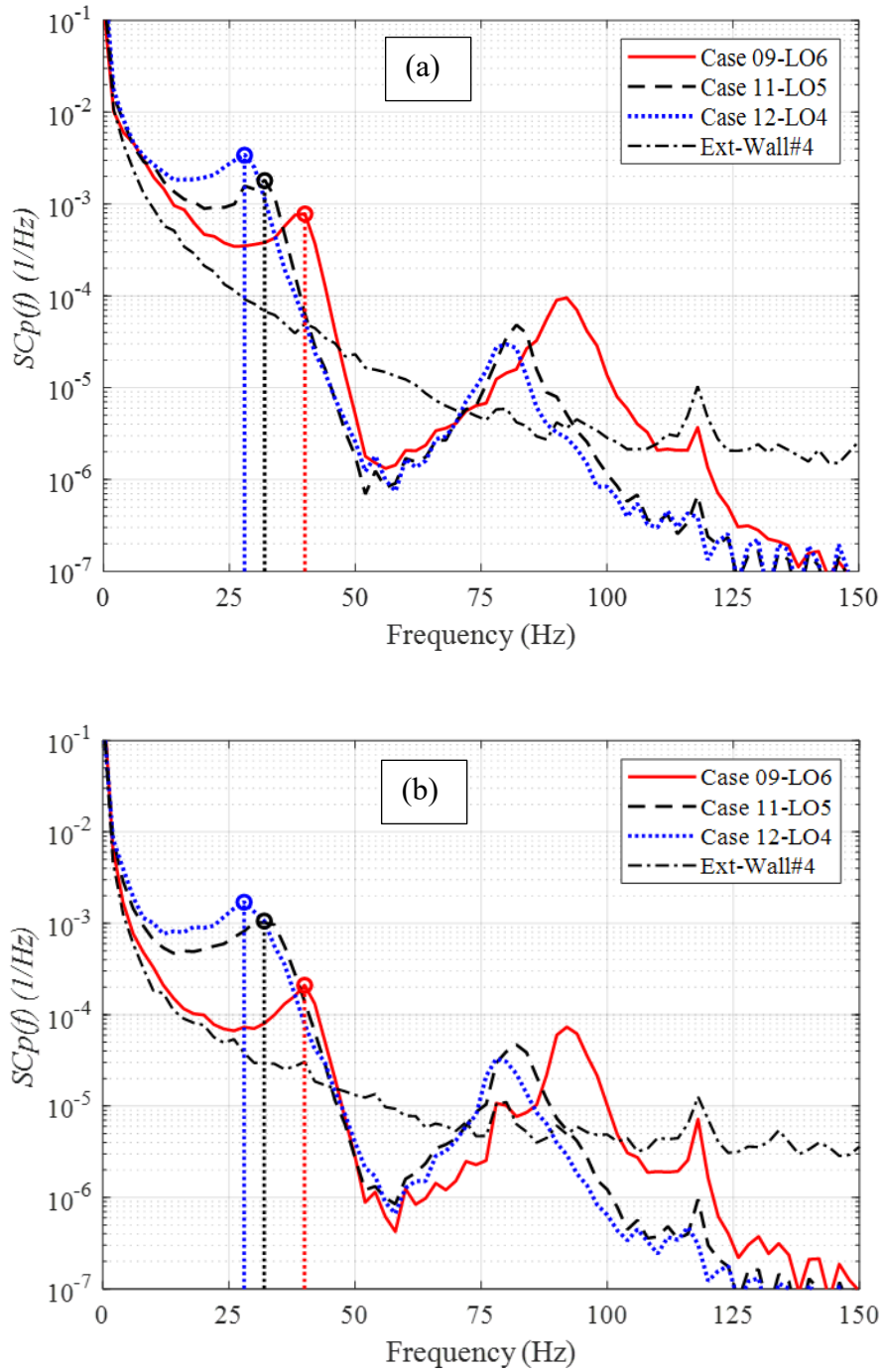


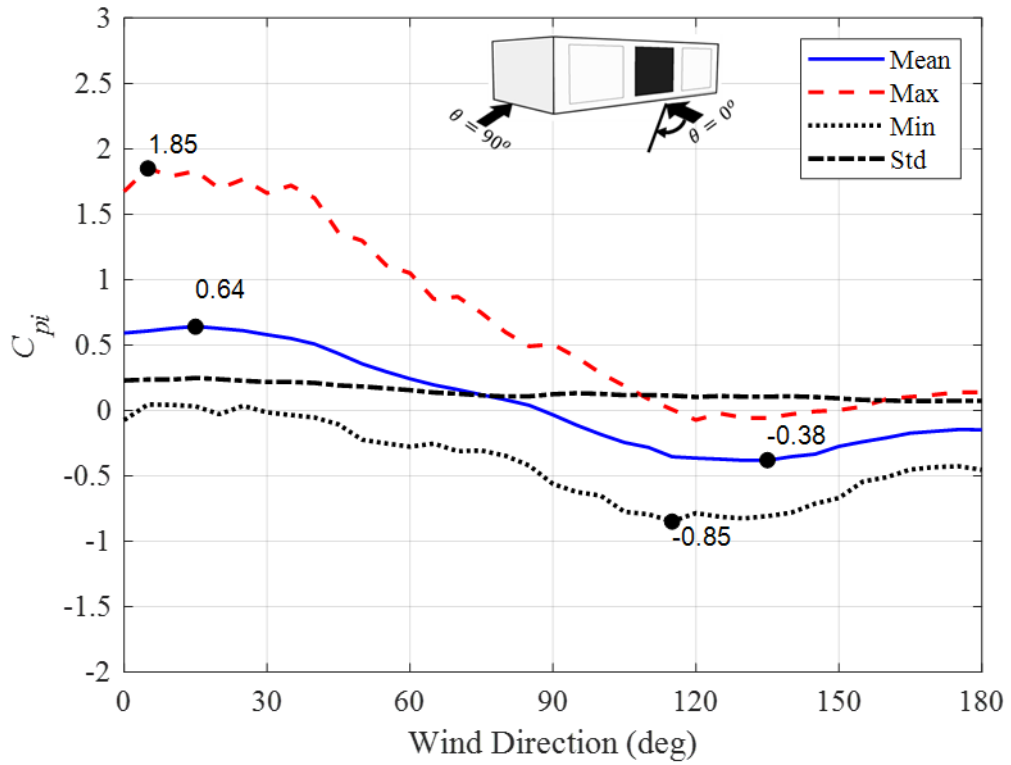
Figure 4.11: Area-averaged external pressure spectrum on Wall #4 and internal pressure spectra for Cases #09, #11, and #12, (a) $\theta = 90^\circ$, (b) $\theta = 180^\circ$

(ii) Effect of the opening location

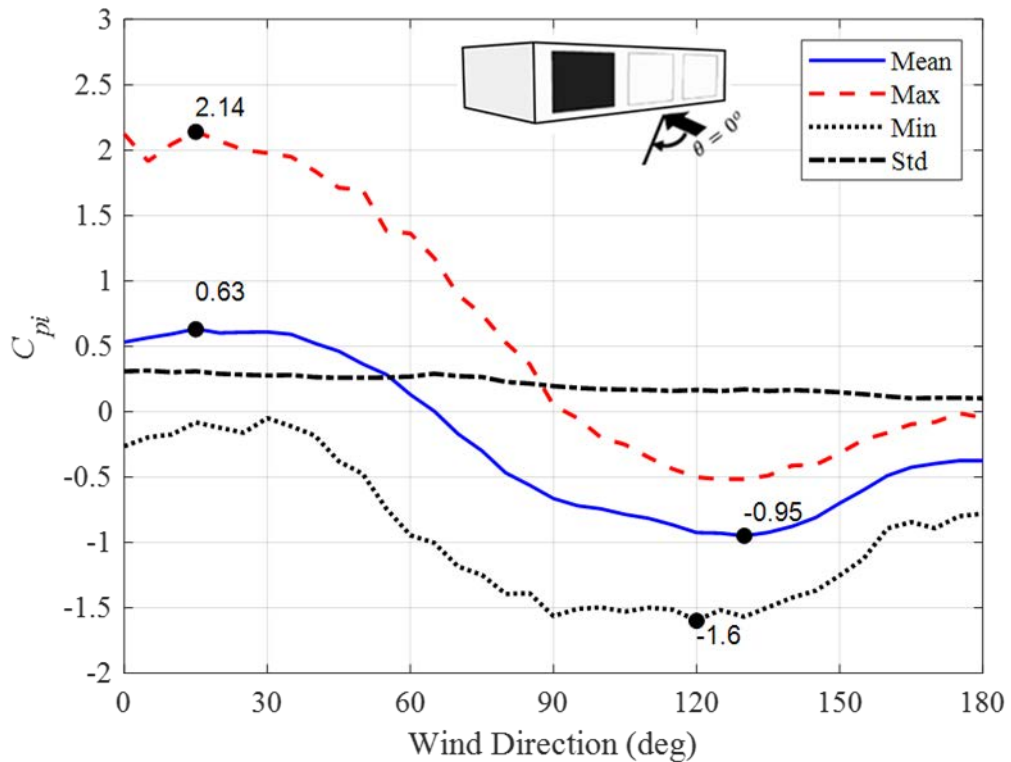
Figure 4.12 shows $C_{\bar{p}i}$, $C_{\sigma pi}$, $C_{\bar{p}i}$ and $C_{\check{p}i}$ in the building with the opening of the same size at two different locations (i.e., LO1 and LO3) for $\theta = 0^\circ$ to 180° . The largest positive $C_{\bar{p}i}$ is about +0.64 for both Cases #04 and #08 at the wind direction $\theta = 15^\circ$. When the

openings are on side wall, largest negative $C_{\bar{p}i}$ are about -0.4 and -0.95 for Cases #4 and #8 at $\theta = 135^\circ$ and 130° , respectively. In Case #08, $C_{\bar{p}i}$ increases up to -0.95 for $\theta = 60^\circ$ to 130° as LO3 is closer to wall leading edge than LO1. Further, as shown in Figures 4.5(a) and 4.12(a), when the building has a single large wall opening, $C_{\bar{p}i}$ is approximately equal to $C_{\bar{p}e}$ at the opening, which satisfies the quasi-static mean internal pressure equation [i.e., Equation (2.2) in Section 2.2], which also agrees with the results of the full-scale study by Humphreys et al. (2019).

For wind directions of $\theta = 0^\circ$ to 45° , the largest $C_{\hat{p}i}$ values are about +1.85 and +2.1 for Case #04 and #08, respectively. The $C_{\sigma p i}$ is higher for Case #08 for wind directions 0° to 80° due to highly fluctuating external pressures closer to the windward edge region which leads to large $C_{\hat{p}i}$. The measured $C_{\hat{p}i}$ and $C_{\check{p}i}$ follows the same trend as the $C_{\hat{p}e}$ and $C_{\check{p}e}$ at the opening, however, Helmholtz resonance amplifies the peak internal pressures in the building with large opening. In a similar model-scale study, Sharma et al. (2010) obtained the pressure gust factor, $C_{\hat{p}i}/C_{\bar{p}i}$ about 2.78 and 2.96 for different opening locations (i.e., 25 mm square opening) which are similar to the $C_{\hat{p}i}/C_{\bar{p}i}$ of about 2.9 and 3.28 for Cases #04 and #08. The largest $C_{\check{p}i}$ of -1.6, for Case #08, is twice the magnitude of $C_{\check{p}i}$ from Case #04, due to the closer proximity of Case #08 wall opening behind the side wall edge for $\theta = 90^\circ$ (LO3) compared to Case #04, whose wall opening which is in the middle of the wall (LO1).



(a) Case #04 – LO1



(b) Case #08 – LO3

Figure 4.12: Mean, standard deviation, minimum, and maximum internal pressure coefficient for single large opening on Wall #1- Cases #04 and #08

Figure 4.13 presents the area-averaged external pressure spectrum for LO1 and the internal pressure spectra for Cases #04 and #08 for $\theta = 0^\circ$ and $\theta = 90^\circ$. For both wind directions, Helmholtz resonance was observed at the same frequency of 36 Hz irrespective of the opening location (Case #04, and #08). However, the magnitude of the Helmholtz resonance is larger in Case #08 because of increased internal pressure fluctuations generated by the higher external pressures at LO3.

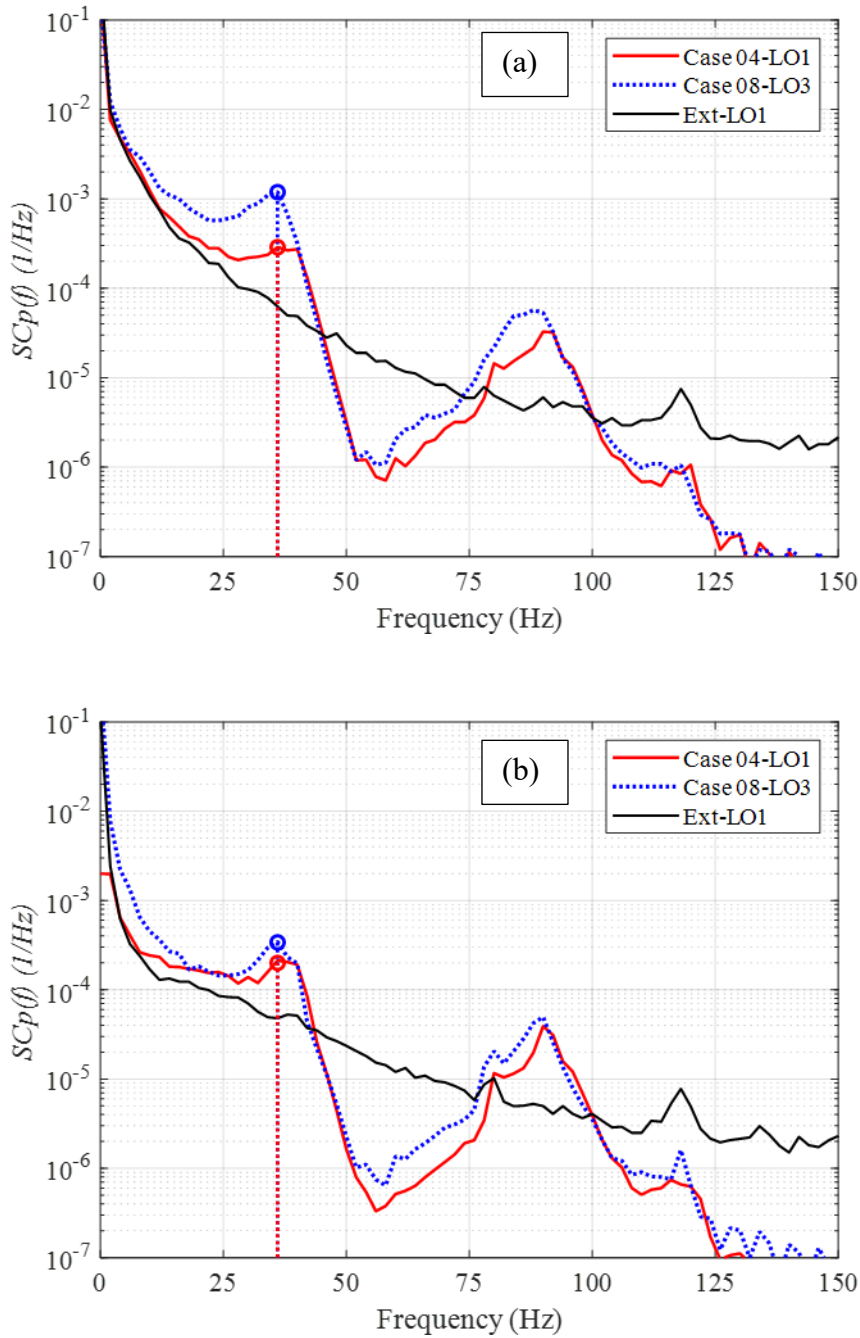


Figure 4.13: Area-average external pressure spectrum and internal pressure spectra for Cases #04, #07, and #08 - (a) $\theta = 0^\circ$, (b) $\theta = 90^\circ$

4.2.3 A large opening in a building with background porosity

Internal pressures were measured in the building with large opening LO1 on Wall #1 and wall porosities of 0.6%, 0.30%, and 0.08% (Cases #30, #31, and #32 in Table 3.4, respectively). Walls #2, #3, and #4 contain 1.5 mm and 3 mm diameter holes to maintain uniform porosity levels across all walls. Figure 4.14 gives the mean, maximum, and minimum internal pressure coefficients for LO1 wall opening with three different porosities for Cases #04, #30, #31, and #32.

The $C_{\bar{p}i}$ are very similar for Cases #30, #31 and #32 with different porosities that $C_{\bar{p}i}$ is about 4.6% less than $C_{\bar{p}i}$ of +0.64 in Case #4 (i.e., zero porosity, LO1 open). Accordingly, the change in porosity does not greatly affect the internal pressure fluctuations in model-scale studies. However, Humphreys et al. (2020) showed that porosity (i.e., 0.58% to 1.39% in JCU-ASIS test building) has a measurable impact on internal pressure fluctuations in full-scale studies. The porosity only has a small influence on the internal pressure fluctuations when the total porous area is less than 10% of the total open area for Cases #30, #31, and #32 (i.e., in case #30, total open area is 8000 mm², and total background porous area \approx 450 mm²), as shown by Vickery and Bloxham (1992). Mean and minimum internal pressures coefficients are more negative in the porous buildings with a large opening compared to Case #04, as the $A_W/A_L < 1$ in Cases #30 to #32.

Furthermore, Woods and Blackmore (1995) explained that porosity has a negligible influence on the mean internal pressure when $A_W > A_L$. Kim and Ginger (2013) also demonstrated that internal pressure is attenuated by 10% to 20% by background porosity when A_W/A_L is less than 5. However, full-scale studies by Humphreys et al. (2020) showed that the porosity of the building damps internal pressure fluctuations and the quasi-static approach to design internal pressures is conservative in industrial buildings with a large opening. These observations showed that background porosity tends to attenuate the internal pressure but may not be accurately modelled in model-scale studies, as explained in Section 4.2.1.

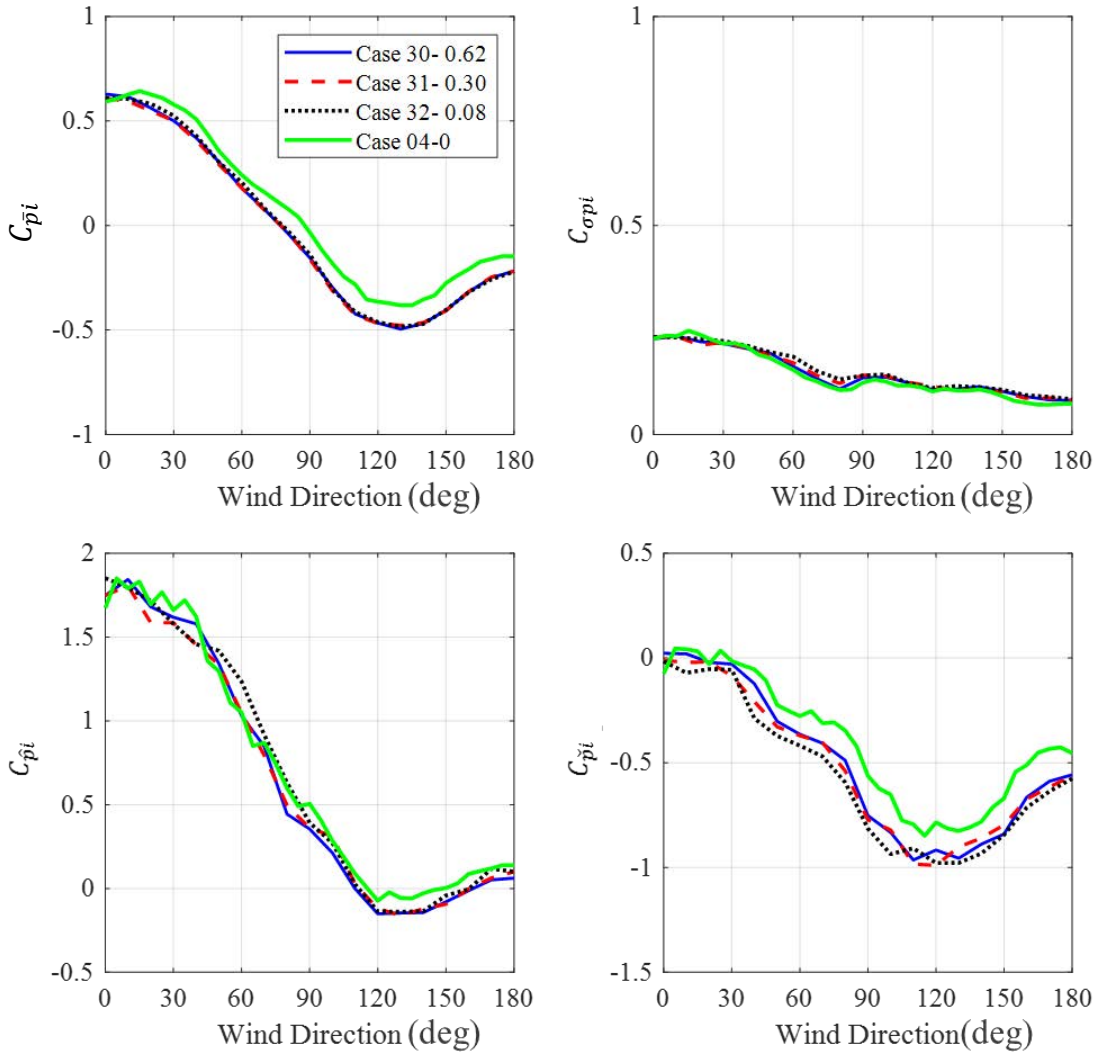


Figure 4.14: Mean, standard deviation, minimum, and maximum internal pressure coefficient for single large opening in Case #04, and LO1 with three different porosities, 0.62, 0.30 and 0.08 for Cases #30, #31 and #32

4.2.4 Effect of the building volume

The effect of the building volume was investigated by considering five single opening configurations in Models #1 and #2. Figure 4.15 shows the $C_{\bar{p}i}$, $C_{\sigma pi}$, $C_{\hat{p}i}$ and $C_{\check{p}i}$ for Cases #04 and #52 in Models #1 and #2. The largest $C_{\bar{p}i}$ for Case #04 is 8% higher than Case #52, and $C_{\hat{p}i}$ of 1.85 in Case #04 is 27% higher than Case #52 when the opening is on the windward wall at $\theta = 5^\circ$. The building volume significantly influences the peak internal pressure when the wind is approaching from $\theta = 0^\circ$ to 45° (i.e., windward opening), due to the attenuation of internal pressure in the larger internal volume. When

the opening is on the side wall ($\theta = 90^\circ$), C_{pi} in the building is different because the distance from the windward leading edge to the opening is different for the two models and the highest C_{pi} occurred at 115° and 145° for Cases #04 and #52, respectively.

Ginger et al. (2008, 2010), and Kim and Ginger (2013) showed that mean internal pressures coefficients are nearly equal for different building volumes for the same opening area. These studies have presented peak internal pressure coefficients with respect to the non-dimensional parameter, S^* . In this thesis, the ratio between internal and external pressure standard deviation and the ratio between peak internal and external pressures coefficients are compared in Section 4.3 with respect to the opening non-dimensional parameter, S^* .

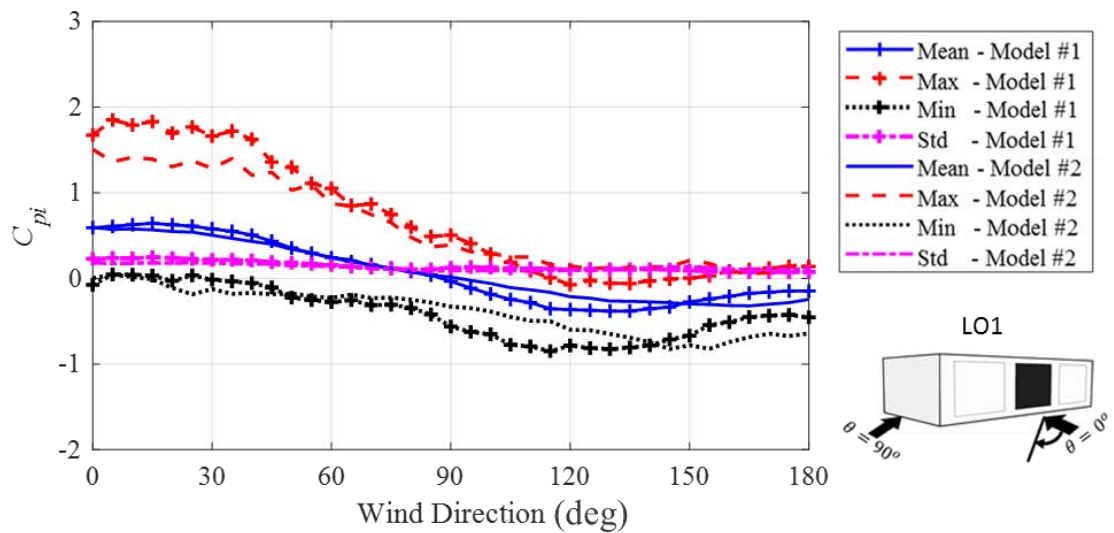


Figure 4.15: Mean, standard deviation, minimum, and maximum internal pressure coefficient for a single large opening, LO1 for two volumes, Case #04 in Model #1 and Case #52 in Model #2

The Helmholtz frequency, f_H decreases with increasing the building volume and f_H is 38 Hz and 20 Hz for Cases #04 and #52, as shown in Figure 4.16. The volume of Case #52 is twice the volume of Case #04, and its Helmholtz frequency is about half of Case #04. Ginger et al. (2010) also showed that Helmholtz resonance frequency decreases with increasing building volume. Figure 4.16 shows secondary peaks for internal pressure spectra at about 18 Hz above the Helmholtz frequency. However, as mentioned earlier, this secondary peak has less influence on internal pressure fluctuations as its peak is more than an order of magnitude lower.

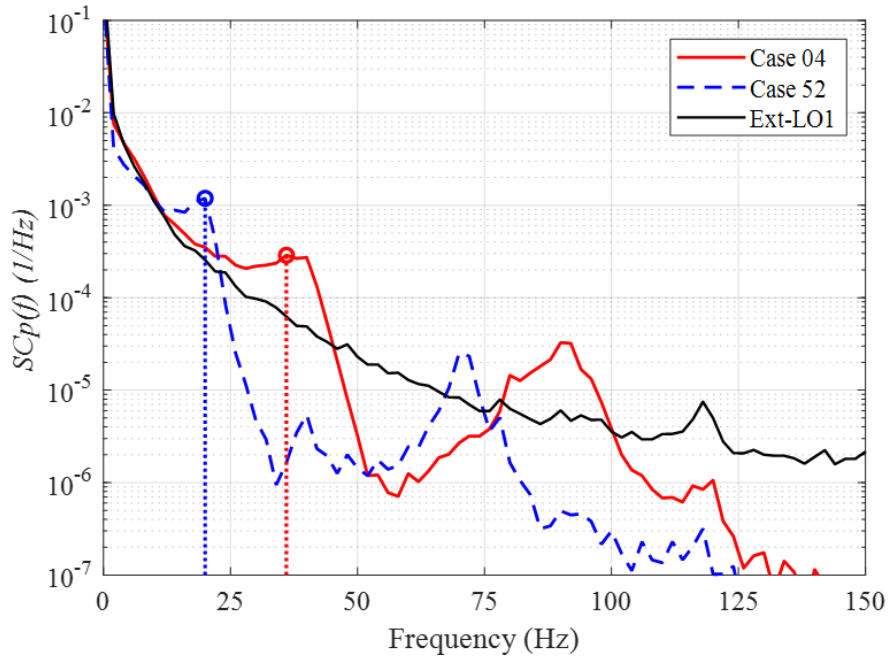
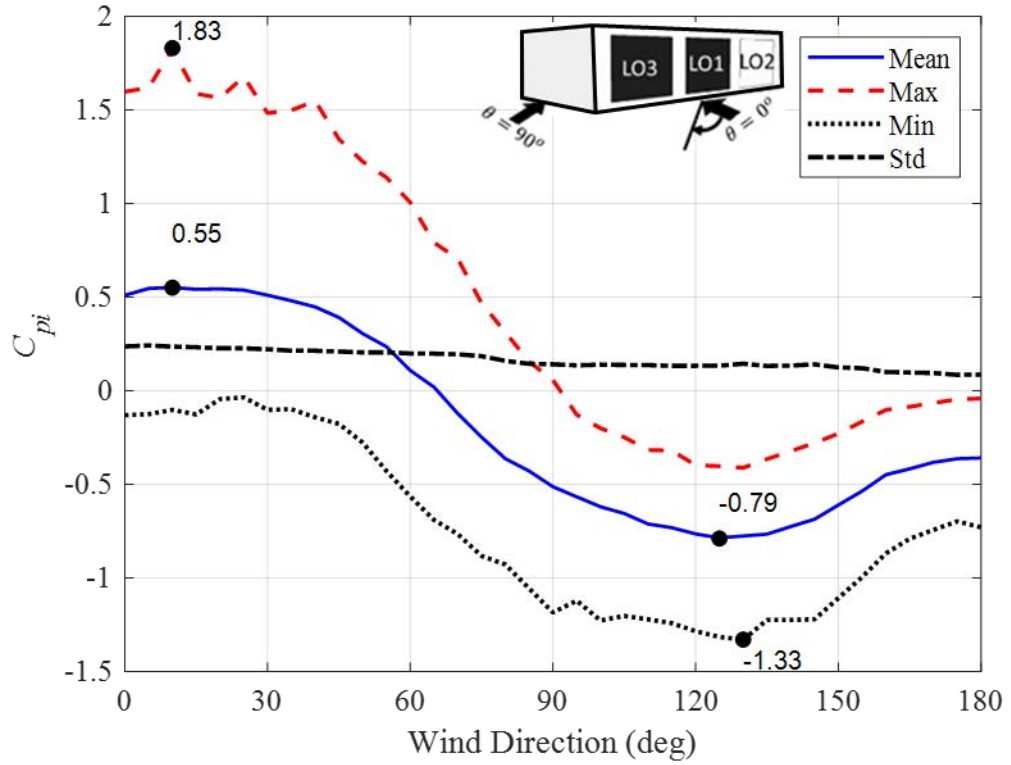


Figure 4.16: Area-average external pressure spectrum and internal pressure spectra for Case #4 (Model #1) and #52 (Model #2) at $\theta = 0^\circ$

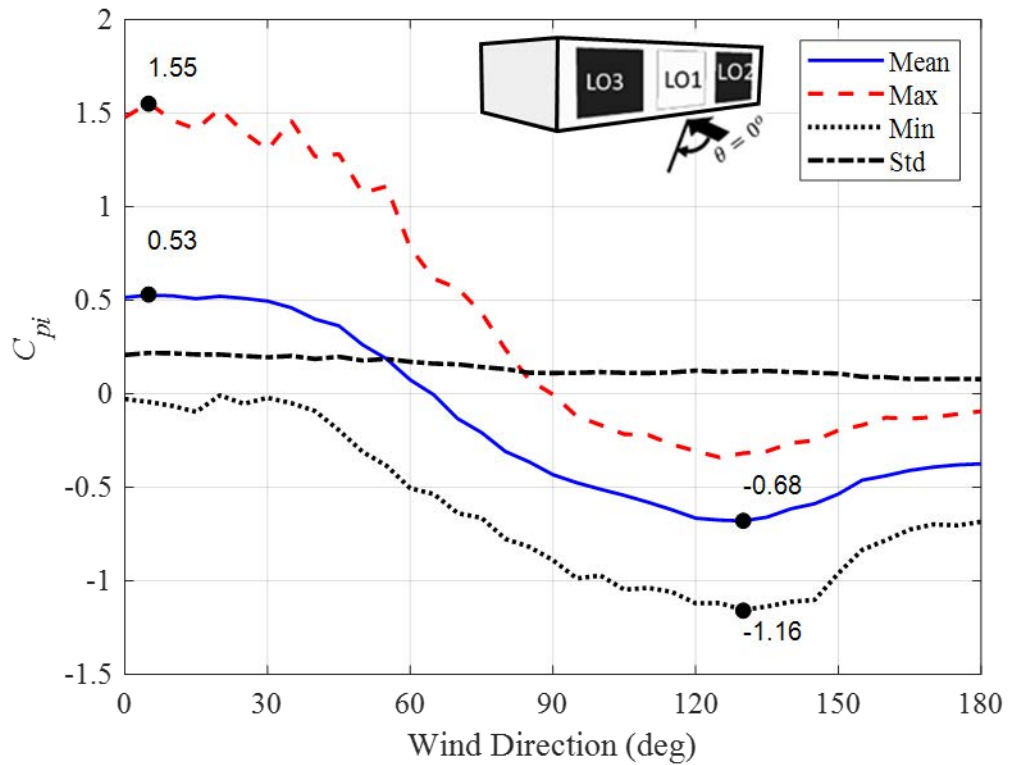
4.2.5 Building with multiple openings on the same wall

Figure 4.17 shows the $C_{\bar{p}i}$, $C_{\sigma p i}$, $C_{\hat{p}i}$ and $C_{\check{p}i}$ for Cases #13, #14, and #15 (Table 3.4) for wind directions 0° to 180° . As shown in Figure 4.17, largest positive $C_{\bar{p}i}$ of about +0.5 is similar for all three cases within the wind directions $\theta = 0^\circ$ to 30° and its 28% lower than the single opening case, LO1 (Case #04), shown in Figure 4.12(a). Further, largest suction $C_{\bar{p}i}$ of -0.79, -0.68 and -0.66 are observed at $\theta = 90^\circ$ to 135° such that the air-flow into and out of the building through multiple openings on the same wall creates the difference for Cases #13, #14, and #15.

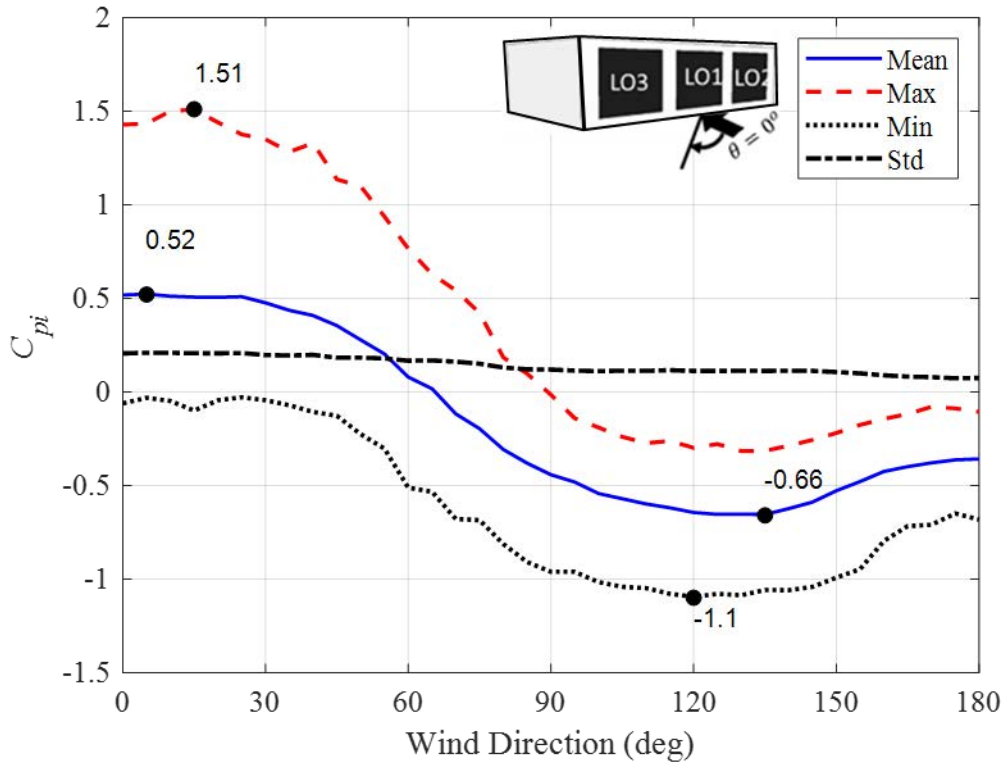
Figure 4.17 further shows the highest $C_{\hat{p}i}$ of 1.83 at $\theta = 10^\circ$ is 20% less and the lowest $C_{\check{p}i}$ of -1.3 at $\theta = 130^\circ$ is 18% less for Case #13 compared to the single opening Case #08 as given in Figure 4.12(b). However, internal pressure fluctuations are attenuated for different opening configurations for Cases #13, #14, and #15, resulting in a decrease in the peak internal pressures due to the lack of spatial correlation of external pressures across multiple large openings. In the multiple opening cases, the relation between peak internal to peak external pressures are further discussed in Section 4.3 with respect to the non-dimensional parameter, S^* .



(a) Case #13 – LO1+LO3



(b) Case #14 – LO2+LO3



(c) Case #15 – LO1+ LO2 +LO3

Figure 4.17: Mean, standard deviation, maximum and minimum internal pressure coefficients for Cases #13, #14 and #15

Figure 4.18 shows the internal pressure and area-averaged external pressure spectra across the openings LO1, LO2 and LO3 for Cases #13, #14, and #15 for wind direction $\theta = 0^\circ$. Helmholtz resonance was observed at frequencies of 40 Hz, 38 Hz, and 44 Hz for Cases #13, #14, and #15, respectively. In Cases #13 and #14, Helmholtz resonance occurred at two slightly different frequencies for a similar opening area. This may be because openings are at different locations resulting in different inertial coefficients for the openings. In Case #15, Helmholtz resonance occurred at higher frequencies with a smaller magnitude than the single opening cases explained in Figure 4.13. The spatial and temporal variations in external pressures at three different opening areas (LO1, LO2 and LO3) reduce internal pressure fluctuations for multiple opening cases so that the magnitude of the energy contained in the Helmholtz frequency changes accordingly.

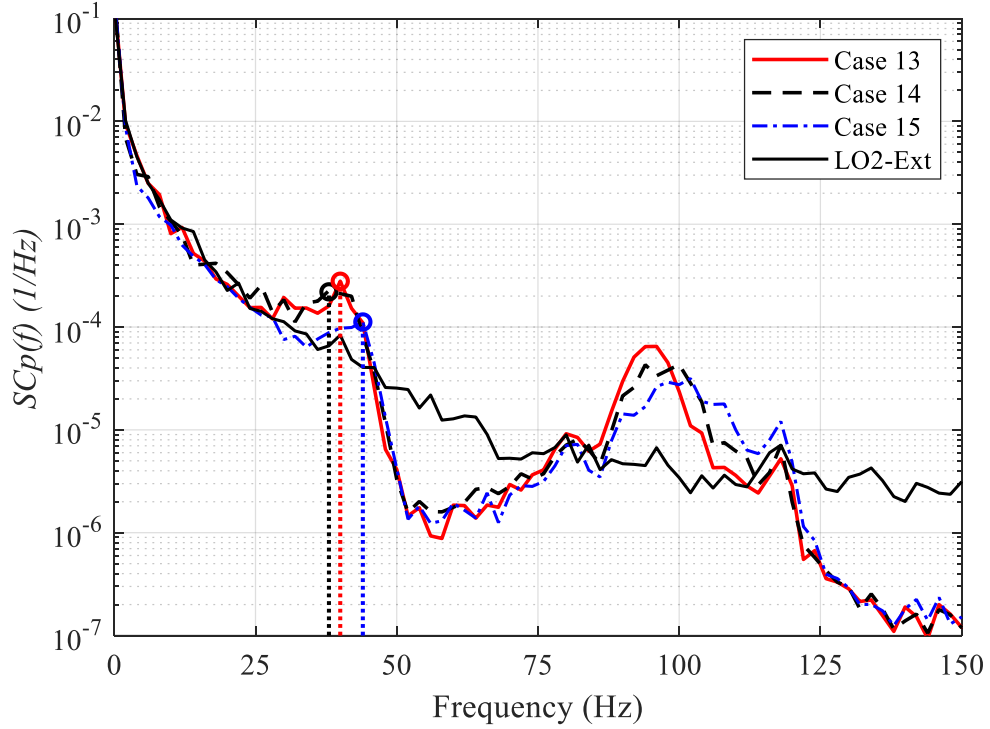


Figure 4.18: Area-average external pressure spectrum for LO2 and internal pressure spectra for $\theta = 0^\circ$

4.3 Non-dimensional representation

Internal pressure fluctuations in a building with a single windward wall opening are described by non-dimensional parameters by Holmes (1979), Sharma and Richards (2003), Yu et al. (2006), Ginger et al. (2008), Guha et al. (2011), and Kim and Ginger (2013), as detailed in Section 2.3. The dimensional analysis of the governing internal pressure equation (Equation 2.7) shows that the internal pressure response is a function of the parameter, $S^* = (A^{3/2}/V) \times (a_s/\bar{U}_h)^2$ and the integral length-scale of turbulence to opening area ratio, $\Phi_5 = \lambda_u/\sqrt{A}$.

Table 4.1 presents the S^* and Φ_5 values for different opening configurations where $a_s = 340$ m/s, mean wind speed at roof height, ($\bar{U}_h \sim 9.0$ m/s), and $\lambda_u = 0.436$ m from the model scale study. The variation of the building volume and opening area of Models #1 and #2 produced a range of S^* and Φ_5 values from 0.76 to 350 and 2.8 to 11, respectively. For configurations with multiple openings on the same wall, the calculation of S^* and Φ_5 considers the combined opening areas on the wall.

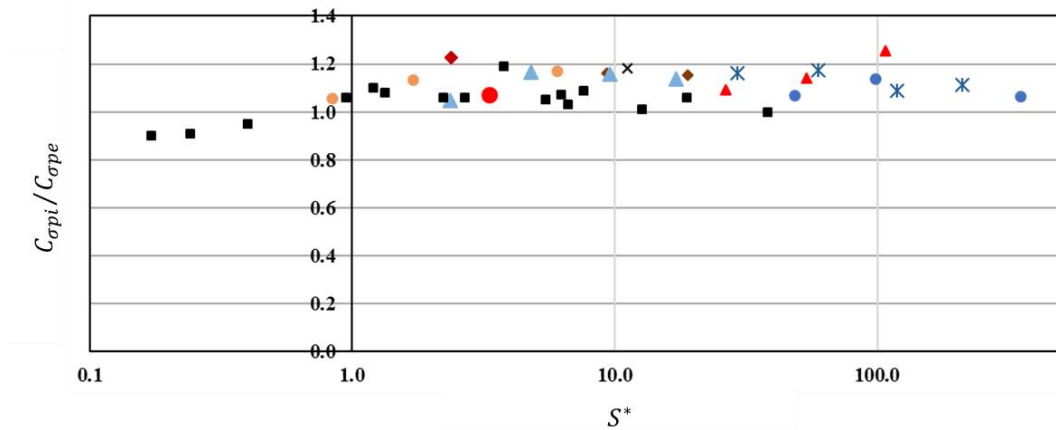
Table 4.1: Area to volume ratio for different single opening configurations

Case #	Opening	Volume $\times 10^6$ (mm ³)	Opening area (mm ²)	S^*	Φ_5
29	LO1+LO2+LO3	16	24000	310	2.81
15	LO1+LO2+LO3	56	24000	88.6	2.81
54	LO1+LO2+LO3	112	24000	44.3	2.81
31	LO2+LO3	28	16000	96.4	3.45
26	LO2+LO3	56	16000	48.2	3.45
55	LO2+LO3	112	16000	24.1	3.45
23	LO6	16	17100	186	3.33
21	LO6	28	17100	107	3.33
9	LO6	56	17100	53.3	3.33
49	LO6	112	17100	26.6	3.33
53	LO11	112	13500	18.7	3.75
47	LO10	112	9000	10.2	4.60
4	LO1	56	8000	17.0	4.87
52	LO1	112	8000	8.5	4.87
5	LO8	56	4000	7.6	6.89
48	LO8	112	4000	3.0	6.89
6	LO9	56	2000	2.1	9.75
24	LO5	16	3200	15.1	7.71
22	LO5	28	3200	8.6	7.71
11	LO5	56	3200	4.3	7.71
50	LO5	112	3200	2.2	7.71
25	LO4	16	1600	5.3	10.9
12	LO4	56	1600	1.5	10.9
51	LO4	112	1600	0.8	10.9

Figure 4.19 shows the standard deviation ratio, $C_{\sigma pi}/C_{\sigma pe}$ for each configuration when the wind flows perpendicular to the opening. The standard deviation ratio, $C_{\sigma pi}/C_{\sigma pe}$ varies around 1.1 for the majority of S^* values (for $0.79 \leq S^* \leq 350$) which is in agreement

with previous model-scale studies conducted by Vickery (1991), Holmes and Ginger (2012), and Kim and Ginger (2013) where the $C_{\sigma pi}/C_{\sigma pe} = 1.1$ when the $S^* \geq 1.0$. Guha et al. (2013) also showed that $C_{\sigma pi}/C_{\sigma pe}$ varied in the range of about 0.85 to 1.05 for the S^* in the range of 25 to 200. Furthermore, the full-scale study by Humphreys et al. (2019) presented that $C_{\sigma pi}/C_{\sigma pe} < 1.0$ for larger S^* and Φ_5 values (i.e., $34 > \Phi_5 > 14$ and $390 \geq S^* \geq 24$) in the JCU-ASI shed primarily due to additional damping induced by background leakage.

This study presents additional data for large S^* values ($50 < S^* < 350$) and small Φ_5 values ($2.8 < \Phi_5 < 3.3$) shown in Figure 4.19 where $C_{\sigma pi}$ exceeds $C_{\sigma pe}$ by about 10% to 20%. Furthermore, when there are multiple openings on the same wall, $C_{\sigma pi}/C_{\sigma pe}$ is larger than 1.0, showing a significant increase in internal pressure fluctuation for large S^* values.



Symbol	●	▲	◆	●	▲	×	●	◆	×	■
Cases #	15,29,54	26,31,55	4,52	12,25,51	11,22,24,50	9,21,23,49	5,48	6	47	Previous Data
Φ_5	2.8	3.5	4.9	11	7.7	3.3	6.9	9.8	4.6	4.7,6,8.5,15

Figure 4.19: Internal and external pressure standard deviation ratio versus S^* for different opening configurations- when wind perpendicular to the opening

Figure 4.20 presents the internal to external peak positive pressure ratio ($C_{\hat{p}i}/C_{\hat{p}e}$) with respect to S^* from the range of single windward openings and volume configurations studied, for winds approaching perpendicular to the openings. When the S^* ranges between 1 and 10, $C_{\hat{p}i}/C_{\hat{p}e}$ ratios are in good agreement with the model scale study conducted by Kim and Ginger (2013).

Furthermore, Yu et al. (2006), Ginger et al. (2008), and Kim and Ginger (2013) have shown that the internal pressure fluctuations increase as S^* increases and Φ_5 decreases. According to Guha et al. (2013), the peak internal to external pressure ratios ($C_{\hat{p}_i}/C_{\hat{p}_e}$) varied between 0.7 to 1.0 for $25 < S^* < 200$. However, Figure 4.20 shows that the $C_{\hat{p}_i}/C_{\hat{p}_e}$ approximately equals 1.0 for large S^* values and small Φ_5 values ($2.8 < \Phi_5 < 3.3$) when the building has a complete wall opening (Cases #9,#21, #23 and #49). For $50 < S^* < 350$, when the building contains multiple openings on the same wall, the spatial variations in the external pressure fluctuations leads to lower peak external pressures that produce larger $C_{\hat{p}_i}/C_{\hat{p}_e}$ (i.e., >1.2) in Cases #15, #29, #31, and #55. In a full-scale study, Humphreys et al. (2020) showed that $\hat{p}_i/\hat{p}_{ew} < 1.0$ and internal pressure is attenuated by 3% to 12% due to the background leakage in the JCU-ASI shed relative to the external pressure when S^* varies from 123 to 24. Another full-scale study by Ginger et al. (1997) showed that $C_{\hat{p}_i}/C_{\hat{p}_e}$ approximately equals 1.0 for S^* values of 1.1 and 6.9, and Φ_5 values of 71 and 112, respectively.

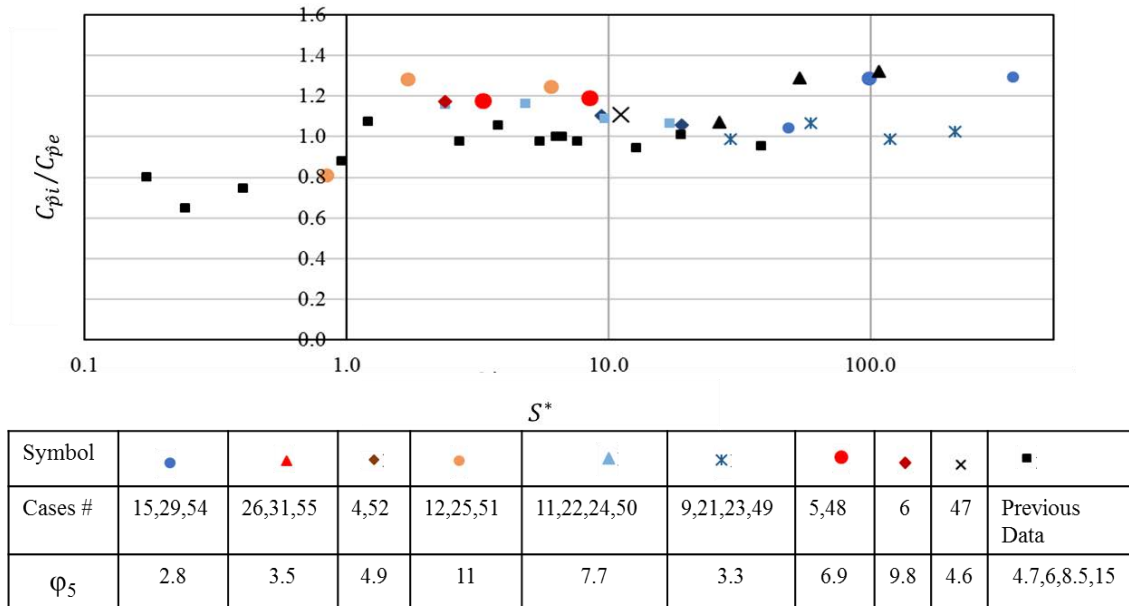


Figure 4.20: Peak internal and peak external pressure ratio versus S^* for different single opening configurations- when wind perpendicular to the opening

4.4 Chapter summary

The fluctuating internal and external pressures on a rectangular industrial building were determined using a 1/200 scale wind tunnel model study. The internal pressure fluctuations were measured and analysed for a range of building configurations, including different sizes and locations of wall openings, combinations of wall openings, building volume, and wall porosity with approaching wind direction. The spatially and temporally varying external pressures on Wall #1, Wall #4 and the roof were also assessed with wind direction to clarify external pressure variations across the envelope. Further, internal pressures in the building resulting from large openings were compared with the area-averaged external pressures at the opening for these building configurations. The outcomes of this Chapter are;

- The mean external pressure coefficients on the windward wall, leeward wall, sidewall and the roof of buildings are similar to previous full-scale and model-scale studies. The mean external pressure coefficients are consistent with quasi-steady coefficients in the wind loading standard AS/NZS 1170.2.
- The magnitude of peak suction external pressures high in regions of flow separation on the roof and walls compared to regions further away from leading edges and are dependent on approach wind direction.
- Internal pressure coefficients in nominally sealed buildings are small and fluctuate between 0 and -0.4 with small variations between wind directions. In this model scale study, the variation of porosity in the nominally sealed building has very little influence on internal pressure fluctuations so that the background porosity in industrial buildings may not be modelled satisfactorily at the model-scale.
- When a building has a large opening, the internal pressure fluctuations generate Helmholtz resonance. As the opening size decreases, increase in damping reduces the energy in the internal pressure fluctuations.
- For multiple openings on the same wall, internal pressure fluctuations are attenuated, resulting in a decrease in the peak internal pressures due to the greater spatial variation of external pressures across multiple large openings. Further, Helmholtz resonance can occur while there are multiple openings in a wall with f_H increasing as the opening area increases.
- For larger S^* values ($50 < S^* < 350$) and small Φ_5 values ($2.8 < \Phi_5 < 3.3$);

- The $C_{\sigma pi}$ exceeds $C_{\sigma pe}$ by about 10% - 20% showing a significant increase in the energy of the internal pressure fluctuation due to Helmholtz resonance.
- $C_{\hat{p}i}/C_{\hat{p}e}$ approximately equals to 1.0 when the building has a whole wall opening (3- wall building)
- $C_{\hat{p}i}/C_{\hat{p}e} > 1.2$ for multiple wall openings on the same surface due to spatial and temporal variation in external pressures that produce lower peak external pressures compared to internal pressure.

This Chapter analysed a series of building configurations to understand internal pressure dynamics in the building and the external pressure fluctuations on different locations on walls and roof. This knowledge leads to a need for understanding the correlation between external and internal pressures, net pressures, and net reductions factors in different locations and structural components in the building envelope that the detailed explanations are included in Chapter 5 with respect to the non-dimensional parameter, S^* .

5 CORRELATION OF EXTERNAL AND INTERNAL PRESSURE FLUCTUATIONS

Chapter 5 presents a detailed discussion of the correlation between internal and external pressure fluctuations (r_{pepi}), net pressures fluctuations and reduction factors for net pressures on nominally sealed buildings and buildings with large openings. The correlation is assessed for wall and roof cladding, purlins and girts for different building configurations. The peak internal, external and net pressures are analysed, and the relationship between peak events and the correlation between internal and external pressures are used to derive the net pressure factor (F_C) which defines peak net pressures on roof and wall cladding of the building.

5.1 Cross-correlation coefficient

Cross-correlation coefficient is a measure of the magnitude of the similarity between two series. The simultaneously measured internal and external pressure time-history signals are used to calculate the cross-correlation coefficient defined in Equation 5.1 as a function of lag time (τ) between internal pressure fluctuations relative to the external pressure fluctuations (explained in Section 2.4).

$$r_{pepi}(\tau) = \frac{1}{T \times C_{\sigma pe} \times C_{\sigma pi}} \int_0^T [(C_{pe}(t) - \bar{C}_{pe}) \times (C_{pi}(t + \tau) - \bar{C}_{pi})] dt \quad (5.1)$$

The cross-correlation between internal and external pressures are obtained for the five repeat wind tunnel runs. Typically the $r_{pepi}(\tau)$ for the five repeat runs are shown in Figure 5.1. The averaged correlation coefficients at zero lag time ($\tau = 0$) is taken as the correlation coefficient of particular internal and external pressure fluctuations. The

$r_{p_e p_i}(0)$ is the cross-correlation coefficient at the zero lag time ($\tau = 0$), that describes the relationship between internal and external pressure fluctuations at the different locations on the building envelope at the same moment in time. The correlation at zero lag time provides a relationship between the external and internal pressures and the resulting net pressure acting on selected areas of the surfaces.

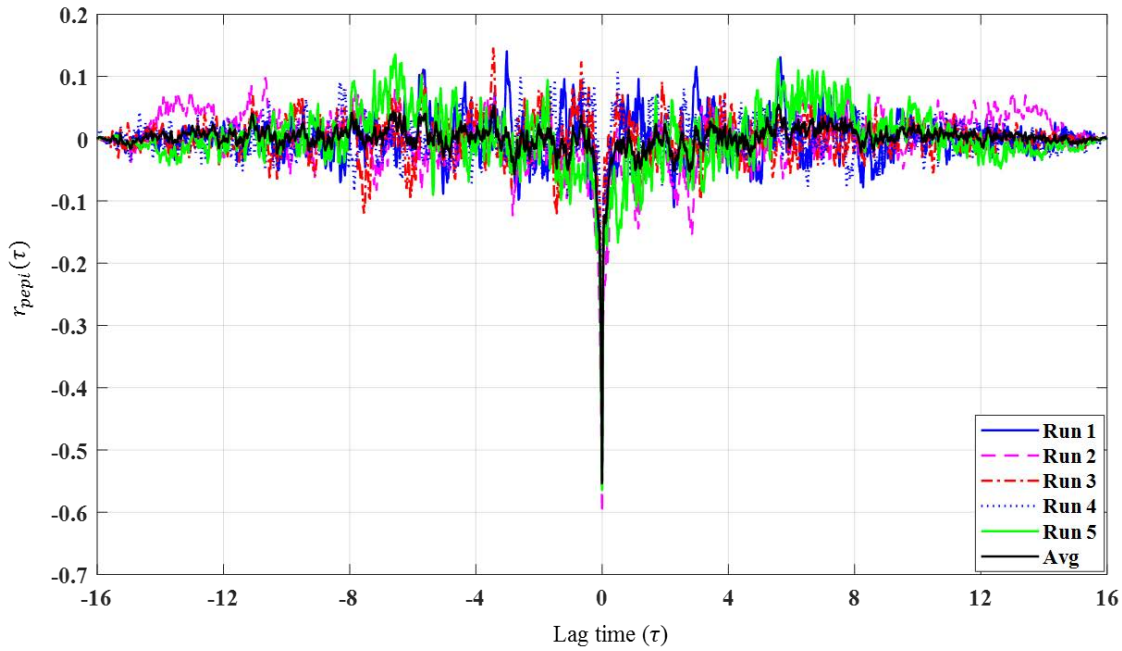


Figure 5.1: Typical cross-correlation between internal and external pressures vs lag time (τ)

The correlation coefficient varies between -1.0 and +1.0, and a correlation of ± 1.0 describes a perfect positive or negative correlation of two fluctuating signals. The results of correlation coefficients in this Chapter are interpreted, as defined in Table 5.1.

Table 5.1: Interpretation for cross-correlation coefficient

Range of $r_{p_e p_i}(0)$	Description
$ 0.7 < r_{p_e p_i}(0) < 1 $	Highly correlated
$ 0.4 < r_{p_e p_i}(0) < 0.7 $	Moderately Correlated
$0 < r_{p_e p_i}(0) < 0.4 $	Poorly Correlated

The external and internal pressures acting towards a surface are defined as positive, and the pressures acting away from a surface are considered as negative (i.e., suction). Figure 5.2(a) shows the negative external pressures and negative internal pressures measured on the roof cladding of the building with a sidewall opening. These pressures are positively correlated, as shown in Figure 5.2 (b). The two pressure signals act in opposite directions such that an increase in external suction pressure and an increase in the internal suction pressure produce a positive correlation coefficient at zero lag-time.

If the external and internal pressure fluctuations act in the same direction (i.e. negative external and positive internal pressure fluctuation, or positive external and negative internal pressure fluctuations) at the same time, the two pressure signals are negatively correlated at zero lag time, as shown in Figure 5.3(a)-(b). Figure 5.3 shows the two signals are poorly negatively correlated with and $r_{pepi}(0) = -0.32$, suggesting the occurrence of the increase in external suction pressure with an increase in positive internal pressure is generating the resulting outward net pressures ($C_{pe} - C_{pi}$). The $r_{pepi}(0)$ is an important parameter to understand the net pressure fluctuations.

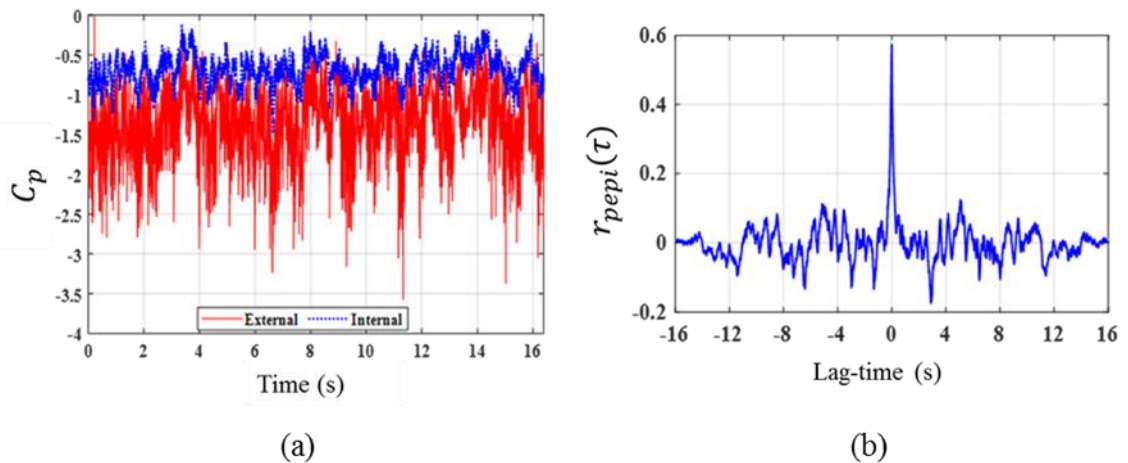


Figure 5.2: (a) Negative internal and negative external pressures in the building (b) Positive correlation between negative external and negative internal pressure

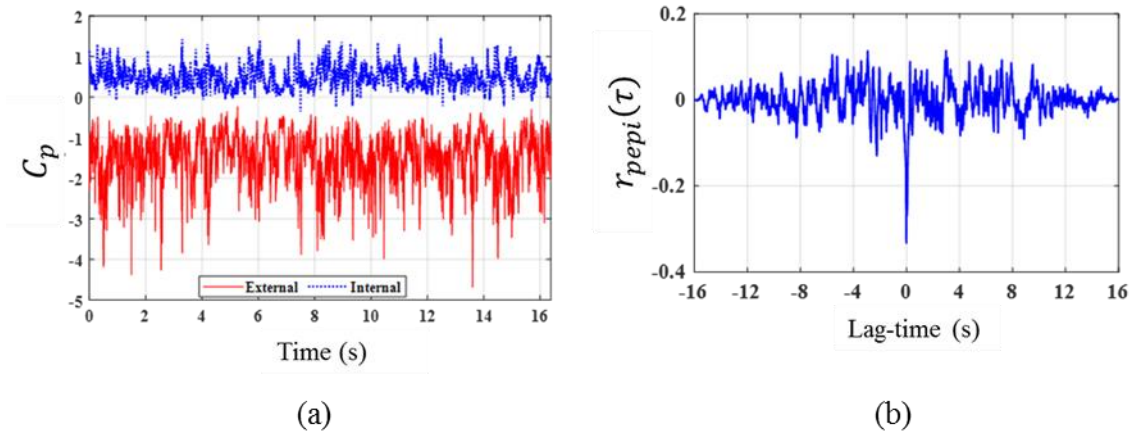


Figure 5.3: (a) Negative external and positive internal pressures in the building, (b) negative correlation between negative external and positive internal pressures

5.2 Building with a large opening- effect of opening size and locations

The internal pressure fluctuations in a building with a large opening are affected by the opening size and location in the envelope, as discussed in Chapter 4. Table 5.2 shows the five selected cases for a detailed analysis of the correlation between external and internal pressure in a building with a large opening. This section discusses the correlation between internal and external pressures on the roof and walls on the building envelope.

Table 5.2: Selected single opening cases for detail analysis

Case #	Description	Opening size	Opening area to wall area [#] ratio
4	LO1 on Wall #1	100mm × 80mm	0.2
8	LO3 on Wall #1	100mm × 80mm	0.2
9	LO6 on Wall #4	190mm × 95mm	0.92
11	LO5 on Wall #4	80mm × 40mm	0.16
12	LO4 on Wall #4	40mm × 40mm	0.08

[#] wall area –Wall #4 = 100 × 200 mm²; Wall #1 = 100 × 400 mm²

5.2.1 Correlation coefficients on the roof cladding- openings on the Wall #4

Correlation coefficients between the external and internal pressure can be determined for each pressure tap to indicate their variation across different areas of the roof and wall surfaces. Figure 5.4 shows the correlation coefficient for 17×6 grid of external taps on one half of the roof of the nominally sealed building (Case #02) and the building with single openings (Cases #9, #11, and #12) for $\theta = 90^\circ$, when the upstream flow is perpendicular to Wall #4. Additionally, Figure 5.4 also shows the colour scale of the correlation coefficient. Here, the same internal pressure fluctuations apply on all tap locations on the grid.

Figure 5.4(a) shows that internal and external roof pressures on the nominally sealed building are poorly, positively correlated for the orthogonal wind direction ($\theta = 90^\circ$). Six tap locations (shown in black rectangles in Figure 5.4a) are selected to study the external and internal pressure fluctuations in Case #02. Figure 5.5 shows the internal and external pressure fluctuations at these six different locations on the roof cladding of nominally sealed building for $\theta = 90^\circ$. The magnitude of the internal pressure fluctuations is lower than the external pressure fluctuations shown in Figure 5.5. Figure 5.5 further illustrates that the external pressures near the windward roof edge are highly fluctuating, and the magnitude of the external pressure fluctuations decreases towards the middle of the roof. These external pressures on roof and internal pressures are independent and do not directly correlate as they are poorly correlated.

When a building has a large windward wall opening, internal pressures are large and highly fluctuating, and correlation between internal and external pressures on the roof cladding varies from -0.6 to +0.1 as shown in Figure 5.4(b)-(d). Further, the external pressure decreases towards the middle of the roof (away from the windward edge) and reduces the correlation, as shown by the colour scale of Figure 5.4. Figure 5.4 also shows that the external pressures on RP1-1 are highly fluctuating following the flow separation at the windward corner that the internal and external pressures are poorly, negatively correlated regardless of the size of the opening. In the first row from the windward roof edge, the $r_{pepi}(0)$ varies between -0.3 and -0.4 in Figure 5.4(b) and $r_{pepi}(0)$ varies between -0.4 and -0.5 in Figure 5.4(c) – (d).

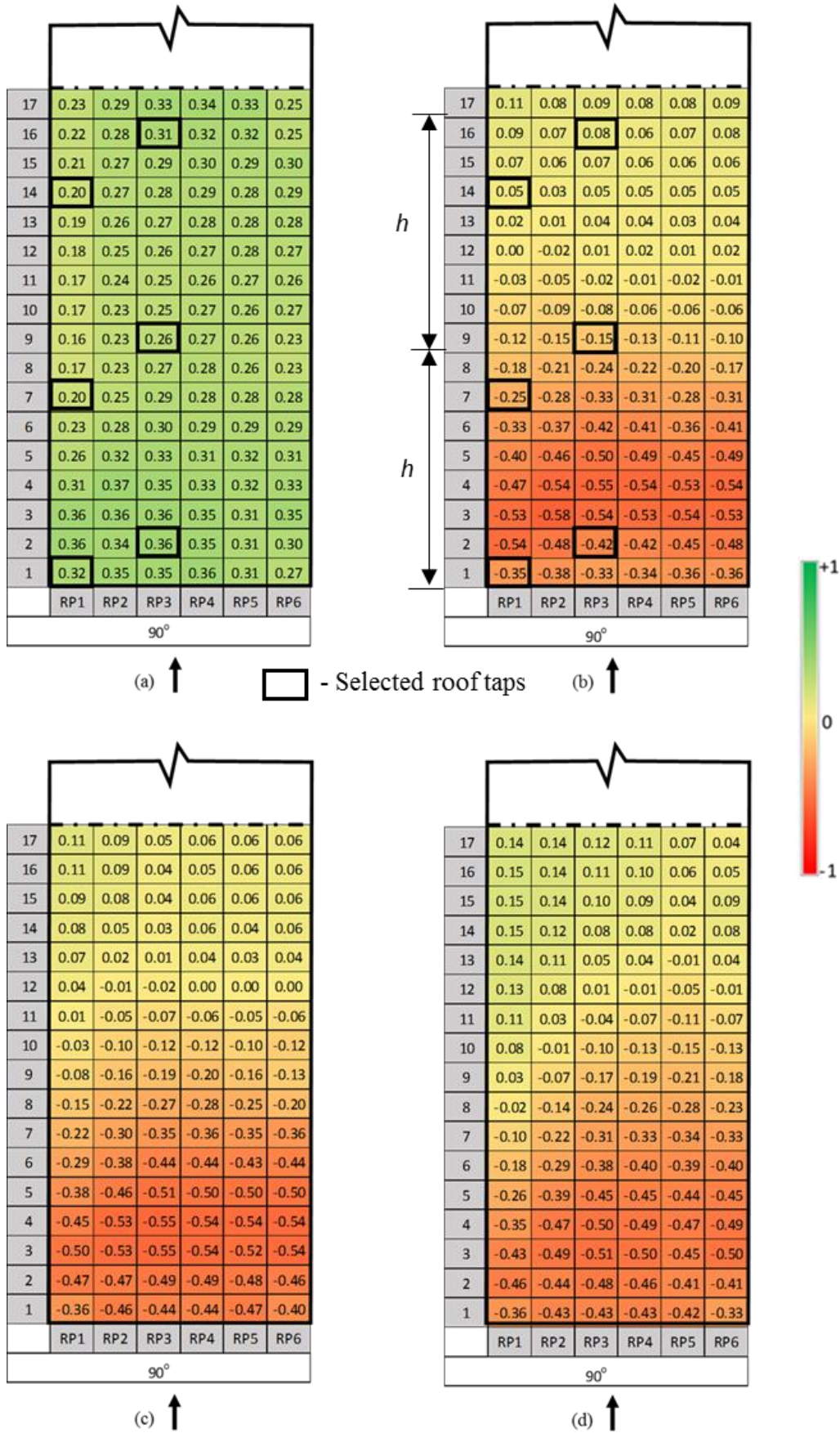


Figure 5.4: Correlation between external and internal pressure on roof cladding for $\theta = 90^\circ$ (a) Case #02, (b) Case #09, (c) Case #11, and (d) Case #12

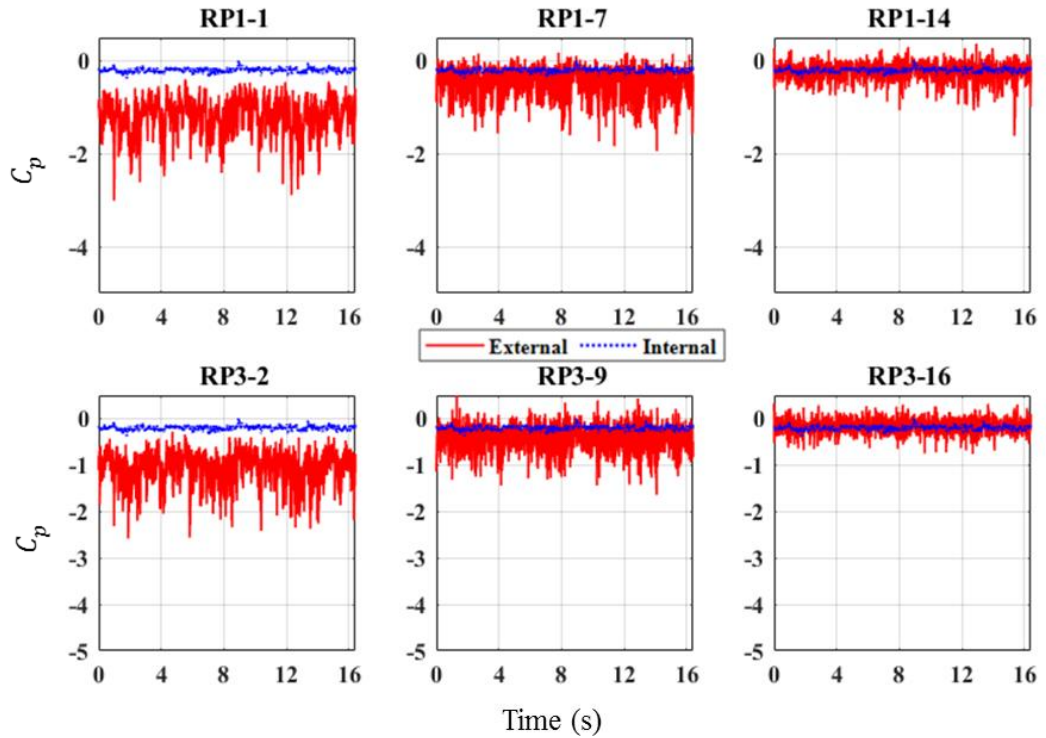


Figure 5.5: External and internal pressure fluctuations on the roof of the nominally sealed building, for $\theta = 90^\circ$ – Case #02

Several tap locations (shown in black rectangles in Figure 5.4b) are studied in further detail to examine the relationship between external pressure fluctuations and correlation coefficients across the roof locations. Figure 5.6. shows the fluctuating components, $C'_p(t) = C_p(t) - \bar{C}_p$ of external and internal pressure at these six locations for Case #09 at $\theta = 90^\circ$. The external pressures are decreasing towards the middle of the roof (i.e., RP1-1 to RP1-14) resulting in a small $C_{\sigma_{pe}}$ at the RP1-14, as shown in Figure 5.6. Time-varying fluctuating components of internal and external pressures in Figure 5.6 explain the negative and positive correlation between internal and external pressures.

The external and internal pressures at the RP3-2 are moderately correlated as the external pressures have higher fluctuations compared to the internal pressures fluctuations. Similarly, internal and external pressures are moderately correlated near the flow reattachment area at rows #3, #4 and #5 parallel to the windward edge. The $r_{pepi}(0)$ is around -0.5 at most of the locations, which are $0.3h$ away from the windward edge (between $0.3h$ and $1h$) in Cases #9, #11 and #12. RP1-7 and RP3-9 in Figure 5.6 show a similar fluctuation of external and internal pressures, which are moderately correlated on

the roof. $r_{pepi}(0)$ is dependent on the size of the large windward opening and that the percentage of variation is about 10% - 15% of the correlation coefficients between Cases #9, #11 and #12.

Internal and external pressures are poorly correlated in the middle of the roof after the flow reattachments (i.e., rows between #8 to #17, within $1h$ and $2h$) that $r_{pepi}(0)$ varies between -0.1 and $+0.1$ at $\theta = 90^\circ$, as shown in Figure 5.4. Figure 5.6 also shows that external pressures fluctuations at the taps RP1-14 and RP3-16 are smaller than the internal pressure fluctuations, with poor correlation indicating a random relationship between internal and external pressure fluctuations which have a relatively small variance from the mean external pressure.

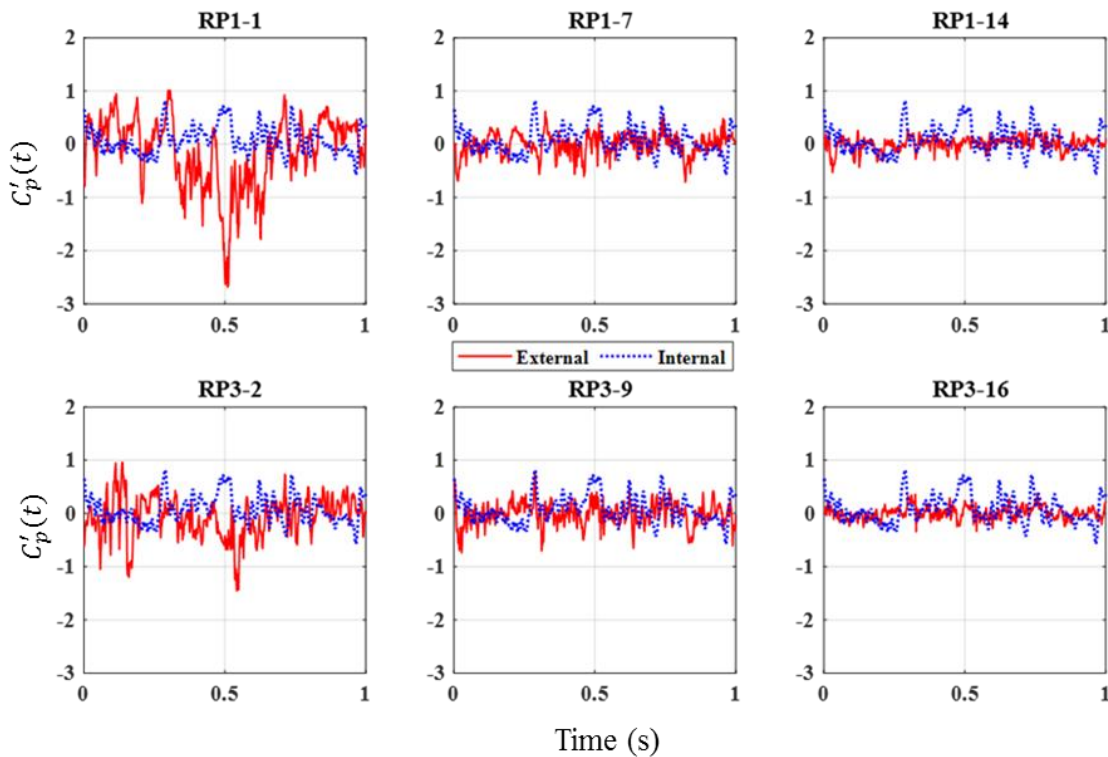


Figure 5.6: Fluctuating component of external and internal pressures ($C_p(t) - C_{\bar{p}}$) on the roof for Case #09 at $\theta = 90^\circ$

Figure 5.7 shows the correlation between external and internal pressures at RP3-1 and RP3-17 for Case #09 at $\theta = 90^\circ$. The largest r_{pepi} does not always occur at zero lag time as exemplified by the $r_{pepi}(0)$ is 0.09 (Figure 5.4b) and $r_{pepi}(0.032)$ is 0.18 for RP3-17 as shown in Figure 5.7 for Case #09 at $\theta = 90^\circ$. Figure 5.7 also shows that the external

pressure at RP3-17 has 0.032 s lag time which has poor correlation with internal pressure compared to the external pressure at the leading windward edge. This time difference in external pressures is the time taken to travel along the roof may increase along the roof purlin that the external and internal pressures are poorly correlated at the middle of the roof. Further, external pressures at windward roof edge (RP3-1) and internal pressures influenced by external pressures at the windward wall have similar variations to generate large $r_{pepi}(0)$ compared to middle of the roof. However, correlation between internal and external pressures at zero lag time is more important in building designing.

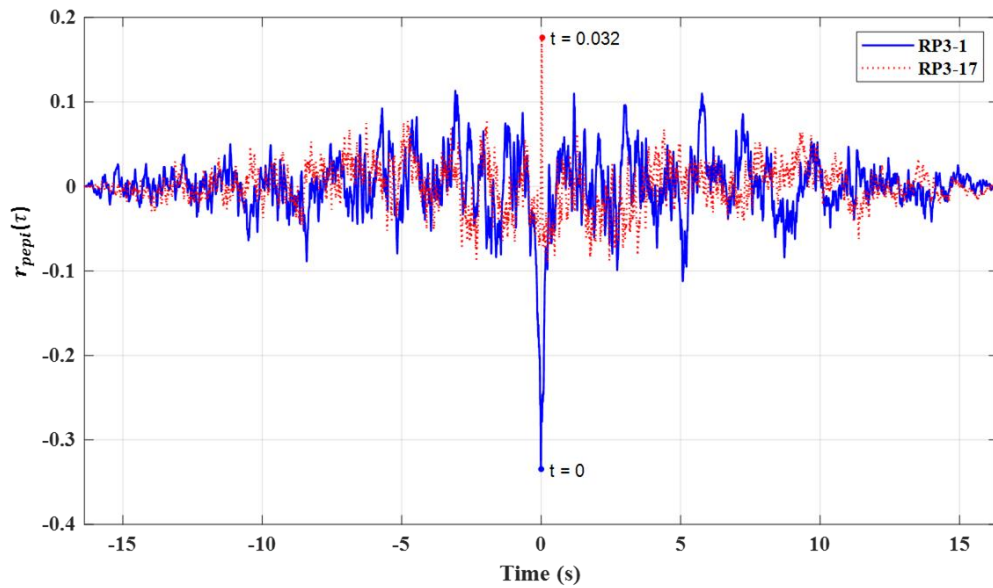


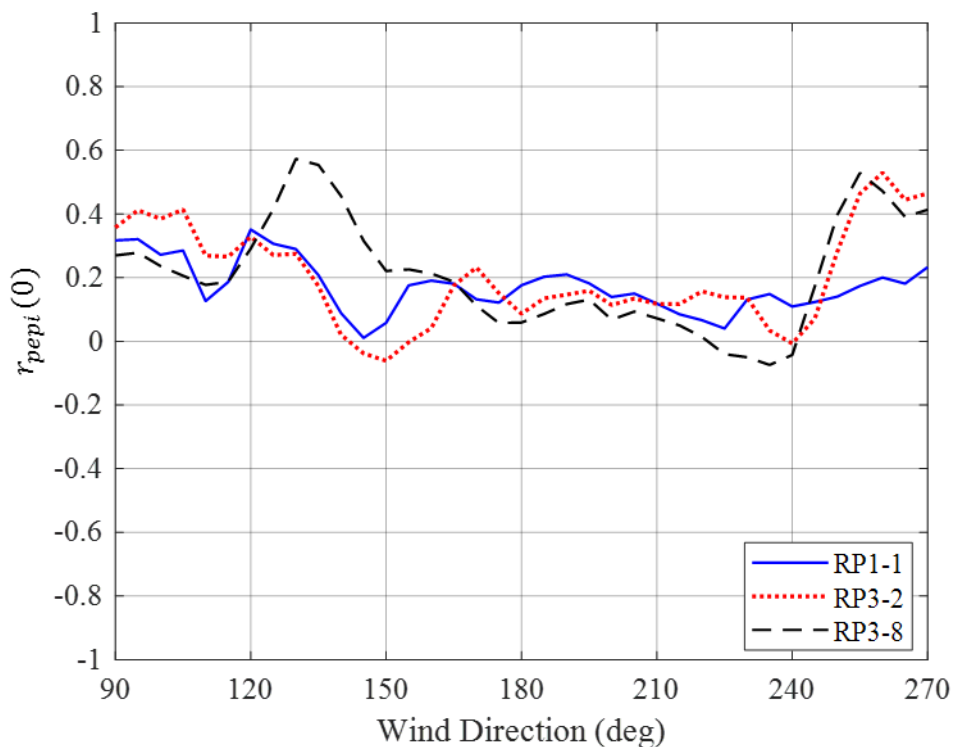
Figure 5.7: Correlation between internal and external pressure fluctuations at RP3-1 and RP3-17 for Case #09 at $\theta = 90^\circ$

Figure 5.8(a) – (d) show the correlation between internal and external pressures at RP1-1, RP3-2, and RP3-8 for Cases #02, #09, #11, and #12 for wind directions $\theta = 90^\circ$ to 270° . The internal pressure fluctuations are negative in Case #02, and the internal and external pressures are positively correlated, where $r_{pepi}(0)$ is less than 0.6 for all wind directions, as shown in Figure 5.8(a). Figure 5.8(b) – (d) show that external roof suction pressures at the roof windward edge (i.e., RP3-2), above the opening, have a high negative correlation with the positive internal pressures for $90^\circ \leq \theta \leq 135^\circ$, while external suction and negative internal pressures are positively correlated for $180^\circ \leq \theta \leq 270^\circ$.

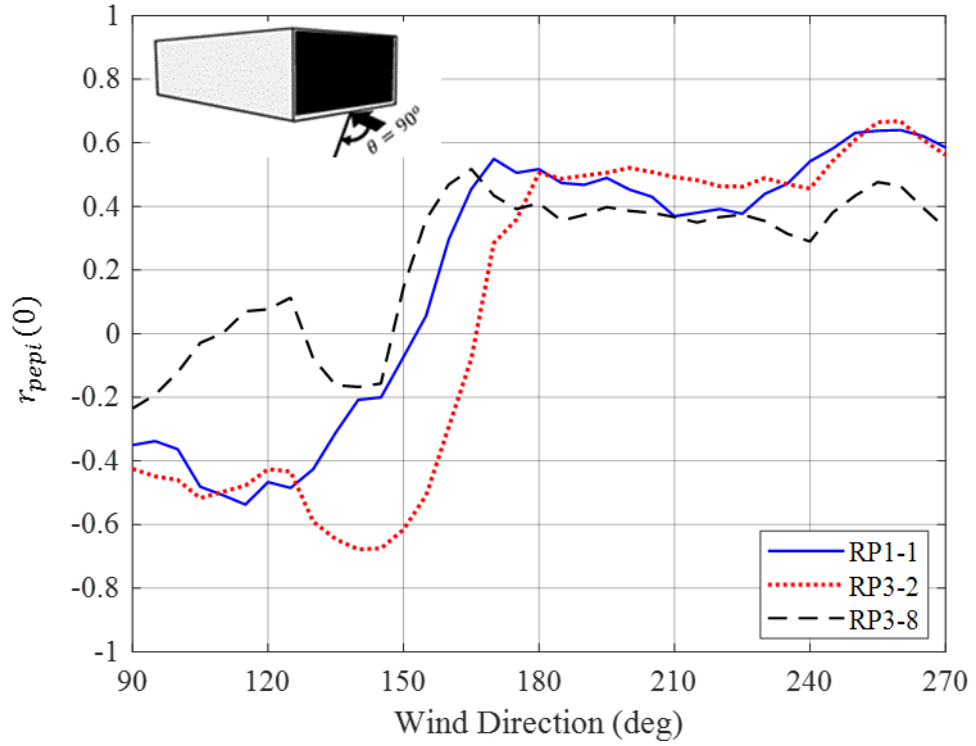
Figure 5.8(c) and (d) further shows that $r_{pepi}(0)$ decreases towards the middle of the roof for $\theta = 90^\circ$ to 135° . $r_{pepi}(0)$ for Cases #11 and #12 varying in a similar manner to the

results obtained by Xu and Lou (2017), Ginger and Letchford (1999) and Bodhinayake et al. (2020) that the large external suction pressures at the windward leading roof edge were well correlated with large positive internal pressures. Furthermore, for wind directions $90^\circ \leq \theta \leq 135^\circ$, $r_{pepi}(0)$ varied between -0.4 to -0.7 at the windward roof edge for Cases #09, #11 and #12, which is similar to results obtained by Sharma and Richards (2005) from model-scale tests of a building with a $40 \text{ mm} \times 20 \text{ mm}$ (i.e., $S^* = 17$) opening at the centre of the windward wall. The correlation of external and internal pressures in the middle of the roof for Cases #09, #11 and #12 are also similar to the results presented for three different single dominant opening cases by Xu and Lou (2017) when the openings are on the windward wall or sidewall.

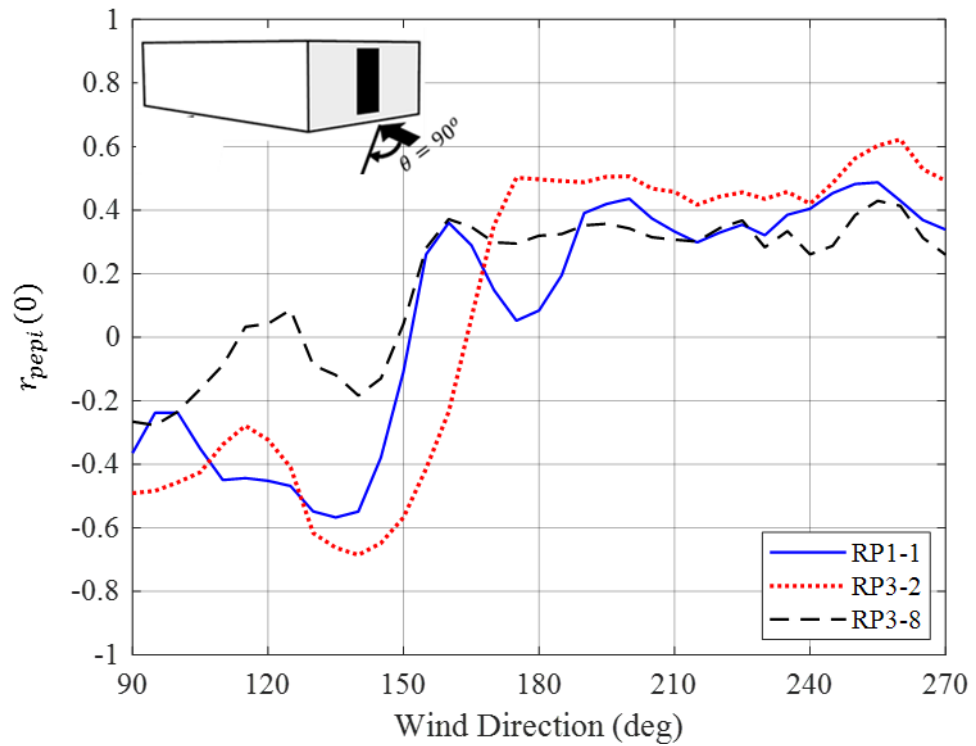
The correlation coefficient between negative internal pressure and external suction pressure varied between +0.4 to +0.6 for Cases #09, #11, and #12, at $180^\circ \leq \theta \leq 270^\circ$. Here, external pressure taps are located $2h$ or more away from the leading windward edge. This positive correlation leads to downward acting net pressures on the downwind side of the roof with the combination of positive external pressure and negative internal pressure at the roof cladding.



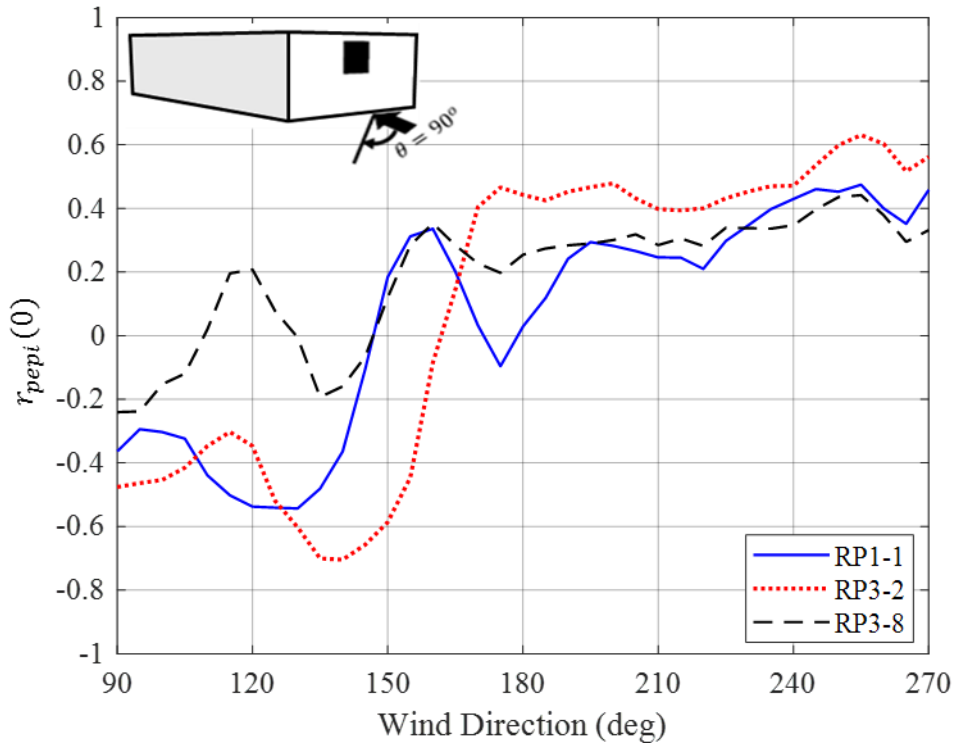
(a) Case #02



(b) Case #09



(c) Case #11



(d) Case #12

Figure 5.8: $r_{pepi}(0)$ for RP1-1, RP3-3, and RP3-8 for wind directions 90° to 270° ; (a) Case #02, (b) Case #09, (c) Case #11, (d) Case #12

Figure 5.8(c – d) show increasing higher negative correlations for oblique approach wind directions 120° to 150° for RP1-1 and RP3-2 when the internal pressures are positive, and the external pressures are negative resulting in high net suction pressures. Accordingly, $r_{pepi}(0)$ on whole roof purlin tributaries were further analysed as presented in Figure 5.9 at $\theta = 135^\circ$ to see a better understanding the correlation between internal and external pressure for oblique wind directions. Colour scales in Figure 5.9 show the contrast of correlated external and internal pressures due to conical vortex formation along the windward edges for the oblique wind flows.

For wind direction $\theta = 135^\circ$, external and internal pressures are poorly correlated in the nominally sealed building at the first and second rows and columns in Figure 5.9(a) such that the $r_{pepi}(0)$ is less than $|0.4|$. Here external pressures are highly fluctuating at the windward roof edges due to the formation of conical vortex along the edge, and internal pressures are small as illustrated in Figure 5.10(a). Figure 5.10(b) shows that external pressures are small at the roof middle (RP5-13) following the flow reattachment and

rollups. Here external pressure at the leeward roof edge and internal pressure fluctuations have similar temporal variation since both pressures have a relationship with the external pressure fluctuations at the leeward wall.

When the building has an opening on the gable end wall in Cases #09, #11, and #12, $r_{pepi}(0)$ is negative and external and internal pressures are moderately correlated where the flow separation occurs causing high suction pressures near the windward roof edge (i.e., first two rows) for the cornering wind direction $\theta = 135^\circ$. However, high suction external pressure due to conical vortices along with the roof purlins, RP1 and RP2 (i.e., first two columns) are poorly correlated with internal pressures.

When the whole gable end wall is open (Case #9), the conical vortices generating the external suction pressure at the windward roof edge creates a high correlation between internal pressure, as shown in Figure 5.9(b). Here it is more likely that conical vortices formed a single separation bubble adjacent to the wall and roof resulting in similar fluctuation of external and internal pressures. When the opening is on the middle of the gable end wall (Cases #11 and #12), flow separation happens over the gable end wall causing high suction pressures near the leading roof edge. Here, external pressures in a separated region independent of the opening are unlikely to be strongly correlated with internal pressures and pressure fluctuations caused by conical vortices are very likely to be poorly correlated with internal pressures. The colour scales of Figure 5.9(c)-(d) show a similar trend in correlation coefficients compared with Figure 5.9(b) showing a higher correlation coefficient about -0.7 at the flow separation regions.

Figure 5.9(c)-(d) also shows that highly fluctuating external pressures are poorly correlated with internal pressures for oblique wind directions along the roof edge above Wall #3 (i.e., Wall #3 is adjoining to Wall #4 with a large opening). The time lag between external and internal pressure fluctuations created the different $r_{pepi}(0)$ at two adjoining windward roof edges for oblique wind flows. Figure 5.11 shows the r_{pepi} at RP1-7 and RP2-1 for Case #09 at $\theta = 135^\circ$. Here, time lag of 0.053 s shows between highest correlation coefficient since RP2-1 located at top of the opening and suction pressure at RP2-1 is influenced by the external pressures at the windward wall, which is a driving pressure for internal pressure fluctuations. Thus, external and internal pressures are moderately correlated at RP2-1 compared to RP1-7 at the zero lag time.

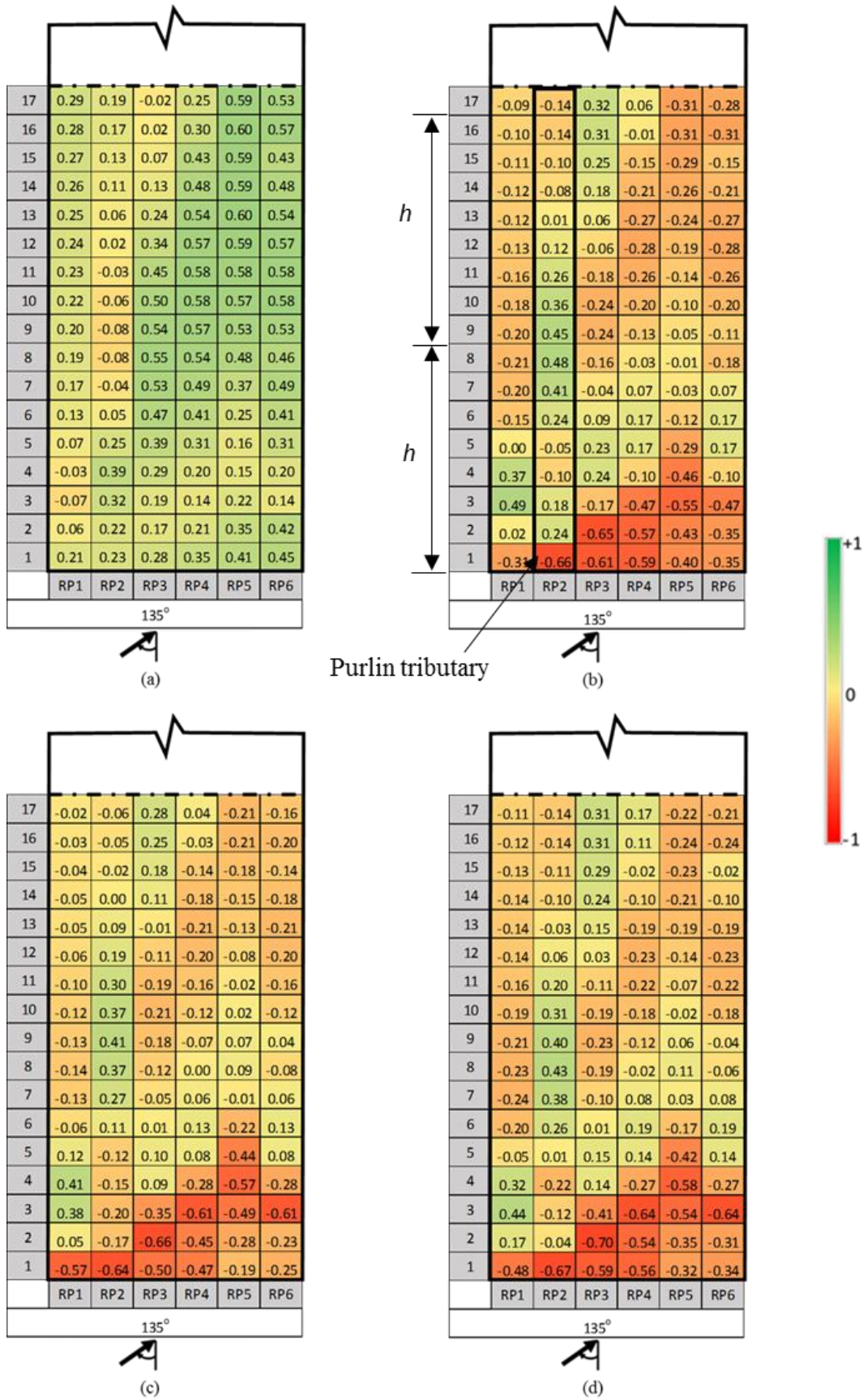


Figure 5.9: $r_{pepi}(0)$ on roof cladding for $\theta = 135^\circ$ (a) Case #02-nominally sealed, (b) Case #09-LO6 open, (c) Case #11-LO5 open, and (d) Case #12-LO4 open

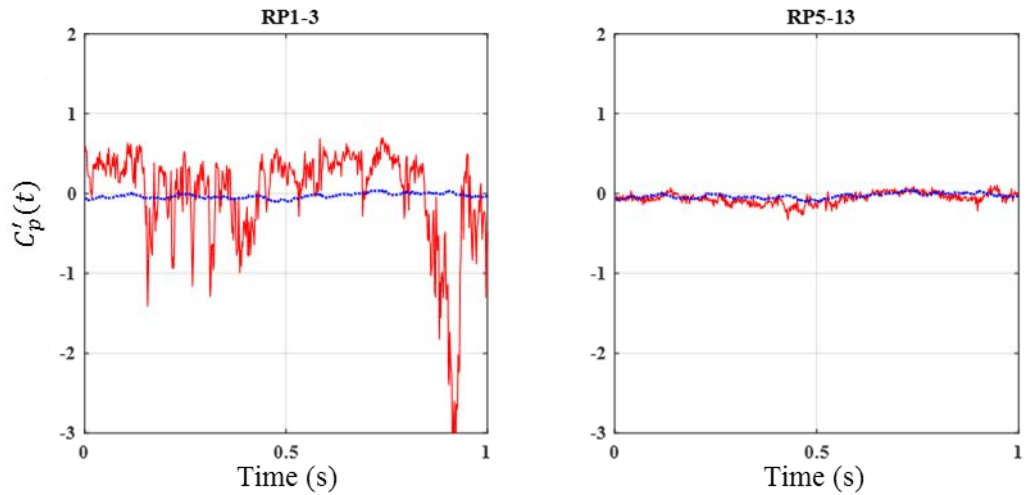


Figure 5.10: Fluctuating component of external and internal pressure at RP1-3 and RP5-13 for Case #02 at $\theta = 135^\circ$

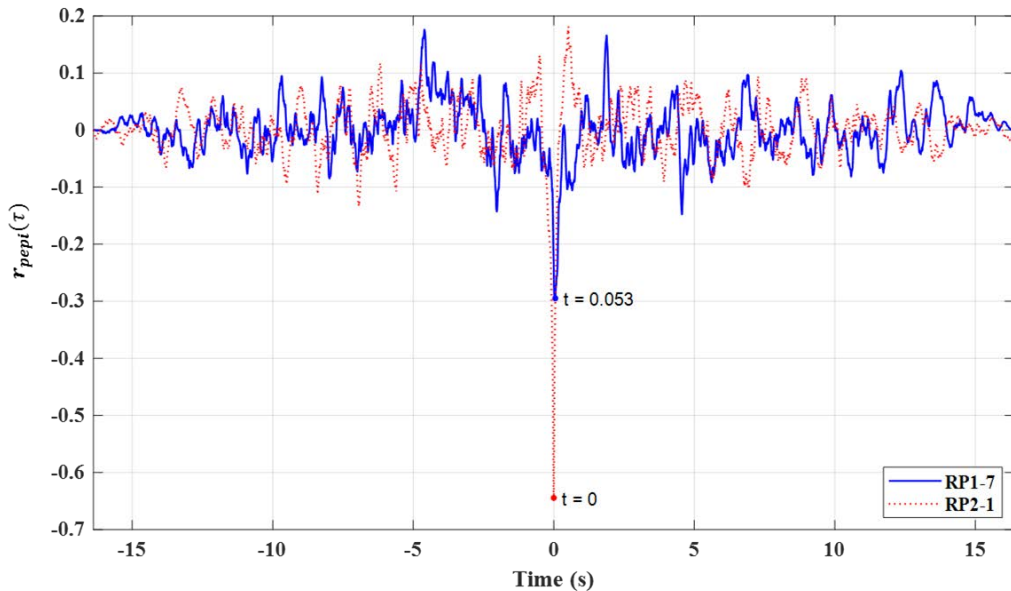


Figure 5.11: Correlation between internal and external pressures at RP1-7 and RP2-1 for Case #09 at $\theta = 135^\circ$

Figure 5.12 shows the fluctuating components of external and internal pressures at four different locations for Case #09 at $\theta = 135^\circ$. For roof locations, RP2-1 and RP4-2, the highly fluctuating components of the external pressures are negatively correlated with positive internal pressure. In contrast, fluctuating components of external pressures on roof locations RP1-3 and RP2-8 are positively correlated with positive internal pressure. The external and internal pressure changes as seen in Figure 5.12 (RP2-1 and RP4-2) the increase in external pressure coincides with the decrease in internal pressure and vice-

versa. However, for pressure tap locations RP1-3 and RP2-8, external and internal pressures increase or decrease together.

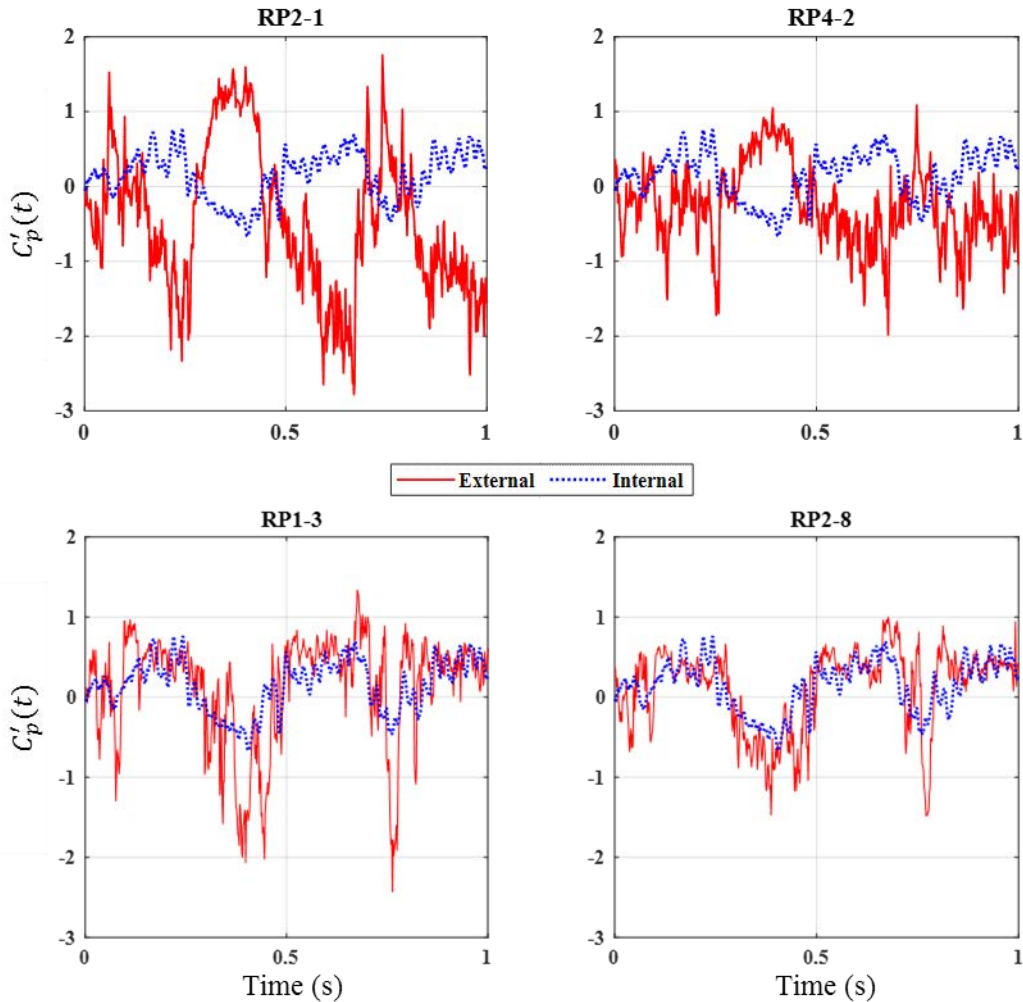


Figure 5.12: Fluctuating component of internal and external pressures at RP2-1, RP4-2, RP1-3 and RP2-8 for Case #09 at $\theta = 135^\circ$

Figure 5.13 shows the fluctuating components of internal and external pressures at RP5-13 and RP6-7 for Case #09 at $\theta = 135^\circ$. Figure 5.13 shows the significantly smaller external pressure fluctuations at the roof taps RP5-13 and RP6-7, which are poorly correlated with highly fluctuating internal pressure. The time lag between external and internal pressure fluctuations at the middle of the roof cladding, as shown in Figure 5.7 continued for other wind directions to produce the poor correlation between internal and external pressures.

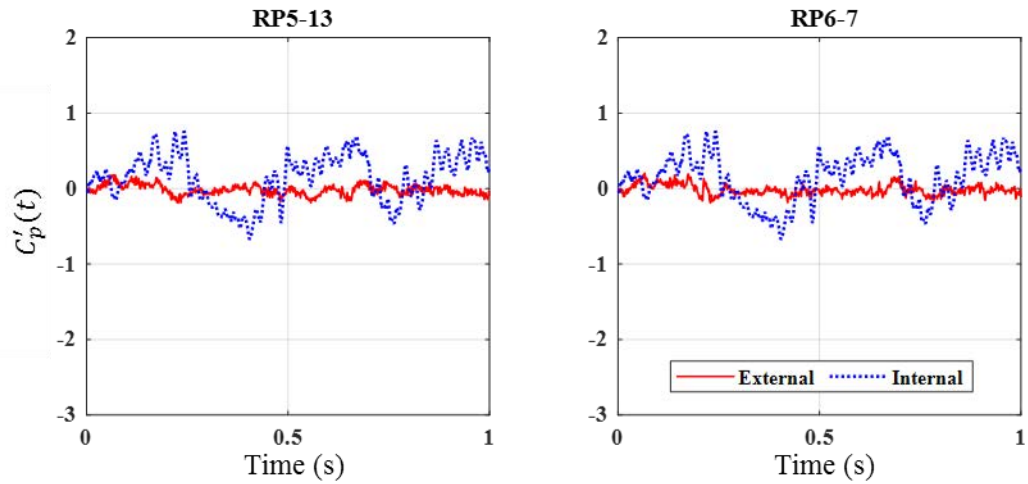


Figure 5.13: Fluctuating component of internal and external pressures at RP5-13, and RP6-7 for Case #09 at $\theta = 135^\circ$

5.2.1.1 Correlation between external, internal and net pressures- Case #09

Figure 5.14 and Figure 5.15 show the correlation between internal and external pressures (r_{pepi}), correlation between external and net pressures (r_{pepn}) and correlation between internal and net pressures (r_{pipn}) at the locations along RP3 and RP4 for a building with a large opening (Case #09) for $\theta = 90^\circ$ to 135° . The r_{pepn} is always positive and r_{pipn} is negative since the external and net pressures are acting in the same direction, while internal pressure acts in the opposite direction. The $r_{pepi}(0)$ values are less than $r_{pipn}(0)$ and $r_{pepn}(0)$ since internal and external pressures are independent events while net pressure depends on the combination of external and internal pressures.

Figure 5.14 and Figure 5.15 further show that the external and net pressures, and internal and net pressures are highly correlated at the windward edge (RP3-1 and RP4-1), thus $r_{pepn}(0)$ is higher than 0.9 and $r_{pipn}(0)$ is around 0.75 for $\theta = 90^\circ$ to 135° . Here, net pressure fluctuation mainly follows the external pressure fluctuations at the windward edge. At the middle of the roof (RP3-16 and RP4-16), external and net pressures are poorly correlated, while internal and net pressures are highly correlated. Here net and internal pressure have similar fluctuations since external pressures have less effect on net pressure fluctuations. Thus, the correlation between external and net pressure decreased, while the correlation between internal and net pressure increased towards the middle of the roof from the windward edge when the opening is perpendicular to approaching wind.

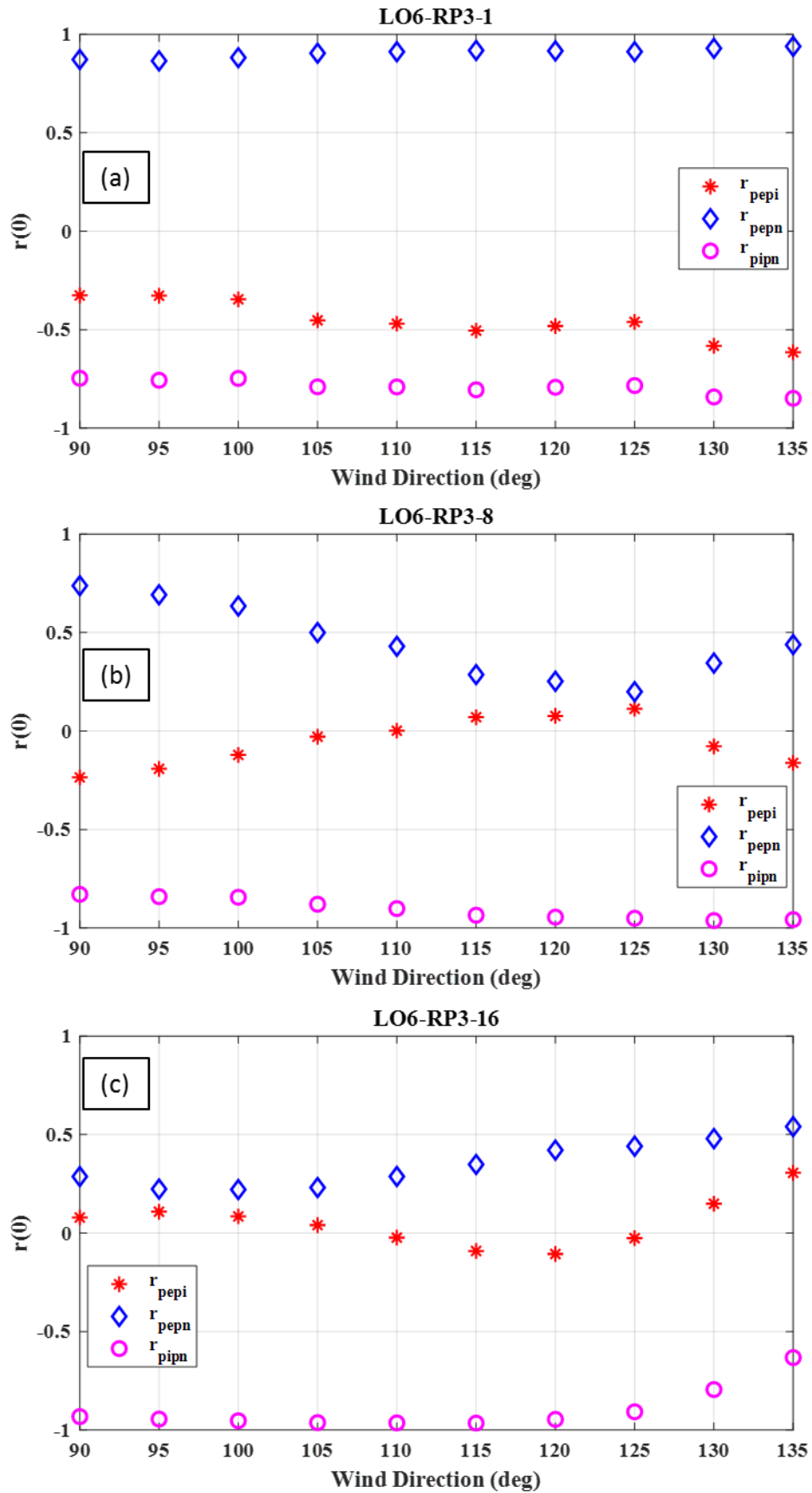


Figure 5.14: Correlation between internal, external and net pressure time-histories of Case #09 for wind directions 90° to 135° (a) RP3-1, (b) RP3-8, and (c) RP3-16

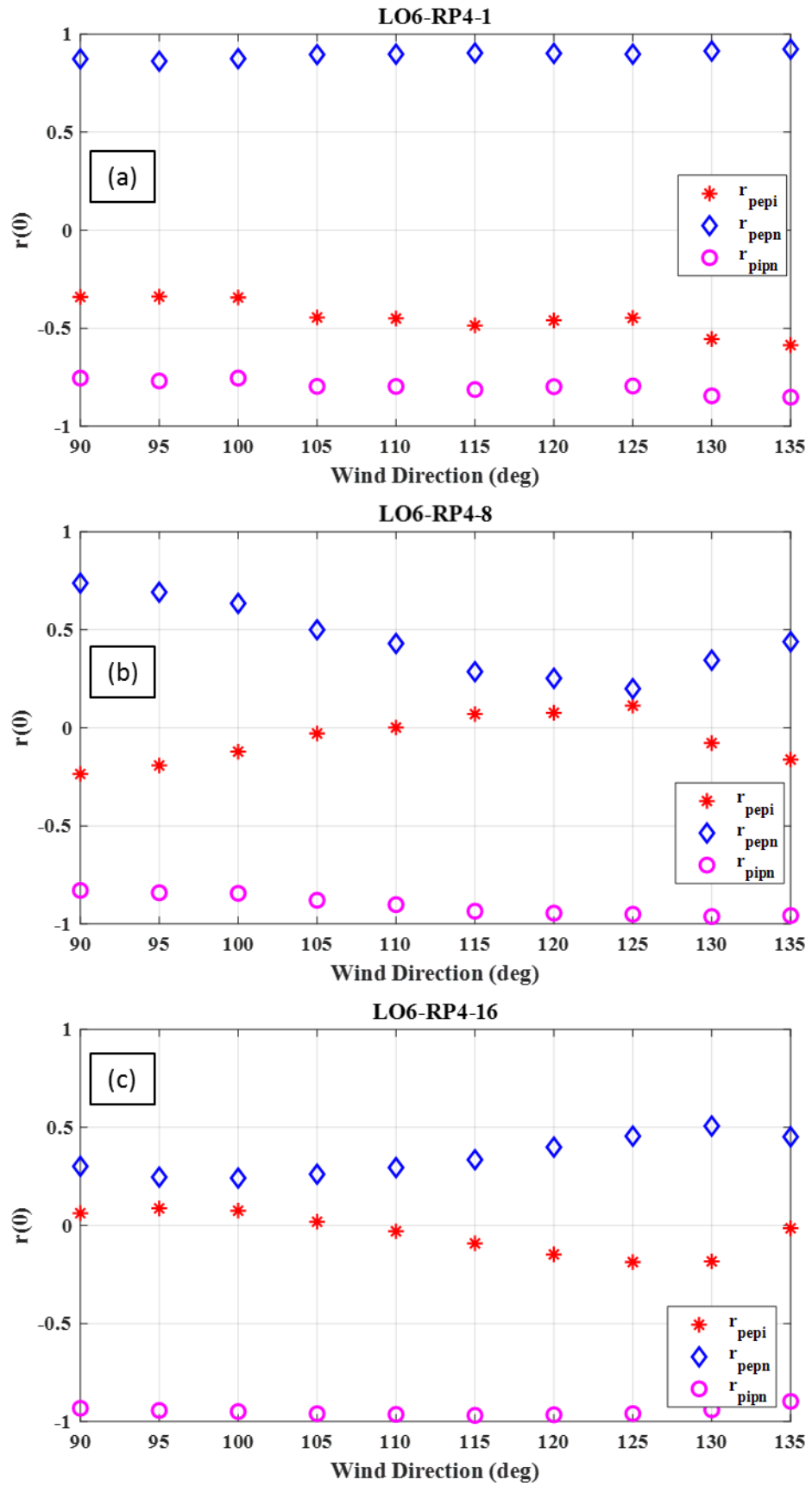


Figure 5.15: Correlation between internal, external and net pressure time-histories of Case #09 for wind directions 90° to 135° (a) RP4-1, (b) RP4-8, and (c) RP4-16

5.2.2 Correlation coefficients on the roof cladding- opening on Wall #1

The effect of the location of the opening the r_{pepi} is studied through openings LO1 and LO3 described in Cases #04 and #08. Figure 5.16 shows the $r_{pepi}(0)$ for selected roof locations when the LO1 is opened for wind directions 0° to 180° . For wind directions, $0^\circ \leq \theta \leq 45^\circ$, negative external and positive internal pressures are negatively correlated between -0.4 and -0.5. When the opening is on the windward wall, external pressures on the upwind part of the roof are negatively correlated with internal pressure and $r_{pepi}(0)$ decreases for sidewall opening. When the opening is at the leeward wall for wind directions 135° to 180° , external pressures at RP5-14 and RP6-17 are positively well correlated with negative internal pressure since the tap locations are near the leeward roof edge above the opening. For Case #04 windward opening, external pressures on upwind roof edge (RP6-17) has a high correlation with internal pressure and is poorly correlated on the roof corners (RP6-2) in agreement with the results of Ginger and Letchford (1999) and Beste and Cermak (1997).

Figure 5.17 shows the $r_{pepi}(0)$ for selected roof taps on the building with an opening at the edge of Wall #1 (LO3) for wind directions 0° to 180° . External pressures on the windward roof edge near the opening (RP6-2 and RP5-5) and internal pressures are moderately correlated compared to RP6-17 located away from the windward wall opening for wind direction $\theta = 0^\circ$. Comparison of Figure 5.16 and Figure 5.17 shows that the location of the opening significantly affects the correlation between external and internal pressures on the roof cladding. Especially when the opening is near the edge of the windward wall, $r_{pepi}(0)$ decreased from -0.5 to -0.1 for wind direction 10° to 50° at the windward corner region of the roof and increased positively till +0.6 at $\theta = 80^\circ$.

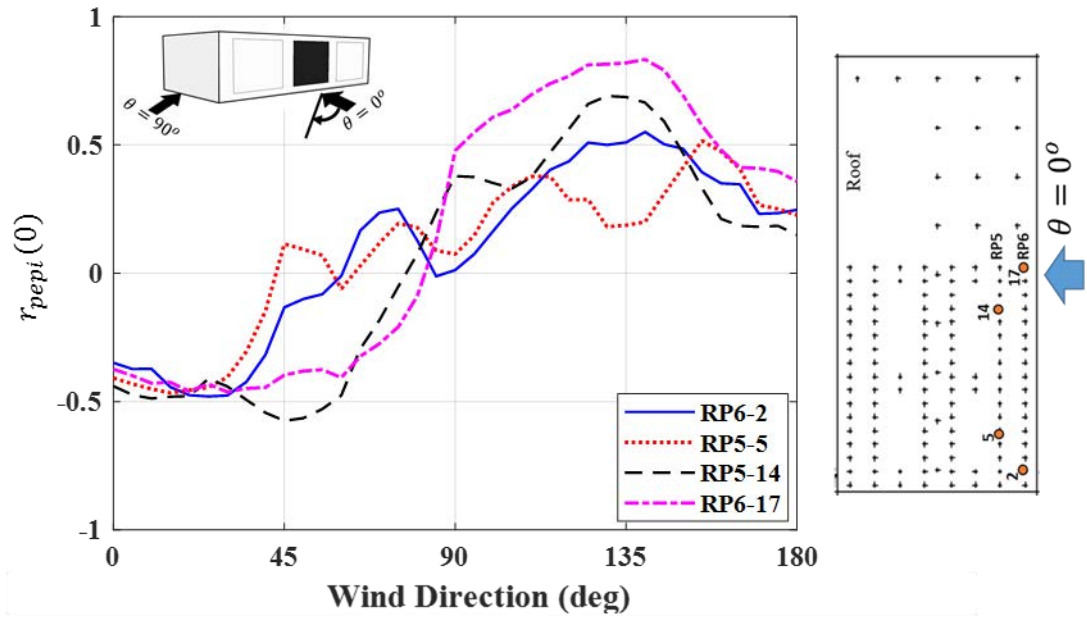


Figure 5.16: $r_{ppepi}(0)$ for selected locations on the roof purlins, RP5 and RP6 for LO1 opening (Case #04) – $\theta = 0^\circ$ to 180°

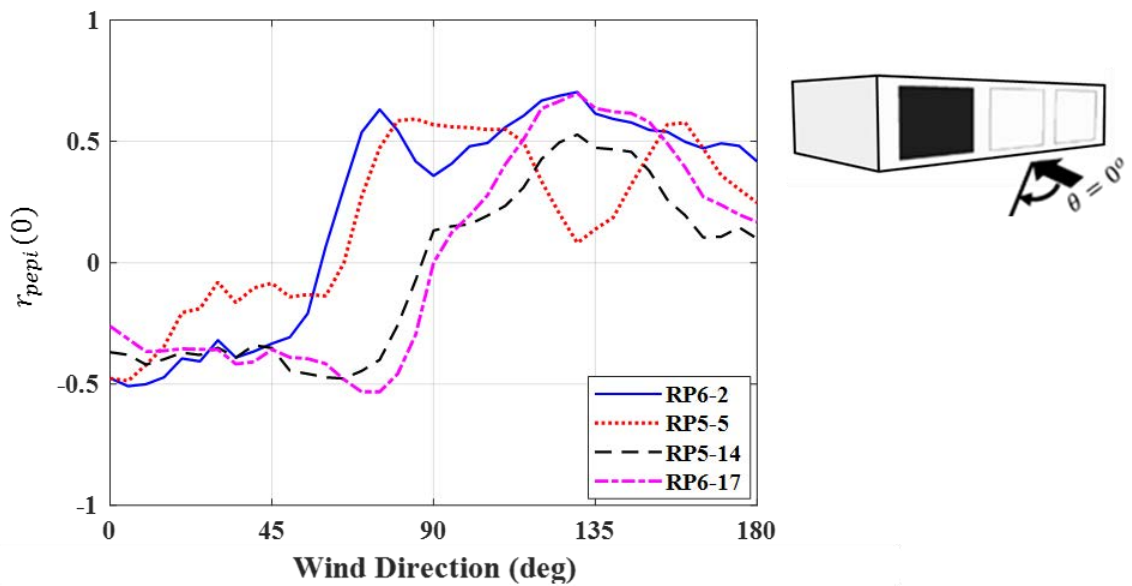


Figure 5.17: $r_{ppepi}(0)$ for selected locations on the roof purlins, RP5 and RP6 for LO3 opening (Case #08) – $\theta = 0^\circ$ to 180°

The $r_{ppepi}(0)$ explained in Sections 5.2.1 and 5.2.2 for different cladding locations on the roof shows that the external suction and positive internal pressure fluctuations in the building with large opening is negatively correlated. The $r_{ppepi}(0)$ is less than $|0.7|$ regardless of the opening size and approaching wind directions. The external and internal

pressure fluctuations are poorly correlated at the roof windward corner and moderately correlated at the windward roof edge ($< 1h$ from the windward edge). Furthermore, $r_{pepi}(\tau)$ is less than $|0.2|$ due to the time taken for external pressure fluctuations to travel along the roof, compared to the internal pressure fluctuations caused by external pressure at the windward wall opening.

5.2.3 Correlation coefficients on the wall cladding

(i) Opening on Wall #4

Correlation between external and internal pressures are analysed on four locations, WG2-1, WG2-3, WG2-8, and WG2-17 on Wall #1, as shown in Figure 5.18. Figure 5.19 presents the correlation coefficient for selected tap locations on the wall girt tributary (i.e., WG2) for Cases #02, #09 and #11 with an opening on Wall #4 for wind directions 90° to 270° .



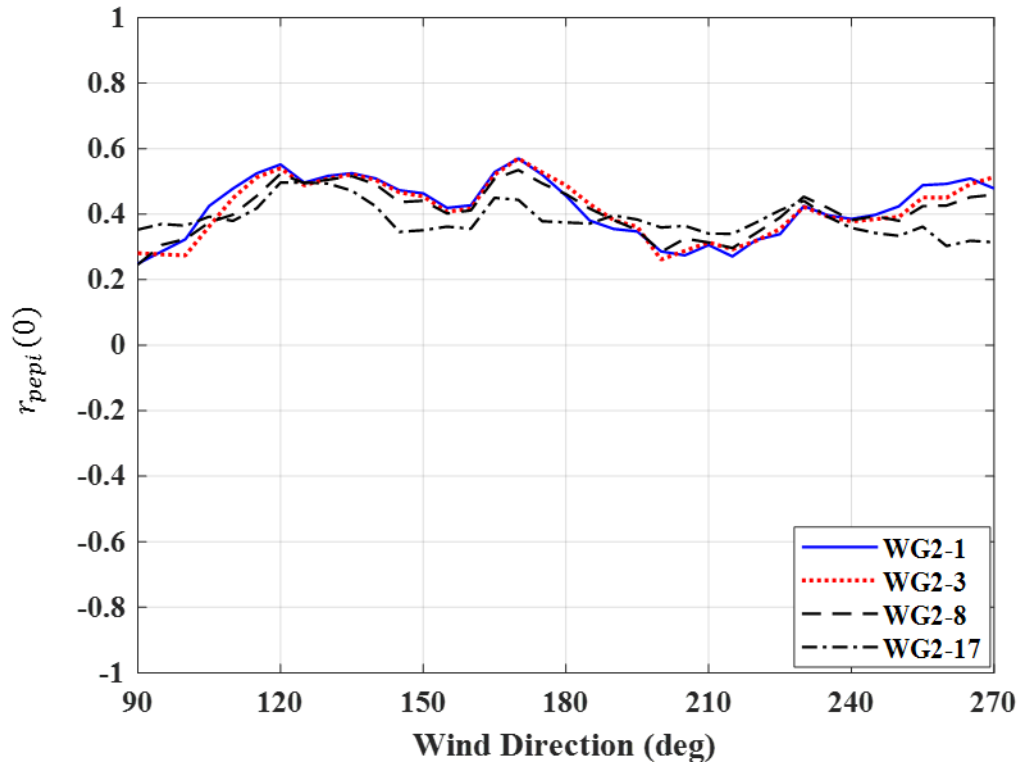
Figure 5.18: Selected external pressure taps on Wall #1

For the nominally sealed building (Case #2), Figure 5.19(a) shows that $r_{pepi}(0)$ varies between 0.2 and 0.5 for all wind directions $\theta = 90^\circ$ to 270° . Further, correlation coefficients on the wall and roof of the nominally sealed building have similar variation as shown in Figure 5.8(a) and Figure 5.19(a) because the internal pressures are generated by leakage through all walls which are not related to external pressure fluctuations at a single tap location.

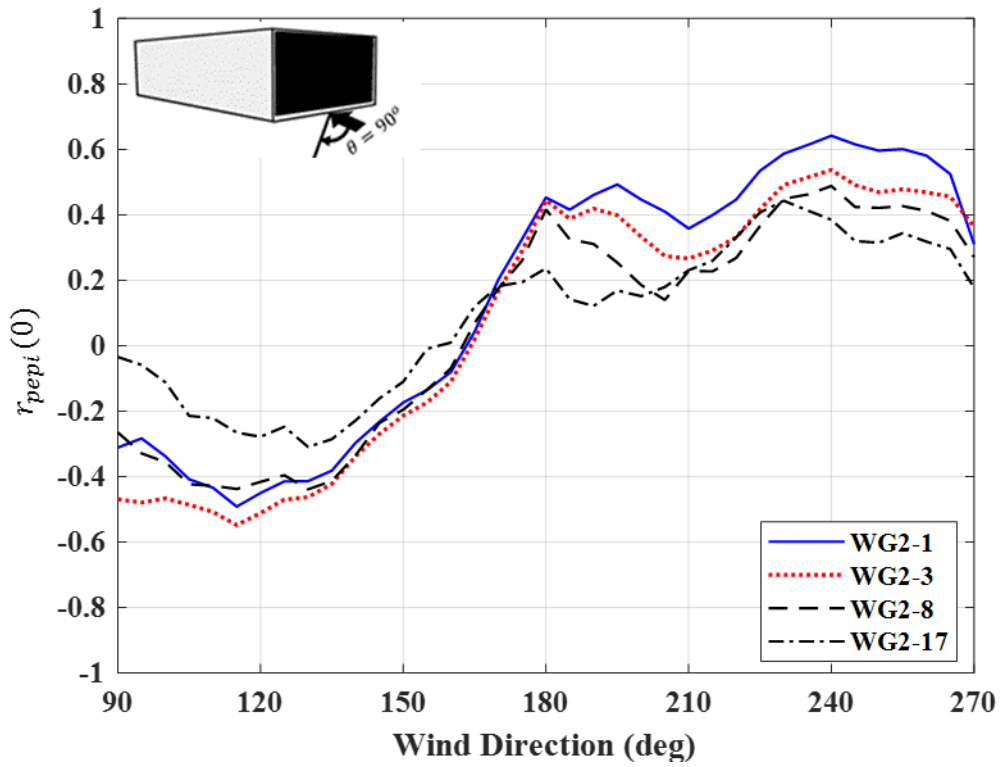
For wind directions $90^\circ \leq \theta \leq 135^\circ$, WG2 is on the side wall of the building and $r_{pepi}(0)$ is negative, as shown in Figure 5.19(b) - (c) for Cases #09 and #11. External pressures

near the leading edge of Wall #1 (WG2-1 and WG2-3) are moderately correlated with internal pressure fluctuations compared to the middle of the side wall (WG2-17) for $\theta = 90^\circ$ to 135° . $r_{pepi}(0)$ on the roof and side wall have similar variations for Cases #09 and #11 following a similar external pressure fluctuation patterns at the leading edge and reattachment area caused by conical vortices and rollups. However, the correlation coefficient on the roof leading edge is higher in magnitude compared to the side wall for the oblique wind directions (i.e., $\theta = 135^\circ$). The $r_{pepi}(0)$ is slightly higher at WG2-3 for the whole wall opening (Case #09) since the pressure tap is near the opening at the separation bubble which influenced internal pressure fluctuations compared to the opening at the middle of the Wall #4 (Case #11).

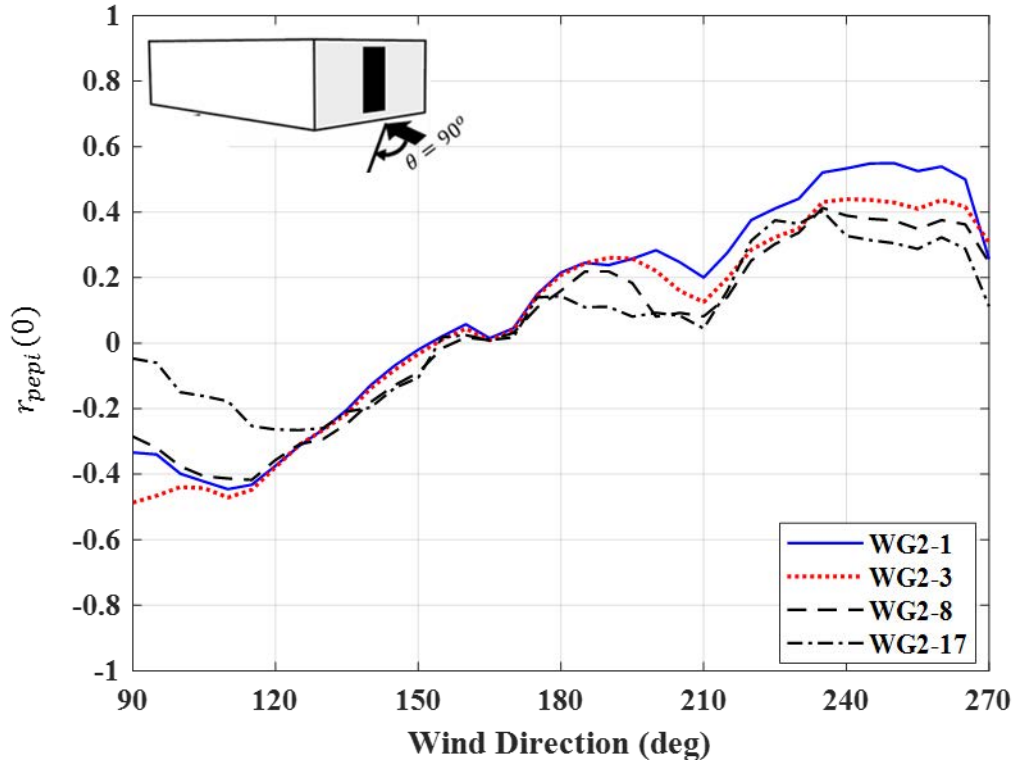
When the opening is on the side wall, WG2 is on the leeward wall and $r_{pepi}(0)$ changes from negative to positive with the negative internal and negative external pressures being positively correlated for wind directions $165^\circ \leq \theta \leq 225^\circ$. Here, external and internal pressures are moderately correlated at WG2-1 and WG2-3 for Case #09, because these are near to the opening edge of LO6 with similar temporal variations in internal and external pressures compared to Case #11. For wind directions $225^\circ \leq \theta \leq 270^\circ$, $r_{pepi}(0)$ increases from WG2-17 to WG2-1 along the side wall $2h$ away from windward leading edge when the opening is on the leeward wall. Here, small internal pressure fluctuations depend on the small external pressures at the leeward opening that the negative external and negative internal pressures are positively correlated caused by the spatial and temporal variations in external and internal pressure fluctuations.



(a) Case #02



(b) Case #09



(c) Case #11

Figure 5.19: $r_{pepi}(0)$ on WG2-1, WG2-3, WG2-8 and WG2-17 on Wall #1 for wind directions 90° to 270° (a) Case #02, (b) Case #09, and (c) Case #11

(ii) Opening on Wall #1

Figure 5.20 shows the correlation between internal and external pressure fluctuations at WG3-2, WG3-5, WG3-9 and WG3-12 on Wall #1 for $\theta = 0^\circ$ to 180° when LO1 is open (Case #04). For windward wall opening ($0^\circ \leq \theta \leq 45^\circ$), positive internal pressure and positive external pressures are positively correlated. $r_{pepi}(0)$ is large near to the opening (WG3-12) and decreases towards the side wall (WG3-2) due to the spatial variations in external pressure fluctuations from WG3-12 to WG3-2. Figure 5.20 also shows that negative external pressures at the leading edge are poorly correlated with negative internal pressure and $r_{pepi}(0)$ increases toward the side wall opening for $\theta = 45^\circ$ to 135° . When the opening is on leeward side ($135^\circ \leq \theta \leq 180^\circ$), external and internal pressures are moderately correlated and $r_{pepi}(0)$ is almost similar at all locations due to less temporal variations in external pressure fluctuations on the leeward wall.

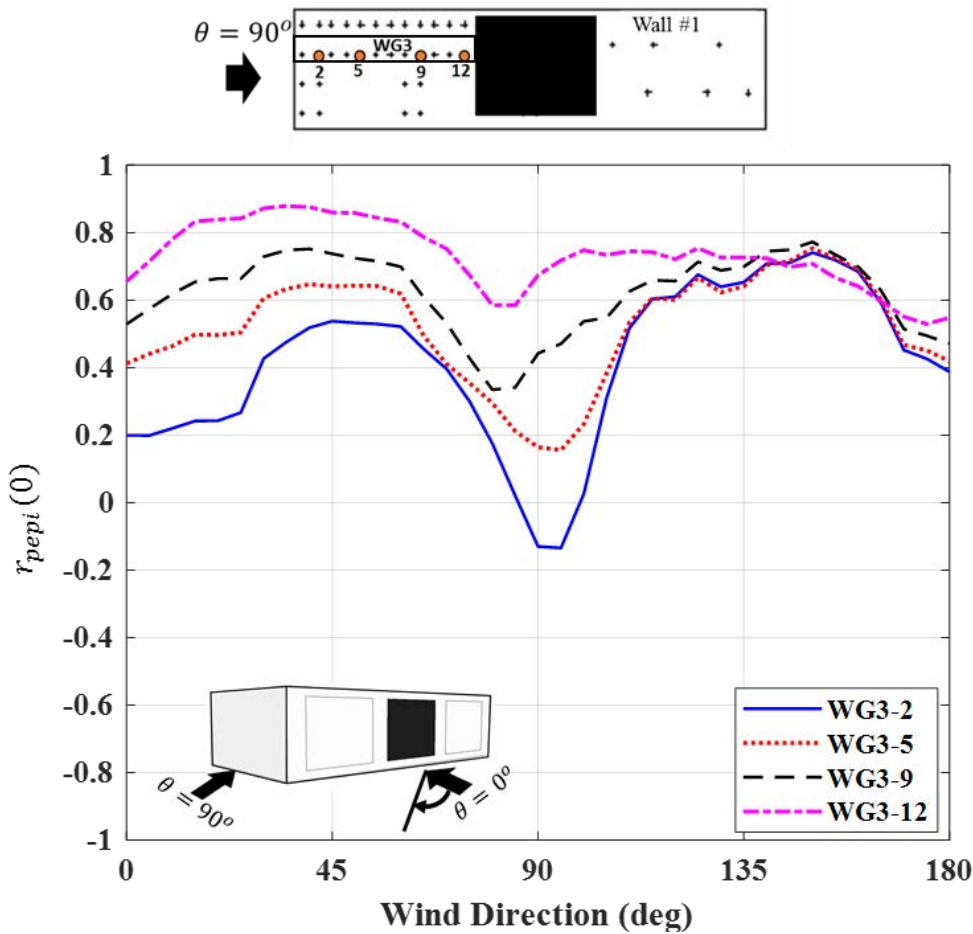


Figure 5.20: $r_{pepi}(0)$ on WG3-2, WG3-5, WG3-9 and WG3-12 on Wall #1 with the opening on Wall #1 for wind directions 0° to 180° for Case #04

The internal and external pressures are poorly correlated on Wall #3 for $\theta = 0^\circ$ to 180° when the opening is on the opposite wall (Wall #1) as shown in Figure 5.21. For wind direction 0° to 45° , negative external pressures and positive internal pressures act on Wall #3, negative internal and negative external pressures applied on Wall #3 for $\theta = 45^\circ$ to 135° , while negative internal and positive external pressures occurred on Wall #3 for $\theta = 135^\circ$ to 180° . The internal pressures are generated by the external pressure at the opening on Wall #1. The external pressures on Wall #3 are generated by the flow around the building and such do not have a direct relationship with internal pressure fluctuations that leads to poor correlation between internal and external pressure fluctuations on Wall #3.

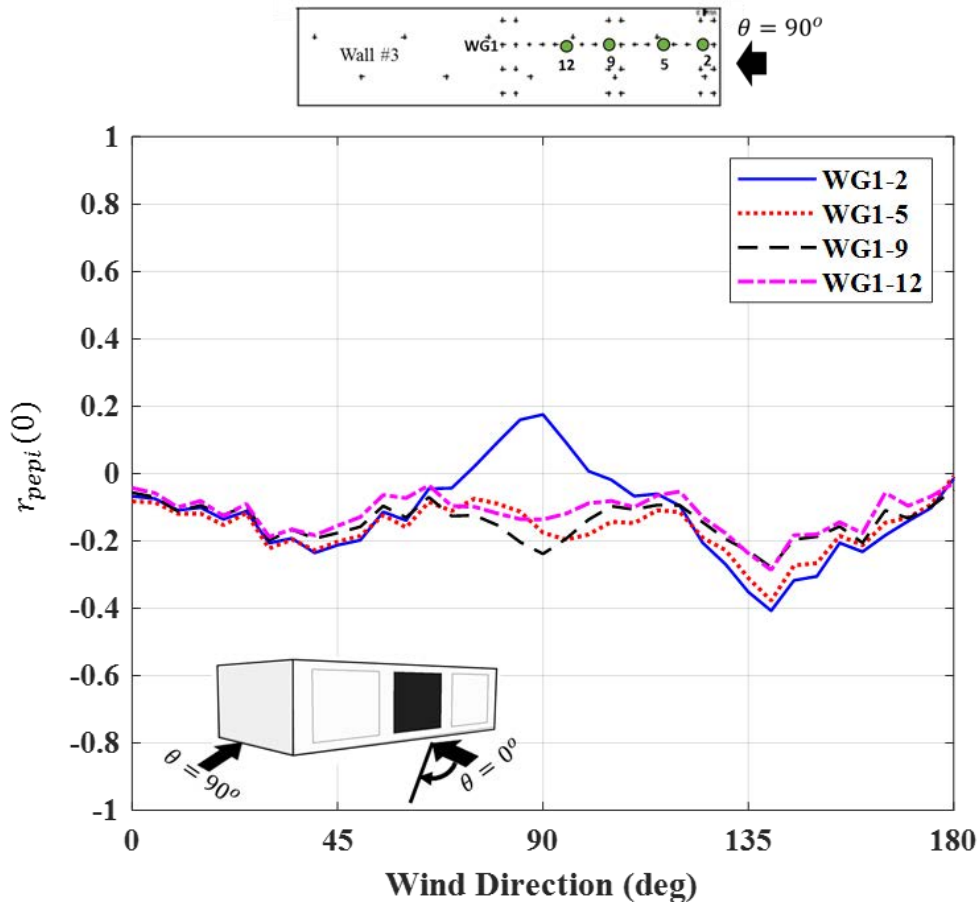


Figure 5.21: $r_{pepi}(0)$ on WG1-2, WG1-5, WG1-9 and WG1-12 on Wall #3 with the opening on Wall #1 for wind directions 0° to 180° for Case #04

5.3 Effect of the building volume on the correlation coefficient

Figure 5.22 shows the $r_{pepi}(0)$ for single taps in Zone #1 and Figure 5.23 shows the area-averaged external pressures of four taps in Zone #1 for Cases #09 and #23 for $\theta = 90^\circ$ to 270° . Taps RP1-1 and RP2-2 are in the same roof Zone #1B where $r_{pepi}(0)$ are different at the windward roof edge for $\theta = 90^\circ$ to 150° , as shown in Figure 5.22. Figure 5.22 also shows that the $r_{pepi}(0)$ has small variation when the building volume is changed from Case #09 to Case #23. r_{pepi} as each tap is sensitive to the wind direction since the external pressure fluctuations depend on the flow separation, reattachment and formation of vortices. The area-averaged external pressures on roof Zone #1B (i.e., 4 taps) gives the effect of the averaging external pressures. Accordingly, different $r_{pepi}(0)$ on roof Zone #1B are derived between area-averaged external pressures (i.e., 4 taps) and internal pressure fluctuations as shown in Figure 5.23. For the windward wall opening, the largest

$r_{pepi}(0)$ is about -0.6 for Cases #9 and #23 at $\theta= 105^\circ$. Similarly, $r_{pepi}(0)$ is about +0.6 when the opening is on side wall for $\theta= 180^\circ \pm 45^\circ$ and +0.7 for leeward wall opening at 250° . Figure 5.23 also shows that area-averaged $r_{pepi}(0)$ has similar variations for two different building volumes with same opening size.

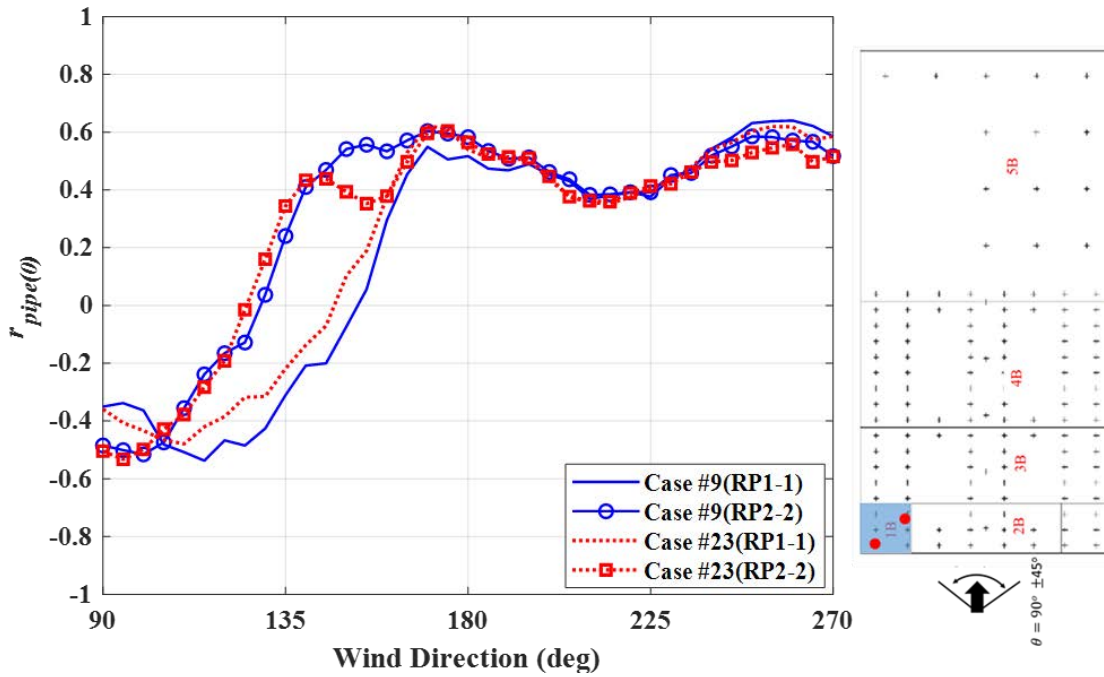


Figure 5.22: $r_{pepi}(0)$ for Cases #9 and #23 at RP1-1 and RP2-2 for $\theta = 90^\circ$ to 270°

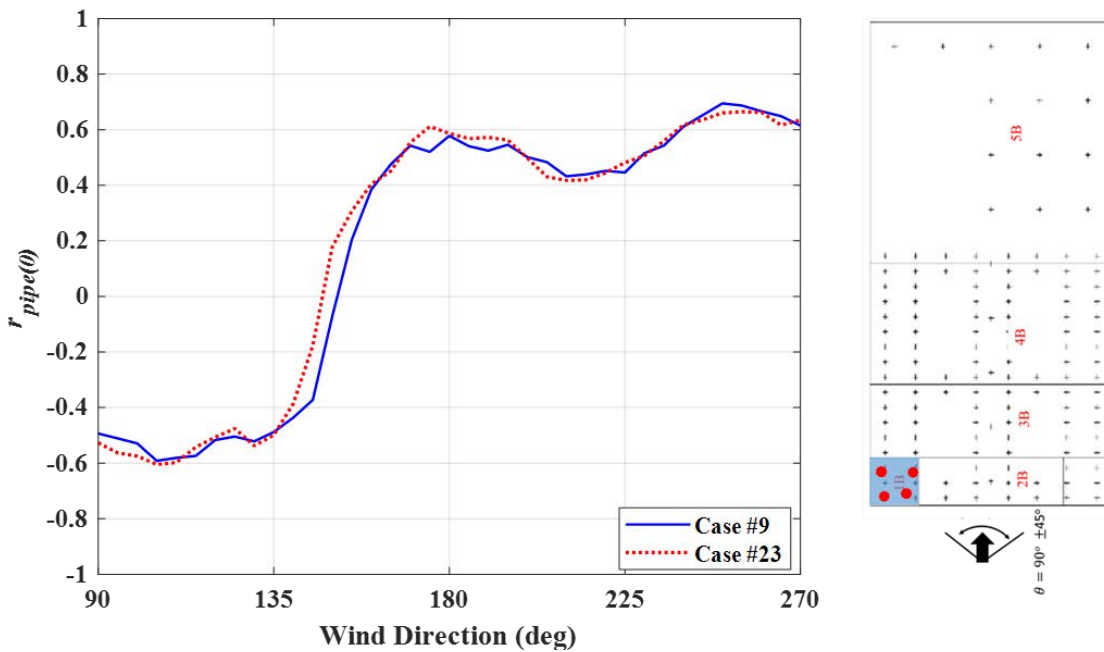


Figure 5.23: Area-averaged $r_{pepi}(0)$ for Zone #1B for Cases #9 and #23 for $\theta = 90^\circ$ - 270°

The correlation between area-averaged external and internal pressure fluctuations are presented relative to the non-dimensional parameter, S^* in Figure 5.24. For wind directions 90° to 135° , largest $r_{pepi}(0)$ for Zone #1B varies between -0.6 and -0.7 for windward wall opening configurations, LO6 (Cases #09, #21, and #23), LO5 (Cases #11, #22, and #24) and LO4 (Cases #12, and #25) as presented in Figure 5.24. Accordingly, area-averaged external and internal pressure fluctuations are moderately correlated and nearly constant for the whole wall opening cases (Cases #09, #21, and #23), because external pressure on Zone #1B and internal pressure are influenced by the external pressures at the opening LO6. However, the effect of correlation between internal and external pressures to generate peak net pressures is analysed in Section 5.4.

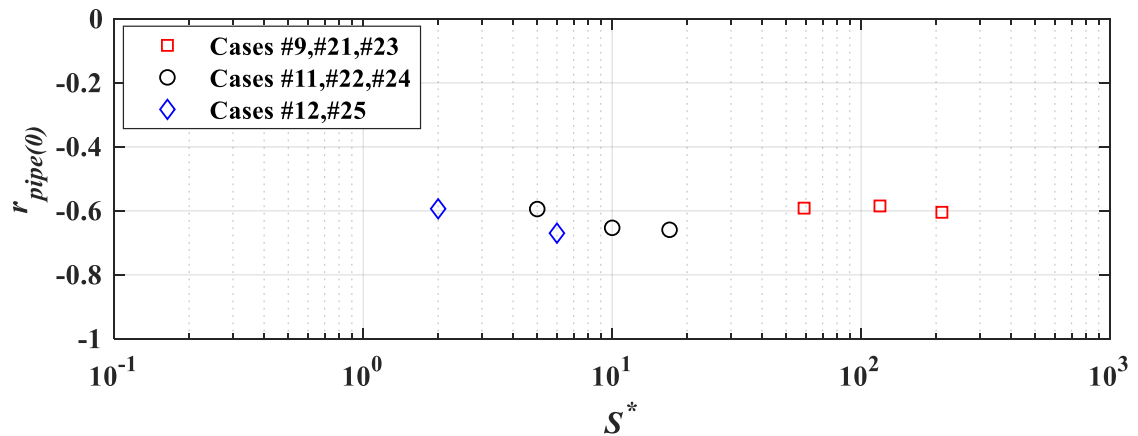


Figure 5.24: Largest $r_{pepi}(0)$ for roof zone #1B for single opening cases LO6, LO5 and LO4 for different building volumes- $\theta = 90^\circ$ to 135°

Figure 5.25 shows area-averaged $r_{pepi}(0)$ relative to the non-dimensional parameter, S^* for different building configurations. The area-averaged external pressures at Zone #2B and internal pressure fluctuations are highly correlated for the building with a large windward opening, as shown in Figure 5.25. Zone #2B is located near the leading edge above the opening and experiences large suction pressure from the formation of conical vortices. The spatial averaging of high frequencies of the suction pressure and the positive internal pressure at the windward wall produce high negative correlation. The $r_{pepi}(0)$ on Zone #2B is similar to the values from the previous studies conducted by Beste et al. (1997) and Sharma and Richards (2005).

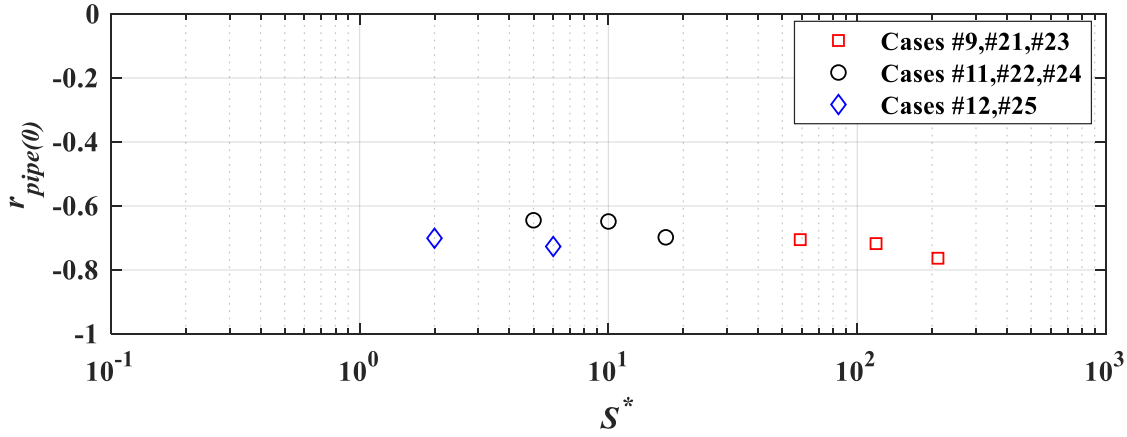


Figure 5.25: Largest $r_{pepi}(0)$ for roof zone #2B for single opening cases LO6, LO5 and LO4 for different building volumes- $\theta = 90^\circ$ to 135°

5.4 Net pressure and net pressure factors for roof and wall cladding

The combination of pressures on external and internal surfaces generates the net pressures on the roof and wall cladding. The net pressure is a critical design criterion for cladding and structural components, and the peak net pressure on different parts of the roof and wall cladding is required for design. As explained in Section 5.2.1, external pressures in different areas have varying correlation patterns with the internal pressure for the same wind direction. The different net pressure fluctuations are identified in different parts of the roof and wall cladding.

The peak external and peak internal pressures do not occur at the same time due to the lack of correlation between internal and external pressure fluctuations. Accordingly, the magnitude of the peak net pressure coefficient is less than the difference between peak external and peak internal pressures for a specific wind direction. Two net pressure factors, F_{C1} and F_{C2} , are defined by Bodhinayake et al. (2020) based on the maximum net pressure coefficient ($C_{\hat{p},net}$) and the minimum net pressure coefficient, $C_{\check{p},net}$, as given in Equations 5.2 and 5.3. Here, F_{C1} accounts for the inward pressures while F_{C2} accounts for the outward pressure on the building envelope.

$$F_{C1}(\theta) = \frac{C_{\hat{p},et}(\theta)}{C_{\hat{p}e}(\theta) - C_{\check{p}i}(\theta)} \quad (5.2)$$

$$F_{C2}(\theta) = \frac{C_{\check{p},net}(\theta)}{C_{\check{p}e}(\theta) - C_{\check{p}i}(\theta)} \quad (5.3)$$

The wind loading standard AS/NZS 1170.2 (2011) specifies combination factors, K_C similar to the net pressure factor, to account for the lack of correlation of pressures on different surfaces that influence a local effect. Here, K_C is applied to the peak external and internal pressures derived from a 90° quadrant of wind directions. That is for pressures on two contributing surfaces (i.e. large external and internal pressure), AS/NZS 1170.2 specifies a K_C of 0.9, where $C_{\check{p},net} = 0.9(C_{\check{p}e} - C_{\check{p}i})$. The net pressure factors, F_C from this study are compared with the combination factor (K_C), given in AS/NZS 1170.2 (2011). AS/NZS 1170.2 specifies that $K_C = 1$ for net cladding loads when $|C_{\check{p}i}| < 0.2$, which accounts for the minor contribution of the internal pressure (i.e., Case #2). For other instances, $K_C = 0.9$ for deriving net cladding loads, when pressures act on two effective surfaces, (e.g., Case #15).

Higher F_C values represent a smaller reduction to the difference in peak pressures contributing to net loads. Peak net, external and internal pressures are used to derive the net pressure factors for five runs for each approach wind direction, θ . The average of five net pressure factors is taken as the F_C for a particular location on the envelope.

5.4.1 Roof cladding - net pressures

Figure 5.26 and Figure 5.27 show the mean, standard deviation, maximum and minimum net pressure coefficients on the roof for Cases #02 and #09, respectively at $\theta = 90^\circ$. Here, the net pressure coefficient distribution shows that the highest negative pressures occur near windward roof edge and decreases towards the middle of the roof. The internal pressure coefficients are small in the nominally sealed building such that the net pressure coefficients (Figure 5.26) are mostly influenced by the external suction pressures, which are poorly correlated with internal pressure fluctuations as was noted in Figure 5.4(a). Figure 5.27 shows that the net pressure coefficients are significantly higher in Case #09 because of large positive internal pressure fluctuations when the building has a windward wall opening. The $C_{\check{p},net}$ creates a higher uplift force on the roof cladding and structural components for wind direction $\theta = 90^\circ$, and largest $C_{\check{p},net}$ occurs at the roof windward

corner (i.e., RP1-1). However in this region (i.e., first row), external and internal pressures are poorly correlated where $r_{pipe}(0)$ is less than $|0.4|$. Accordingly, peak net pressure are not greatly influenced by the correlation coefficients between internal and external pressures. The coincidence of peak external and peak internal pressures and generation of peak net pressures needs to be analysed further by considering “peak events” within the observed time.

Chapter 5: Correlation of External and Internal Pressure Fluctuations

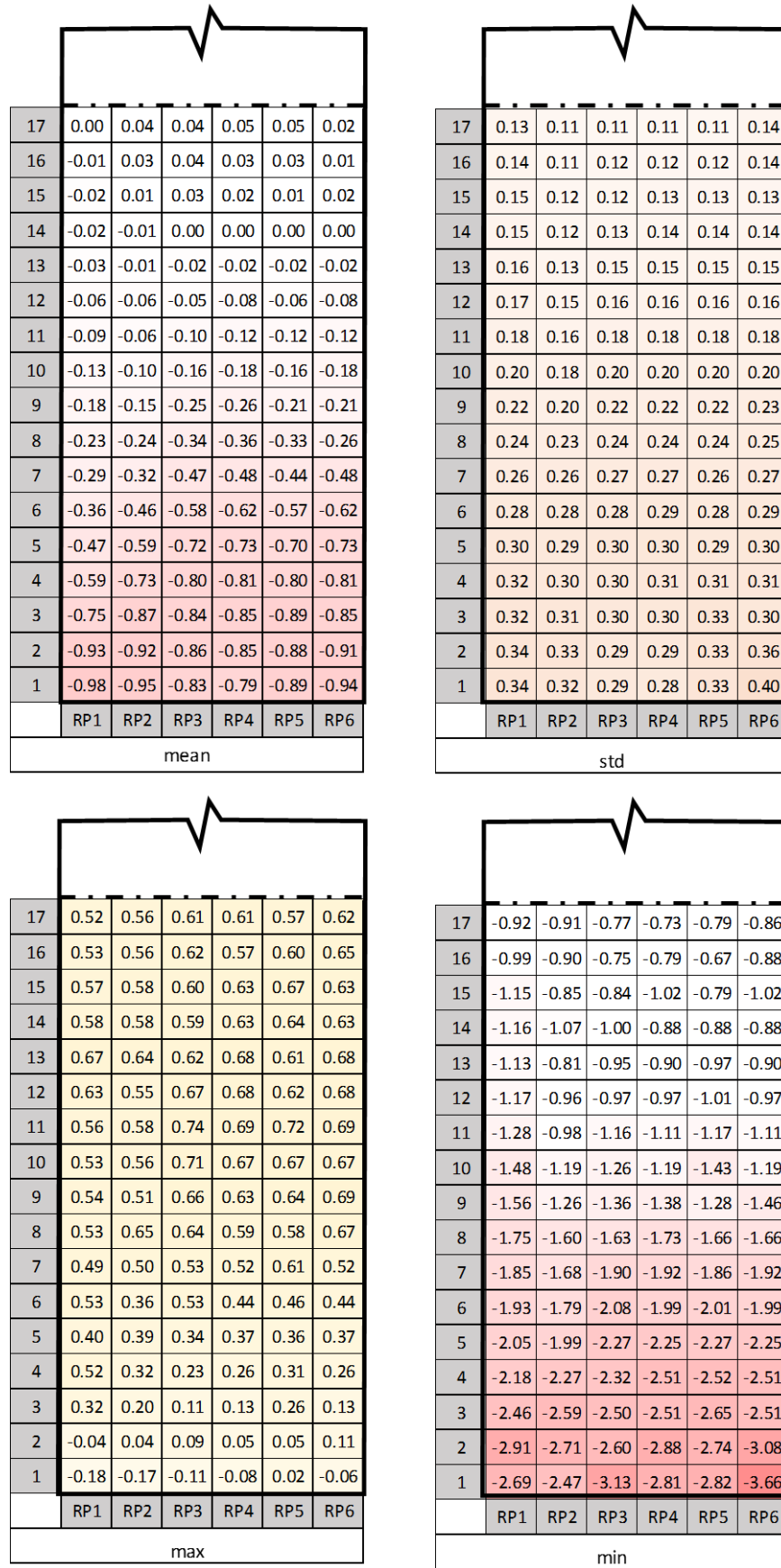


Figure 5.26: Mean, standard deviation, maximum and minimum net pressure coefficients for Case #02 at $\theta = 90^\circ$

Correlation of internal and external pressure fluctuations in industrial buildings

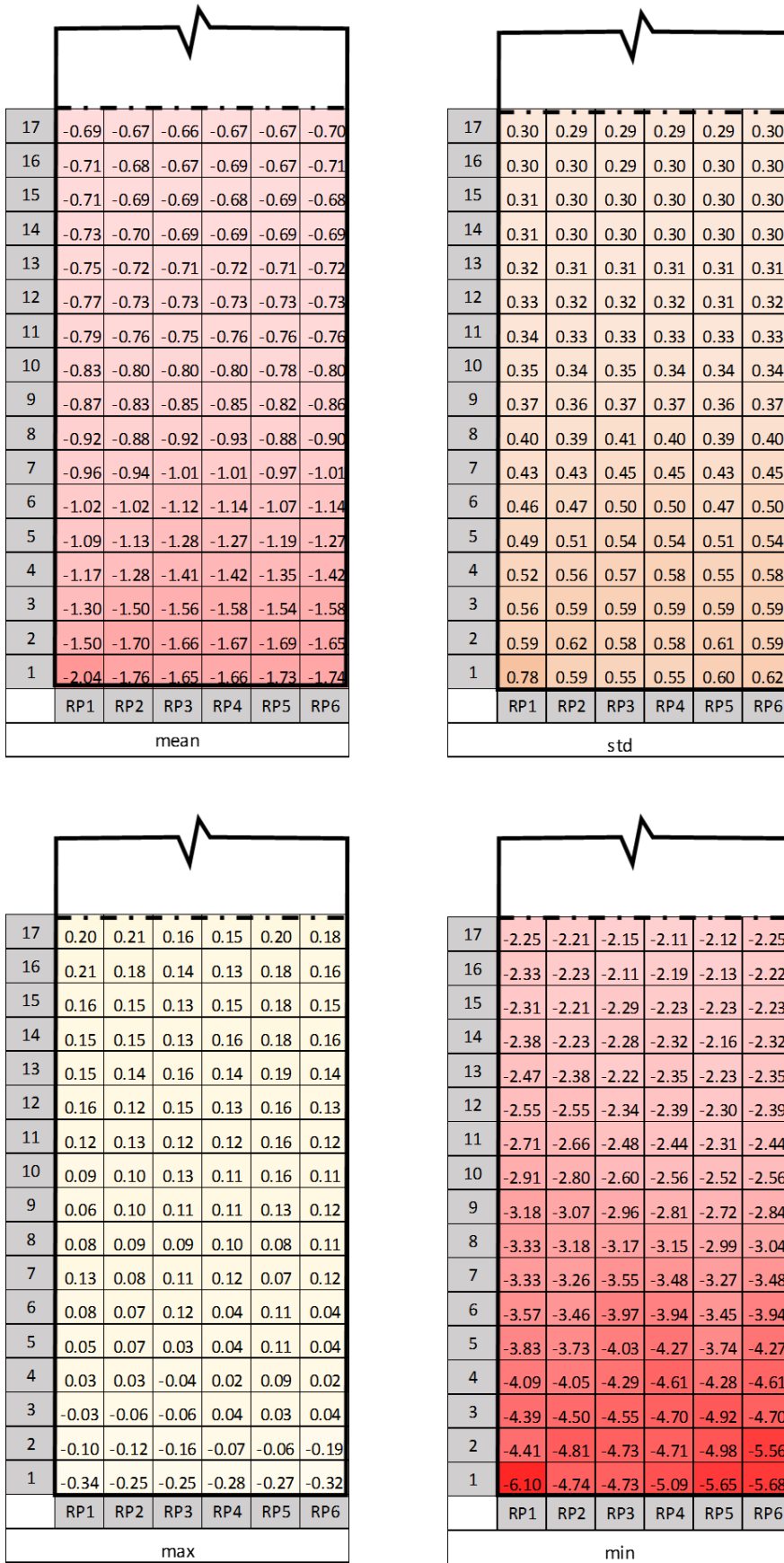
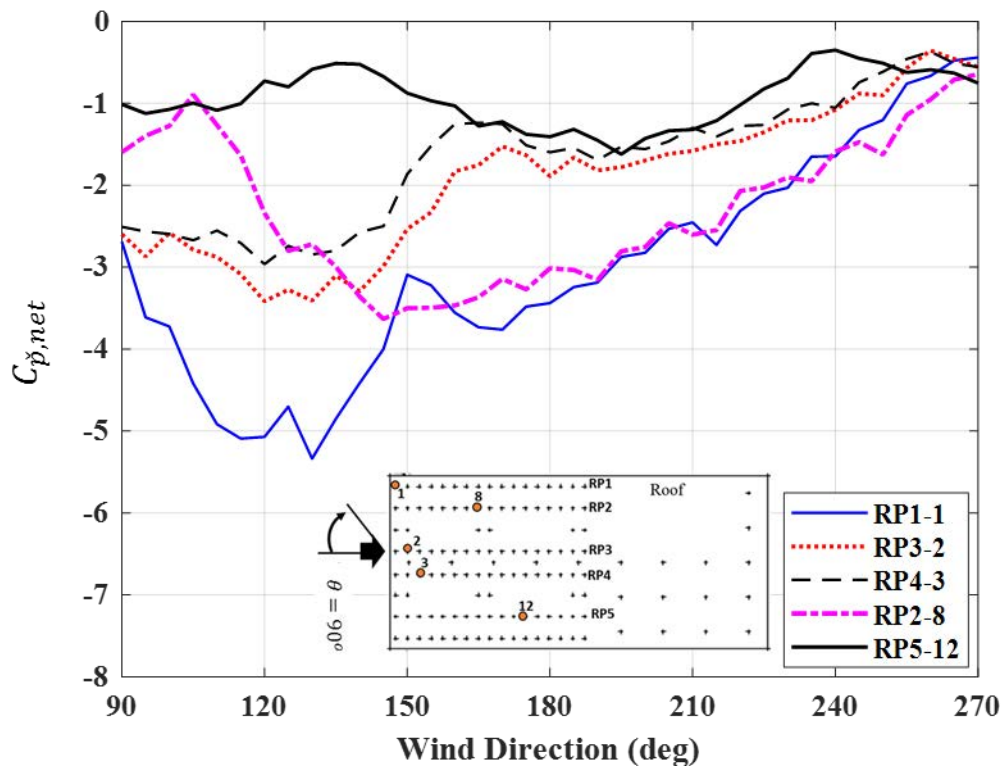


Figure 5.27: Mean, standard deviation, maximum and minimum net pressure coefficients for Case #09 at $\theta = 90^\circ$

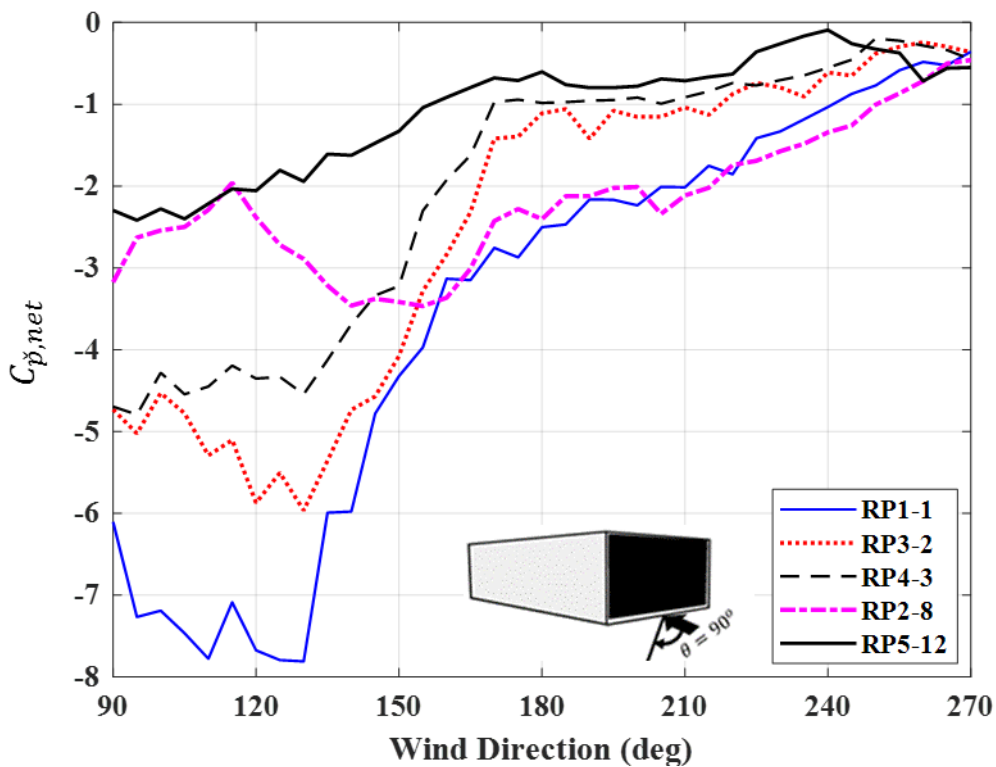
The largest minimum net pressure occurs at the windward roof corner (RP1-1) for all Cases #02, #09, and #11 within the wind directions $90^\circ \leq \theta \leq 135^\circ$, as shown in Figure 5.28(a)-(c). The large suction external pressures at leading roof edge due to flow separation for cornering wind flows are combined with high positive internal pressure to generate large minimum net pressure for Cases #09 and #11. Figure 5.28(a)-(c) also shows $C_{\check{p},net}$ of -5.3, -7.8, and -7.4 at $\theta = 130^\circ, 130^\circ$ and 105° for Cases #02, #09, and #11, respectively. Such $C_{\check{p},net}$ at the roof corner on the building with a large windward opening have also been found by Ginger and Letchford (1999) in a full-scale study.

Figure 5.28(a)-(c) further show that $C_{\check{p},net}$ have similar variations for wind directions $160^\circ \leq \theta \leq 270^\circ$ (i.e., RP1-1, and RP2-8 decrease from -3.0. to -0.5 and RP3-2 decreases from -1.0 to -0.5) on the leeward roof corner and edge for Cases #02, #09, and #11. Furthermore, the largest $C_{\check{p},net}$ on different parts of the roof are generated at different wind directions. These large net pressures depend on the combination of large suction external pressure and positive internal pressure at critical wind directions $\theta = 90^\circ$ to 135° . However, $C_{\check{p},net}$ at RP3-2 is smaller compared to RP1-1 even though the highest $r_{pipe}(0)$ was measured for RP3-2 at $\theta = 135^\circ$, as shown in Figure 5.9.

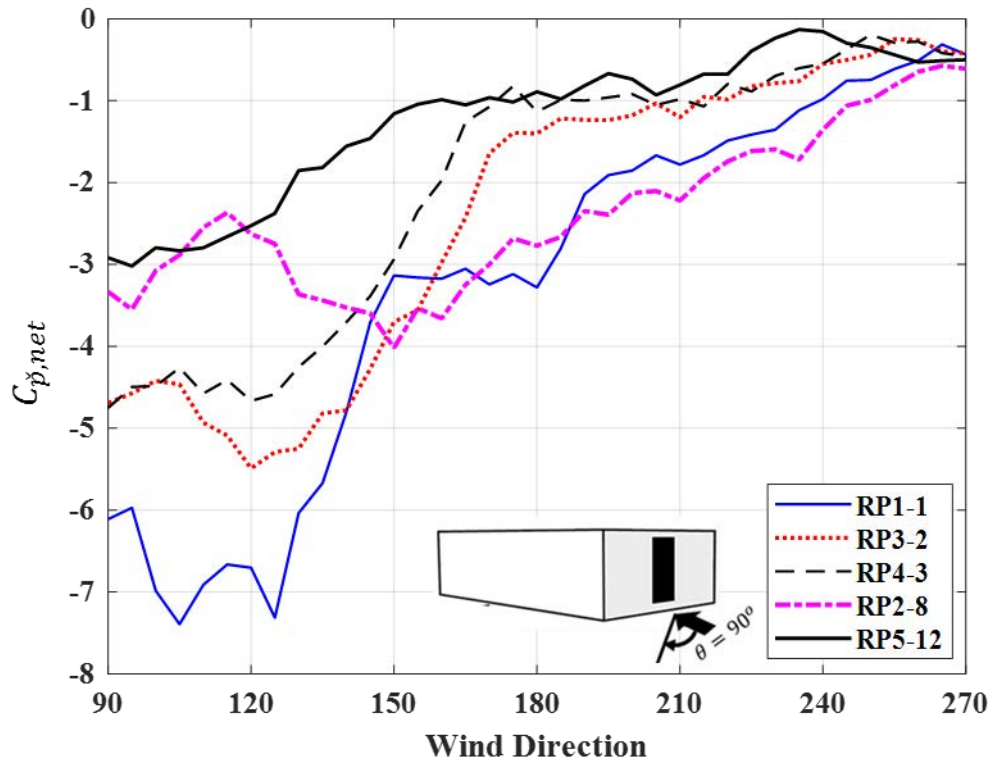
The measure of the correlation between external and internal pressure fluctuations does not entirely define the cause of net pressure peaks. Furthermore, $r_{pepi}(0)$ varies around zero at the middle of the roof for wind directions 90° to 135° . However, the external pressure peaks contribute to generating the large net suction pressures which are significantly higher than the mean net pressures (i.e., $C_{\check{p},net} = 2.5$ and $C_{\bar{p},net} = 0.9$ at the RP3-17 for $\theta = 90^\circ$). A large correlation coefficient indicates that the positive internal pressure and negative external pressure are likely to act together and generate large negative net pressures. This is also likely to give large peak negative net pressures. The peak positive internal pressure and the peak negative external pressure are generated at different times to the peak net pressures. The relations between correlation coefficient and the peak net pressure coefficients are further analysed based on the correlation of peak external and internal pressures in the next section.



(a) Case #02- Nominally sealed building



(b) Case #09- LO6 Opening



(c) Case #11- LO5 Opening

Figure 5.28: Minimum net pressure coefficient at wind directions $\theta = 0^\circ$ - 270°
 (a) Case #02, (b) Case #09, and (c) Case #11

5.4.1.1 Application of Covariance Integration method

The covariance integration method described in Section 2.6 is used to estimate the peak net pressure on cladding elements based on the external and internal pressure fluctuations on the cladding element for Case #09. This shows how the correlation between external and internal pressures influences the net pressure on a cladding element.

Accordingly, $N = 2$; and “ j ” and “ k ” are the external and internal surfaces of the cladding element. The influence coefficients for obtaining the net pressure on the cladding element are $\beta_j = 1$ for external pressure, and $\beta_k = -1$ for internal pressure, and areas, $A_j = A_k = 1$. Equation 2.15 and 2.16 in Section 2.6 are rearranged to give peak factor for net pressure as shown in Equation 5.4.

$$g_{net} = \left(\sum_{j=1}^2 \sum_{k=1}^2 \beta_j \beta_k g_{p_j} g_{p_k} r_{p_j p_k}(0) C_{\sigma p_j} C_{\sigma p_k} \right)^{1/2} / C_{\sigma p, net} \quad (5.4)$$

Equation 5.4 can be expanded as given in Equation 5.5; here, subscript j denotes the external pressure surface, and subscript k denotes the internal pressure surface. Equation 5.5 is further simplified to Equation 5.6 by substituting β values and $r_{pj pj} = r_{pk pk} = 1$.

$$g_{net} C_{\sigma p, net} = \left(\beta_j \beta_j g_{pj} g_{pj} r_{pj pj} C_{\sigma pj} C_{\sigma pj} + \beta_j \beta_k g_{pj} g_{pk} r_{pj pk} C_{\sigma pj} C_{\sigma pk} + \beta_k \beta_j g_{pk} g_{pj} r_{pk pj} C_{\sigma pk} C_{\sigma pj} + \beta_k \beta_k g_{pk} g_{pk} r_{pk pk} C_{\sigma pk} C_{\sigma pk} \right)^{1/2} \quad (5.5)$$

$$g_{net} C_{\sigma p, net} = \left(g_{pj} g_{pj} C_{\sigma pj} C_{\sigma pj} - 2g_{pj} g_{pk} r_{pj pk} C_{\sigma pj} C_{\sigma pk} + g_{pk} g_{pk} C_{\sigma pk} C_{\sigma pk} \right)^{1/2} \quad (5.6)$$

Using Equation 2.14 in Section 2.6, the peak net pressure coefficient is estimated by Equation 5.7.

$$\check{C}_{p, net} = \bar{C}_{p, net} - g_{net} C_{\sigma p, net} \quad (5.7)$$

Table 5.3 shows the measured internal, external and net pressure coefficients, calculated peak factors for net pressures and the estimated peak net pressures for selected roof locations RP1-1, RP2-8, RP3-2, RP4-3 and RP5-12 for Cases #02 and #09 wind direction 90° (see sample calculation for RP1-1). The external pressure peak factors, g_{pj} are 4.76 and 6.93, in good agreement with Ginger et al. (2000) and internal pressure peak factor, g_{pk} vary between 3.70 and 4.43 is in good agreement with Guha et al. (2012). Table 5.3 shows that the estimated minimum net pressure coefficients for both Cases #02 and #09 closely match measured values within $\pm 10\%$. Furthermore, Figure 5.29 shows that measured minimum net pressures at RP1-1 are in good agreement with estimated minimum net pressures using Covariation Integration method within the wind directions 90° to 270° for Cases #09 and #11. Accordingly, Covariation Integration method satisfactorily estimates the peak net pressures based on the measured external and internal pressures and correlation between external and internal pressures.

Sample calculation for RP1-1;

$$(g_{pj})_{RP1-1} = (-1.53 - (-4.92)) / 0.63 = 5.33$$

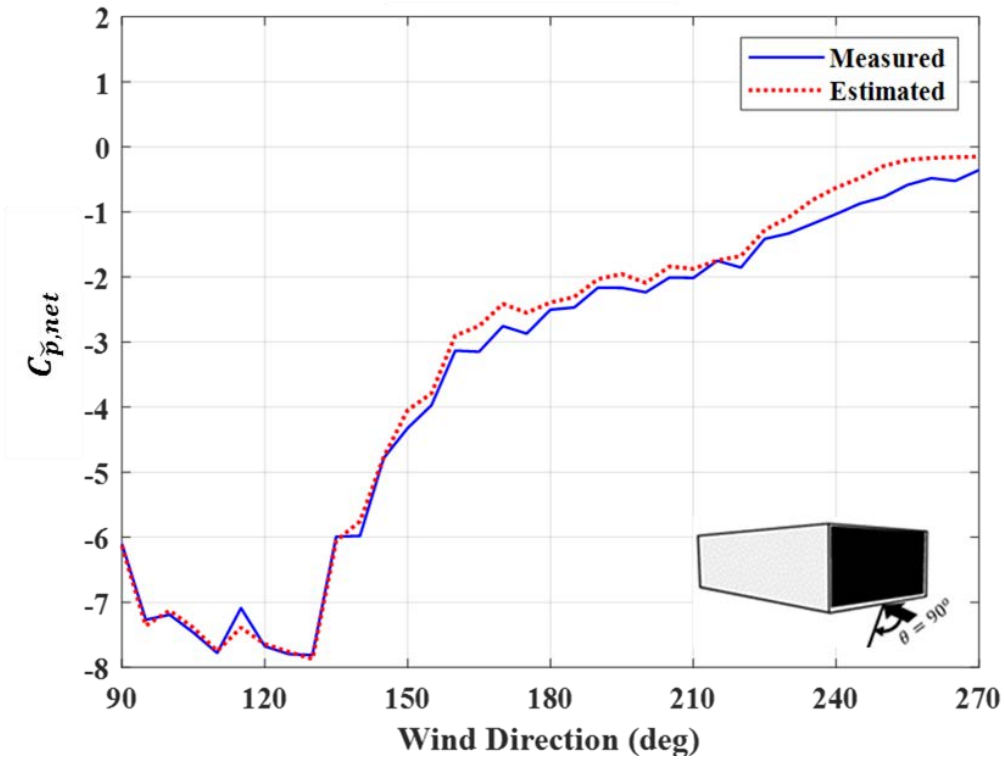
$$(g_{pk})_{RP1-1} = (1.76 - 0.51) / 0.28 = 4.43$$

$$(g_{net} \sigma_{net})_{RP1-1} = (4.43 \times 4.43 \times 0.28 \times 0.28 - 2 \times 5.33 \times 4.43 \times (-0.35) \times 0.28 \times 0.63 + 5.33 \times 5.33 \times 0.63 \times 0.63)^{1/2} = \pm 4.00$$

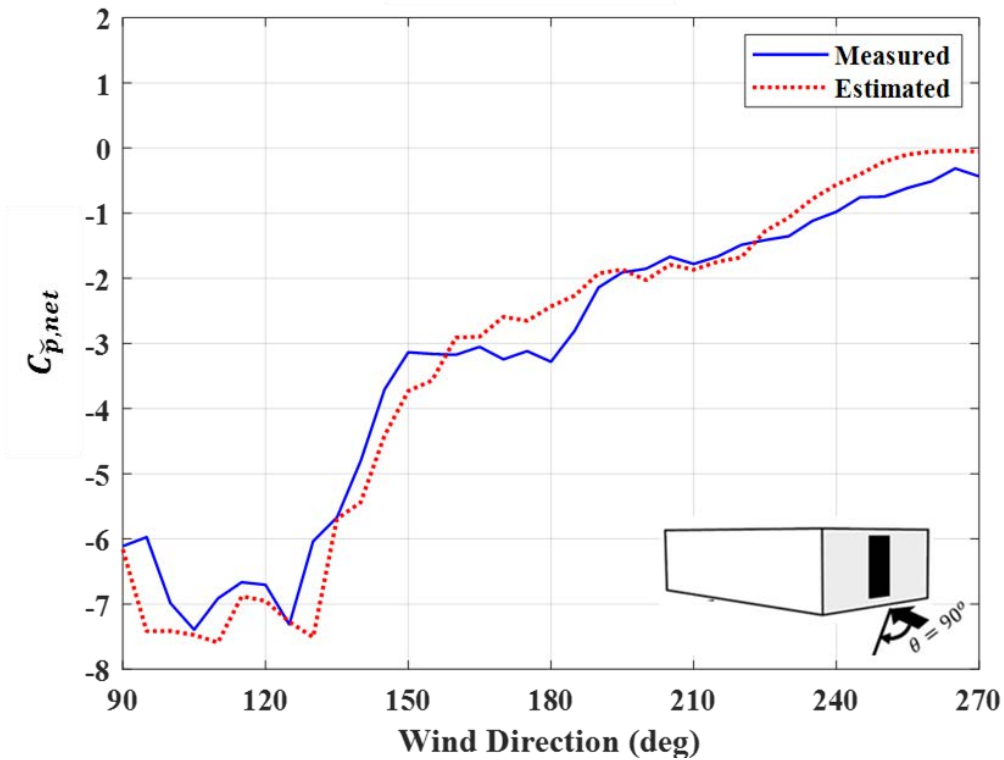
$$\text{Estimated } (\check{C}_{p,net})_{RP1-1} = (-1.53 - 0.51) - 4.00 = -6.04$$

Table 5.3: Estimated minimum net pressures using covariance integration method and measured minimum net pressures on selected roof locations for (a) Case #02 and (b) Case #09 for $\theta = 90^\circ$

Tap #	Measured								r_{pipe}	$g_{net} C_{\sigma p,net}$	Estimated	Measured
	External pressure coefficients				Internal pressure coefficients							
RP	$C_{\bar{p}e}$	$C_{\check{p}e}$	$C_{\sigma pj}$	g_{pj}	$C_{\bar{p}i}$	$C_{\check{p}i}$	$C_{\sigma pk}$	g_{pk}		$C_{\check{p},net}$	$C_{\check{p},net}$	
(a) Case #02- Nominally sealed building												
1-1	-1.19	-2.86	0.35	4.76	-0.21	-0.03	0.05	3.70	0.32	1.62	-2.61	-2.69
3-2	-1.07	-2.83	0.31	5.73					0.36	1.71	-2.57	-2.60
4-3	-1.05	-2.75	0.32	5.40					0.35	1.65	-2.49	-2.51
2-8	-0.44	-1.81	0.24	5.75					0.23	1.33	-1.57	-1.60
5-12	-0.26	-1.25	0.17	5.93					0.28	0.96	-1.01	-1.02
(b) Case #09 – Building with a large opening (LO6)												
1-1	-1.53	-4.92	0.63	5.33	0.51	1.76	0.28	4.43	-0.35	4.00	-6.04	-6.10
3-2	-1.16	-3.86	0.40	6.79					-0.42	3.44	-5.10	-4.73
4-3	-1.07	-3.39	0.39	5.92					-0.53	3.17	-4.75	-4.70
2-8	-0.37	-1.76	0.22	6.40					-0.21	2.06	-2.94	-3.18
5-12	-0.22	-1.18	0.14	6.93					0.01	1.57	-2.30	-2.30



(a) Case #09- LO6 open



(b). Case #11- LO5 open

Figure 5.29: Estimated and measured minimum net pressure coefficients at RP1-1 for Cases #09 and #11 for wind directions 90° to 270°

5.4.1.2 Peak pressure on roof cladding

The largest positive or negative pressure within an observation time is considered to be the peak pressure for that particular time-history. The maximum internal, minimum external and minimum net pressure acting within a 16 s observation time on RP1-1 shown in Figure 5.30 indicates that these peaks occur at three different times. The peak net pressure of -5.22 is generated by the combination of the external pressure of -4.22 and the internal pressure of 1.02 as shown in Figure 5.30. Accordingly, the peak net pressure is independent of peak external and peak external pressures, and the coincidence of peaks are further analysed based on the peak events in external, internal, and net pressure signals at the RP1-1 for Cases #02, #09 and #11 at $\theta = 90^\circ$.

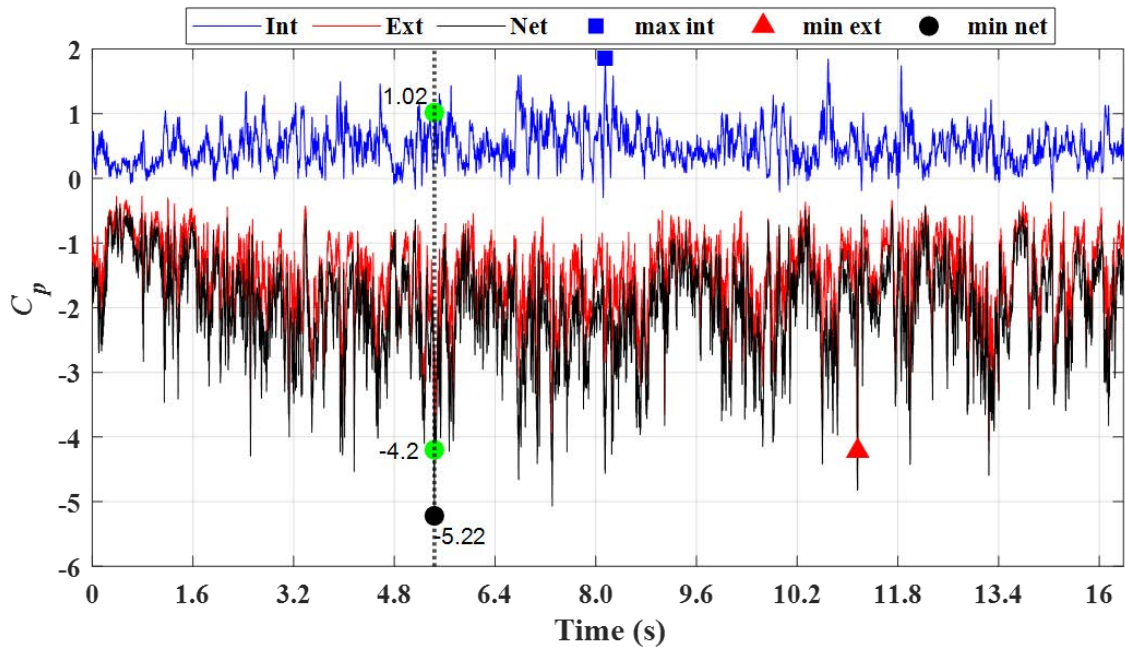


Figure 5.30: External, internal, and net pressures (Run #5) vs time with respective peaks at the RP1-1 at $\theta = 90^\circ$ for Case #09

Table 5.4 shows the external, internal and net pressure peak to standard deviation ratios for RP1-1 at $\theta = 90^\circ$. The standard deviation of net pressure is larger than the external and internal pressure standard deviation indicating a higher fluctuating component in net pressure. Further, peak to standard deviation ratios in internal pressure fluctuations are the smallest of the three ratios. The coincidence of peak external, internal, and net pressure is studied by identifying “peak events” where the pressure exceeds the mean value by $3 \times$ standard deviations (i.e., the threshold value for pressure = $C_{\bar{p}} + 3 \times C_{\sigma p}$).

Accordingly, peak events were selected programmatically using standard and in-built MATLAB® function for the net, external and internal pressure time-histories of 16 s. The standard function “*findpeaks*” is used including properties of zero “*Minimum Peak Distance*” between two peaks, the threshold as “*Minimum Peak Height*” and zero “*Minimum Peak Width*”. Further, “*Minimum height difference*” between neighbour peaks is fixed as zero to determine all peak events higher than the threshold because the coincidence of any peak external and peak internal can generate large net peak event.

Table 5.4: Peak to standard deviation ratios for external, internal and net pressures of an average of five runs for $\theta = 90^\circ$, RP1-1

Case #	External			Internal			Net		
	C_p -peak	$C_{\sigma p}$	peak/std	C_p -peak	$C_{\sigma p}$	peak/std	C_p -peak	$C_{\sigma p}$	peak/std
02	-2.9	0.34	8.8	-0.36	0.05	7.2	-2.6	0.33	7.8
09	-4.7	0.6	7.8	1.46	0.26	5.5	-5.63	0.72	7.8
11	-4.8	0.5	9.6	2.27	0.35	6.5	-6.4	0.71	9.0

The selected external, internal, and net pressure peak events for a particular observation time is shown in Figure 5.31. Internal and external pressure peak events do not coincide with each other and do not align with the peak net pressure event as shown in Figure 5.31 as is further explained by the number of peak events for each run of internal, external and net pressure fluctuations in Table 5.5. If the minimum external and maximum internal pressures coincide, it generates the largest net peak event, which is the critical peak for the design criteria.

Figure 5.32 shows the empirical PDFs for wind tunnel data and histograms of the internal, external and net pressure peak events distribution. The empirical PDFs closely follow the measured wind tunnel data showing the accurate selection of peak events. The peak events in internal pressures are positively skewed between +1.4 and +1.5, and external and net pressure peak events are negatively skewed between -3.5 and -4.0 and between -4.5 and -5.5. Figure 5.32 also shows that a small number of net peak events higher than -5.5, which shows that internal peak events higher than +1.4 and external pressures peak events higher than -4.0 do not coincide.

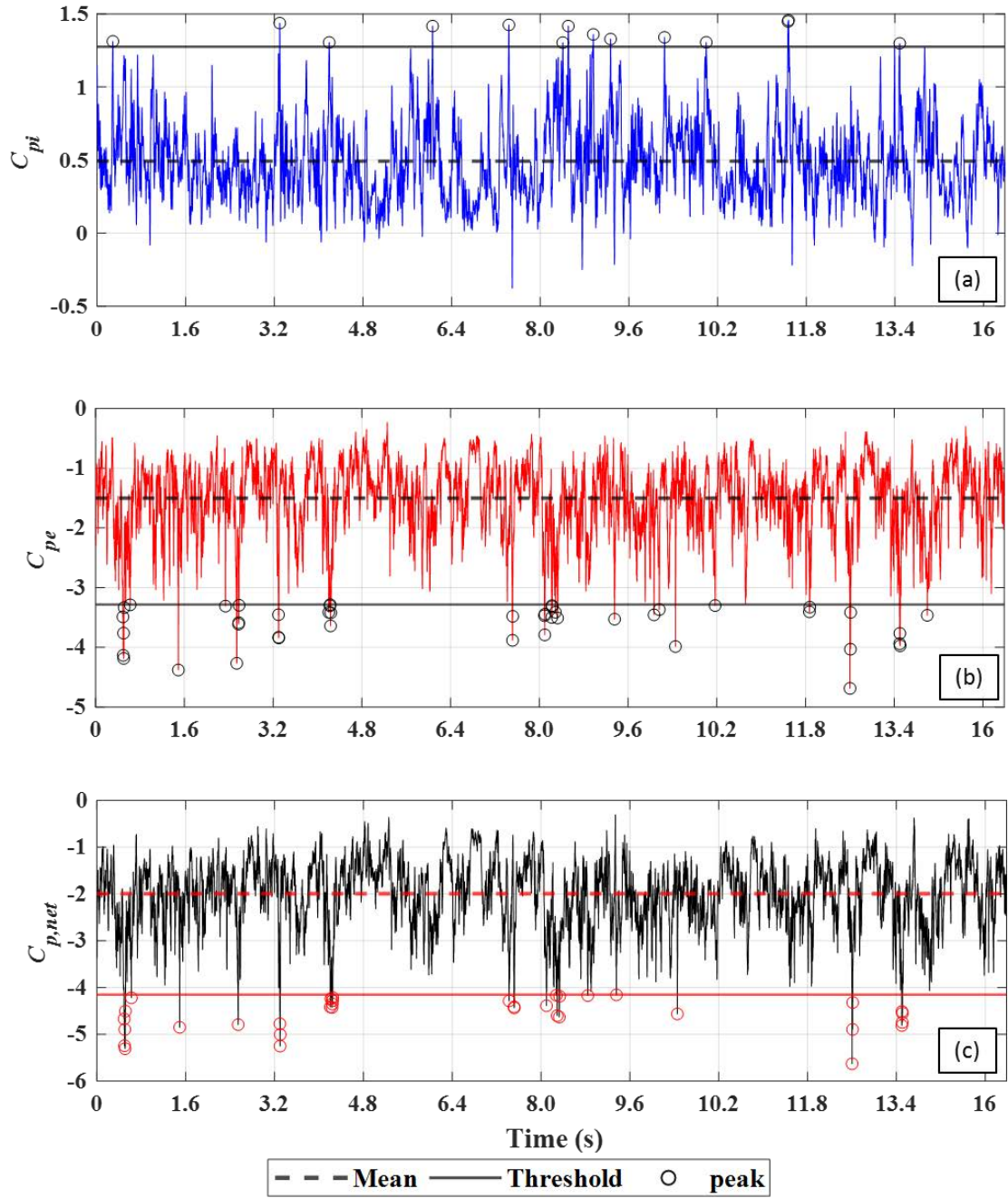


Figure 5.31: Peak events with time on the RPI-1 for Case #09 at $\theta = 90^\circ$; (a) internal pressure fluctuation, (b) external pressure fluctuation, (c) net pressure fluctuation

Table 5.5: Number of peak events exceeding 3 standard deviations from the mean for five runs – Case #09, RPI-1, $\theta = 90^\circ$

Description	Run #1	Run #2	Run #3	Run #4	Run #5	Total
Net	35	34	43	34	22	168
External	44	45	53	40	26	208
Internal	14	21	22	24	14	95

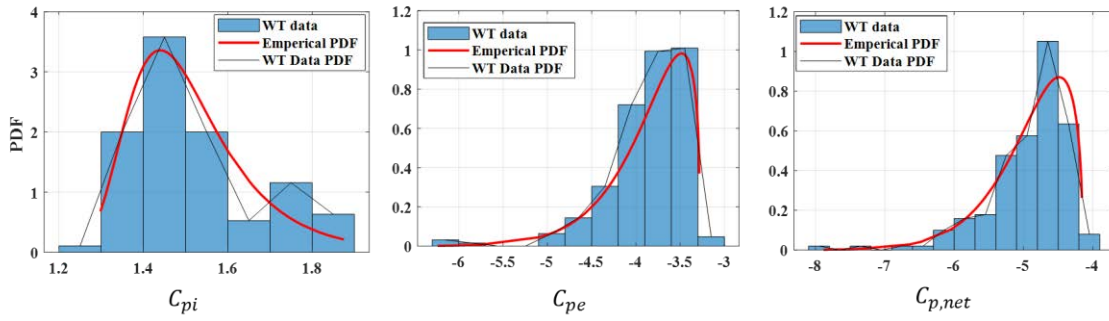


Figure 5.32: Theoretical and wind tunnel data PDFs, and Histogram of peak events for Case #09, RP1-1, $\theta = 90^\circ$

The net, external, and internal pressure peak events and their coincidences are further analysed using the Venn diagram in Figure 5.33 showing the net pressures peaks (N), external pressure peaks (E) and internal pressure peaks (I). Further, “ NEI ” represents the net, external and internal pressure peak events that occur at the same time, and “ NEI' ” presents only the net and external pressure peaks that occur at the same time, where the internal pressure is lower than the threshold value for a peak event.

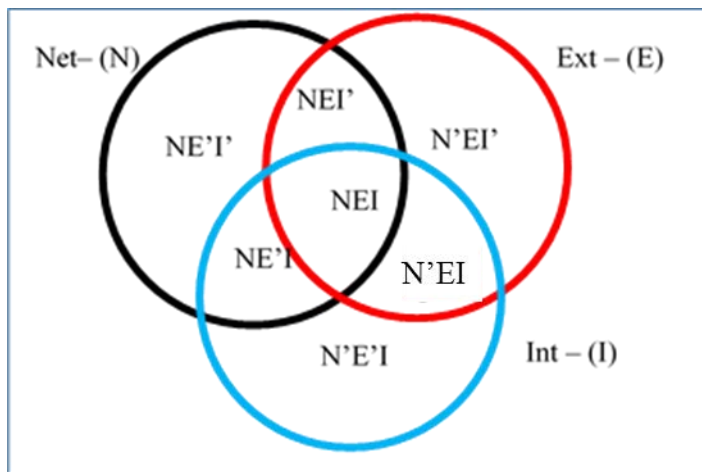


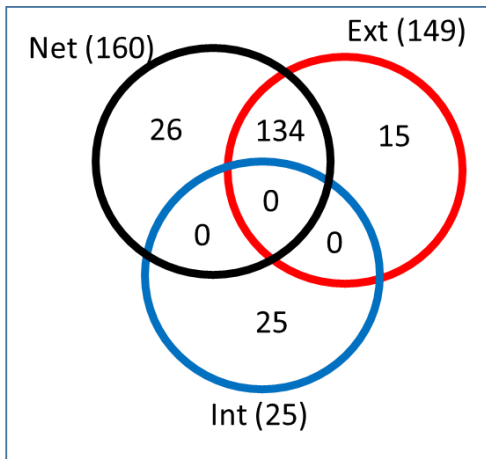
Figure 5.33: Venn diagram for external, internal, and net peak events

The peak events of net, external and internal pressure time-histories were obtained, and individual events are compared between each time-history using the standard inbuilt MATLAB® function to separate the peak events in the Venn diagram. Accordingly, Figure 5.34(a)-(e) represent the individual Venn diagram of RP1-1 at roof corner and

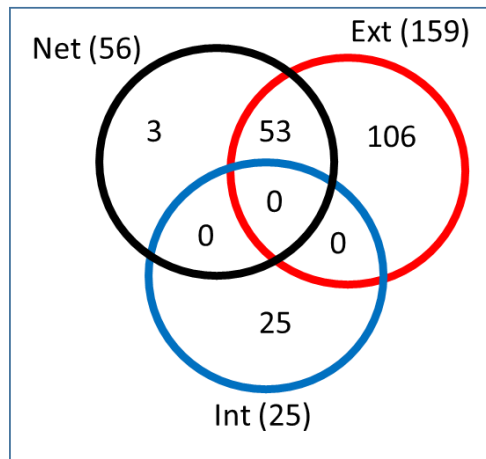
RP3-17 at roof middle for Cases #02, #09, and #11, at $\theta = 90^\circ$. Figure 5.34(a)-(b) show that the internal pressure peaks did not contribute to generating the peak net pressure that the internal pressure fluctuations are not significant in the nominally sealed building. Furthermore, net peak events depend on the external pressures peak events such that over 80% of external pressure peaks and net pressure peaks at RP1-1 occurred at the same time, while 95% of net peaks at RP3-17 coincide with external pressure peak events.

When the building has a large opening, Figure 5.34(c)-(e) shows that net pressure peak events depend on the external pressure peak events at the roof corner or near to the leading edge (RP1-1), and internal pressure peak events at the middle of the roof (RP3-17). The magnitude of external pressure peaks is significantly higher than internal pressure peak events at the roof corner and vice versa at the middle of the roof to generate net peak events. Furthermore, more than 50% (i.e., 127/168 in Figure 5.34c) of external and net pressure peak events have coincided while less than 10% (i.e., 5/57 in Figure 5.34e) of internal and net pressure peak events have coincided at the roof corner.

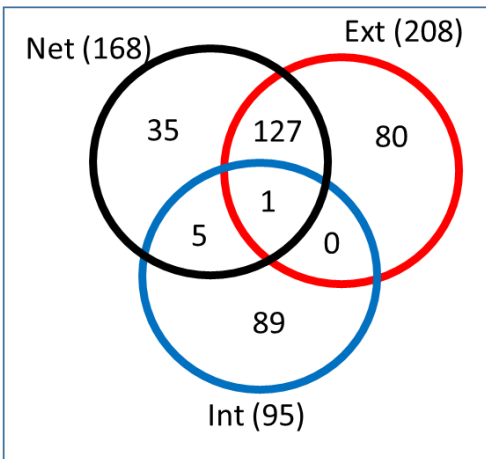
Figure 5.34(c)-(e) further shows that coincidence of peak events in external, internal, and net pressures are less than 1% (i.e., $NEI = 1$ for Case #09, Figure 5.34c). This shows a low probability of occurrence of minimum external, maximum internal, and minimum net pressures at the same time which is considered as critical for design. It is noticed that some internal pressure peak events become net peak events with the combination of external pressure, which are lower than an external threshold pressure. Furthermore, the Venn diagrams show zero number of common peak events for the external and internal pressures (i.e., $N'EI = 0$) that indicates if the external and internal peak events have coincided that peak event becomes a net peak event.



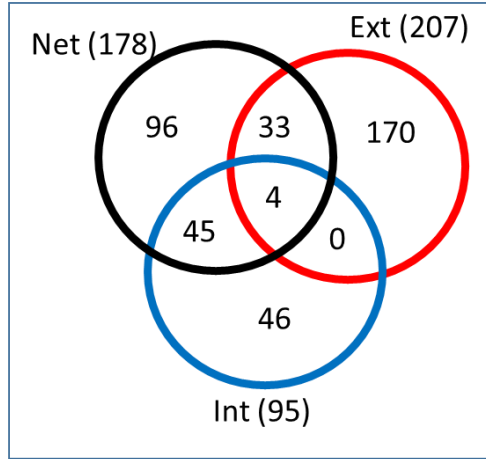
(a) Case 02-RP1-1



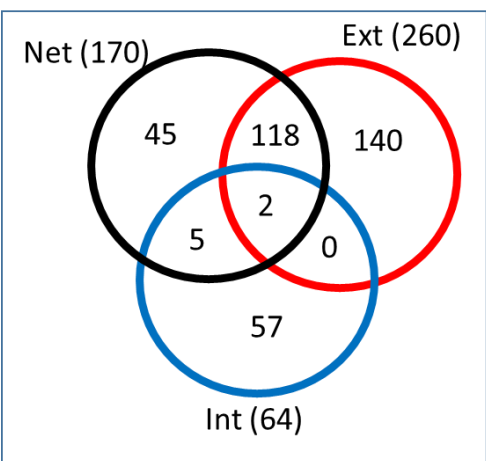
(b) Case 02-RP3-17



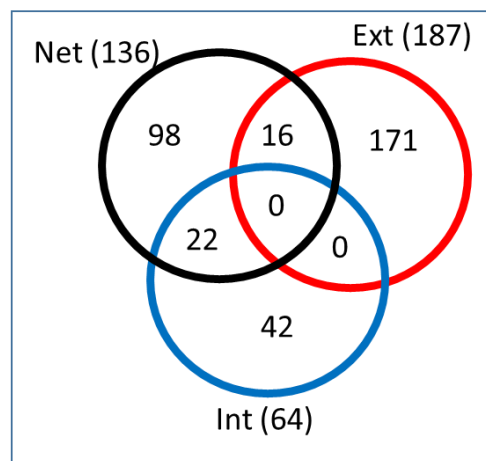
(c) Case 09-RP1-1



(d) Case 09-RP3-17



(e) Case 11-RP1-1



(f) Case 11-RP3-17

Figure 5.34: Venn diagrams for peak events for Cases #02, #09, and #11 for RP1-1 and RP3-17 at $\theta = 90^\circ$

Table 5.6 shows the number of external, internal, and net pressure peak events and the number of coinciding peaks (NEI) for $\theta = 90^\circ$ to 135° at RP1-1. For a nominally sealed building, internal pressure peaks are lower than the threshold value for any wind direction from 90° to 135° . Accordingly, peak events in net, external and internal pressures do not coincide indicating that high internal pressure fluctuations are not required to generate the high net peak events.

For the building with a large windward opening, the number of net pressure peak events is lower than the number of external pressure peak events and higher than the number of internal pressure peak events for most wind directions. The main reason is that the magnitude of the external pressure peak events decreases when combined with internal pressure local minima since the correlation of external and internal pressures at RP1-1 is moderate (0.6). As shown in Table 5.6, internal, external, and net pressure peak events do not coincide for all wind directions 90° to 135° showing a low probability of occurrence of maximum internal, minimum external, and minimum net pressures at the same time. This introduces a reduction factor to the net pressure peaks.

Table 5.6: Number of net, external, and internal peak events for wind directions 90° to 135° for RP1-1

θ (deg)	Case #02				Case #09				Case #11			
	Net	Ext	Int	NEI	Net	Ext	Int	NEI	Net	Ext	Int	NEI
90	160	149	0	0	168	208	95	1	170	260	64	2
95	208	205	0	0	152	201	76	3	180	238	65	2
100	168	163	0	0	199	216	86	4	153	188	67	1
105	149	131	0	0	156	159	100	4	176	206	66	1
110	163	167	0	0	153	149	96	2	164	159	74	1
115	175	180	0	0	128	130	93	3	256	298	87	2
120	156	150	0	0	151	161	72	2	329	416	99	9
125	88	81	0	0	243	259	87	10	309	368	88	12
130	156	161	0	0	338	365	80	7	210	233	93	7
135	189	186	0	0	345	358	64	3	208	245	104	5

*- NEI represents Net, External and Internal peaks which occurred at the same time.

5.4.1.3 Application of L.R.C. method

The L.R.C. method is used to determine the external and internal pressures, which generate the peak net pressure on the cladding element (RP1-1) for Case #9. Equation 5.8 is used to estimate the representative external and internal pressures using their mean and standard deviation pressures, the correlation between net pressures, and net pressure peak factor.

$$(C_{pj})_{\widehat{net}} = \bar{C}_{pj} \pm g_{net} r_{pjpn} C_{\sigma pj} \quad (5.8)$$

As shown in Figure 5.30, external, internal and net pressure peaks occurred at three different time frames, and the peak net pressure of -5.22 is generated by combining corresponding external and internal pressures of -4.20 and +1.02 at RP1-1 (Run #5) for Case #09 at $\theta = 90^\circ$. The calculated net pressure peak factor, g_{net} is 5.10, correlation between external and net pressure, r_{pepn} is 0.80, and correlation between internal and net pressure, r_{pipn} is -0.63 for RP1-1 for Case #09 at $\theta = 90^\circ$. Accordingly, estimated external and internal pressures using the L.R.C. method are -3.72 and +1.32. The estimated peak net pressure of -5.04 (i.e., -3.72-1.32) is about 3.5% less than the measured peak net pressure of -5.22 for RP1-1 for Case #09 at $\theta = 90^\circ$. This further confirmed that generation of peak net pressure is a random process, and the external, internal and net pressure peak events do not coincide.

5.4.2 Roof cladding- net pressure factors based on point pressures

The net pressure factors are determined using the point pressures at each tap on the roof for cladding design. The net pressure factors are derived for the largest outward acting net pressures (negative and positive) for critical wind directions in each case. The net pressure factors derived from the area-averaged external and net negative pressures (on different zones) are analysed in Appendix C.

Point net pressure factors derived for Case #02 are presented in Figure 5.35, for $\theta = 90^\circ$ to 135° . Highest net pressure factor and largest $C_{\check{p},net}$ do not always occur for the same wind direction; for example, the roof tap RP1-1 experiences the largest $C_{\check{p},net}$ at $\theta = 130^\circ$, whilst the largest F_{C2} is at $\theta = 105^\circ$.

Internal pressures in Case #2 (nominally sealed building) are significantly lower than the negative external pressures, and therefore only have a minor influence on the net pressure factors, thus producing high F_C values on the roof. For the nominally sealed building, Figure 5.35 further shows the net pressure factors on windward roof corner (RP1-1; Zone #1) is about 0.97, windward edge (RP3-2; Zone #2) is about 0.95, reattachment area (RP3-8; Zone #3) is also about 0.95 and middle of the roof (RP5-12; Zone #4) is about 0.85 compared to the $K_C = 1.0$ from AS/NZS 1170.2.

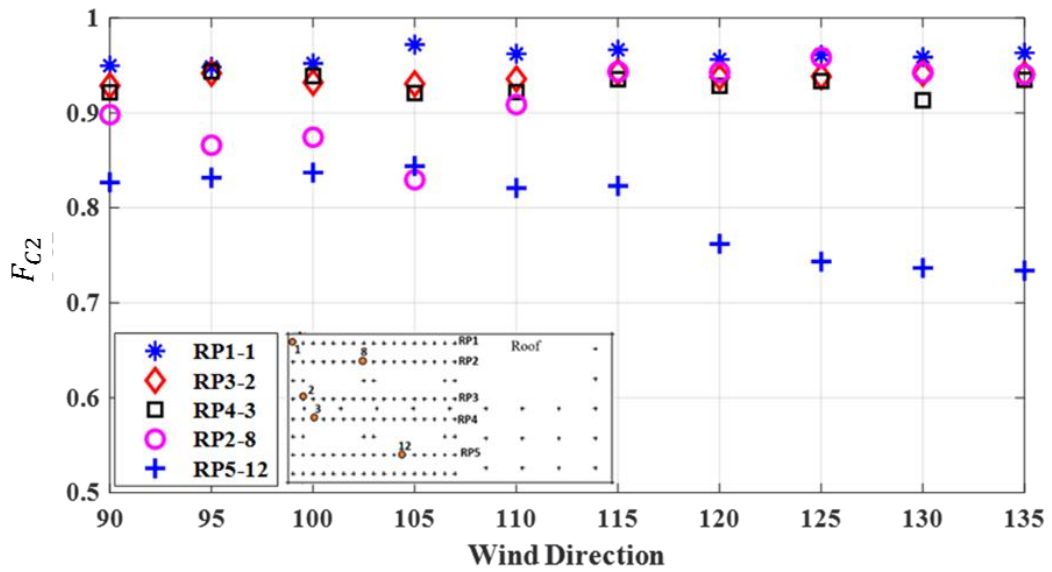


Figure 5.35: Point net pressure factors (F_{C2}) for roof cladding for Case #02 – $\theta = 90^\circ$ to 135°

Figure 5.36 shows the net pressure factors, F_{C2} for Case #09 when the opening is on the windward end wall for wind directions 90° to 135° . The F_{C2} values depends on wind direction and location of the tap and F_{C2} varies between 0.55 to 0.95, as shown in Figure 5.36. The net pressure factors for the roof corner tap (RP1-1) range between 0.9 to 0.95 for Case #09. The largest F_{C2} for windward roof corner was obtained at $\theta = 125^\circ$, which produces the highest net pressures as shown in Figure 5.28(b). However, the wind direction for the largest F_C and the highest net pressure is not always the same, because of different coincidence of peak external and internal pressures on different cladding locations.

Since the highest net pressure coefficient is critical for design, F_C is derived for the wind direction that produces the largest peak net pressures of the particular cladding location. The net pressure factor for RP3-2 of 0.95 ($\theta = 135^\circ$), for RP4-3 and RP5-12 at 90° are about 0.9 and 0.78 for Case #09, compared with $K_C = 0.9$ in the AS/NZS 1170.2 (2011), which are 5% higher on roof corner (RP1-1), and 10% lower on the middle of the roof (RP5-12).

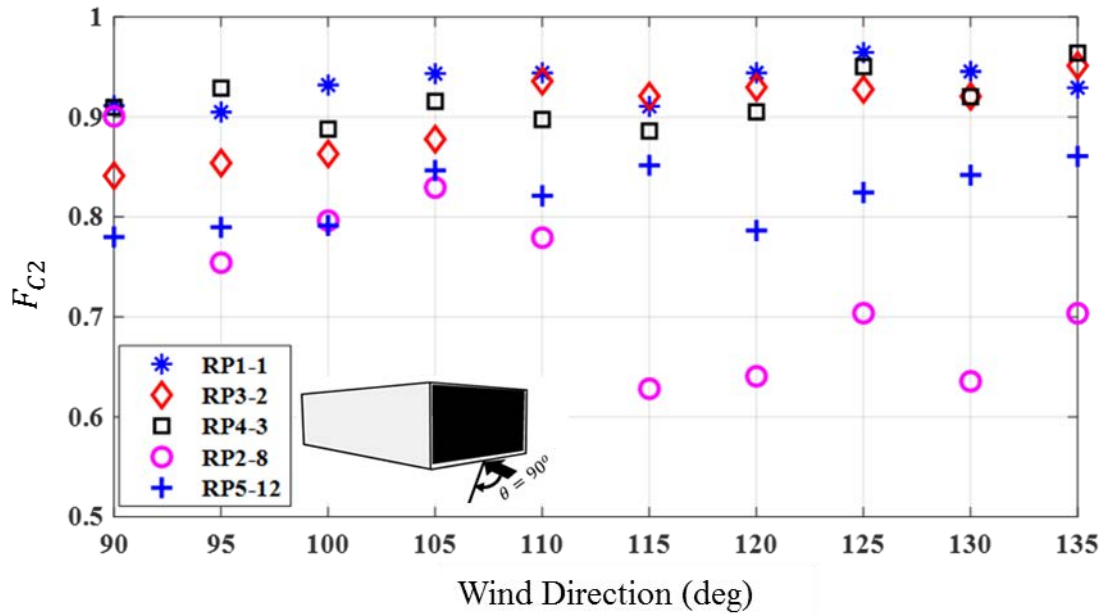


Figure 5.36: Point net pressure factors, F_{C2} for roof cladding for Case #09 – $\theta = 90^\circ$ to 135°

The point net pressure factor, F_{C1} is critical for building design when the opening is on the leading edge of the side wall that produces large negative internal and small negative or positive external pressures at the roof downwind side (near to leeward edge). Figure 5.37 shows the F_{C1} for roof cladding for Case #07 when the LO2 is on side wall for wind directions 225° to 315° . Figure 5.37 also shows that F_{C1} is less than 0.85 for roof cladding and largest F_{C1} observed at the leeward roof edge (i.e., RP1-1, RP4-3). Accordingly, maximum net pressure is 15% less than the combined effect of minimum internal and maximum external pressures at the particular roof cladding.

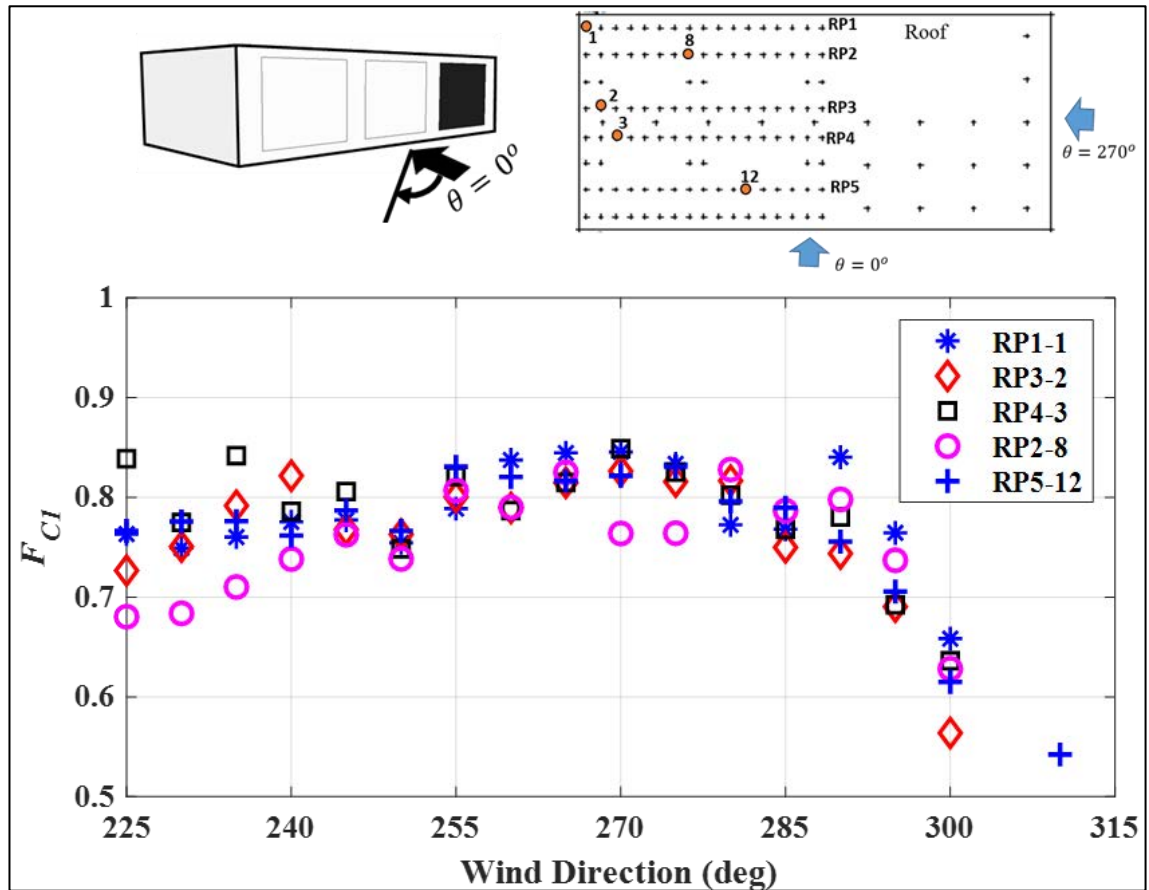


Figure 5.37: Point net pressure factors, F_{C1} for roof cladding for Case #07 (LO2 opening) – $\theta = 225^\circ$ to 315°

The net pressure factors (F_{C1} and F_{C2}) for different roof zones are obtained based on the wind directions that produce the peak maximum or minimum net pressure coefficients. Accordingly, F_{C2} is calculated for wind direction of minimum net pressures when the opening is on the windward wall (i.e., $\pm 45^\circ$ to the orthogonal wind direction to the opening) and F_{C1} is calculated to wind direction of maximum net pressure when the opening is on the leeward or side wall (i.e., for Case #09, $\theta = 225^\circ$ to 270°). Point net pressure factors are presented in simplified form for different roof zones, as shown in Figure 5.38, when the wind flows perpendicular to the opening, $\theta \pm 45^\circ$.

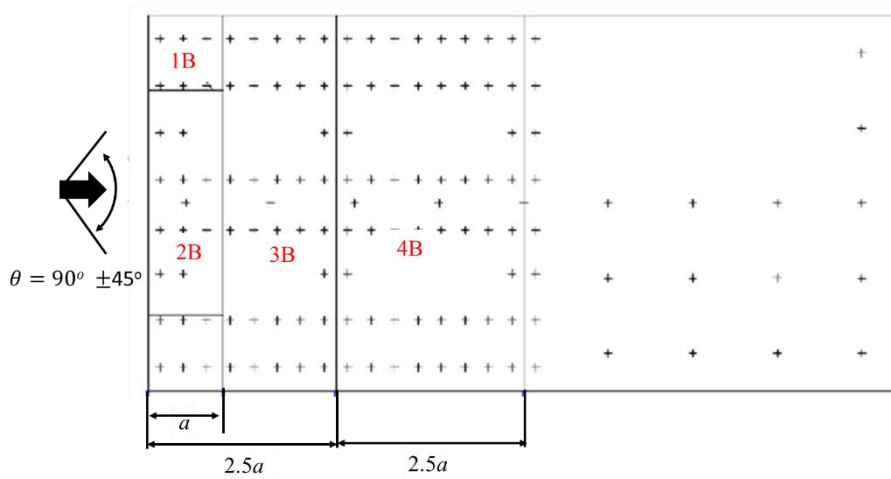


Figure 5.38: Roof zones for the net pressure factors when wind flows $\theta 90^\circ \pm 45^\circ$ perpendicular to the opening.

The calculated F_{C1} and F_{C2} are presented with respect to the non-dimensional parameter, S^* for different roof zones. Figure 5.39 shows the F_{C1} and F_{C2} for Zone #1B for different S^* values that the calculated F_{C2} is higher than 0.9 and F_{C1} is smaller than 0.75 for all S^* values. For building design, F_{C2} represents the critical building configurations with large suction net pressures on Zone #1B, and $F_{C2} = 0.95$ for any S^* value compares to combination factor, K_C (i.e., 0.9) defined in AS/NZS 1170.2.

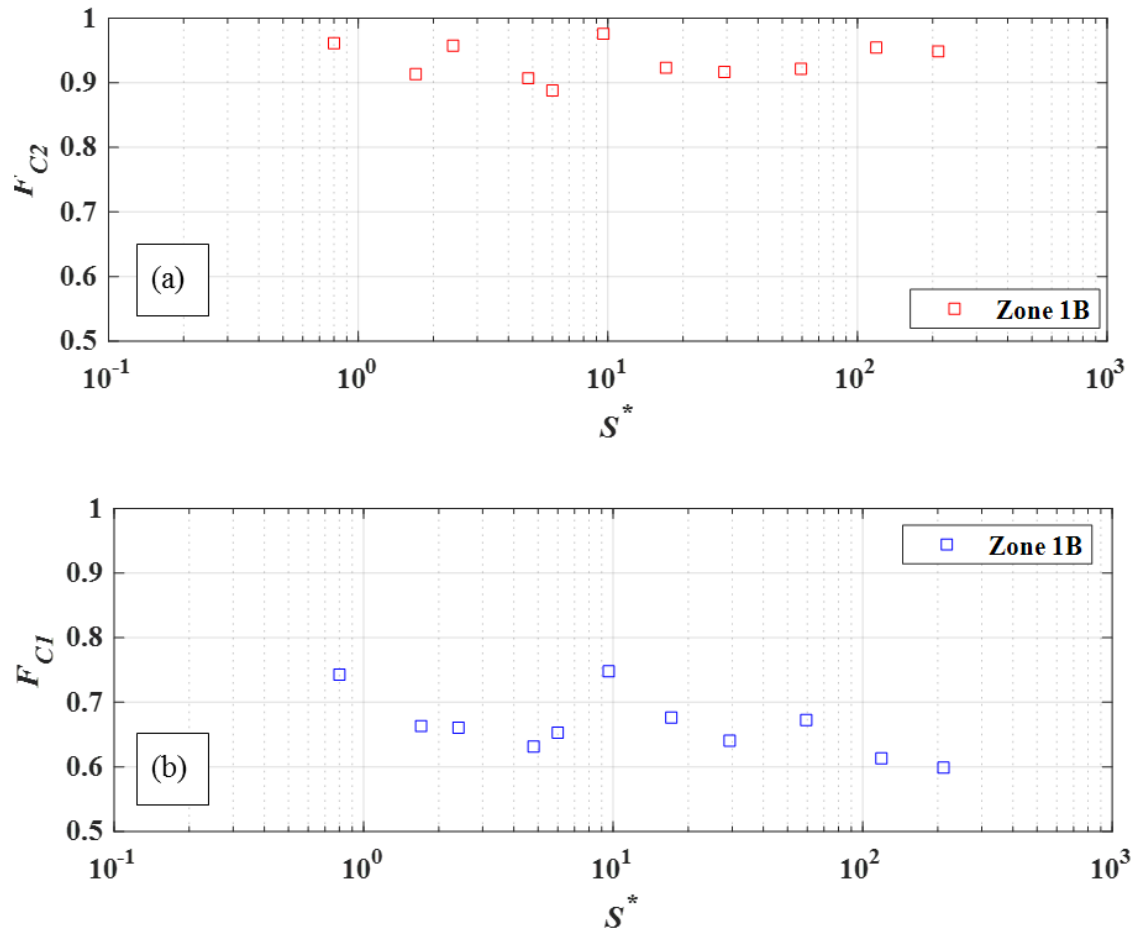


Figure 5.39: Point net pressure factors for Zone #1B vs S^* (a) F_{C2} for windward opening cases; (b) F_{C1} for leeward or side wall opening cases

The point net pressure factors, F_{C1} for roof Zones #2B, #3B, and #4B are smaller than 0.8 (Table 5.7) showing more reduction in the downward net pressure acting on roof cladding when the opening is on leeward or side wall. The F_{C2} is higher than F_{C1} due to the small difference between the magnitude of minimum suction net pressure and magnitude of combined minimum suction external and maximum positive internal pressures. The F_{C2} depends on the opening area to volume ratio and the location of the roof cladding, as shown in Table 5.7 for roof Zones #2B, #3B, and #4B. Accordingly, for roof Zone #2B, F_{C2} is 0.9 and 0.85 when $S^* < 50$ and $S^* > 50$, respectively. For roof Zone #3B, F_{C2} values do not show a trend line and vary between 0.8 and 0.9, and the calculated F_{C2} for roof Zone #4B is less than 0.8 compared to $K_C = 0.9$ in AS/NZS 1170.2.

Table 5.7: Point net pressure factors, F_{C1} and F_{C2} for roof Zones #2B, #3B and #4B for different S^* values

Case #	S^*	Zone #2B		Zone #3B		Zone #4B	
		F_{C1}	F_{C2}	F_{C1}	F_{C2}	F_{C1}	F_{C2}
51	0.8	0.66	0.91	0.76	0.81	0.73	0.73
12	1.7	0.58	0.88	0.73	0.87	0.76	0.79
50	2.4	0.54	0.92	0.63	0.79	0.69	0.76
11	4.8	0.70	0.78	0.71	0.92	0.75	0.77
25	6.0	0.57	0.85	0.78	0.91	0.75	0.83
22	9.6	0.63	0.85	0.76	0.91	0.82	0.84
24	17.1	0.60	0.90	0.73	0.87	0.78	0.84
49	29.3	0.67	0.92	0.67	0.76	0.72	0.79
9	59.4	0.62	0.83	0.75	0.93	0.82	0.81
21	118.9	0.62	0.82	0.73	0.91	0.75	0.75
23	210.7	0.62	0.82	0.72	0.88	0.74	0.85

5.4.3 Wall Cladding

The net pressure coefficients are analysed for Wall #1, Wall #3 and Wall #4 of the building with a windward wall opening, side wall opening and leeward wall opening for critical wind directions by considering critical design scenarios.

5.4.3.1 Wall #1- net pressure and net pressure factor

The peak minimum net pressure coefficients are presented in Figure 5.40 at the selected pressure taps on Wall #1 when the building has an opening on the windward wall for wind directions $\theta = 90^\circ$ to 135° . The $C_{p,net}$ decreases towards the leeward wall along Wall #1 from leading windward edge and in a similar manner to the $C_{p,net}$ on the roof cladding as seen in Figure 5.27. Net pressures fluctuations are higher near the leading edge due to the large suction external and positive internal pressures.

Figure 5.41 shows the point net pressure factor on Wall #1 for wind directions $\theta = 90^\circ$ to 135° which is similar to the F_{C2} variations on roof cladding. The largest F_{C2} of 0.9 occurs at 90° with the highest $C_{p,net}$ at WG1-1 and WG1-3. The net pressure factor increases

from 0.8 to 0.9 in the middle of the wall (i.e., WG1-17) for wind direction 90° to 135° . However, smallest $C_{p,net}$ produced the largest F_{C2} at WG1-5 and WG1-17 which is not the critical design scenario for cladding. Therefore F_{C2} is obtained for wind direction of the largest $C_{p,net}$. Accordingly, the F_{C2} is 0.9 for cladding at the leading edge ($< .5h$ from the windward edge), 0.85 for cladding between $0.5h$ and $1h$ and 0.8 for cladding located between $1h$ and $2h$ along with side wall when the building has an opening on the windward wall.

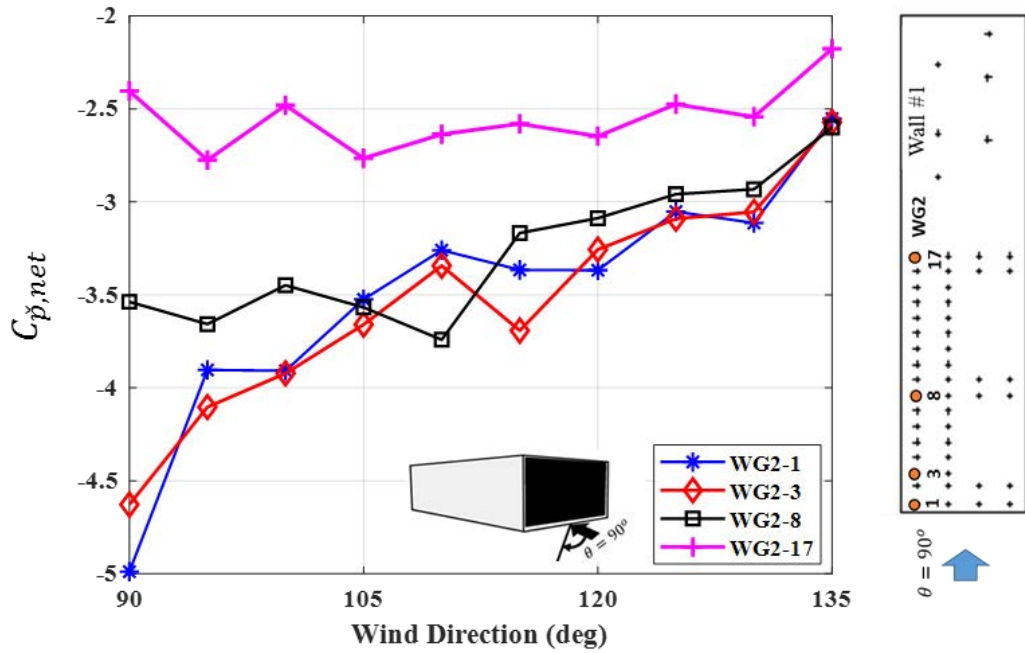


Figure 5.40: Minimum net pressures coefficient on Wall #1 cladding when the LO6 open for $\theta = 90^\circ - 135^\circ$

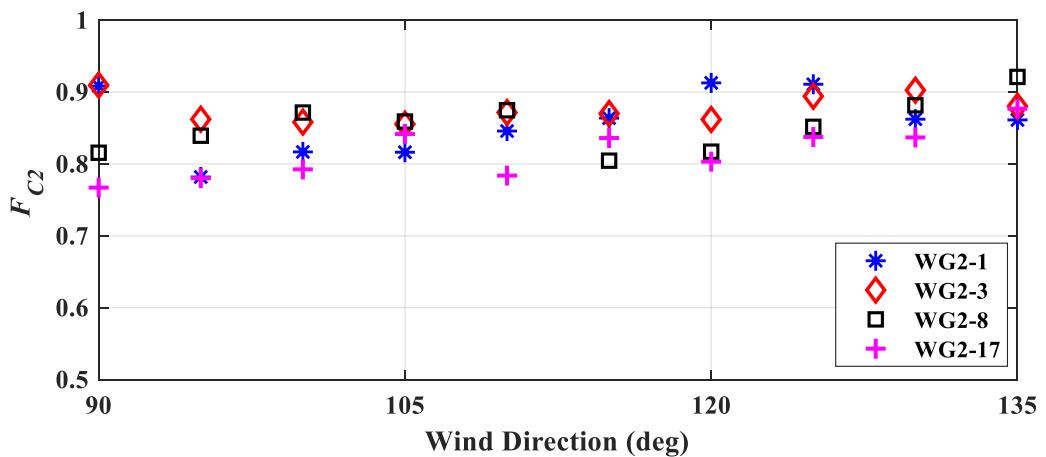


Figure 5.41: Point net pressure factor, F_{C2} for Wall #1 for $\theta = 90^\circ - 135^\circ$

5.4.3.2 Wall #2 – net pressures and net pressure factors

The combination of large negative internal and positive external pressure generates the largest maximum net pressure on Wall #2 when the building contains a large opening at the leading edge of the adjoining wall (i.e., Case #07, LO2 on Wall #1) for wind directions 225° to 315°. Figure 5.42 shows the $C_{\hat{p},net}$ on Wall #2 when LO2 is open for wind directions from 225° to 315°. The largest $C_{\hat{p},net}$ occurred at $\theta = 255^\circ$ to 285° when the opening is at the side wall generating negative internal pressures.

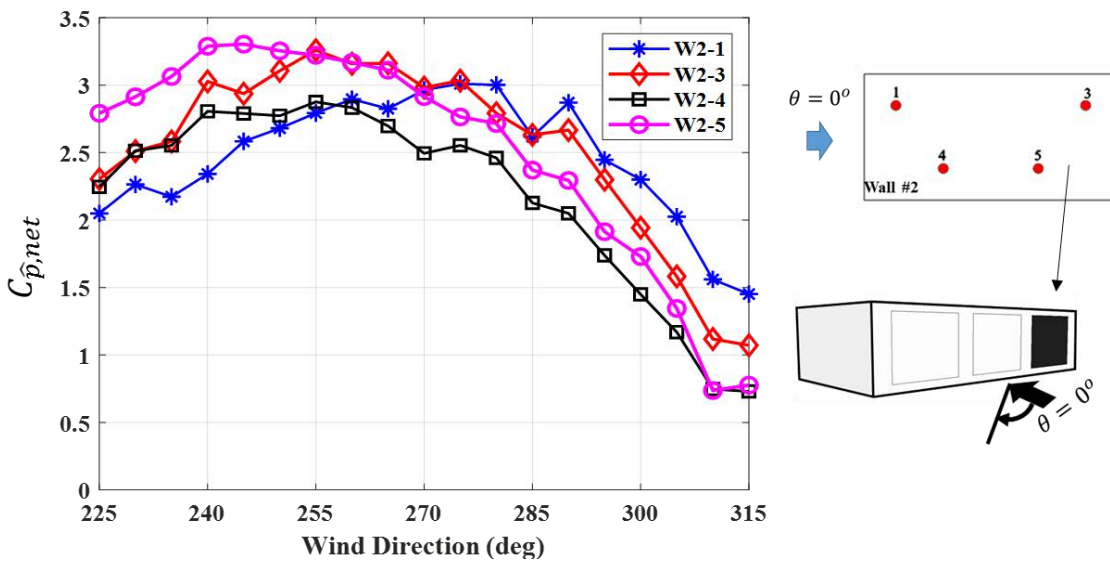


Figure 5.42: Maximum net pressure coefficients on Wall #2 with the opening on Wall #1 in Case #07 – $\theta = 270^\circ \pm 45^\circ$

Figure 5.43 shows the external, internal and net pressure time-histories for two different locations, W2-1 and W2-5 for wind directions 280° and 240°. The highest maximum net pressure at W2-1 and W2-5 occur at $\theta = 280^\circ$ and 240° . The external pressures at these locations fluctuate around +1.0 for particular wind directions 280° and 240°, but internal pressure fluctuates around 0.0 for W2-1 ($\theta = 280^\circ$) and -0.7 for W2-5 ($\theta = 240^\circ$). Accordingly, combination negative internal pressure and positive external pressure at W2-5 produces the positive large net pressure ($\theta = 280^\circ$) while external pressure dominates at W2-1 ($\theta = 240^\circ$) to generate large maximum net pressure.

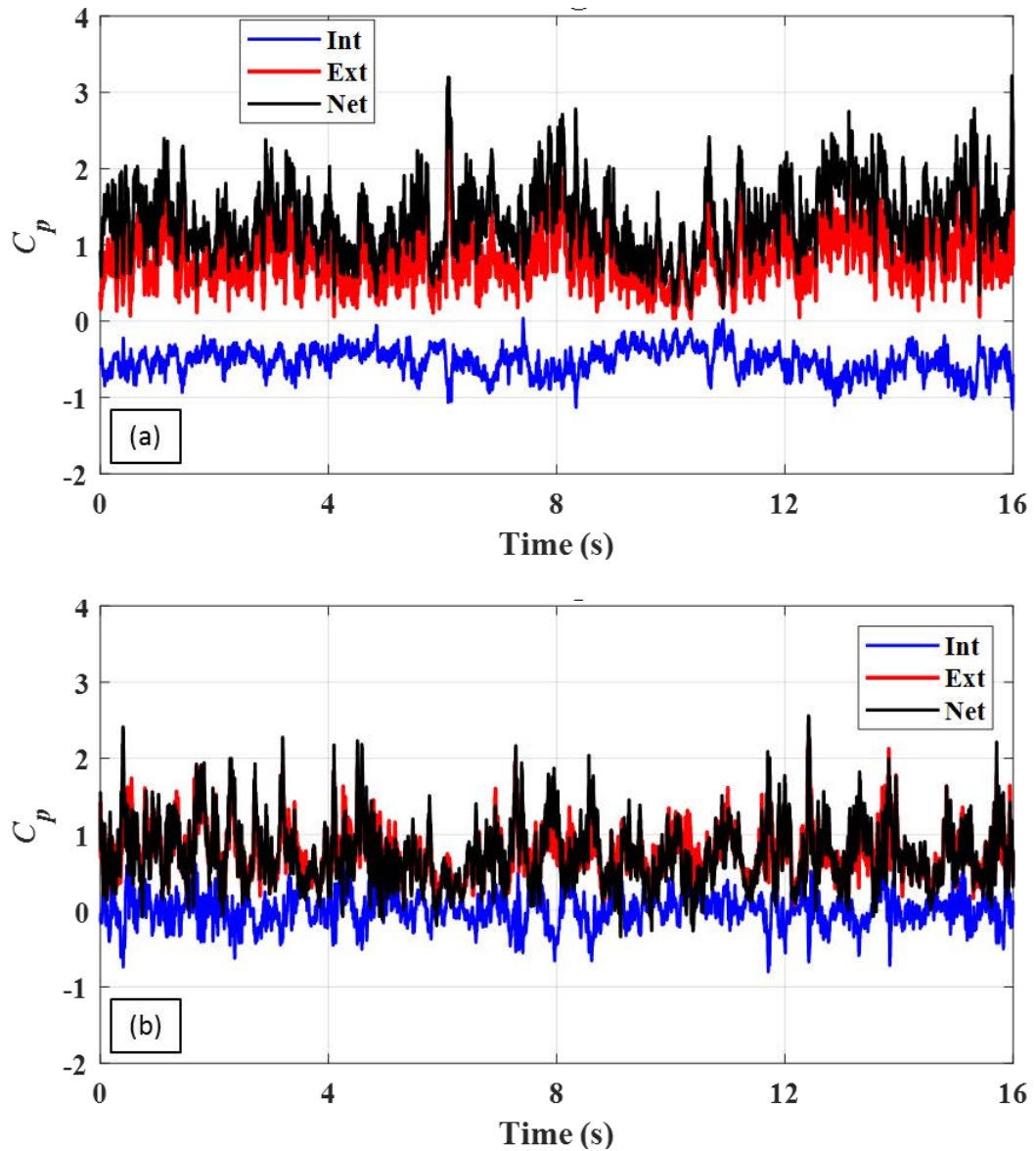


Figure 5.43: External, internal and net pressure time-histories for Wall #2 (a) W2-5 for $\theta = 260^\circ$, (b) W2-1 for $\theta = 290^\circ$

The F_{C1} is the critical net pressure factor for Wall #2 following this building configuration that Wall #2 is the windward wall when the opening is on the adjacent side wall for $\theta = 270^\circ \pm 45^\circ$. Figure 5.44 shows that F_{C1} varies between 0.9 and 0.95 for wind directions 255° to 285° following the largest $C_{\hat{p},net}$ on Wall #2. Net pressure factor can be concluded as 0.95 compares to the combination factor, $K_C = 0.9$. The maximum net pressure can be calculated using measured external and internal pressure data and given K_C , such that $C_{\hat{p},net} = K_C(C_{\hat{p},net} - C_{\hat{p},i})$. Accordingly, calculated $C_{\hat{p},net}$ for W2-1 for $\theta = 280^\circ$ is 2.97 (i.e., $0.9[2.32 - (-0.98)]$) which has good agreement with measured $C_{\hat{p},net}$ of 3.0. But

calculated $C_{\hat{p},net}$ for W2-5 for $\theta = 240^\circ$ is 3.15 (i.e., $0.9[2.25 - (-1.25)]$) which is ~5% less than the measured $C_{\hat{p},net}$ of 3.3.

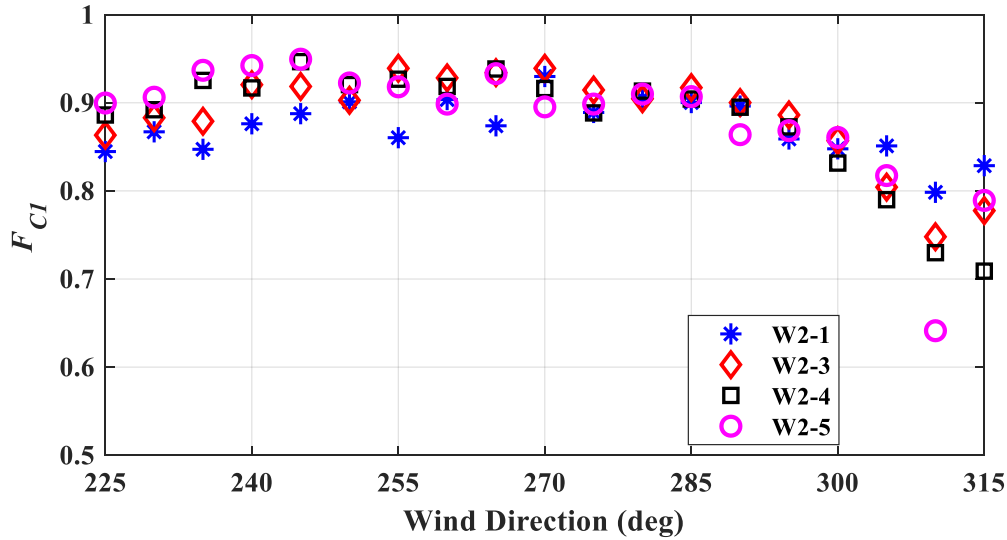


Figure 5.44: Point net pressure factor, F_{CI} for Wall #2 when the opening on adjacent side wall for $\theta = 270^\circ \pm 45^\circ$

5.4.3.3 Wall #3- net pressure and net pressure factor

Figure 5.45 and Figure 5.46 show the maximum and minimum net pressure coefficients on Wall #3 when the opening is on the opposite wall (i.e. Wall #1). Figure 5.45 shows that the $C_{\hat{p},net}$ can be critical on Wall #3 when the opening is on leeward wall for $\theta = 135^\circ$ to 180° and highest $C_{\hat{p},net}$ observed for W3-1 at the windward edge and decrease along with wall towards the wall middle. On Wall #3 for wind directions 0° to 45° , the $C_{\hat{p},net}$ can be critical for design when the opening is on the windward wall. The combination of large positive internal and suction external pressures generates large net pressures on the leeward wall, as shown in Figure 5.46. The highest peak net pressure is 3 times larger than the peak external pressure since the positive internal pressure fluctuations reasonably influenced net pressure fluctuation on the leeward wall.

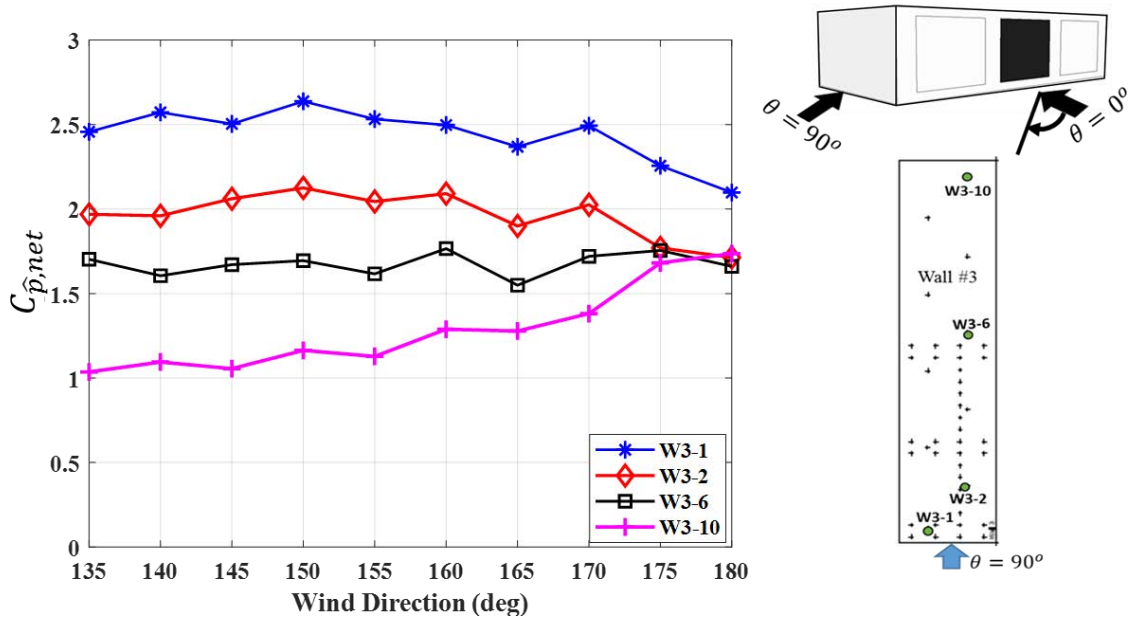


Figure 5.45: Maximum net pressure coefficient for Wall #3 with the opening on Wall #1, Case #04 for $\theta = 135^\circ - 180^\circ$

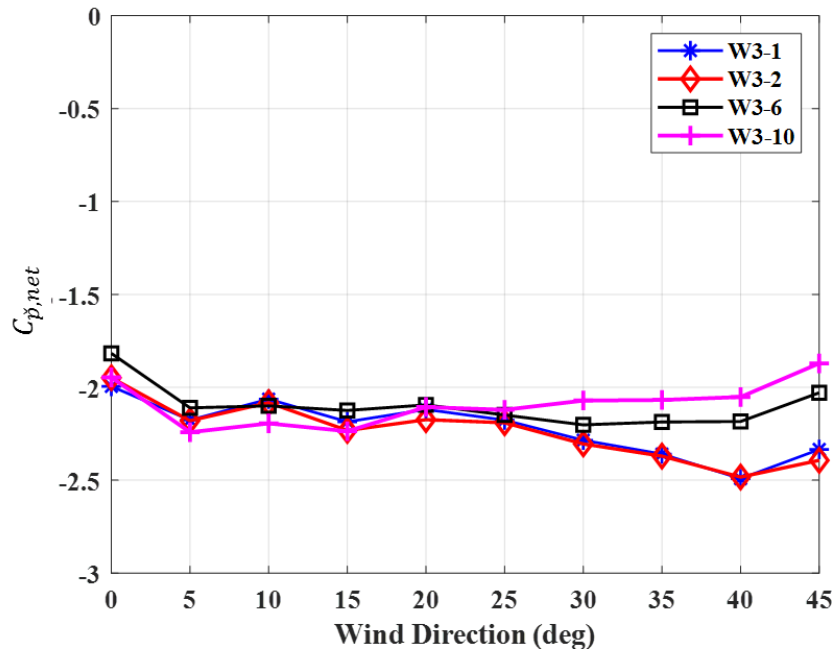


Figure 5.46: Minimum net pressure coefficient for Wall #3 with the opening on Wall #1, Case #04 for $\theta = 0^\circ - 45^\circ$

Figure 5.47 shows the point net pressure factors, F_{C1} for windward wall (Wall #3) when the building has an opening on the leeward wall. The F_{C1} is ~ 0.9 for Wall #3 by considering the wind direction of the largest $C_{p,net}$ as shown in Figure 5.47. Figure 5.48 shows the F_{C2} for leeward wall (Wall #3) when the opening is on the windward wall. For wind direction 0° , minimum net and external pressures on all cladding locations produced a F_{C2} of 0.85 because positive internal pressure influenced the net pressure factor. However, F_{C2} is about 0.9 for some wind directions due to the small minimum net and maximum internal pressures compared to wind direction $\theta = 20^\circ$. The comparison of F_{C1} and F_{C2} suggest the most conservative net pressure factor is 0.9 for Wall #3 when the building contains an opening on the opposite wall.

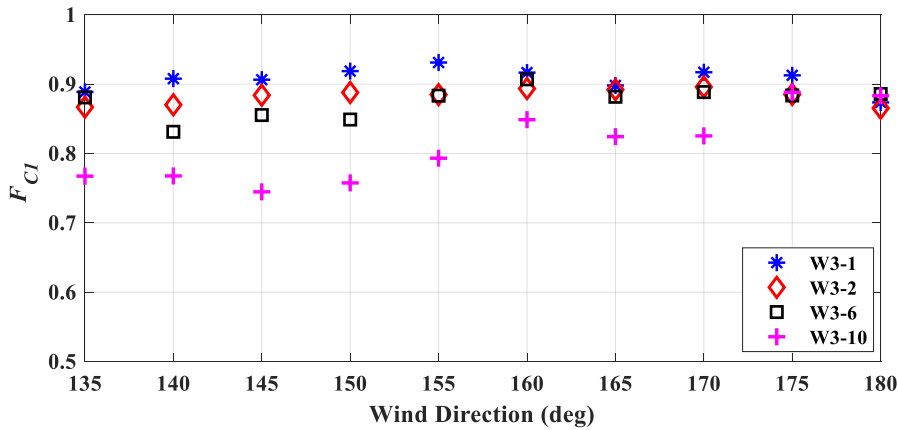


Figure 5.47: Point net pressure factor, F_{C1} for Wall #3 (windward wall) with the opening on Wall #1, Case #4, $\theta = 135^\circ - 180^\circ$

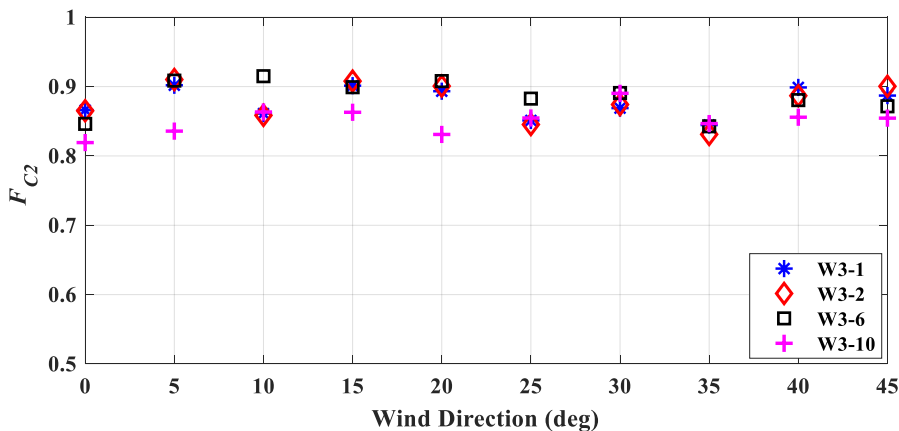


Figure 5.48: Point net pressure factors, F_{C2} for Wall #03 (leeward wall) with the opening on Wall #1 - Case #04, $\theta = 0^\circ - 45^\circ$

5.5 Chapter summary

The correlations between external and internal pressure fluctuations were determined using simultaneously measured external and internal pressure observations on model-scale buildings. The correlation coefficients at the zero-lag time, $r_{pepi}(0)$ were derived for roof and wall cladding at different locations with respect to the approaching wind directions for different building configurations. The combination of external and internal pressure fluctuations which generate net pressures on roof and wall cladding were also analysed. Furthermore, the net pressure factors were defined for roof and wall cladding based on the peak net, external and internal pressures, as illustrated in Figure 5.49. The outcome of this Chapter are;

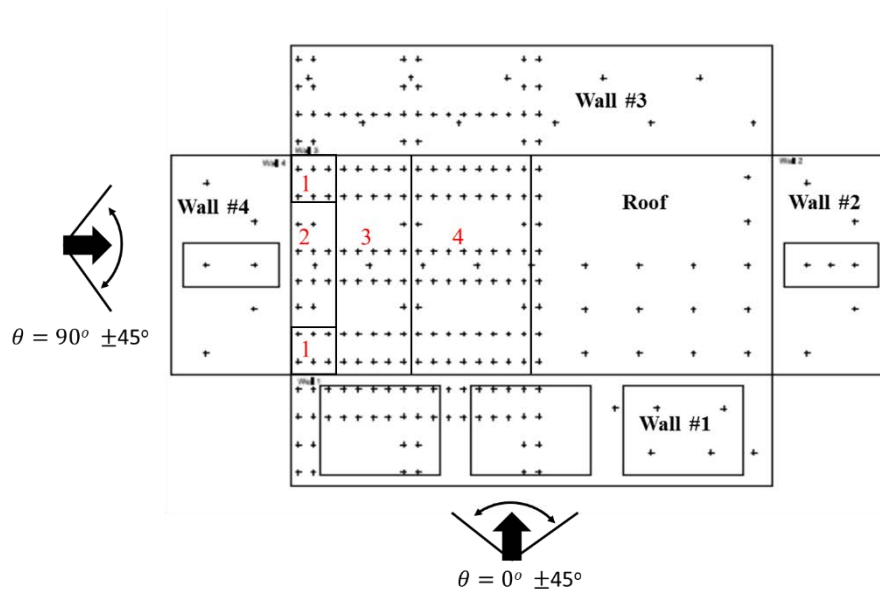


Figure 5.49: Schematic view of the walls and roof zones on the building envelope

The level of correlation between the external and internal pressures is a critical parameter that defines the estimation to the net pressure. The covariation integration method can satisfactorily estimate the peak net pressures on cladding element of nominally sealed building and building with a large opening.

Nominally sealed building-

- Small internal pressure fluctuations are poorly correlated with the external pressure fluctuations on the walls and roof because the internal pressures are

generated by leakage through all walls which are not related to external pressures fluctuations at a single tap location.

- Peak net pressures mostly influenced by the peak external pressures since the small internal pressure fluctuations do not significantly contribute to net peak pressures.
- The peak net suction pressures are large at the leading roof edge for wind directions within a sector $\pm 45^\circ$ to the orthogonal directions (i.e., Zone 1 and 2 for $\theta = 90^\circ \pm 45^\circ$) and decrease towards the leeward roof end.
- The net pressure reduction factors for windward roof corner (Zone #1) is about 0.97, windward edge and reattachment area (Zone #2 and #3) is about 0.95, and middle of the roof (Zone #4) is about 0.9.

Building with a large opening-

- Highly fluctuating positive internal pressures are moderately correlated with large negative external pressures (i.e., opening on Wall #4 for $\theta = 90^\circ \pm 45^\circ$), at the roof windward leading edge above the opening (Zone #1 and #2) because the internal positive pressure fluctuations are generated through the area-averaged external pressure fluctuations over the opening.
- The correlation coefficients between area-averaged external pressures and internal pressures are -0.6 and -0.7 at the windward roof corner and windward roof edge respectively which agrees with previous studies by Beste and Cermak (1997) and Sharma and Richards (2005)
- Highly fluctuating internal pressure fluctuations are poorly correlated with small external suction pressures at the roof locations $1.5h$ away from the leading roof edge after the reattachment area (Zone #4) that $r_{pepi}(0)$ varies between -0.2 and +0.3 due to the time for the external pressure fluctuations to travel to the middle of the roof from the leading roof edge.
- When the opening is on the windward wall (i.e., Wall #1 for $\theta = 0^\circ \pm 45^\circ$);
 - For windward wall cladding and wall girt (Wall #1), $r_{pepi}(0)$ is +0.8 near the opening and decreases further toward the sides of the wall, where $r_{pepi}(0)$ is less than +0.4 at the edge of the windward wall.

- For side wall cladding and wall girt (Wall #4), $r_{pepi}(0)$ is -0.5 near the leading edge and decrease towards the middle of the wall with $r_{pepi}(0)$ less than -0.2 which similar to $r_{pepi}(0)$ in the middle of the roof.
- For leeward wall cladding and wall girt (Wall #3), external and internal pressures are poorly correlated and $r_{pepi}(0)$ varies between -0.3 and +0.2.
- When the opening is on the side wall (i.e., Wall #1 for $\theta = 90^\circ \pm 45^\circ$);
 - For windward wall cladding and wall girt (Wall #2), external and internal pressures are poorly correlated and $r_{pepi}(0)$ varies between -0.4 to 0.1 along the wall girt.
 - For side wall cladding and wall girt (Wall #1), external and internal pressures are poorly correlated at the windward leading wall edge, $r_{pepi}(0)$ increases towards the opening edge along the wall girt that $r_{pepi}(0)$ varies between -0.1 to +0.7. In contrast, on the opposite side wall, internal and external pressures are poorly correlated and $r_{pepi}(0)$ is -0.3.
 - For leeward wall cladding and wall girt (Wall #2), $r_{pepi}(0)$ varies between -0.1 to 0.4 along the wall girt.
- The occurrence of peak net pressure is a random process which does not depend on the coincidence of the peak internal and peak external pressure at the same time.
- For $1 < S^* < 120$, net reduction factor (F_{C2}) for Zone #1 is 0.95, and F_{C2} is 0.9 and 0.85 for Zone #2 when $S^* < 50$ and $S^* > 50$, respectively. For Zone #3 and #4, F_{C2} is 0.8 ($1 < S^* < 120$).
- When the opening is on the windward wall, the net reduction factor, F_{C2} is 0.8 and 0.85 for windward wall and leeward wall, respectively and F_{C2} is 0.9 at the leading edge and 0.85 at the middle of side wall.

6 CONCLUSIONS AND RECOMMENDATIONS

Internal pressure can contribute significantly to the high net wind loads generated by a combination of external and internal pressures across the building envelope. Satisfactory estimation of internal pressure fluctuations and their correlation with external pressures fluctuations enables the optimal design of cladding in buildings. Wind load standards (i.e., AS/NZS 1170.2) provide internal and external pressure data based on quasi-steady approximations to specify the net wind loads on the building envelope. The parameters specified in the wind loading standards to account for the lack of correlation between internal and external pressures are not well understood and have not been satisfactorily characterised previously from model-scale wind tunnel tests, full-scale tests or analytical techniques.

The aim of this thesis is to characterise the wind-induced internal pressure fluctuations and assess the net pressures that generate peak net wind loads on industrial-type buildings and to define the net pressure reduction factors.

Model-scale studies were conducted on two open-plan, rectangular, low roof pitch industrial buildings, 80 m long \times 40 m wide \times 20 m high, and 160 m long \times 40 m wide \times 20 m high at a length scale of 1/200. A total of 55 configurations were tested, including, nominally sealed buildings, buildings with single large and multiple openings in the envelope, porous buildings with large openings and different building volumes. These studies provide an understanding of the internal pressure fluctuations in different building configurations and their combination with the external pressures fluctuations that generate net wind loads on roof and wall cladding. The results are also represented non-dimensionally to enable their approach in structural design for a range of typical industrial buildings.

The conclusions and recommendations derived are detailed as follows:

6.1 Conclusions

The preliminary objective of this study was to determine internal and external pressure fluctuations and how they to generate net pressures on cladding elements of typical industrial buildings with a range of opening configurations, building volume, and building porosity. The aim of this study is successfully accomplished by characterising internal and external pressure fluctuations and their correlations to generate the peak net pressures on roof and wall cladding of industrial buildings. The study found that;

A probabilistic assessment of the internal, external and net pressure peak events acting on roof and wall (when the peak exceeds the mean by 3σ) shows that these peak events do not coincide (i.e., random events). This finding is confirmed by the application of the covariance integration method, which showed that these peak net pressure can be estimated very satisfactorily using the mean, peak and standard deviation of the internal and external pressures and their correlations (determined from the overall signals).

External pressures on walls and roof

- The mean external pressure coefficients on the windward wall, leeward wall, sidewall and the roof of buildings are similar to previous full-scale and model-scale studies. The magnitude of peak suction external pressures is high in flow separation regions on the roof and walls and are dependent on approach wind direction.
- The magnitude of peak positive and negative external pressures decreases as the size of the area-averaged pressure region increases as per area reduction factor, K_a in AS/NZS 1170.2 with significantly greater decreases in highly turbulent pressure regions due to the spatial variation of external pressures. Area reductions factors applicable to the windward and leeward wall have been produced in this study.

Internal pressures

Nominally sealed building;

- Internal pressure coefficients in nominally sealed buildings are small and fluctuate between 0 and -0.4 with small variations across all approach wind directions. The

mean internal pressure coefficient is negative and fluctuates around -0.2, which has in good agreement with quasi-steady coefficient in AS/NZS 1170.2.

- The restricted flow in and out through the porous holes around the building envelope produces damped internal pressure fluctuations and small mean suction internal pressures compared to the external pressures on walls.
- The magnitude of the nominally sealed model scale internal pressure fluctuations cannot be directly compared to a full-scale building, due to the inability to correctly scale flow through the small openings. However, characteristics of the internal pressure fluctuations obtained for a nominally sealed building are considered representative of wind flow through typical porous openings in the envelope.

Buildings with a large opening;

- The internal pressure follows the external pressure fluctuation at the opening in accordance with previous studies with the positive internal pressure fluctuations decreasing with increasing opening area following a decrease in area-averaged external pressures over the opening due to lack of spatial correlation.
- As the opening size decreases, the Helmholtz frequency f_H decreases, while the magnitude of the energy associated with the internal pressure fluctuations increases.
- The amplification and attenuation of peak and fluctuating internal pressures are presented as a function of the non-dimensional parameter, $S^* = (A^{3/2}/V)(a_s/\bar{U}_h)^2$. Ratio, $C_{\sigma pi}/C_{\sigma pe}$ varies around 1.1 and $C_{\hat{p}i}/C_{\hat{p}e}$ varies around 1.2, which agrees with previous studies conducted by Vickery (1992), Holmes and Ginger (2012), and Kim and Ginger (2013).
- Tests of multiple large openings on the same wall have shown that mean internal pressures are similar to a single opening on the same wall of similar size. The peak internal pressure fluctuations decreases, because of a decrease in the peak external pressures over the multiple large openings.

The main objectives of this thesis were achieved by determining the correlation between internal and external pressure fluctuations and analysing the peak net pressures on walls and roof. The following are the main findings.

Nominally sealed building

- The internal and external pressure fluctuations are poorly, positively correlated near to windward roof edge and moderately correlated $2h$ away from the leading edge of roof.
- The internal and external pressure fluctuations on the windward wall, are poorly correlated ($r_{pepi} < 0.3$). $r_{pepi}(0)$ is 0.4 and approximately constant along the side wall and the external and internal pressures are moderately correlated on the leeward wall.
- The peak net suction pressures are significantly large on the leading roof edge and decrease towards the leeward roof end.
- The peak net pressures on the roof are mostly influenced by the peak external pressures as the small internal pressure fluctuations, which are poorly correlated with the external pressure fluctuations have a minimal contribution to peak net pressures.

Building with a large opening

- The external pressures near the windward roof edge are moderately, negatively correlated with high positive internal pressure in the building with a large windward opening.
- For oblique wind flows (i.e., $\theta = 135^\circ$), the large external suction pressures generated by the flow separation and conical vortices formed above the opening on the roof edge are highly, negatively correlated, while external pressures above the other leading edge (i.e., above the adjacent wall) are poorly correlated with internal pressure fluctuations.
- The correlation coefficients between area-averaged external pressures and internal pressures are about -0.6 to -0.7 at the windward roof corner and windward roof edge and $r_{pepi}(0)$ does not vary significantly on these roof locations for different building configurations when the S^* varies between 1 to 120.
- At the middle of the roof ($1h$ away from leading-edge), internal and external pressures are poorly correlated following the flow reattachment such that $r_{pepi}(0)$ varies between -0.2 and +0.3.

- When the opening is on the windward wall, internal and external pressures on the side wall are moderately correlated near the leading edge and poorly correlated at the middle of the wall, and has a similar variation as on the roof cladding.
- The probability of peak external, internal and net pressure events occurring at the same time is less than 1%. More than 60% of external peak events and net peak events at the windward roof edge coincided while more than 50% of internal peak events coincide with peak net pressures at the middle of the roof.

The net pressure reduction factors are derived for different roof and wall locations as a function of S^* (considering the coincidence of the peak internal and peak external pressures) as the secondary objective of the study. The largest correlation coefficient, peak net pressure coefficient and largest net pressure reduction factor generally occur for three different approach wind directions on most of roof and wall cladding zones. The key extracts for the net pressure factors are as follows;

Nominally sealed building,

- The net pressure reduction factors, F_{C2} for windward roof corner (Zone #1) is about 0.95, windward edge and reattachment area (Zone #2 and #3) is about 0.95, and middle of the roof (Zone #4) is about 0.9.

Building with a large opening

- For $1 < S^* < 120$, net reduction factor (F_{C2}) for the windward roof corner is 0.95, and for the windward roof edge, F_{C2} is 0.9 and 0.85 when $S^* < 50$ and $S^* > 50$, respectively. For the middle of the roof F_C is 0.8.
- When the opening is on the windward wall, the net reduction factor (F_{C2}) is 0.8 and 0.85 for windward wall and leeward wall, respectively and F_{C2} is 0.9 at the leading edge and 0.85 at the middle of the side wall.

The outcomes of this study have identified that characteristics of external and internal pressure responsible for generating large net pressures on the roof and wall of industrial type buildings. The study has shown that characteristics are dependent on the type and

size of the opening in the envelope, the wind direction and the location of the roof and wall cladding. In nominally sealed buildings, large external suction pressures generate large net pressures with minimal influence from small internal pressure fluctuations. In a building with a large windward opening, large external suction pressures at the leading windward roof edge in combination with the positive internal pressure generate large net negative pressures. The large positive internal pressure dominates combination with small external pressures to produce small net suction pressures at the roof middle. The occurrence of peak net pressure is a random process which depends on the coincidence of the peak external and peak internal pressures at different locations on the wall and roof cladding.

6.2 Recommendations

The following recommendations and further research is suggested;

- Design of net pressure coefficients on the roof and wall cladding of industrial buildings can be achieved by applying the net pressure factors defined in this thesis across different regions of the building envelope by considering the possible building opening configurations.
- Full-scale studies are required to identify the influence of background leakage on the correlation between peak internal and peak external pressures in an industrial building with respect to the opening area.
- More research into the coincidence of internal and external pressures on other building elements, (i.e., uplift and shear force on the portal frame footings, racking forces).

REFERENCES

- ASCE standard. (2011). "Minimum Design Loads for Buildings and Other Structures." *American Society of Civil Engineers* 7-10. New York.
- Beste, F. and J. E. Cermak (1997). "Correlation of internal and area-averaged external wind pressures on low-rise buildings." *Journal of Wind Engineering and Industrial Aerodynamics* 69–71: 557-566. [https://doi.org/10.1016/s0167-6105\(97\)00186-4](https://doi.org/10.1016/s0167-6105(97)00186-4).
- Bodhinayake, G.G., Ginger, J. D., & Henderson, D. J. (2019). "Internal and External Pressure Fluctuations, Combination and Area Reduction Factors", *The 15th International Conference on Wind Engineering*, China.
- Bodhinayake, G.G., Ginger, J. D., & Henderson, D. J. (2020). "Correlation of internal and external pressures and net pressure factors for cladding design", *Journal of Wind and Structures*, <https://doi.org/10.12989/was.2020.30.2.000>
- Davenport, A.G., Surry, D. , Stathopoulos, T., "Wind Loads on Low-Rise Buildings", The University of Western Ontario, London, Ontario, Canada (1977)
- Davenport, A., & Surry, D. (1984). "The estimation of internal pressures due to wind with application to cladding pressures and infiltration." *Paper presented at the Proc., Wind pressure workshop*.
- Ghanadi, F., Arjomandi, M., Cazzolato, B.S., and Zander, A.C. (2014) " Control of turbulent boundary layer by a self-excited Helmholtz resonator", *Journal of fluid mechanics*
- Ghanadi, F., Arjomandi, M., Cazzolato, B.S., and Zander, A.C. (2013) " Numerical simulation of grazing flow over a self-excited Helmholtz resonator", *Engineering letters, Vol.21, no3, pp.137-142*
- Ginger, J. D., Mehta, K. C., & Yeatts, B. B. (1997). "Internal pressures in a low-rise full-scale building." *Journal of Wind Engineering and Industrial Aerodynamics*, 72(1-3), 163-174. doi:10.1016/S0167-6105(97)00241-9
- Ginger, J. D. (1997). "Internal and net pressures on low-rise full-scale buildings." *Cyclone Testing Station. technical report 45*.
- Ginger, J. D. and C. W. Letchford (1999). "Net pressures on a low-rise full-scale building." *Journal of Wind Engineering and Industrial Aerodynamics* 83: 239-250. [https://doi.org/10.1016/s0167-6105\(99\)00075-6](https://doi.org/10.1016/s0167-6105(99)00075-6).
- Ginger, J. D., Holmes, J. D., & Kopp, G. A. (2008). "Effect of building volume and opening size on fluctuating internal pressures." *Wind and Structures An International Journal*, 11(5), 361-376. doi:10.12989/was.2008.11.5.361
- Ginger, J. D., Holmes, J. D., & Kim, P. Y. (2010). "Variation of internal pressure with varying sizes of dominant openings and volumes." *Journal of Structural Engineering*, 136(10), 1319-1326. doi:10.1061/(ASCE)ST.1943-541X.0000225

- Guha, T. K., Sharma, R. N., & Richards, P. J. (2011a). "Internal pressure dynamics of a leaky building with a dominant opening." *Journal of Wind Engineering and Industrial Aerodynamics*, 99(11), 1151-1161. doi:10.1016/j.jweia.2011.09.002
- Guha, T. K., Sharma, R. N., & Richards, P. J. (2011b). "Influence factors for wind induced internal pressure in a low rise building with a dominant opening." *Journal of wind and Engineering*, 8(02), 1-17.
- Guha, T. K., Sharma, R. N., & Richards, P. J. (2012). "Internal pressure in a building with multiple dominant openings in a single wall: Comparison with the single opening situation." *Journal of Wind Engineering and Industrial Aerodynamics*, 107-108, 244-255. doi:10.1016/j.jweia.2012.04.023
- Guha, T. K., Sharma, R. N., & Richards, P. J. (2013a). "Field studies of wind induced internal pressure in a warehouse with a dominant opening." *Wind and Structures An International Journal*, 16(1), 117-136. doi:10.12989/was.2013.16.1.117
- Guha, T. K., Sharma, R. N., & Richards, P. J. (2013b). "Internal Pressure in a Building with a Single Dominant Opening: An Experimental and Numerical Case Study." *Journal of Structural Engineering (Madras)*, 41(1), 243-252. doi:10.3850/978-981-07-8012-8_156
- Harris, R. I. (1990). "The propagation of internal pressures in buildings." *Journal of Wind Engineering and Industrial Aerodynamics*, 34(2), 169-184. doi:10.1016/0167-6105(90)90142-Y
- Holmes, J. D. (1979). "Mean and fluctuating internal pressures induced by wind." Paper presented at the *Fifth international conference on wind engineering*, Fort Collins, Colorado, U.S.A.
- Holmes, J.D., and Best, R. J. (1981). "An approach to the determination of wind load effects on low-rise buildings", *Journal of Wind Engineering and Industrial Aerodynamics*, 7(3), 273-287 doi: 10.1016/0167-6105(81)90054-4
- Holmes, J.D., and Sym, M.J. (1994). "Wind loads on steel-framed low-rise buildings" *steel construction (Australian Institute of Steel Constructions)*, 28:2-12
- Holmes, J. D. (2007). "Wind Loading of Structures:" *Taylor & Francis*.
- Holmes, J. D., & Ginger, J. D. (2012). "Internal pressures - The dominant windward opening case - A review." *Journal of Wind Engineering and Industrial Aerodynamics*, 100(1), 70- 76. doi:10.1016/j.jweia.2011.11.005
- Humphreys, M. T., Ginger, J. D., & Henderson, D. J. (2019). "Internal pressures in a full-scale test enclosure with windward wall openings." *Journal of Wind Engineering and Industrial Aerodynamics*, 189, 118-124. doi:https://doi.org/10.1016/j.jweia.2019.03.024
- Humphreys, M. T. (2020).. " Characteristics Wind-Induced Internal Pressures in Industrial Buildings with wall opening", PhD thesis, *James Cook University, Townsville, Australia*.
- Irwin, P. A., & Dunn, G. (1994). *Review of internal pressures on low rise buildings*. RWDI:Report: 93-270.
- Kim, P. Y., & Ginger, J. D. (2013). "Internal pressures in buildings with a dominant opening and background porosity." *Wind and Structures An International Journal*, 16(1), 47-60. doi:10.12989/was.2013.16.1.047

- Kim, S.I., and Metha, K.C. (1977). "Wind loads on flat roof area through full-scale experiments", *Texas Tech University, Institute for Disaster Research Report*.
- Kopp, G. A., and Morrison, M. J. (2011). Discussion of "Tornado-induced wind loads on low-rise buildings" by F. L. Haan, V. K. Balaramudu, and P. P. Sarkar, *J. Struct. Eng.* 137, 1620–1622.
- Liu, H. (1975). "Wind pressure inside buildings." *Proceedings of the 2nd US National Conference on Wind Engineering Research*, Colorado State University, June.
- Liu, H., & Saathoff, P. J. (1981). "Building Internal Pressure: Sudden Change." *Journal of the Engineering Mechanics Division*, 107(2), 309-321.
- Liu, H., & Rhee, K. H. (1986). "Helmholtz oscillation in building models." *Journal of Wind Engineering and Industrial Aerodynamics*, 24(2), 95-115. doi:10.1016/0167-6105(86)90001-2
- Oh, J. H. (2004). "Wind-Induced Internal Pressures In Low-Rise Buildings." (*Master of Engineering Science*), University of Western Ontario.
- Oh, J. H., Kopp, G. A., & Inculet, D. R. (2007). "The UWO contribution to the NIST aerodynamic database for wind loads on low buildings: Part 3. Internal pressures." *Journal of Wind Engineering and Industrial Aerodynamics*, 95(8), 755-779. doi:10.1016/j.jweia.2007.01.007
- Roy, R.J., and Holmes, J.D. (1981). "Total force measurements on wind-tunnel models of low-rise buildings", *proceedings Colloque, Construire avec, Nantes, France*.
- Sharma, R. N. (1996). "The influence of internal pressure on wind loading under tropical cyclone conditions." *University of Auckland*.
- Sharma, R. N., & Richards, P. J. (1997). "Computational modelling in the prediction of building internal pressure gain functions." *Journal of Wind Engineering and Industrial Aerodynamics*, 67–68, 815-825. doi: [http://dx.doi.org/10.1016/S0167-6105\(97\)00121-9](http://dx.doi.org/10.1016/S0167-6105(97)00121-9)
- Sharma, R. N., & Richards, P. J. (2003). "The influence of Helmholtz resonance on internal pressures in a low-rise building." *Journal of Wind Engineering and Industrial Aerodynamics*, 91(6), 807-828. doi: [http://dx.doi.org/10.1016/S0167-6105\(03\)00005-9](http://dx.doi.org/10.1016/S0167-6105(03)00005-9)
- Sharma, R. N. and P. J. Richards (2005). "Net pressures on the roof of a low-rise building with wall openings." *Journal of Wind Engineering and Industrial Aerodynamics* 93(4): 267-291. <https://doi.org/10.1016/j.jweia.2005.01.001>.
- Sharma, R.N., Mason, S., Driver, P.,(2010). "Scaling methods for wind tunnel modelling of building internal pressures induced through openings", *Journal of Wind and Structures* 13: 363-374.
- Sharma, R. N. (2013). "The Fundamentals of Building Internal Pressure Dynamics Induced Through a Dominant Opening." *Paper presented at The Eighth Asia-Pacific Conference on Wind Engineering*, Chennai India. December 10-14
- Standards Australia, & Standards New Zealand. (2011). "AS/NZS 1170.2:2011 (A5) Australian and New Zealand Standard – Structural Design Part 2:" *Wind Actions*.
- Stathopoulos, T., & Luchian, H. D. (1989). "Transient Wind - Induced Internal Pressures." *Journal of Engineering Mechanics*, 115(7), 1501-1514. doi:10.1061/(asce)0733-9399(1989)115:7(1501)

- Stathopoulos, T., Surry, D., & Davenport, A. G. (1979). "Internal pressure characteristics of low-rise buildings due to wind action." *Paper presented at the 5th International Conference on Wind Engineering*, Fort Collins, Colorado USA.
- Vickery, B. J. (1986). "Gust-Factors for Internal-Pressures in Low Rise Buildings." *Journal of Wind Engineering and Industrial Aerodynamics*, 23(1-3), 259-271. doi:10.1016/0167-6105(86)90047-4
- Vickery, B. J. (1991). "Comments on the propagation of internal pressures in buildings" by R.I. Harris. *Journal of Wind Engineering and Industrial Aerodynamics*, 37(2), 209-212. doi:http://dx.doi.org/10.1016/0167-6105(91)90074-7
- Vickery, B. J., & Bloxham, C. (1992). "Internal pressure dynamics with a dominant opening." *Journal of Wind Engineering and Industrial Aerodynamics*, 41(1-3), 193-204. doi:10.1016/0167-6105(92)90409-4
- Vickery, B. J. (1994). "Internal pressures and interactions with the building envelope" by R.I. Harris. *Journal of Wind Engineering and Industrial Aerodynamics*, 37(1-2), 125-144. doi:http://dx.doi.org/10.1016/0167-6105(94)90022-1
- Woods, A. R., & Blackmore, P. A. (1995). "The effect of dominant openings and porosity on internal pressures." *Journal of Wind Engineering and Industrial Aerodynamics*, 57(2-3), 167-177. doi: 10.1016/0167-6105(95)00003-A
- Xu, H., Yu, S., & Lou, W. (2014). "The inertial coefficient for fluctuating flow through a dominant opening in a building." *Wind and Structures, an International Journal*, 18(1), 57-67. doi:10.12989/was.2014.18.1.057
- Xu, H., Yu, S., & Lou, W. (2016). "Estimation Method of Loss Coefficient for Wind-Induced Internal Pressure Fluctuations." *Journal of Engineering Mechanics*, doi: 10.1061/(asce)em.1943-7889.0001097
- Xu, H., Yu, S., & Lou, W. (2017). "The loss coefficient for fluctuating flow through a dominant opening in a building." *Wind and Structures*, 24(1), 79-93. doi:10.12989/was.2017.24.1.079
- Xu, H., and W. Lou (2017), "Combined effects of internal and external pressures for a building with wall openings," *9th Asia-Pacific conference on wind engineering*, Auckland, New Zealand.
- Yu, S.C., Lou, W.J., & Sun, B.N. (2006). "Wind-induced internal pressure fluctuations of structure with single windward opening." *Journal of Zhejiang University SCIENCE A*, 7(3), 415-423. doi:10.1631/jzus.2006.A0415
- Yu, S.C., Lou, W.J., & Sun, B.N. (2008). "Wind-induced internal pressure response for structure with single windward opening and background leakage." *Journal of Zhejiang University- SCIENCE A*, 9(3), 313-321. doi:10.1631/jzus.A071271

APPENDICES

Appendix A : Wind tunnel model details.....	165
Appendix B : Area averaged external pressure coefficient and area reduction factor (K_a)	173
Appendix C: Area-averaged net pressure and net pressure factor for roof Zones	181

APPENDIX A : WIND TUNNEL MODEL DETAILS

This appendix describes the wind tunnel models used in this model-scale testings. This includes the external pressure layout for both Model #1 and Model #2.

A.1. External pressure tap layout – Model #1

Figure A.1 shows a total of 254 external pressure taps on the Model #1. External pressure tap layout on the roof and walls with dimensions are shown in Figure A.2, Figure A.3, Figure A.4 and Figure A.5.

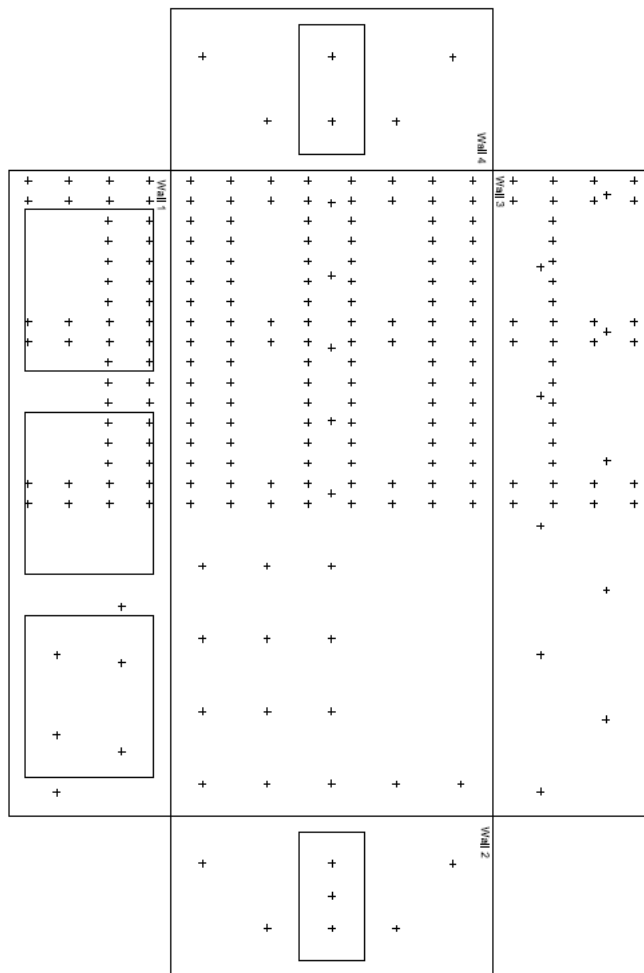


Figure A.1: External pressure taps layout - Model #1

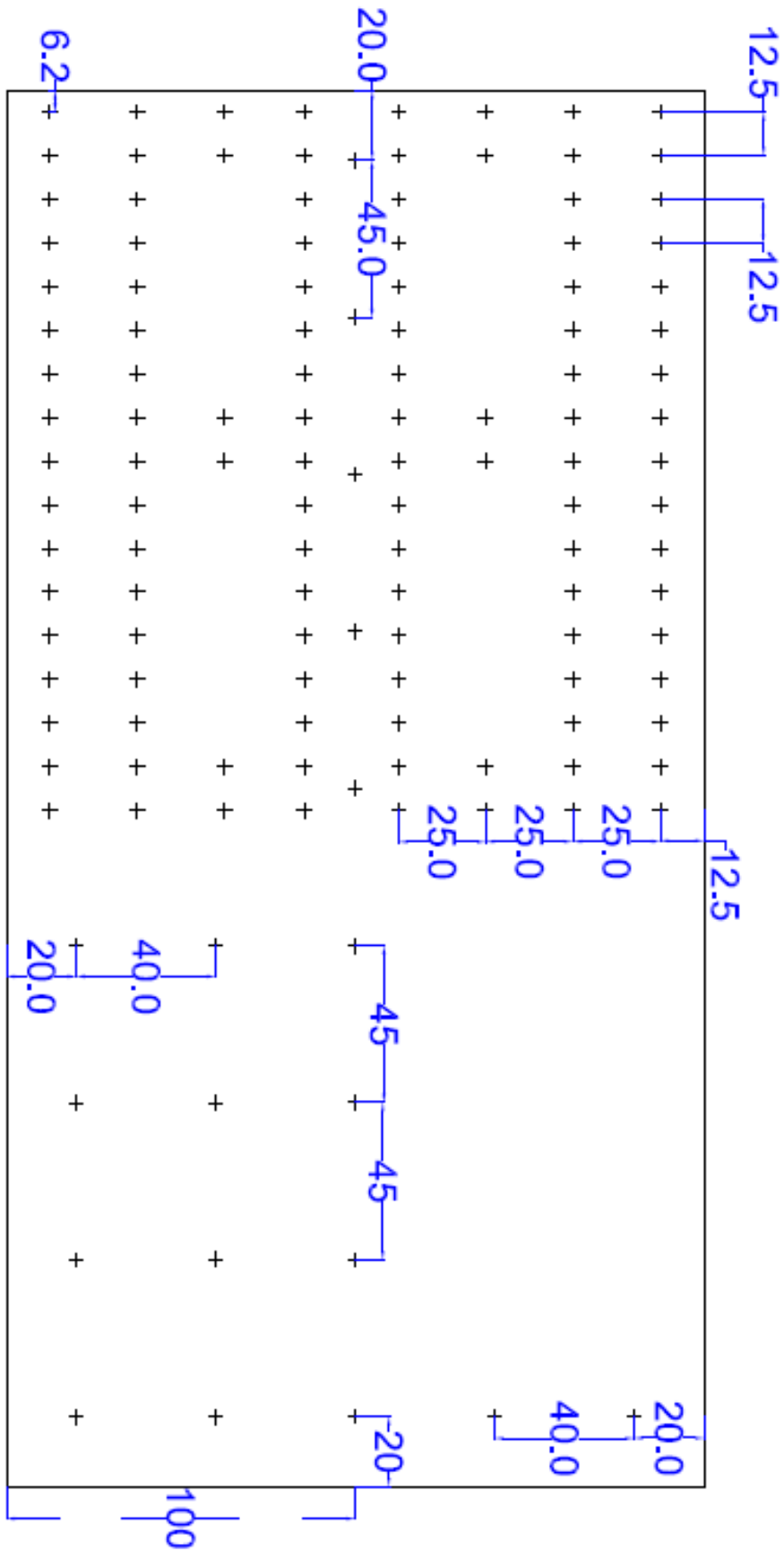


Figure A.2: Model #1-external pressure taps layout on the roof (All dimensions in millimetres)

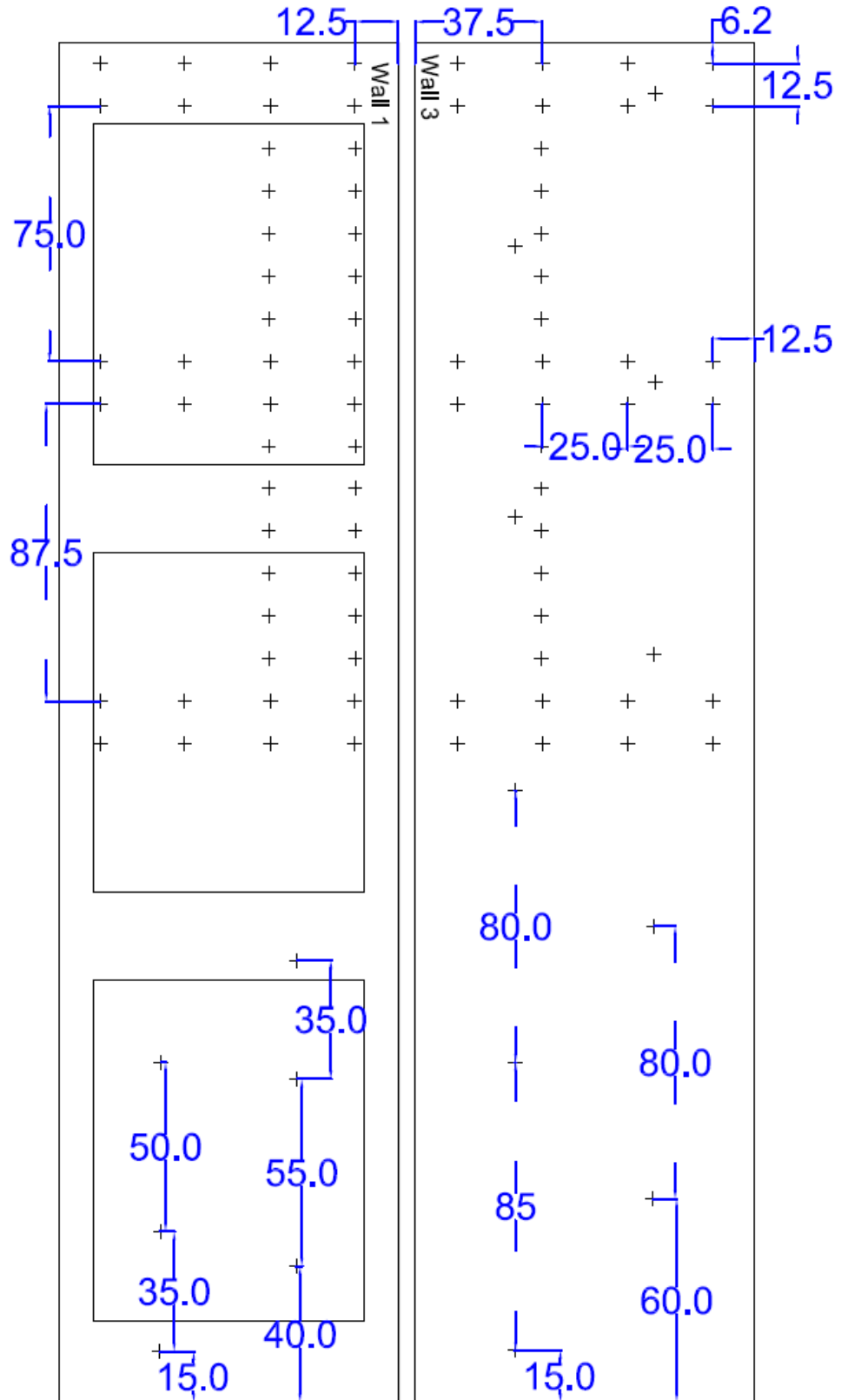


Figure A.3: Model #1-external pressure taps layout on Wall #1 and #3 (All dimensions in millimetres)

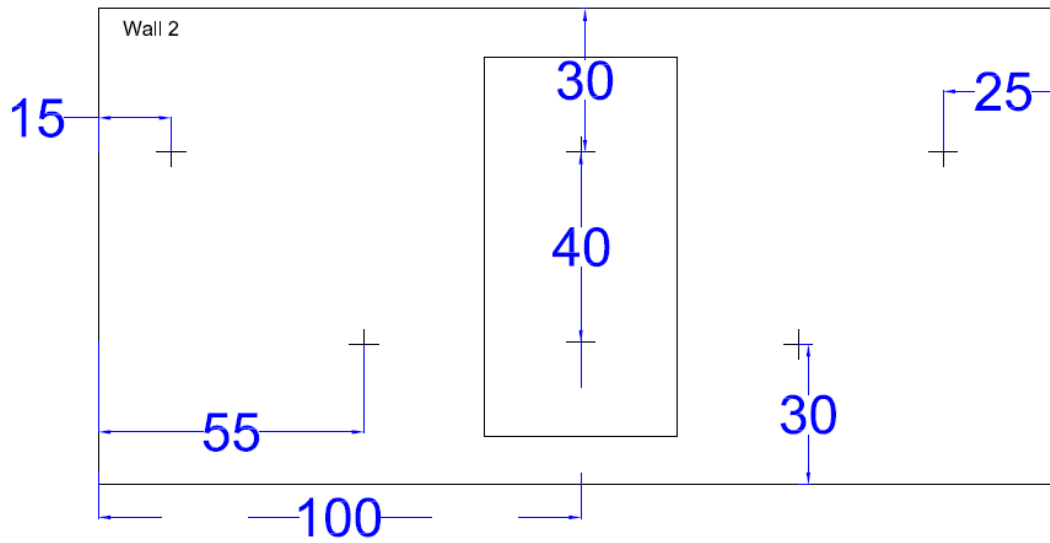


Figure A.4: Model #1-external pressure taps layout on Wall #2 (All dimensions in millimetres)

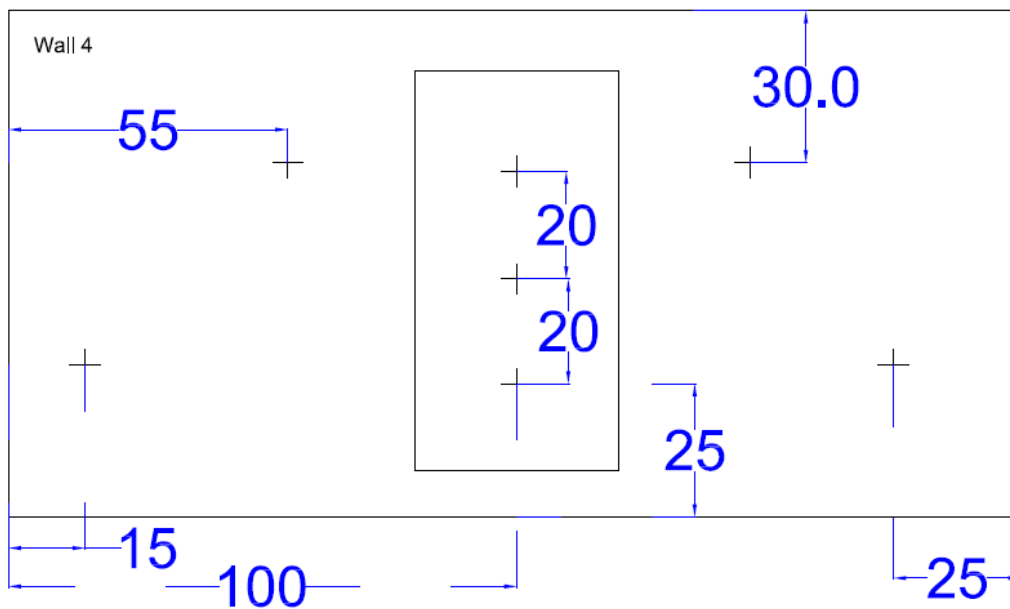


Figure A.5: Model #1-external pressure taps layout on Wall #4 (All dimensions in millimetres)

A.2. External pressure tap layout – Model #2

Figures A.6 and A.7 show the dimensions and openings locations for Model #2. External pressure tap layout on roof and walls are shown in Figures A.8, A9, A10, and A.11.

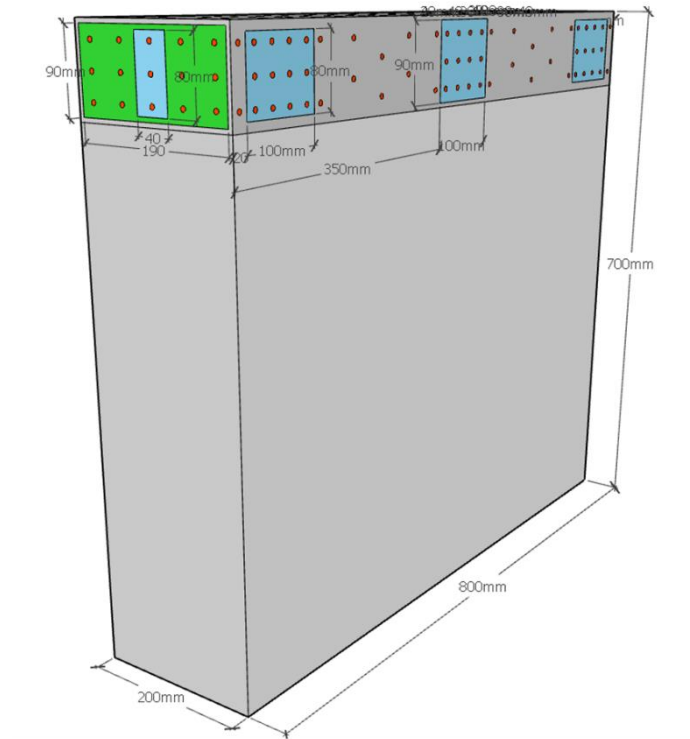


Figure A.6: Model #2 dimensions and opening locations (All dimensions in millimetres)

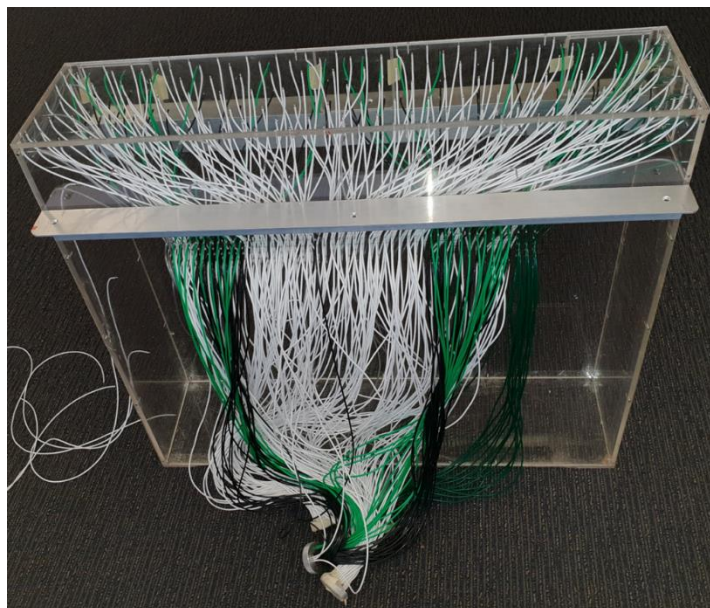


Figure A.7: External and internal pressure tubes are connected to Model #2

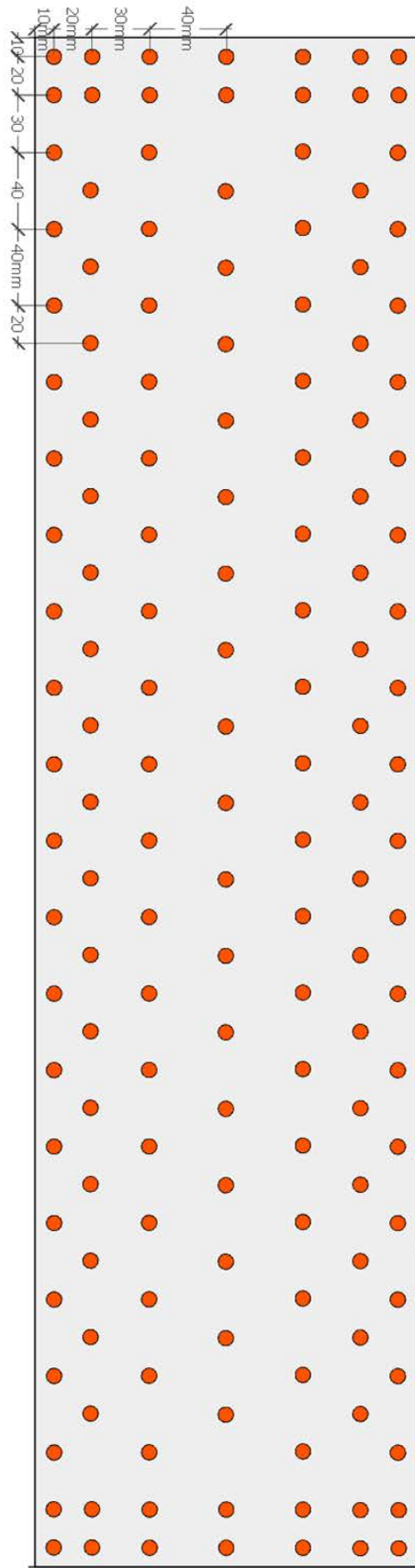


Figure A.8: Model #2-external pressure taps layout on the roof (All dimensions in millimetres)

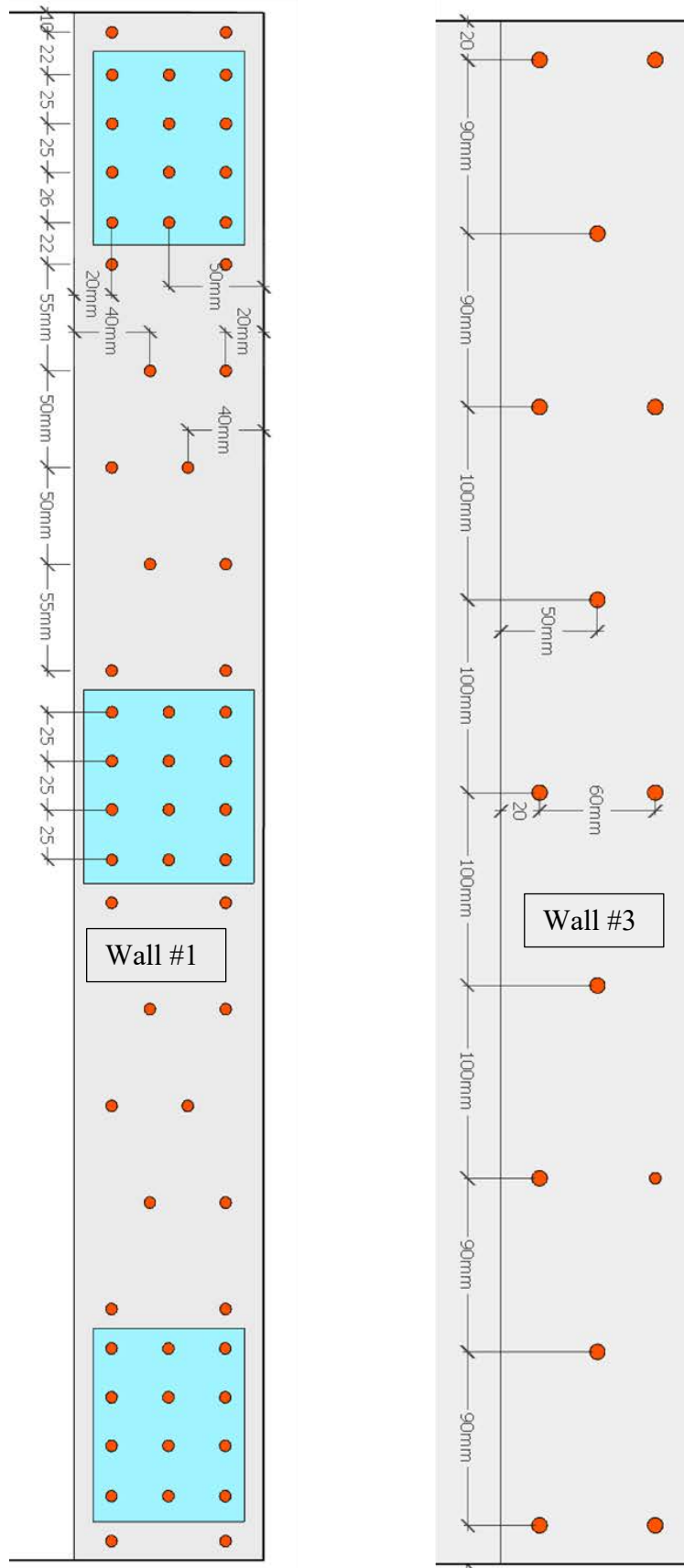


Figure A.9: Model #2- external pressure taps layout on Wall #1 and #3 (All dimensions in millimetres)

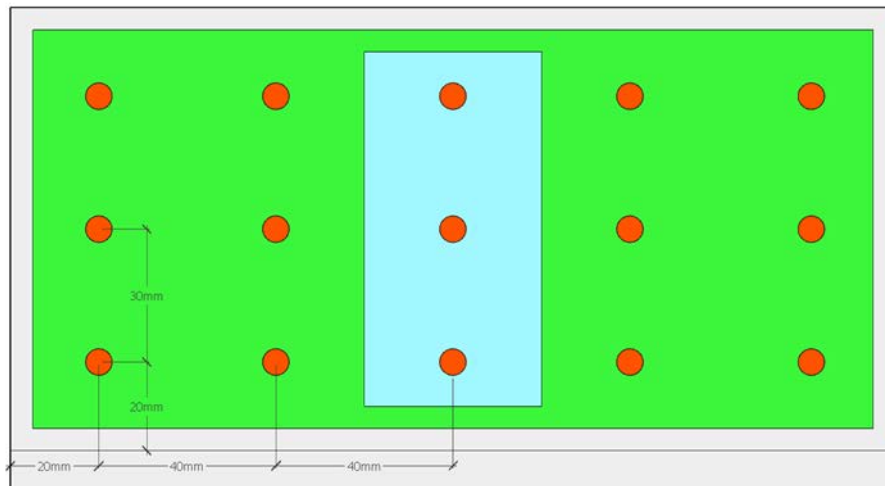


Figure A.10: Model #2- external pressure taps layout on Wall #4 (All dimensions in millimetres)

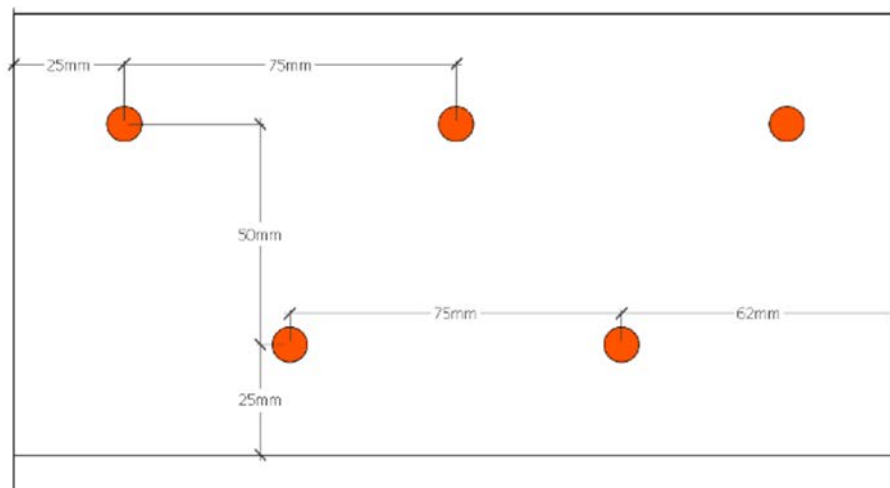


Figure A.11: Model #2- external pressure taps layout on Wall #2 (All dimensions in millimetres)

APPENDIX B : AREA AVERAGED EXTERNAL PRESSURE COEFFICIENT AND AREA REDUCTION FACTOR (K_a)

B.1. Wall patches on the nominally sealed building

Eight patches are selected to compare area-averaged external pressures on each patch (Figure B.1) on the nominally sealed building. Four external pressures taps were evenly distributed in each patch as shown in Figure B.2. Area of each patch is 50 m^2 in full scale. Time histories of four external pressure taps were averaged and created area average time history of the particular patch from a to h, and different time histories were generated for tributary areas shown in Table B.1.

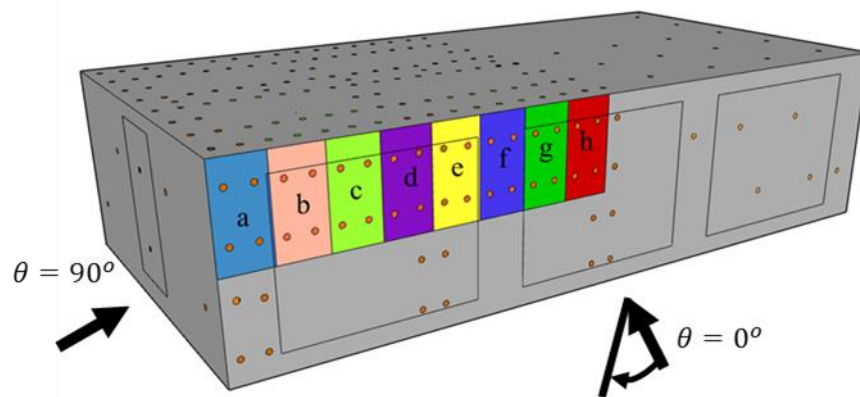
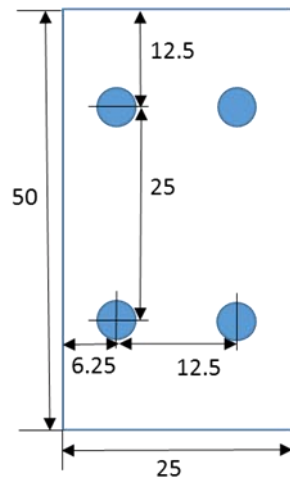


Figure B.1: Eight patches on the nominally sealed building



* Dimension in Millimetres

Figure B.2: External pressure tap layout on each patch

Table B.1: Patch combinations and notations

Patch Combination	Notation
Single Patch –a,b,c,d,e,f,g,h	a,b,c,d,e,f,g,h
Two adjacent patches a+b, b+c, c+d, d+e, e+f, f+g, g+h	a-b, b-c, c-d, d-e, e-f, f-g, g-h
Three adjacent patches a+b+c, b+c+d, c+d+e, d+e+f, e+f+g, f+g+h	a-c, b-d, c-e, d-f, e-g, f-h
Four adjacent patches a+b+c+d, b+c+d+e, c+d+e+f, d+e+f+g, e+f+g+h	a-d, b-e, c-f, d-g, e-h
Five adjacent patches a+b+c+d+e, b+c+d+e+f, c+d+e+f+g, d+e+f+g+h	a-e, b-f, c-g, d-h
Six adjacent patches a+b+c+d+e+f, b+c+d+e+f+g, c+d+e+f+g+h	a-f, b-g, c-h
Seven adjacent patches a+b+c+d+e+f+g, b+c+d+e+f+g+h	a-g, b-h
Eight adjacent patches a+b+c+d+e+f+g+h	a-h

B.2. Data analysing method

- Find external pressure maximum, minimum and mean of each tap location for five test runs, each wind direction.
- Find area-averaged external pressure maximum, minimum and mean from generated time histories by averaging four-time histories for each tributary area for five test runs, each wind direction.
- Averaged five means, maximums, and minimums
- Area reduction factor for each tap considered as follows (Bodhinayake et al. (2019));

$$K_{a1} = \frac{\text{Maximum of particular tributary area}}{\text{Maximum of individual pressure tap}}$$

$$K_{a2} = \frac{\text{Minimum of particular tributary area}}{\text{Minimum of individual pressure tap}}$$

B.3. Area-averaged external pressures on side walls $\theta = 90^\circ \pm 45^\circ$

Figure B.3 shows the area-averaged minimum external pressure coefficients on side wall for all patch combinations shown in Table B.1. Largest C_{pe} occurred at the patch ‘a’ and decreased towards the middle of the wall (h). Furthermore, this minimum pressure coefficients decrease significantly when the tributary area is increased, as shown in Figure B.3 in different colours. Table B.2 shows the area reduction factors in each tap location as a matrix that the K_a is significantly decreased with increasing the tributary area. This calculated area reduction factors are in accordance with the wind loading standard AS/NZS 1170.2 for side wall cladding design as proposed in Table B.5.

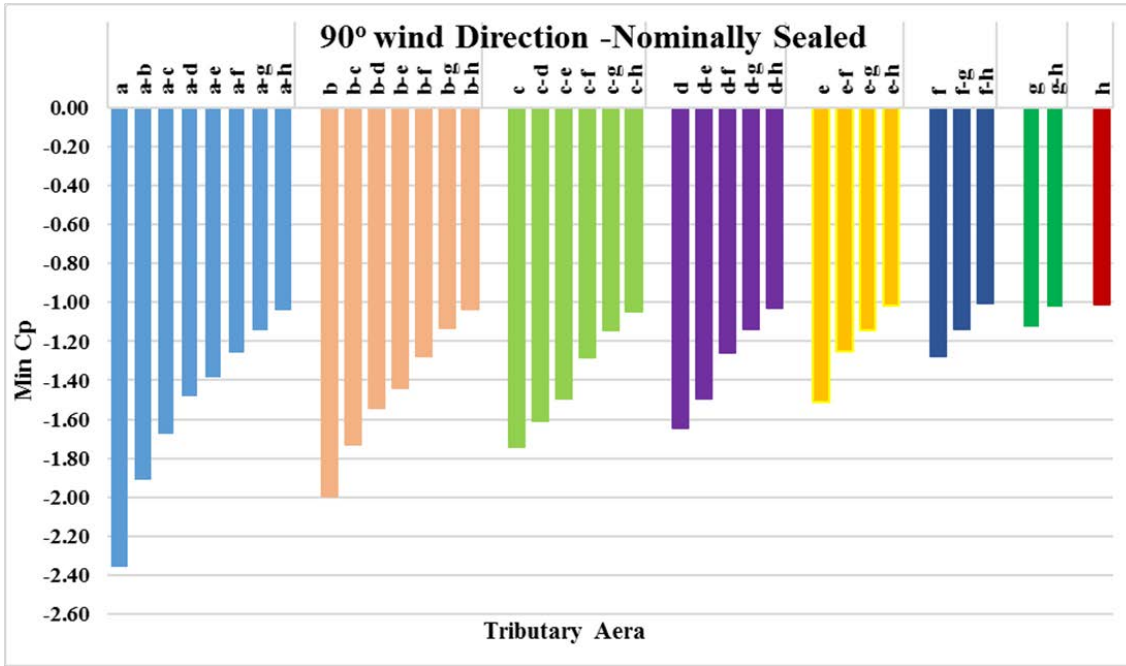


Figure B.3: Area-averaged minimum external pressure coefficients for each tributary area on side wall

Table B.2: Individual area reduction factors for each tap location on the side wall patch by adding one patch at a time to patch “a”

	a														
a	0.97	1.00													
	0.80	0.77	b												
a	0.78	0.82	0.74	0.72											
	0.65	0.63	0.81	0.92	c										
a	0.69	0.72	0.65	0.63	0.76	0.68									
	0.57	0.55	0.71	0.81	0.79	0.94	d								
a	0.61	0.64	0.57	0.56	0.67	0.60	0.55	0.76							
	0.50	0.49	0.63	0.71	0.70	0.83	0.74	0.86	e						
a	0.57	0.59	0.54	0.52	0.63	0.56	0.51	0.71	0.67	0.76					
	0.47	0.45	0.59	0.67	0.65	0.78	0.69	0.80	0.67	0.92	f				
a	0.52	0.54	0.49	0.48	0.57	0.51	0.47	0.65	0.61	0.69	0.76	0.77			
	0.43	0.41	0.53	0.61	0.59	0.71	0.63	0.73	0.61	0.84	0.94	0.95	g		
a	0.47	0.49	0.44	0.43	0.52	0.46	0.43	0.59	0.55	0.63	0.69	0.70	0.84	0.78	
	0.39	0.38	0.48	0.55	0.54	0.64	0.57	0.66	0.55	0.76	0.86	0.86	0.84	0.93	
a	0.43	0.45	0.40	0.39	0.47	0.42	0.39	0.53	0.50	0.57	0.63	0.64	0.77	0.71	
	0.35	0.34	0.44	0.50	0.49	0.59	0.52	0.60	0.50	0.69	0.78	0.78	0.76	0.84	

B.4. Area-averaged external pressures on windward walls $\theta = 0^\circ \pm 45^\circ$

Figure B.4 shows the maximum area-averaged external pressures on the windward wall for each patch combinations shown in Table B.1. As illustrated in Figure B.4, maximum C_{pe} is less on patch ‘a’ compared to all other patches due to the flow separation effects at the wall edge and it continued to area-averaged C_{pe} combining patch ‘a’ with other patches. Maximum C_{pe} also are decreased with increasing the tributary area; however, the percentage of decrease is small in the middle of the wall due to less spatial variation and stagnation of external pressure fluctuations.

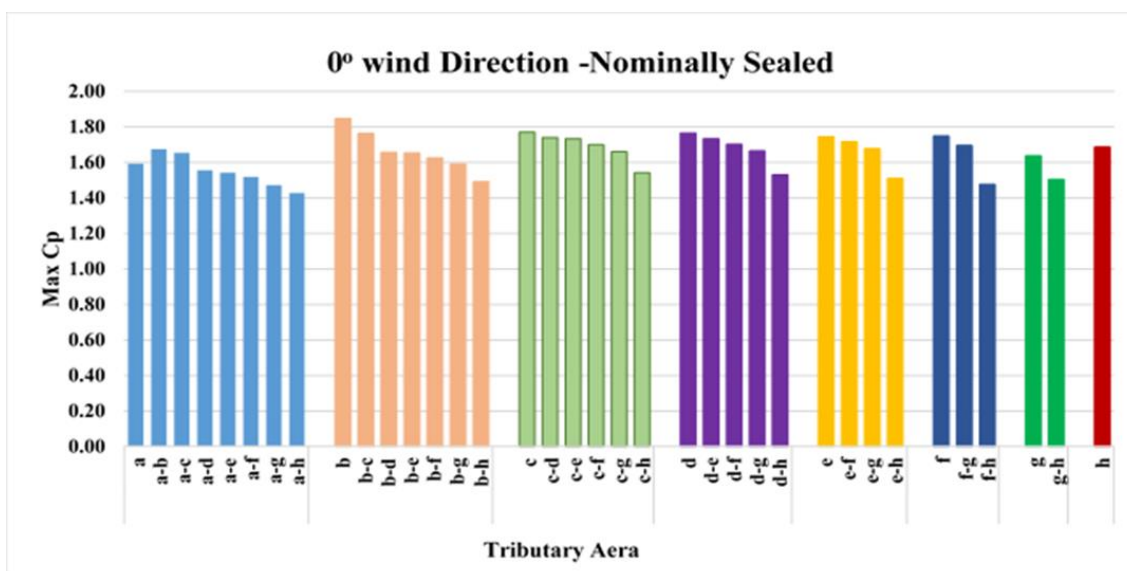


Figure B.4: Area-averaged minimum external pressure coefficients for each tributary area on the windward wall

Table B.3 shows the area reduction factors for individual cladding locations based on the Equation in Section B.2. When the tributary area is increased over 100m² lowest area reduction factor is about 0.8, which suggest a reduction to the maximum external pressures on the windward wall compared to AS/NZS 1170.2. Proposed K values based on the tributary area is shown in Table B.5.

Table B.3: Individual area reduction factors for each tap location on the windward wall patch by adding one patch at a time to patch “a”

	a													
a	0.84	0.76												
	0.98	0.86	b											
a	0.89	0.80	0.88	0.84										
	1.00	0.90	0.88	0.88	c									
a	0.88	0.79	0.87	0.83	0.86	0.92								
	1.00	0.89	0.87	0.87	0.89	0.88	d							
a	0.82	0.74	0.82	0.78	0.81	0.87	0.87	0.86						
	0.96	0.84	0.82	0.82	0.84	0.83	0.83	0.80	e					
a	0.82	0.74	0.81	0.77	0.80	0.86	0.86	0.85	0.84	0.83				
	0.95	0.83	0.81	0.81	0.83	0.82	0.83	0.80	0.84	0.81	f			
a	0.80	0.73	0.80	0.76	0.79	0.85	0.85	0.84	0.82	0.82	0.83	0.83		
	0.94	0.82	0.80	0.80	0.81	0.81	0.81	0.78	0.82	0.80	0.80	0.85	g	
a	0.78	0.70	0.77	0.74	0.76	0.82	0.83	0.81	0.80	0.80	0.81	0.81	0.81	0.73
	0.91	0.79	0.78	0.77	0.79	0.79	0.79	0.76	0.80	0.77	0.77	0.83	0.88	0.90
a	0.76	0.68	0.75	0.72	0.74	0.80	0.80	0.79	0.78	0.77	0.78	0.78	0.78	0.71
	0.88	0.77	0.75	0.75	0.77	0.76	0.77	0.74	0.78	0.75	0.75	0.80	0.85	0.87

B.5. Area-averaged external pressures on leeward walls $\theta = 180^\circ \pm 45^\circ$

Figure B.5 shows the minimum area-averaged external pressure coefficients on leeward wall for all patch combinations shown in Table B.1. Here, minimum C_{pe} values are nearly constant when the tributary area is increased due to small external pressure fluctuations on the leeward wall following the wake region. Accordingly, the calculated area-reductions factor equals to 1 for single patches when the tributary area less than 25m^2 as shown in Table B.4. Further lowest area reduction factor can be defined as 0.9 when the tributary area is over 100m^2 .

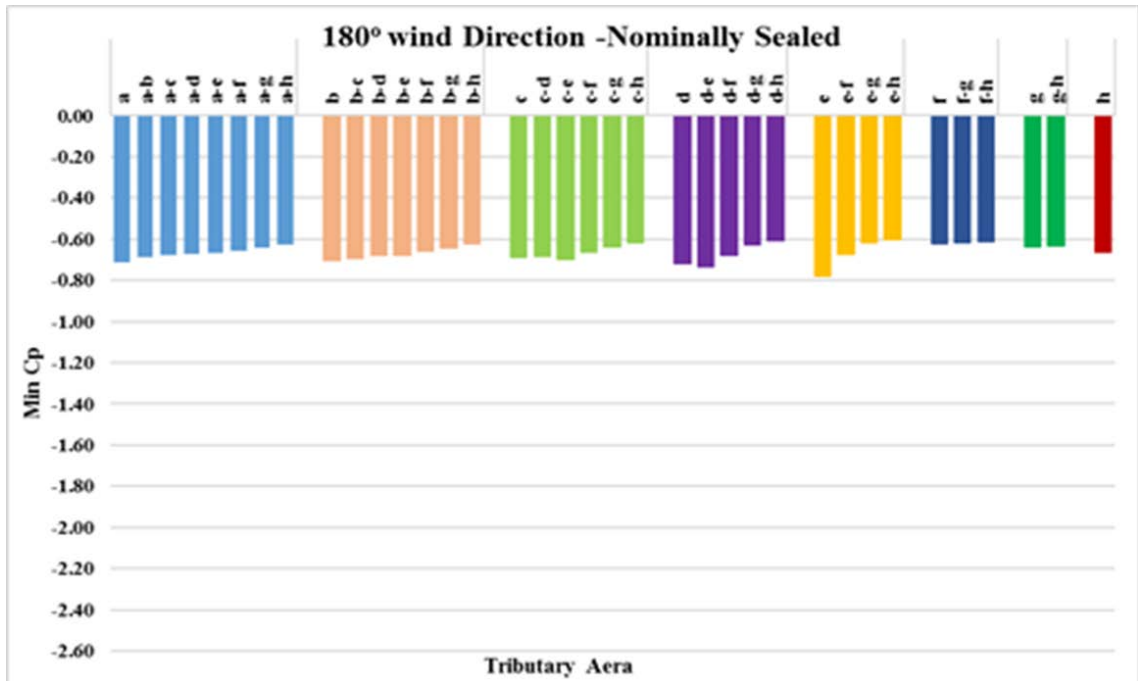


Figure B.5: Area-averaged minimum external pressure coefficients for each tributary area on the leeward wall

Table B.4: Individual area reduction factors for each tap location on the Leeward wall patch by adding one patch at a time to patch “a”

	a															
a	0.92	0.96														
	0.98	0.99	b													
a	0.88	0.92	0.90	0.89												
	0.94	0.95	1.00	1.00	c											
a	0.87	0.91	0.89	0.88	0.87	0.89										
	0.93	0.94	1.00	1.00	1.00	1.00	d									
a	0.86	0.90	0.88	0.87	0.85	0.88	0.83	0.76								
	0.92	0.93	0.99	0.99	1.00	1.00	1.00	1.04	e							
a	0.85	0.89	0.88	0.86	0.85	0.87	0.83	0.76	0.77	0.77						
	0.91	0.93	0.98	0.98	1.00	1.00	1.00	1.00	0.77	0.95	f					
a	0.84	0.88	0.86	0.85	0.83	0.86	0.81	0.74	0.75	0.76	0.93	0.92				
	0.90	0.91	0.97	0.96	0.99	0.99	0.99	1.00	0.75	0.93	1.00	1.02	g			
a	0.82	0.86	0.84	0.83	0.82	0.84	0.80	0.73	0.74	0.74	0.91	0.90	0.83	0.90		
	0.88	0.89	0.95	0.94	0.97	0.97	0.97	0.99	0.74	0.91	1.00	1.00	0.99	0.99	h	
a	0.80	0.84	0.82	0.81	0.80	0.82	0.77	0.71	0.72	0.72	0.89	0.88	0.81	0.88	0.79	0.70
	0.85	0.87	0.92	0.92	0.94	0.95	0.95	0.97	0.72	0.89	1.00	0.97	0.97	0.97	0.97	1.02

B.6. Proposed area reduction factors, K_a

Table B.5 shows the simplified area reduction factors for side wall, windward wall and leeward wall of the building envelope. K_a values for side wall have a good agreement with AS/NZS 1170 and new K_a values can be proposed to windward wall and leeward wall as shown in Table B.5.

Table B.5: Proposed area reduction factor for wall cladding design for $h < 20m$

Tributary area (A), m ²	Side wall	Windward wall	Leeward wall
≤ 25	0.95	0.95	1.00
50	0.9	0.9	0.95
≥ 100	0.8	0.85	0.9

APPENDIX C: AREA-AVERAGED NET PRESSURE AND NET PRESSURE FACTORS FOR ROOF ZONES

Figure C.1 shows the roof zones considered for area-averaged pressures on the roof by averaging the pressures of 4, 8, 30, and 42 pressure taps on Zones 1B, 2B, 3B, and 4B respectively. The critical wind directions for roof zones are $\theta \pm 45^\circ$ when the wind flows perpendicular to the opening. Therefore, wind directions $90^\circ \pm 45^\circ$ are considered for further analysis of nominally sealed case (i.e., Cases #02), and building with large openings on Wall #4 (i.e. Case #09).

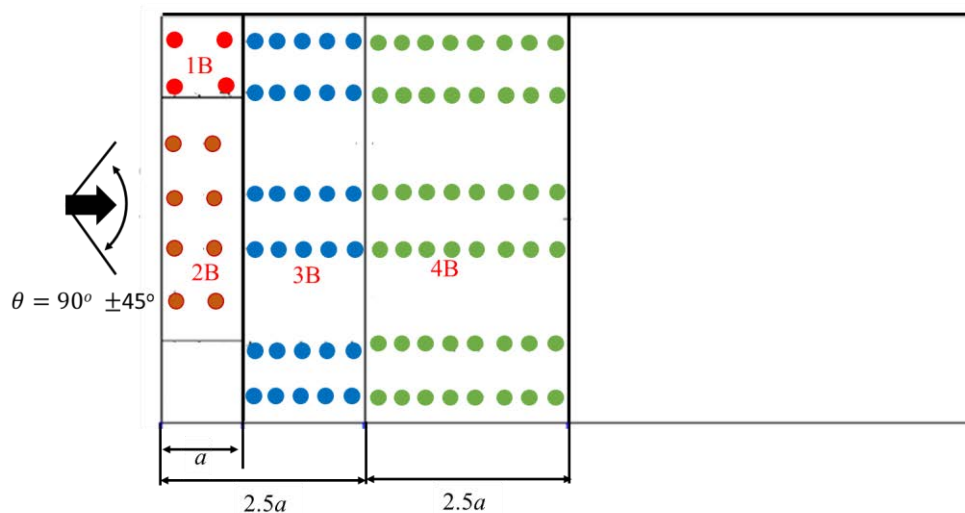


Figure C.1: Roof zones for the net pressure factors when wind flows $90^\circ \pm 45^\circ$

C.1. Nominally sealed building – Case #02

Figures C.2(a) and (b) show the minimum external and minimum net point pressures (i.e., considering a single tap in the zone) and area-averaged pressures for Zone #1B of the nominally sealed building for wind directions 90° to 135° . The highest suction external and net pressures occurred at RP1-1 for wind directions 110° to 125° . As explained in Section 4.2.1, the internal pressure fluctuations are small in the nominally sealed building, and the minimum external and minimum net pressures have similar trends as shown in Figures C.2(a) and (b). The area-averaged minimum external and net pressures vary

around -3.0, lower than the point pressures in the zone due to the spatial filtration. The area-averaged minimum net pressures decrease towards the middle of the roof as shown by the reduction in the minimum pressures proposed from Zones #1B, 2B, 3B and 4B in Figure C.3. The area-averaged $C_{p,net}$ of -3.0 ($\theta = 110^\circ$), -2.8 ($\theta = 120^\circ$), -1.3 ($\theta = 90^\circ$), and -1.0 ($\theta = 135^\circ$) are identified for roof Zones #1B, 2B, 3B and 4B, respectively.

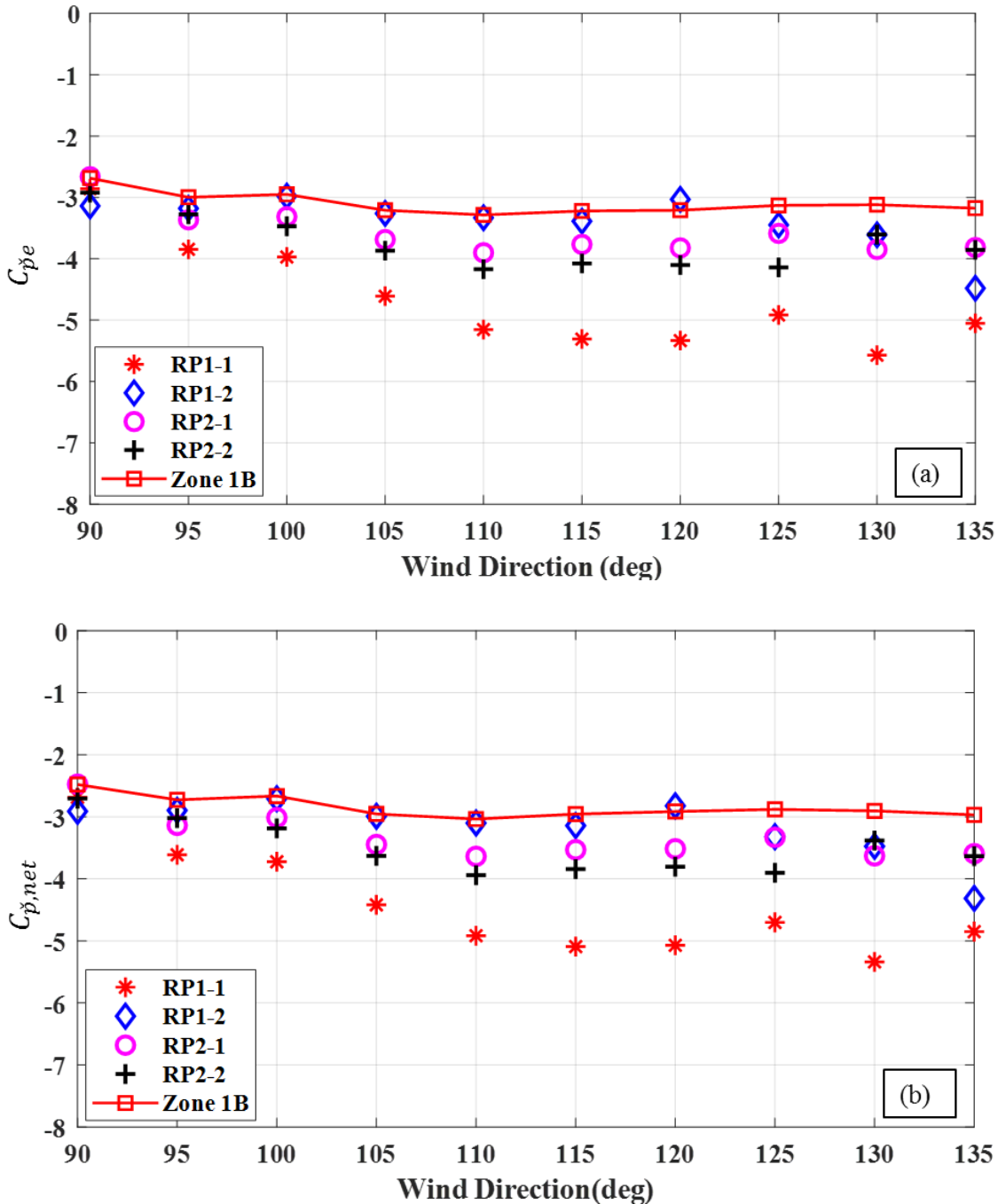


Figure C.2: Point pressures and area-averaged pressures for Zone #1B of nominally sealed building (Case #02) (a) Minimum external pressures (b) minimum net pressures for $\theta = 90^\circ$ to 135°

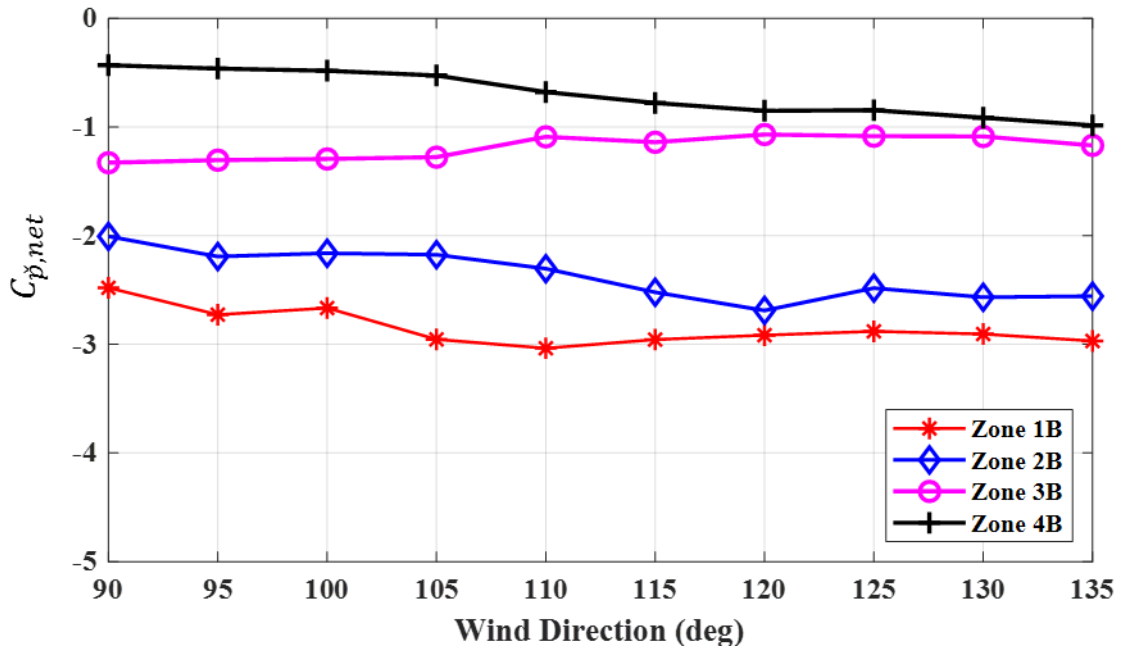


Figure C.3: Area-averaged minimum net pressures for roof Zones 1B, 2B, 3B and 4B of the nominally sealed building (Case #02) for $\theta = 90^\circ$ - 135°

Figure C.4 shows the area-averaged net pressure factors determined using the area-averaged minimum and maximum pressures for the nominally sealed building (Case #02) roof zones wind directions 90° to 135° . As discussed in net pressure factors for point pressures, largest suction net pressure and largest net pressure factor do not occur at the same wind direction. Thus, net pressure factor related to the largest suction net pressure is selected as a particular net pressure factor for roof zone for further comparison. Accordingly, area-averaged F_{C2s} are 0.95, 0.90, 0.85, and 0.85 for Zones #1B, 2B, 3B, and 4B respectively, which is 5% less for some roof areas than the net pressure factors calculated at the point pressures (Section 5.4.2, Figure 5.35) for each roof zone. This is because the spatial filtration on area-averaged net pressures has a greater reduction than area-averaged external pressures with less affect form internal pressure fluctuations.

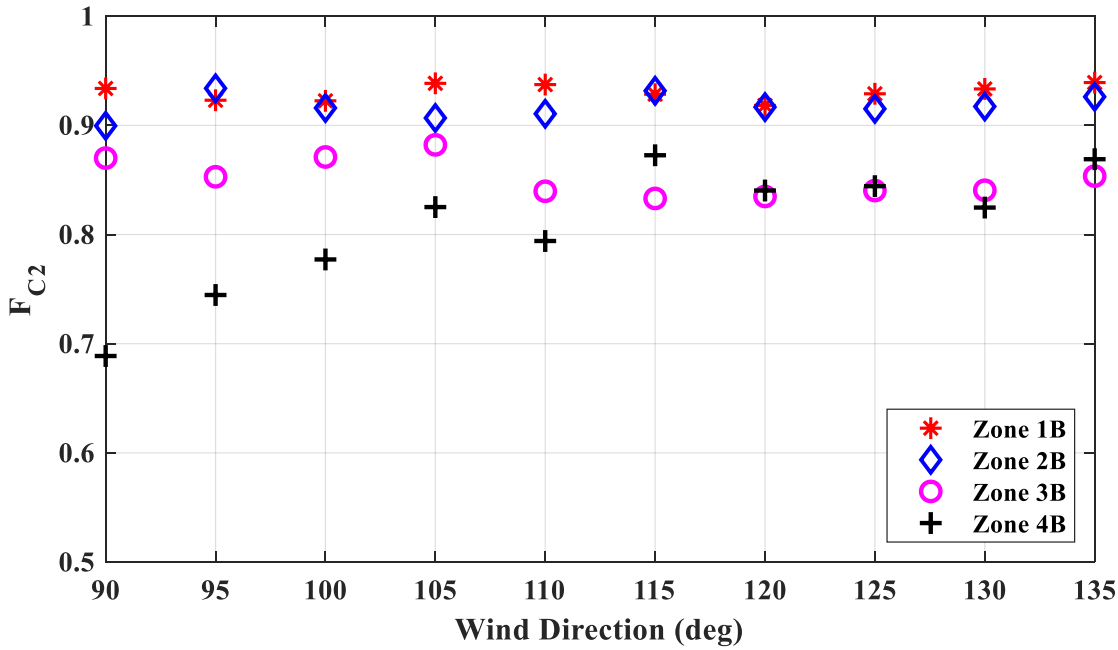


Figure C.4: Area-averaged net pressure factors (F_{C2}) for roof zones based area-averaged external and net pressures for nominally sealed building (Case #02), $\theta = 90^\circ$ to 135°

C.2. Building with a large opening – Case #09

Figures C.5(a)-(b) show minimum external and minimum net pressures of single pressure taps and area-averaged pressures for Zone #1B for the building with a large opening (Case #09) for $\theta = 90^\circ$ - 135° . As explained in Section 5.4.1, the highest C_{pe} and $C_{p,net}$ are identified at RP1-1 and RP2-1 for critical wind directions. The area-averaged minimum external pressures vary around -3.5 and area-averaged $C_{p,net}$ varies around -4.5, which is 40% less than the largest minimum pressures at RP1-1 for $\theta = 110^\circ$. This is due to the spatial filtrations in the individual time-histories of four pressure taps when producing the area-averaged external and net pressure time-histories. Figure C.6 shows the minimum area-averaged net pressures on Zones 1B, 2B, 3B, and 4B of a building with a large opening (Case #09) for $\theta = 90^\circ$ - 135° . Figure C.6 further shows that $C_{p,net}$ decreases towards the middle of the roof due to spatial filtrations of 30 and 42 pressure taps on the area-averaged pressures. Zone #1B experiences the largest area-averaged $C_{p,net}$ of -5.0 at $\theta = 105^\circ$, while -4.5 at $\theta = 130^\circ$ for Zone #2B, -3.0 and -2.0 at $\theta = 90^\circ$ for Zone #3B and #4B, respectively.

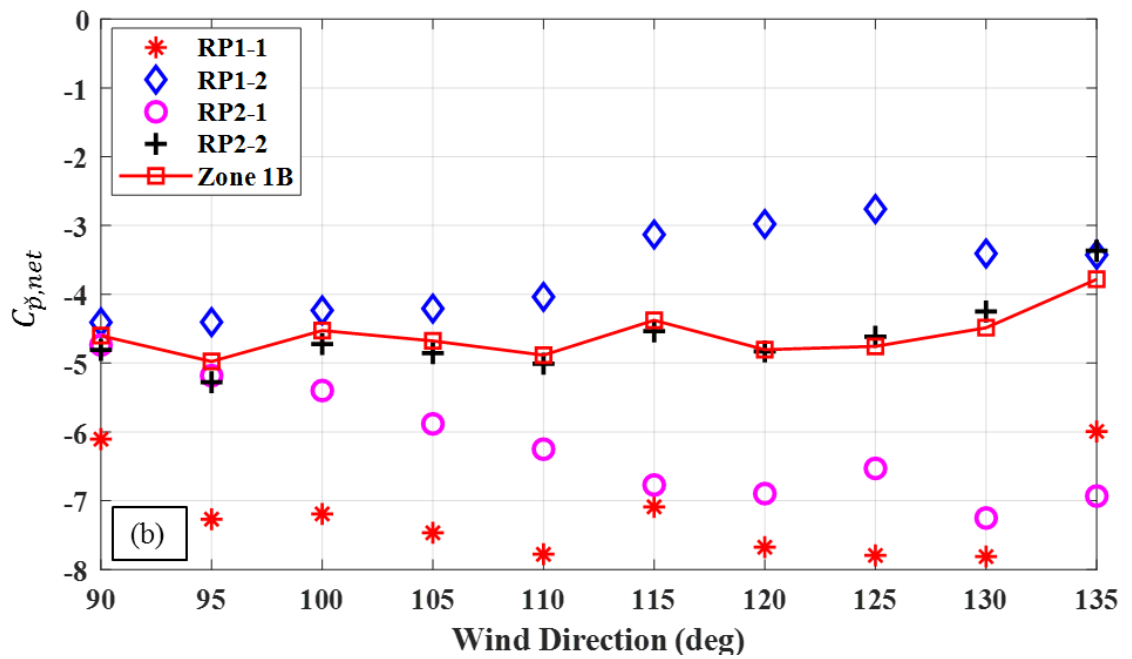
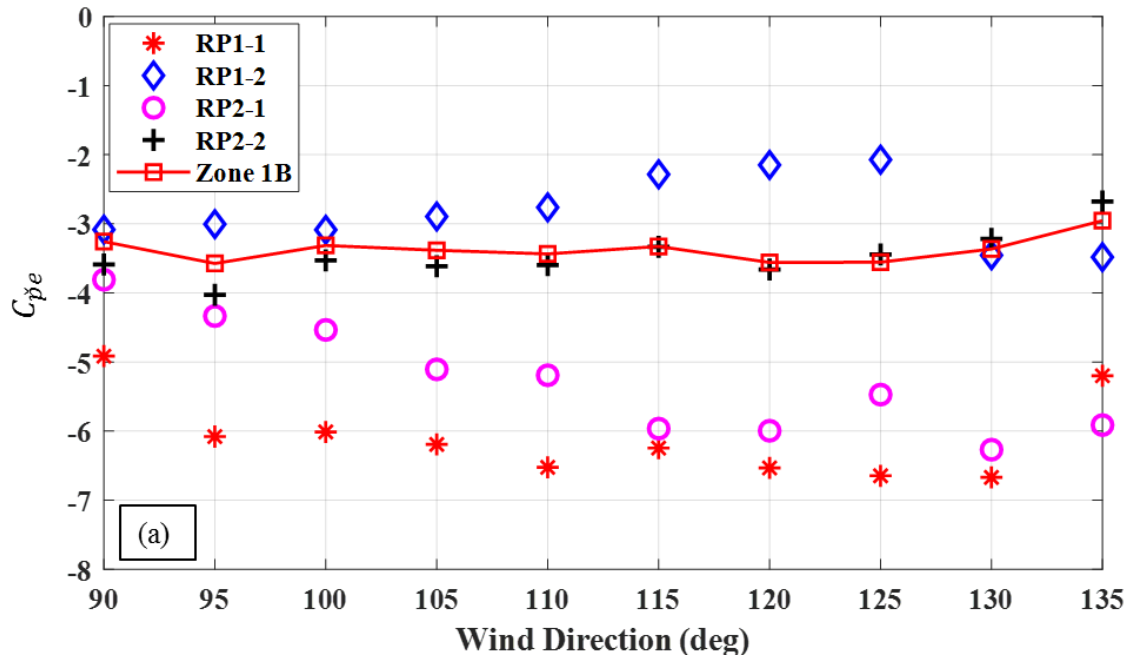


Figure C.5: Point pressures and area-averaged pressures for Zone #1B of a building with a large opening (Case #09) (a) Minimum external pressures (b) minimum net pressures for $\theta = 90^\circ$ to 135°

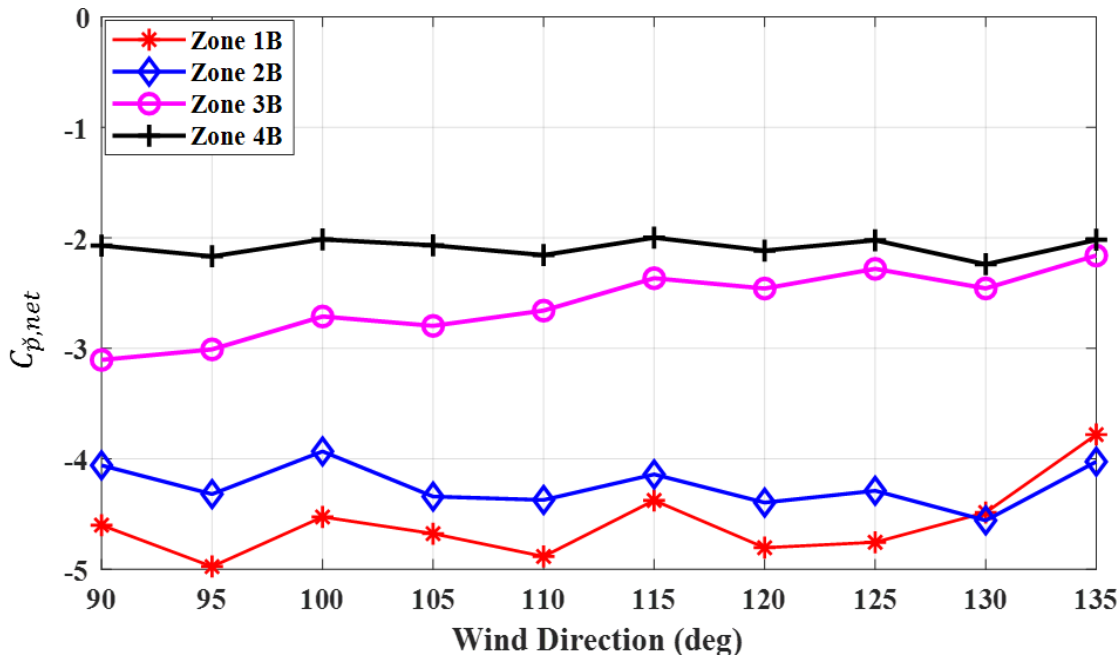


Figure C.6: Area-averaged minimum net pressures for roof Zones 1B, 2B, 3B, and 4B of a building with a large opening (Case #09) for $\theta = 90^\circ$ - 135°

Figure C.7 shows the calculated net pressure factors for different roof zones for Case #09 based on the area-averaged external, net, and internal pressures. The area-averaged net pressure factors for each roof zone are selected considering the wind direction of highest suction net pressures on particular roof zone. Accordingly, the largest F_{C2} for Zone #1B is 0.9 at $\theta = 95^\circ$, which produces the highest net suction pressure, as shown in Figure C.6. Similarly, the area-averaged net pressure factors for Zone 2B of 0.95 ($\theta = 130^\circ$), for Zones 3B and 4B at 90° are about 0.90 and 0.85 for Case #09. The calculated net pressure factors based on the point pressures are within $\pm 5\%$ from the area-averaged net pressure factors (i.e. RP1-1 (0.95), RP3-2 (0.95), RP2-8 (0.9) and RP5-12 (0.8) in Figure 5.36, Chapter 5). The spatial filtration reduces the higher external and net peaks, so area-averaged net pressure factor may not represent the actual reduction to the peak net pressures in cladding design. Therefore, the net pressure factors based on point pressures are more appropriate for cladding design.

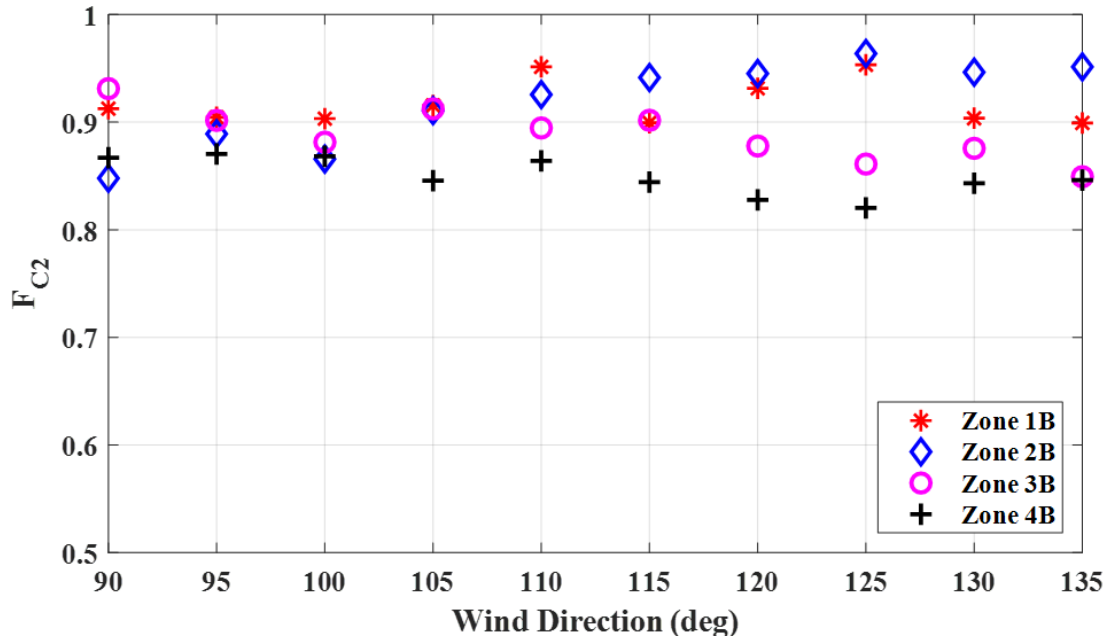


Figure C.7: Area-averaged net pressure factors (F_{C2}) for roof zones based on area-averaged external and net pressures for building with a large opening (Case #09), $\theta = 90^\circ$ to 135°

Table C.1 shows net pressure factors at different roof Zones #1B, 2B, 3B, and 4B based on point pressures and area-averaged pressures for different opening configurations. Most of the area-averaged net pressure factors are higher than net pressure factors for point pressures but are within $\pm 5\%$. This is due to the similar peak internal pressure for both net pressure factors (based on point pressures and area-averaged pressures), but the difference between area-averaged peak external and peak internal pressures are smaller than the difference between point peak pressures. The area-averaged F_{C2} values do not show trends or pattern for different S^* values. However, area-averaged F_{C2} values can be summarised as 0.95 for Zone #1B, 0.9 for Zone #2B and #3B and 0.85 for Zone #3b for any S^* value.

Table C.1: Net pressure factors for different roof Zones #1B, 2B, 3B, and 4B based on point pressures and area-averaged pressures for each S^ values*

Case #	S^*	F_{C2} based on point pressures				F_{C2} based on area-averaged pressures			
		Zone #1B	Zone #2B	Zone #3B	Zone #4B	Zone #1B	Zone #2B	Zone #3B	Zone #4B
12	1.7	0.91	0.88	0.87	0.79	0.94	0.94	0.93	0.84
11	4.8	0.91	0.78	0.92	0.77	0.93	0.90	0.86	0.82
25	6.0	0.88	0.85	0.91	0.83	0.94	0.91	0.94	0.88
22	9.6	0.98	0.85	0.91	0.84	0.92	0.90	0.96	0.90
24	17.1	0.92	0.90	0.87	0.84	0.95	0.93	0.93	0.88
9	59.4	0.92	0.95	0.93	0.81	0.90	0.95	0.90	0.85
21	118.9	0.95	0.82	0.91	0.75	0.94	0.91	0.91	0.82
23	210.7	0.95	0.82	0.88	0.85	0.94	0.94	0.92	0.82